

**Faculty of Science and Engineering
Department of Chemical Engineering**

**Magnetic Field Treatment to Control Scale Growth and Oxygen
Scavenger Performance in Mono Ethylene Glycol Regeneration
Process**

Ammar Wadullah Ahmed Al Helal

**This thesis is presented for the Degree of Doctor of Philosophy of
Curtin University**

2021

DECLARATION

This thesis contains no material that has been submitted for the award of any degree or diploma in any university or institution.

To the best of my knowledge and belief, the work as presented in this thesis is original except as acknowledged.

Ammar Wadullah Ahmed Al Helal

Date: 20/01/2021

ABSTRACT

Magnetic fields application (MFs) is gaining increased importance in all areas of industry and scientific research. This includes physical and chemical applications, which have remarkable potential in a wide range of purposes, including medical applications, electrical power generation, hard water treatment (scale formation control), scanning and analyzing imaging devices and materials separation process. Even though these have excellent prospects, it is not understood whether magnetic fields treatment can work efficiently at MEG regeneration systems in oil and natural gas industries (i.e. pretreatment vessel, reboiler units, and transportation pipelines), specifically at high-salinity concentration, high temperature and high-oxygen content. Magnetic fields applications, the focus of this study, proposes non-chemical techniques to control scale (CaCO_3) formation growth and oxygen contamination after conventional approaches have been exhausted. However, successful implementation of non-chemical techniques requires the understanding of the underlying controlling mechanisms in the MEG regeneration systems, including transportation pipelines.

In the first study of this thesis, an investigation whether the pretreatment process could be minimized without negatively influencing the MEG regeneration process by forming scale on the heater bundle in the presence of low concentrations of divalent cations in the rich MEG stream. In the next part of this research, three experimental studies of CaCO_3 formation with MEG and mineral ions after exposure to a permanent MF in a MEG regeneration pilot plant, modified dynamic scale loop (DSL), and sealed jar cell are reported. In addition, the performance of chemical scale inhibitors in the prevention of CaCO_3 formation in magnetized and non-magnetized MEG solutions was investigated. Furthermore, in this thesis, the performances of non-sulfite products in magnetized and non-magnetized conditions to scavenge oxygen molecules and to mitigate corrosion and sulfate scale formation are presented. Moreover, a new method for the on-site determination of the MEG concentration in brine solutions is proposed. In this new method, measurable physical properties using a portable refractometer and electrical conductivity measurement devices are utilized.

The investigated synthetic solutions contained fresh MEG, degraded MEG and thermally aged MEG solutions, mineral ions, erythorbic acid and two commercial chemical scale inhibitors (HEDP and phosphate ester). Scale formation was analyzed under MEG regeneration process conditions using a modified DSL apparatus, followed by verification experiments using a MEG regeneration and reclamation pilot plant facility at Curtin University. The results generated from the first study using the DSL system and pilot plant indicate that the degree of pretreatment cannot be reduced, even if the divalent ion concentration is lower than ca. 5 ppm total dissolved solids.

The results of this study were sufficient to follow up on this research using magnetic fields technology to study the CaCO_3 formation behavior in MEG regeneration systems. The aim of the second study is to examine the effect of MF treatment on CaCO_3 formation behavior in brine–water solutions and brine–mono ethylene glycol solutions. The differential pressure build-up obtained from each experiment was used to determine any increase or decrease in scaling to guide the development of the new non-chemical scale inhibition techniques. The aqueous and glycolic brine solutions were conducted by using a DSL and autoclave techniques, and thus the differential pressure build-up, scale morphology, pH, and electrical conductivity were then recorded for further analysis. The results indicate that aqueous solutions containing high concentrations of bicarbonate or equal concentrations of bicarbonate and calcium species showed inhibited scale formation following MF exposure at 150°C . In addition, MFs can significantly reduce scale formation in the rich MEG solutions within the capillary coil. Thirdly, the study of glycolic brine solutions with chemical scale inhibitors and a MF treatment established that the MF reduced scale inhibitor performance and the calcium carbonate deposit formed a stable phase morphology at 80 vol. % lean MEG concentrations. An advanced study was conducted to evaluate four physical properties to determine the volume fraction of MEG solutions at various ionic strengths. The physical properties evaluated were the refractive index, electrical conductivity, total dissolved solids (TDS), and non-modified volume fraction. Detailed regression data were generated to model the volume fraction of MEG in terms of these four physical properties. Furthermore, novel MEG volume fraction prediction models were developed.

This work concludes that the use of magnetic field treatments and non-sulfite oxygen scavengers to control scale formation is possible. Furthermore, a method for on-site MEG concentration measurement has been developed that is applicable in the MEG regeneration plant.

ACKNOWLEDGMENT

Firstly, I would like to express my sincere gratitude to my advisor Associate Professor Ahmed Barifcani and Professor Rolf Gubner for the continuous support of my Ph.D. study and related research, for their patience, motivation, and immense knowledge. Their guidance helped me through my research and writing of this thesis. I could not have imagined having better advisors and mentors.

A sincere vote of thanks also is devoted to Professor Shaobin Wang, the chairperson of this research. Besides my advisors, I would like to thank the rest of my thesis committee: Professor Stefan Iglauer and Professor Moses Tade for their insightful comments and encouragement, but also for the hard questions that encouraged me to widen my research from various perspectives.

My sincere thanks also go to Mr. Yu Long, as the laboratory technician at the Curtin Corrosion Centre, who provided assistance to buy the chemicals, instruments and setup the laboratory experiments.

I want to acknowledge Adam Soames, my right-hand friend, who always shared his thoughts, and new ideas with me. I thank my fellow labmates Edith Odeigah and Marisa for the stimulating discussions, for the sleepless nights we were working together before the deadlines, and for all the fun we have had in the last four years. Also, I thank my friends at Curtin University. In particular, I am grateful to Dr. Franca Jones for enlightening me in the first steps of research.

Last but not the least, I would like to thank my family: Kuhel, Yousif, Yaseen, Ibraheem, my parents and to my brothers and sister for supporting me spiritually throughout writing this thesis.

LIST OF PUBLICATIONS

(Refer to the Appendix – for full manuscripts)

Primary Author

Al Helal, A.; Soames, A.; Gubner, R.; Iglauer, S.; Barifcani, A., Influence of Magnetic Fields on Calcium Carbonate Scaling in Aqueous Solutions at 150°C and 1 Bar. *Journal of Colloid and Interface Science* 2018, 509, 472-484 (**Chapter 5**)

Al Helal, A.; Soames, A.; Iglauer, S.; Gubner, R.; Barifcani, A., The Influence of Magnetic Fields on Calcium Carbonate Scale Formation within Ethylene Glycol Solutions at Regeneration Conditions. *Journal of Petroleum Science and Engineering* 2018, 173, 158-169 (**Chapter 6**)

Al Helal, A.; Soames, A.; Iglauer, S.; Gubner, R.; Barifcani, A., Evaluating Chemical-Scale-Inhibitor Performance in External Magnetic Fields Using a Dynamic Scale Loop. *Journal of Petroleum Science and Engineering*, 2019, 179, 1063-1077 (**Chapter 7**)

Al Helal, A.; Soames, A.; Gubner, R.; Iglauer, S.; Barifcani, A., Performance of Erythorbic Acid as an Oxygen Scavenger in Thermally Aged Lean MEG. *Journal of Petroleum Science and Engineering* 2018, 170, 911-921. (**Chapter 8**)

Al Helal A., Iglauer S, Gubner R, and Barifcani A, Performance of erythorbic acid as an oxygen scavenger in salted fresh and degraded monoethylene glycol under a magnetic memory effect. *Asia-Pacific Journal of Chemical Engineering*, 2019, 14, p. e2364. (**Chapter 9**)

Al Helal, A.; Soames, A.; Gubner, R.; Iglauer, S.; Barifcani, A., Measurement of Mono Ethylene Glycol Volume Fraction at Varying Ionic Strengths and Temperatures. *Journal of Natural Gas Science and Engineering* 2018, 54, 320-327 (**Chapter 10**)

Secondary Author

Soames, A.; **Al Helal, A.**; Iglauer, S.; Barifcani, A.; Gubner, R., Experimental Vapor–Liquid Equilibrium Data for Binary Mixtures of Methyl-diethanolamine in Water and Ethylene Glycol under Vacuum. *Journal of Chemical & Engineering Data* 2018, 63 (5), 1752-1760

Soames, A.; Odeigah, E.; **Al Helal, A.**; Zaboony, S.; Iglauer, S.; Barifcani, A.; Gubner, R., Operation of a MEG Pilot Regeneration System for Organic Acid and Alkalinity Removal during MDEA to FFCI Switchover. *Journal of Petroleum Science and Engineering* 2018, 169, 1-14

Conference Paper

Al Helal, A.; Soames, A.; Iglauer, S.; Barifcani, A.; Gubner, R., Effect of Pretreatment Process on Scale Formation in the Re-Boiler Section of Monoethylene Glycol Regeneration Plant. in IOP Conference Series: Materials Science and Engineering. 2019. IOP Publishing. (**Chapter 4**)

TABLE OF CONTENTS

DECLARATION	i
ABSTRACT.....	ii
ACKNOWLEDGMENT	iv
LIST OF PUBLICATIONS	v
TABLE OF CONTENTS	vii
LIST OF FIGURES	xv
LIST OF TABLES	xxiii
Chapter 1 Introduction.....	1
1.1 Overview	1
1.2 Background	3
1.2.1 Magnetic Fields as an Alternative Technique in Chemical Industry	5
1.3 Objective	8
1.4 Thesis Outline	9
Chapter 2 Literature Review	13
2.1 Scale Formation Overview.....	14
2.1.1 Polar and Non-Polar Solutions	15
2.1.2 Calcium Ions in Aqueous Solutions.....	16
2.1.3 Carbonate Ion Hydration in Aqueous Solutions	17
2.1.4 Calcium Carbonate Monomer Formation	18
2.1.5 Morphology and Phases of Calcium Carbonate	20
2.2 Calcium Carbonate Formation in Oilfields	22
2.2.1 Mono Ethylene Glycol Regeneration during Oil and Gas Production	24
2.2.2 Addition of Chemical Scale Inhibitors	26
2.2.3 Mechanisms of Chemical Scale Inhibitor Treatment	27

2.2.4	Conventional Strategies for Scale Formation Remediation.....	28
2.2.5	Non-Conventional Strategies for Scale Formation Remediation	29
2.1	Gas Hydrate Inhibitors and Scale Formation in Oilfield	30
2.1.1	Effect of Mono Ethylene Glycol on Scale Formation	31
2.1.2	Hydration Shell of Ions in Mono Ethylene Glycol	33
2.2	Magnetic Field Treatment as a Non-Chemical Remediation Method	34
2.2.1	Magnetic Field Concepts	34
2.2.2	Magnetic Field Treatment Mechanisms	37
2.2.3	Magnetic Field Orientation and Classification	38
2.2.4	Why is Magnetic Field Application Important in Industry?.....	39
2.2.5	Effect of Magnetic Fields on the Physical Properties of Aqueous Saline Solutions	40
2.2.6	Magnetic Fields Treatments as Scale Formation Inhibitors with Gas Hydrate Inhibitors	42
2.3	Mathematical Modelling Related to Magnetic Fields	44
2.3.1	Magnetic Susceptibility of Electrons	45
2.3.2	Magnetic Susceptibility of Substances	46
2.4	Effect of Magnetic Fields on Ionic Solutions	50
2.4.1	Hydrogen Bonds in Ionic Aqueous Solutions.....	50
2.4.2	Ionic Colloid Systems in Aqueous Solutions	52
2.4.3	Memory Effect.....	53
2.5	Effect of Oxygen Contamination on MEG Regeneration Systems.....	53
2.5.1	Degradation of MEG Solutions	53
2.5.2	Carbon Steel Corrosion Risks.....	55
2.5.3	Typical Oxygen Scavenger Application in General Chemical Industries	56
2.5.4	Effect of Magnetic Field on Microscopic Properties of Aqueous System	60
2.5.5	Jar Cell Technique for Oxygen Scavenger Test	61
2.6	Free Radical Reaction Background.....	61

2.6.1	The Definition of a Radical Molecule	62
2.6.2	The Configuration of a Radical	63
2.6.3	Radical Classification of Oxygen Molecules.....	63
2.7	Measurement of MEG Concentration	64
2.7.1	Determination of MEG Concentration using Physical Properties	65
Chapter 3 Scale Formation Testing Apparatus and Procedures for the Modified Dynamic Scale Loop Using Magnetic Fields		66
3.1	Introduction	66
3.1.1	General Overview of the Modified DSL Apparatus	66
3.1.2	Capillary Tube Coil Size, Dimensions, and Construction Material	67
3.1.3	Magnetic Field Generator Types, Materials, and Size.....	67
3.2	Test Methodologies for the Modified DSL Apparatus	70
3.2.1	Synthetic Brine Solutions and DSL Specifications	70
3.2.2	Dynamic Flow Loop Apparatus Operating Procedure	71
3.3	Factors Influencing the Repeatability of DSL Tests	72
3.3.1	Cleaning Procedure	72
3.3.2	Operational Pressure and Temperature	72
3.3.3	Effect of Flow Rate	72
3.4	Experiment Duration	73
3.5	Validation of Laboratory Tests with Actual Industrial Processes.....	74
3.6	Location of Scale in the Capillary Tube Coil.....	75
3.7	Effects of the MF on Thermodynamic Properties of Scale Formation	75
3.7.1	Effect on the Electrical Conductivity.....	75
3.7.2	Effect on Zeta Potential	77
3.7.3	Effect of MF on Scale Crystal Morphology	78
3.8	Conclusions	78
Chapter 4 Effect of Pre-treatment Process on Scale Formation in the Reboiler Section of Mono Ethylene Glycol Regeneration Plant		79

4.1	Introduction	79
4.2	Experimental Methodology.....	79
4.2.1	Test Conditions	79
4.3	Dynamic Scale Loop	82
4.4	Pilot Plant Distillation	83
4.5	Experimental Results and Discussion	85
4.5.1	Alkalinity Measurements: Case-1 and Case-2 after and before DSL Testing.....	85
4.5.2	Scale Formation Analysis	85
4.5.3	Dynamic Scale Loop Method	86
4.5.4	MEG Pilot Plant Distillation.....	91
4.5.5	Proposed Scale Cleaning	96
4.6	Conclusions	97
Chapter 5 Influence of Magnetic Fields on Calcium Carbonate Scaling in Aqueous Solutions at 150°C and 1 Bar		99
5.1	Introduction	99
5.2	Experimental Methodology.....	99
5.2.1	Chemicals and Equipment Used.....	99
5.2.2	Cleaning Procedure.....	101
5.2.3	Magnet Field Unit.....	101
5.2.4	Experimental Setup.....	103
5.3	Results and Discussion.....	104
5.3.1	Concentrated HCO ₃ ⁻ Solution.....	104
5.3.2	Concentrated Ca ²⁺ Solution	107
5.3.3	Equal Concentration of Bicarbonate and Calcium Ions Solution	111
5.3.4	Magnetic Field Influence upon the Hydration Shell of Ionic Species	112
5.4	Conclusions	115

Chapter 6 The Influence of Magnetic Fields on Calcium Carbonate Scale Formation within Mono Ethylene Glycol Solutions under Regeneration Conditions.....	118
6.1 Introduction.....	118
6.2 Experimental Methodology.....	118
6.2.1 Experimental Equipment and Chemicals.....	118
6.2.1 Experimental Design.....	119
6.2.2 Magnetic Field Device.....	120
6.3 Results and Discussion.....	123
6.3.1 Influence of Magnetic Fields on Scale Formation at 80 vol. % MEG Solution.....	123
6.3.2 Influence of Magnetic Fields on Scale Formation at 50 vol. % MEG Solution.....	126
6.3.3 Morphology of the Precipitates Calcium Carbonate after Exposed to External Magnetic Field.....	129
6.3.4 Discussion of Mechanism Caused after Exposure to Magnetic Fields...	134
6.4 Conclusions.....	137
Chapter 7 Evaluating Chemical-Scale-Inhibitor Performance in External Magnetic Fields Using a Dynamic Scale Loop System	139
7.1 Introduction.....	139
7.2 Materials and Methods.....	139
7.2.1 Brine Solutions	139
7.2.2 Dynamic Tube Blockage Test.....	140
7.2.3 Analytical Method	142
7.3 Results and Discussion.....	143
7.3.1 Effect of Magnetic Field on Brine Solution without CSIs.....	143
7.3.2 Effect of Magnetic Field on CSI-A.....	143
7.3.3 Effect of Magnetic Field on CSI-B.....	145

7.3.4	Effect of Magnetic Field on Electrical Conductivity	147
7.3.5	Effect of Magnetic Field on Turbidity	148
7.3.6	Morphology of the Formed CaCO ₃ Scale	149
7.3.7	Particle-size Analysis	154
7.3.8	Zeta Potential	156
7.3.9	Effects of Magnetic Field on Individual Parameters	159
7.4	Conclusions	161
Chapter 8 Performance of Erythorbic Acid as an Oxygen Scavenger in Thermally Aged Lean MEG..... 163		
8.1	Introduction	163
8.2	Equipment and Chemicals Used	163
8.2.1	pH calibration procedure of TAL-MEG solutions.....	165
8.3	Experimental Methodology.....	165
8.4	Results and Discussion.....	167
8.4.1	Effect of MEG Thermal Aging upon Erythorbic Acid Oxygen Scavenging Performance	167
8.4.2	Effect of Organic Acids on Erythorbic Acid Oxygen Scavenging Performance	168
8.4.3	Evaluation of Erythorbic Acid Performance under Field Conditions (1000 ppb and Saturation).....	169
8.5	Conclusions	174
Chapter 9 The Performance of Erythorbic Acid Oxygen Scavenger within Salty Fresh and Degraded Mono Ethylene Glycol under Magnetic Memory Effect 175		
9.1	Introduction	175
9.2	Experimental Methodology.....	175
9.2.1	Equipment Used and Setup.....	175
9.2.2	Chemicals Used	176
9.2.3	Magnetized Synthetic MEG Solution and Setup	177

9.2.4	Experimental Setup.....	178
9.3	Results and Discussion.....	180
9.3.1	Validation of Mn ²⁺ ion Effect on the Scavenging Process in High-Salt Fresh MEG.....	180
9.3.2	Effect of pH on the Erythorbic Acid Oxygen Scavenging Performance	181
9.3.3	Effect of the Magnetic Field on the Erythorbic Acid Performance in High-Salt Fresh MEG Solutions	181
9.3.4	Effect of MF on Erythorbic Acid Performance in Salt-Free Degraded MEG Solutions	184
9.3.5	Effect of MF on Erythorbic Acid Performance in High Salinity Degraded MEG Solutions	187
9.3.6	pH of Magnetized and Non-magnetized High Fresh MEG and Degraded MEG Solutions	191
9.3.7	Validation of Formic Acid Effect in Combination with Mn ²⁺ Ions on the Scavenging Process in F-MEG.....	192
9.4	Conclusions.....	194
Chapter 10 Measurement of the Mono Ethylene Glycol Volume Fraction at Varying Ionic Strengths and Temperatures.....		195
10.1	Introduction	195
10.2	Experimental Equipment and Chemicals	195
10.2.1	Equipment.....	195
10.2.2	Chemicals.....	196
10.3	Experimental Methodology	196
10.3.1	Experimental Procedure:.....	196
10.3.2	Preparation of Sample Solutions.....	196
10.4	Results and Discussions	197
10.4.1	Application and Testing of the Experimental Data	198
10.4.2	Effect of Ionic Strength on the MEG Volume Fraction Measurements .	199

10.4.3	Correlation Analysis of Experimental Variables Using SPSS Statistics	201
10.4.4	Corrected Volume Fraction of MEG as a Function of Refractive Index, Electrical Conductivity, and TDS	202
10.4.5	Correct Volume Fraction of MEG as a Function of Measured Volume Fraction, and Electrical Conductivity	205
10.4.6	Solution Ionic Strength as a Function of Measured MEG Volume Fraction and Electrical Conductivity	206
10.5	Validation of Proposed Models	207
10.6	Conclusions	208
10.7	Appendix	210
Chapter 11	CONCLUSIONS AND RECOMMENDATIONS.....	211
11.1	CONCLUSIONS	211
11.1.1	Overall Experimental Results	Error! Bookmark not defined.
11.2	RECOMMENDATIONS	217
Chapter 12	REFERENCES.....	220

LIST OF FIGURES

Figure 1-1 Scale deposit on different parts of the MEG pretreatment vessel in a MEG regeneration pilot plant such as sensors, head pumps, and vessels	4
Figure 1-2 Main cations and anions species causing CaCO ₃ scale formation.....	4
Figure 1-3 Cumulative number of magnetic water treatment articles in various leading scientific journals, from the beginning of 2014 to 2018.....	5
Figure 1-4 Dynamic scale loop unit from PSL systemtechnik/Germany	7
Figure 1-5 Layout of thesis objectives and structure.....	12
Figure 2-1 Three-dimensional view of MEG	16
Figure 2-2 Simple demonstration of the stern layer around dissolved Ca ²⁺ ions in aqueous solution.....	16
Figure 2-3 Hydration structure of Ca ²⁺ ions: (a) Seven hydrating water molecules and (b) Six hydrating water molecules.....	17
Figure 2-4 Hydration of carbonate ions: (a) One hydrating water molecule and (b) Six hydrating water molecules	18
Figure 2-5 Monodentate and bidentate bonding in calcium carbonate [77]	19
Figure 2-6 Relationship between the pH of solution and dissociation of carbonic acid in an aqueous solution [99]	20
Figure 2-7 Solubility product of calcite, aragonite, and vaterite with temperature [118]	21
Figure 2-8 MEG loop injection in the pipelines	24
Figure 2-9 CaCO ₃ crystals precipitated from a water + MEG solution (ca. 80% by volume of MEG) at ca. 125°C	32
Figure 2-10 Hydrogen bonding and covalent bonding of a MEG - water system as proposed by Rozhkova, Rozhkova [79]. Images were generated using ACD/ChemSketch freeware [167].....	33
Figure 2-11 Structure of non-polar and polar molecules and their arrangement as they pass through an electromagnetic field	35
Figure 2-12 Lorentz force and the right-hand rule movement of charged molecules	36
Figure 2-13 Recommended MF orientations across the fluid flow in pipelines: Class 4A is diametrically magnetized and class 4B is axially magnetized [19]	39

Figure 2-14 Ferromagnetism: (A) Magnetized material with corresponding MF lines shown and (B) Non-magnetized material	40
Figure 2-15 Diagram of induction and magnetic fields paths	44
Figure 2-16 Electron configuration for diamagnetic and paramagnetic elements.....	45
Figure 2-17 Electronic configuration of sodium atom.....	46
Figure 2-18 Molar susceptibility of the elements at room temperature (cgs units of 10^{-6} cm ³ /mol) [217].....	47
Figure 2-19 Relationship of particle size with MF coercivity [218]	49
Figure 2-20 Ionic polarization under an external MF.....	53
Figure 2-21 Multi-electron oxidation reactions of Mono Ethylene Glycol [236]	54
Figure 2-22 Chemical structure difference between erythorbic acid, ascorbic acid, and dehydroascorbic acid [262].....	57
Figure 2-23 Proposed mechanism of radical scavenging activity of erythorbic acid [262]	59
Figure 2-24 Configuration of triplet and singlet oxygen state.....	64
Figure 3-1 Permanent magnet shapes and configuration.....	68
Figure 3-2 Electromagnetic devices: (A) Continuous MF and (B) Pulsed MF.....	69
Figure 3-3 Electronic circuit diagram of a pulsed power generator, as shown in Figure 3-2-B.....	69
Figure 3-4 Fluid holder for the magnetic pulse technique.....	69
Figure 3-5 Schematic diagram of high-temperature and pressure DSL apparatus.....	72
Figure 3-6 Differential pressure vs. time plot. The various curves indicate blank and different non-CSI trials at 1 bar and a flow rate of 5 mL/min	74
Figure 3-7 Differential pressure vs. time plot. The various curves are for blank and different non-CSI trials at 20 bar and a flow rate of 3.5 mL/min	74
Figure 4-1 pH change in carbonate systems at different temperatures [320]	80
Figure 4-2 DSL configuration and in-line carbon steel disk holder	83
Figure 4-3 MEG pilot plant configuration.....	84
Figure 4-4 Differential pressure build-up over the capillary tube for case-1 and case-2 after pH adjustment to 7.24 (complete blockage).....	88
Figure 4-5 Differential pressure build-up over the capillary tube for case-1 of CO ₂ 0.5 mole % after pH adjustment to 7.24 (semi-blockage)	88
Figure 4-6 Differential pressure build-up over the capillary tube for case-2 of CO ₂ 0.5 mole % after pH adjustment at 7.24 (semi-blockage)	89

Figure 4-7 Differential pressure build-up over the capillary tube for case-1 and case-2 of some of the remaining red indicator trials as shown in Table 4-3 and Table 4-4 after pH adjustment.....	89
Figure 4-8 Scale formation on carbon steel of selected MEG pilot plant trials of case-1	90
Figure 4-9 Effect of CO ₂ removal and hydroxide concentration on system pH.....	91
Figure 4-10 Scale formation on reboiler wall	92
Figure 4-11 Scale formation on carbon steel of selected MEG pilot plant trials of case-1	94
Figure 4-12 Formation of scale upon reboiler wall	95
Figure 4-13 Formation of scale on reboiler bundle and pump head.....	95
Figure 4-14 Mg(OH) ₂ material formed on the micro-filter surface of the MEG pilot plant	96
Figure 5-1 Schematic of the dynamic scale loop	102
Figure 5-2 Dimensions and shape of the diametrically magnetize magnet and depiction of the diametrical MF	102
Figure 5-3 Effect of magnet field exposure upon the tendency of high bicarbonate solution to form scale.....	105
Figure 5-4 Influence of MFs on charged particles (see section 2.4.1).....	105
Figure 5-5 Effect of magnet field exposure upon electrical conductivity of high concentration bicarbonate solution	106
Figure 5-6 Effect of magnet field exposure upon the pH level of high concentration bicarbonate solution.....	107
Figure 5-7 Effect of magnet field exposure upon the tendency of high concentration calcium solution to form scale	108
Figure 5-8 Theorized calcium accumulation following magnetic exposure.....	109
Figure 5-9 Effect of magnet field exposure upon the electrical conductivity of high concentration calcium solution	110
Figure 5-10 Effect of magnet field exposure upon pH level of high concentration calcium solution.....	110
Figure 5-11 Effect of magnet field exposure upon the tendency of equal concentration solution to form scale.....	111
Figure 5-12 Effect of magnet field exposure upon the electrical conductivity of equal concentration solution.....	112

Figure 5-13 Effect of magnet field exposure upon pH level of equal concentration solution.....	112
Figure 5-14 Relationship between hydration shell and electrical conductivity with respect to number of water molecules [89, 168, 169]	114
Figure 5-15 Hydration shell of calcium and bicarbonate ions after diametrically MF exposure [89, 168, 169]	114
Figure 5-16 Comparison of hydration shells of large and small ions	115
Figure 6-1 Schematic of the DSL system	122
Figure 6-2 Schematic diagram of jar cell techniques (Autoclave)	123
Figure 6-3 Effect of MF exposure on the tendency of equal concentration of Ca^{2+} and HCO_3^- solution within 80 vol. % MEG to form scale	124
Figure 6-4 Effect of MF exposure upon EC of equal concentration of Ca^{2+} and HCO_3^- solution within 80 vol. % MEG	125
Figure 6-5 Structure of the solvation shell with MEG molecules after exposure to MFs. The images were generated using ACD/ChemSketch freeware software [167]	126
Figure 6-6 Effect of MF exposure upon the tendency of equal concentration of Ca^{2+} and HCO_3^- solution within 50 vol. % MEG to form scale	127
Figure 6-7 (A) Structure of MEG-bicarbonate ion-water system and (B) Structure of MEG-calcium ion-water system at 50 vol. % MEG after MFs treatment	127
Figure 6-8 Effect of MF exposure upon EC of equal concentration of Ca^{2+} and HCO_3^- solution within 50 vol. % MEG	128
Figure 6-9 SEM images of different MEG concentrations at 150°C by using DSL technique.....	131
Figure 6-10 Low magnification SEM images of 50 % by volume of MEG concentrations at 150°C by using DSL	131
Figure 6-11 High magnification SEM images of 80 % by volume of MEG concentrations at 150°C by using DSL	131
Figure 6-12 SEM images of different MEG concentrations at 30°C and 150°C by using jar cell	134
Figure 6-13 Electrical conductivity of different MEG concentrations of varying ionic strength at 20°C	136
Figure 6-14 Estimated activity coefficient of calcium ions as a function of ionic strength using the extended Debye-Hückel model	136

Figure 6-15 Estimated activity coefficient of calcium ions as a function of temperature using the extended Debye-Hückel model	137
Figure 7-1 Schematic diagram of the DSL system	141
Figure 7-2 Flowchart of experimental procedure	142
Figure 7-3 Flowchart of scale formation analyses for exposed and non-exposed trials	142
Figure 7-4 Changes in pressure (scale formation) as functions of time for calcium carbonate solutions following exposure, or not, to an applied magnetic field	143
Figure 7-5 Changes in pressure (scale formation) as functions of time for calcium carbonate solutions in the presence of CSI-A at 20 ppm concentrations following exposure, or not, to an applied magnetic field	144
Figure 7-6 Changes in pressure (scale formation) as functions of time for calcium carbonate solutions in the presence of CSI-A at 100 ppm concentrations following exposure, or not, to an applied magnetic field	145
Figure 7-7 Changes in pressure (scale formation) as functions of time for calcium carbonate solutions in the presence of CSI-A at 200 ppm concentrations following exposure, or not, to an applied magnetic field	145
Figure 7-8 Changes in pressure (scale formation) as functions of time for calcium carbonate solutions in the presence of CSI-B at 20 ppm concentrations following exposure, or not, to an applied magnetic field	146
Figure 7-9 Changes in pressure (scale formation) as functions of time for calcium carbonate solutions in the presence of CSI-B at 100 ppm concentrations following exposure, or not, to an applied magnetic field	146
Figure 7-10 Changes in pressure (scale formation) as functions of time for calcium carbonate solutions in the presence of CSI-B at 200 ppm concentrations following exposure, or not, to an applied magnetic field	147
Figure 7-11 Electrical conductivities of solutions with various concentrations of CSI-A and CSI-B following exposure, or not, to an applied magnetic field	148
Figure 7-12 Turbidity of solutions with various CSI-A and CSI-B concentrations under an applied MF	149
Figure 7-13 Liquid phase samples of CSI-A and without CSI-A after centrifugation .	149
Figure 7-14 Liquid phase samples of CSI-B after centrifugation.....	149

Figure 7-15 High-magnification SEM images (scale bar: 2 μm) of scales particles formed in magnetized and non-magnetized conditions in the absence of a CSIs: (A) non-magnetized and (B) magnetized	150
Figure 7-16 XRD profiles of (A) Vaterite “V” and Calcite “C” formed during the non-magnetized experiment, and (B) Calcite “C” formed during the magnetized experiment	151
Figure 7-17 High-magnification SEM images (scale bar: 2 μm) of scales formed in magnetized and non-magnetized experiments involving CSI-A	153
Figure 7-18 High-magnification SEM images (scale bar: 2 μm) of scales formed in magnetized and non-magnetized experiments involving CSI-B	154
Figure 7-19 Particle-size distribution patterns from non-magnetized experiments.....	155
Figure 7-20 Particle-size distribution patterns from magnetized experiments.....	156
Figure 7-21 Absolute zeta potentials of solutions with various CSI-A and CSI-B concentrations before and after exposure to MF	157
Figure 7-22 Depicting a possible mechanism for the effect of a magnetic field based on zeta-potential difference [22].....	159
Figure 7-23 Magnetic volume susceptibility of admixtures of substances in the MEG system and water system after exposure to a MF	161
Figure 8-1 Bench scale oxygen scavenger experimental apparatus	164
Figure 8-2 Effect of MEG thermal aging upon oxygen scavenger performance.....	168
Figure 8-3 Effect of acetic acid concentration on erythorbic acid oxygen scavenger performance (at pH = 9) within fresh MEG	169
Figure 8-4 Relationship between pH of solution and dissociation status of acetic acid [362].....	169
Figure 8-5 Effect of pH upon erythorbic acid performance in MEG no salts TAL-MEG	171
Figure 8-6 Effect of pH upon erythorbic acid performance in low organic acid TAL-MEG	171
Figure 8-7 Effect of pH upon erythorbic acid performance in high salinity TAL-MEG	172
Figure 8-8 Effect of pH upon erythorbic acid performance in MEG no salts TAL-MEG	172
Figure 8-9 Effect of pH upon erythorbic acid performance in MEG low organic acids (condensed water only) TAL-MEG	173

Figure 8-10 Effect of pH upon erythorbic acid performance in high salts MEG (full formation water) TAL-MEG	173
Figure 9-1 Bench-scale oxygen scavenger experimental apparatus	176
Figure 9-2 Magnetic treatment setup to circulate MEG solutions	177
Figure 9-3 Scavenging performance of Mn ²⁺ ions in F-MEG solution under alkaline conditions	180
Figure 9-4 Effect of pH level on high-dosage erythorbic acid performance in salt-free F-MEG solutions	181
Figure 9-5 Effect of the MF on low-dosage erythorbic acid performance for ~1000 and ~7000 ppb O ₂ in the high salinity fresh Monoethylene Glycol solutions	182
Figure 9-6 Magnetic memory effect on erythorbic acid scavenging reaction	183
Figure 9-7 Effect of the MF on high-dosage erythorbic acid performance for ~1000 and ~7000 ppb O ₂ in high salinity fresh Monoethylene Glycol solutions	184
Figure 9-8 Effect of the MF on low-dosage erythorbic acid performance for ~1000 and ~7000 ppb O ₂ in salt-free degraded Monoethylene Glycol solutions	185
Figure 9-9 Product formation in aerobic oxidation of formic acid with metal-ion catalyst [368]	185
Figure 9-10 Product formation in aerobic oxidation of formic acid with metal-ion catalyst	186
Figure 9-11 Effect of the MF on high-dosage erythorbic acid performance for ~1000 and ~7000 ppb O ₂ in salt-free degraded Monoethylene Glycol solutions	187
Figure 9-12 Influence of the memory effect on low-dosage erythorbic acid performance for ~1000 and ~7000 ppb O ₂ content in high salinity degraded Monoethylene Glycol solutions	189
Figure 9-13 Influence of the memory effect on high-dosage erythorbic acid performance for ~1000 and ~7000 ppb O ₂ content in high salinity degraded Monoethylene Glycol solutions	189
Figure 9-14 Magnetic memory effect on the pH of the magnetized and non-magnetized high salinity degraded Monoethylene Glycol solutions	190
Figure 9-15 pH measurements after and before exposure to an MF for ~1000 and ~7000 ppb oxygen concentrations in the fresh Monoethylene Glycol solutions	191
Figure 9-16 pH measurements after and before exposure to an MF for ~1000 and ~7000 ppb oxygen concentrations in the degraded Monoethylene Glycol solutions	192

Figure 9-17 Performance of formic acid as oxygen scavenger in F-MEG solutions at pH of 9.0 and 10.0	193
Figure 9-18 Effect of pH level on the scavenging performance of formic acid in F-MEG solution.....	193
Figure 10-1 Refractive index (n_D) for this work and Fogg et al. (1955) as a function of MEG volume fraction at 25°C.....	197
Figure 10-2 Electrical conductivity (EC) at a temperature of 25°C as a function of MEG volume fraction and NaCl.....	198
Figure 10-3 Refractive index (n_D) as a function of MEG volume fraction and ionic strength at 25°C	199
Figure 10-4 Refractive index (n_D) as a function of MEG volume fraction and ionic strength at 25°C	199
Figure 10-5 Effect of ionic strength on the refractive index measurements at 25°C....	201
Figure 10-6 Effect of ionic strength on MEG volume fraction measurement at 25°C.	201
Figure 10-7 MEG volume fraction residual error between actual and calculated values	204
Figure 10-8 Estimated volume fraction of MEG solutions at no salt content, $R^2 = 1.0204$	
Figure 10-9 Residual error between the estimated and actual volume fraction of MEG solutions at ionic strength using measured volume fraction.....	206
Figure 10-10 Ionic strength residual error between actual and estimated values of MEG volume fraction ranging from 10 to 80%.....	207
Figure 10-11 Digital Hand-held Devices from ATAGO company, LTD.....	209

LIST OF TABLES

Table 2-1 Important scale inhibition functional groups and corresponding main classes of inhibitors [157, 159]	28
Table 2-2 Compilation of current experimental conclusions concerning MF treatment	37
Table 2-3 Ionic radius (r_i), hydrated radius (α_i), and ionic mobility of monovalent elements	41
Table 2-4 Description of each symbol and the corresponding SI-Unit of measure.....	45
Table 2-5 Radii of different ions in the periodic table.....	48
Table 2-6 Structural parameters of water and MEG molecules.....	51
Table 2-7 Hydration energy of ions	51
Table 3-1 Parameters affected by MF treatment	66
Table 3-2 Feed concentrations of cations and anions in the DSL test	70
Table 3-3 Dynamic scale loop specifications	70
Table 4-1 Remaining divalent ions compositions in 61.4 wt. % rich MEG solution for different pretreatment (Case-1).....	81
Table 4-2 Remaining divalent ions compositions in 61.4 wt. % rich MEG solution for different pretreatment (Case-2).....	82
Table 4-3 Summary of lab-scale DSL results at high TDS, ppm	86
Table 4-4 Summary of lab-scale DSL results at low TDS (10 to 5 ppm).....	86
Table 5-1 Brine water concentrations for sets 1, 2 and 3	100
Table 5-2 Magnet specifications and dimensions.....	102
Table 5-3 Dynamic scale loop specifications	104
Table 5-4 Radius of ions, r_i , the thickness of ion hydration shell, Δr , and the number of water molecules in the shell, n [89, 169, 330]	113
Table 6-1 Experiments for the exposed and blank tests of DSL technique and non-exposed jar test technique at different conditions.....	119
Table 6-2 Brine, MEG, and water concentrations for sets of 50% and 80% by volume of MEG.....	119
Table 6-3 Magnet specifications and dimensions.....	120
Table 6-4 DSL specifications	122
Table 7-1 Feed concentration of cations and anions for the DSL test.....	139
Table 7-2 CSI concentrations used in the DSL test	140

Table 7-3 DSL specifications	141
Table 7-4 Absolute zeta potentials of various chemical scale inhibitors for magnetized and non-magnetized solutions	157
Table 8-1 Evaluated erythorbic acid based oxygen scavenger [230]	165
Table 8-2 Erythorbic acid dosage rate	166
Table 8-3 MEG salinity levels*	166
Table 9-1 Evaluated erythorbic-acid-based oxygen scavenger [230].....	177
Table 9-2 Magnet Specifications and Dimensions	177
Table 9-3 Experimental design for fresh and degraded MEG solutions under magnetized and non-magnetized conditions	179
Table 9-4 Fresh and degraded MEG solutions at different salinities and organic acid concentrations	179
Table 10-1 Specifications of measurement devices.....	196
Table 10-2 Summary of experimental solutions.....	197
Table 10-3 Mathematical model nomenclature	200
Table 10-4 Relationships between experimental variables by using SPSS statistics ...	202
Table 10-5 Values of parameters of equation 10-2.....	203
Table 10-6 Values of parameters of equation 10-5.....	205
Table 10-7 Values of parameters of equation 10-6.....	207
Table 10-8 Test sample solutions for models validation	208
Table 10-9 Validation of proposed models.....	208
Table 10-10 Experimental values for refractive index (n_D), TDS, EC, uncorrected volume fraction, estimated values of MEG volume fraction and ionic strength for the MEG + NaCl + H ₂ O system.....	210

Chapter 1 Introduction

1.1 Overview

The oil and natural gas sector face many operational obstacles, especially during the extraction and transfer of hydrocarbon products from oil wells. The most important of these obstacles is how to secure the flow of these products from the offshore platforms to onshore facilities, especially with the possibility of forming gas hydrates and corrosion. Although many thermodynamic and mechanical applications have succeeded in resolving these problems, other difficulties have been exacerbated, especially when changes in oilfield conditions have occurred. For instance, mud and water formations could be observed combining with the hydrocarbons for a while. The breaking-through of these substances are often including serious concentrations of divalent ions that developing to an inorganic deposit on the surfaces of transmission pipelines and equipment at alkaline conditions.

Mono ethylene glycol (MEG) is extensively used in the oil and gas pipelines to prevent the formation of gas hydrates [1-4]; however, it increases the carbonate scaling tendency under alkaline conditions [5, 6]. Although some carbonate formation product such as iron carbonate is beneficial in corrosion mitigation when it creates protective layers on the internal surface of the transportation pipeline; calcium carbonate formation has been build-up and causing serious flow assurance issues [5, 7]. During MEG injecting process, calcium carbonate shows lowering in its solubility as well as changing in its morphology, polymath and particle size distributions with increasing concentration of MEG. Therefore, chemical scale inhibitors (CSIs) are commonly recommended to reduce scale formation during liquid-solid separation treatment in MEG regeneration process. Another important issue during MEG regeneration process is dissolved oxygen contamination, which leads to an increase in carbon steel corrosion and contributes to MEG degradation, in turn affects the flow assurance and gas hydrate inhibition performance. Furthermore, most oxygen scavenger agents are sulfite products such as sodium sulfite, bisulfite, or metabisulfite, which increase sulfate scale formation. Therefore, research into scale formation growth under non-chemical treatment and non-toxic oxygen scavenger are crucial for developing strategies for maintenance of transportation pipelines, MEG regeneration plant reboilers, and salty-MEG pretreatment vessels.

Unfortunately, some CSIs promote corrosion in transport pipelines and equipment because of the low pH of the commonly used industrial CSIs such as polyacrylic acid (PAA), polymaleic acids (PMA), maleic acid terpolymers (MAT), poly-phosphono carboxylic acid (PPCA) and diethylenetriamine- penta (methylene phosphonic acid) (DTPMP) [8-12]. Although there are

several strategies to mitigate corrosion phenomena on pipeline surfaces such as cathodic protection, passive films and coatings and corrosion inhibitors agents [13-16], worse scale formation has been observed within transport pipelines because of neutral range and mild alkaline solutions, which provides cathodic corrosion protection [16]. It is not an overemphasis to say that the non-chemical technology, in terms of investment and potential applications, is one of the most significant modern technologies to solve scale and corrosion issues, specifically in oil and natural gas industry.

Magnetics fields (MF) treatment has been reported to effect scale formation growth and radical reactions in aqueous solutions [17-19]. However, it still needs more investigations to propose a systematic procedure illustrating its effect in glycolic solutions. Therefore, to understand the effect of MFs on scale formation as well as oxygen molecules removal, the microscopic properties of brine molecules were investigated by monitoring the differential pressure build-ups, pH and electrical conductivity (EC) of the ionic solutions, and oxygen concentrations level using different MEG concentrations in a dynamic scale loop (DSL) and sealed jar cell systems. Extensive experimental work has been carried out related to the performance of MFs in reducing scale formation and oxygen concentrations in pipelines and reboilers.

This study aims to evaluate the performance of MFs on the scale formation of CaCO_3 in the presence of rich MEG and lean MEG solutions. Furthermore, the chemical scale inhibitors performance in the prevention of calcium carbonate formation using magnetized and non-magnetized MEG solutions was examined. Also investigated was the performance of non-toxic oxygen scavenger substances (erythorbic acid) in fresh, degraded and thermally aged magnetized and non-magnetized MEG solutions. Mathematical models to estimate the MEG volume fraction, including electrolyte species, have also been developed.

A MEG regeneration/reclamation pilot plant at Curtin University was used to investigate the influence of low divalent ions concentrations on the reboiler heating bundle. In addition, a dynamic scale loop system was utilized to determine the effects of the MF on scale formation and the chemical scale inhibitor performance in glycolic solutions. The experimental set-up for this study utilized a dynamic flow loop system designed and supplied by PSL Systemtechnik, Germany. Based on this set-up, a static MF source was developed to generate a MF, and scale formation after MF exposure was studied. A sealed jar cell was utilized to evaluate the performance of a non-sulfite product on the oxygen scavenging process.

Process parameters such as anion and cation solution concentrations, temperature, pH, runtime, and MEG concentrations were changed systematically to evaluate the inhibition effect of the MFs on scale formation. Solutions with different anion and cation saturation levels were pumped through a capillary coil made of stainless steel. The capillary coil was placed inside a controlled

heating chamber. Scale deposition occurred on the inside walls of the capillary coil. The differential pressure build-up over the capillary coil was caused by the deposition of crystalline material, and its morphology was analyzed using Scanning Electron Microscopy (SEM). Thus, relationships between the scale formation behavior and experimental conditions were established. To control sulfate scale formation within the co-solvent solutions, the use of erythorbic acid has been proposed to reduce the use of sulfite oxygen scavenger products. The performance of erythorbic acid as an oxygen scavenger was evaluated under real field conditions using fresh, thermally aged and degraded MEG solutions with different saline and organic acid concentrations. The determination of MEG concentration was done by measuring the electrical conductivity and refractive index data of MEG samples in the field. Thus, several mathematical models have been developed to facilitate this task.

1.2 Background

Scale formation on the surfaces of the pipelines or on the process equipment is an important aspect of flow assurance and causes numerous technical and economic issues in the oil and gas industry (see Figure 1-1). It is common to observe scale in the wellhead structures, reservoir perforations, valves, tubing strings, and separators. The precipitation of foulants reduces the thermal efficiency of the heating and cooling units, as well as causing damage to pipelines and equipment in the field [20, 21]. This leads to loss of production downtime and reduces profits. Furthermore, the accumulated scale increases the pressure buildup, which leads to loss of energy within the pipelines, enhancing the corrosion and pitting because of the restricted flow of corrosive fluid. In the United Kingdom (UK) alone, the build-up of scale in industrial processing plants where hard water is heated or used as a coolant, precisely in 1993, is estimated to be £1.32 billion per year [22]. Such costs can be attributed to descaling or the reduced thermal conductivity of the scaled surfaces; for example, heat transfer is reduced by 90% by a SiO_2 scale layer 0.5 mm thick [23], whereas a CaCO_3 scale layer 25 mm thick results in a 95% reduction in heat transfer [24].

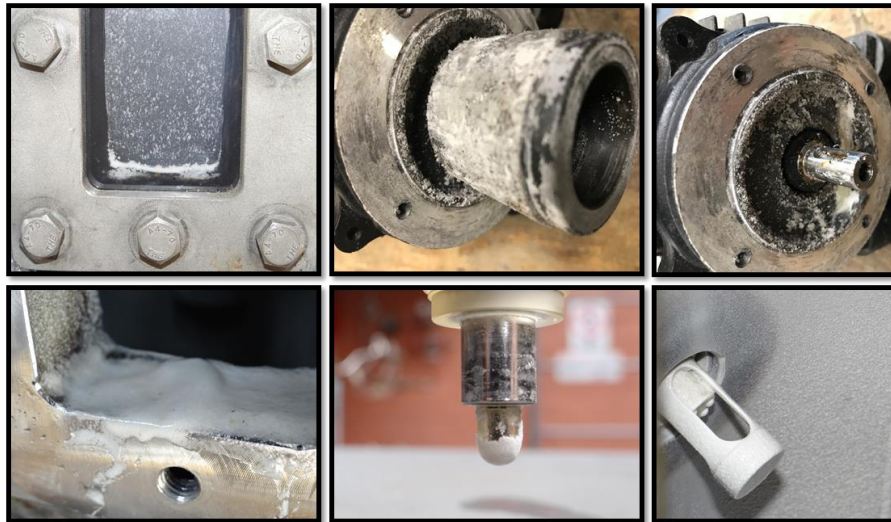


Figure 1-1 Scale deposit on different parts of the MEG pretreatment vessel in a MEG regeneration pilot plant such as sensors, head pumps, and vessels

There are several traditional methods and techniques used to prevent the aggravation of these issues [20]. However, these methods have many disadvantages, which restrict their use. For instance, using chemical treatments and additive inhibitors changes the fluid chemistry [22, 25]. In addition, some of these methods increase the contamination and impurity of the disposed waste, which requires extra purification and separation processes, further increasing expenses. The scale sediment has specific formation conditions, such as high saturation index, high pH, and the presence of carbonate or sulfite ions [10, 22, 25] (see Figure 1-2). Other inorganic scales could also exist within aqueous solutions such as calcium sulfate, barium sulfate, and strontium sulfate, but these types of scale precipitate under different thermodynamic conditions than calcium carbonate [26].

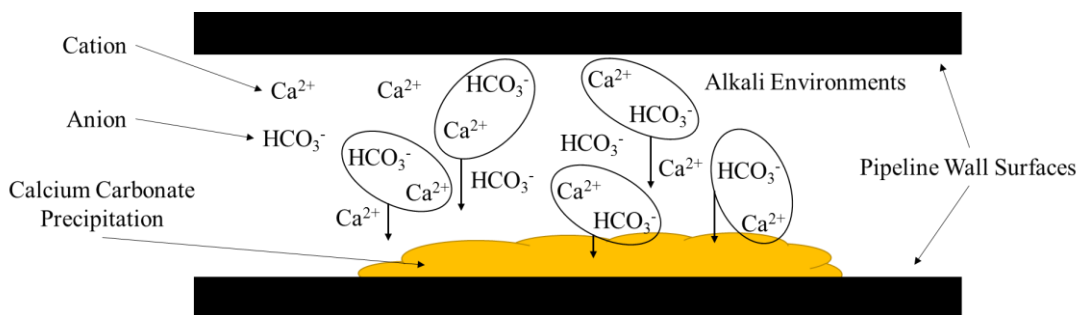


Figure 1-2 Main cations and anions species causing CaCO_3 scale formation

Additionally, although the temperature of the reaction is an indirect factor, it is the main activator for scale formation, accelerating the rate of chemical reaction. Moreover, the crystalline phases and morphology of the deposits are affected by the temperature. Unfortunately, high temperatures accelerate the precipitation of calcium carbonate, unlike other sediments. Because of the low solubility of CaCO_3 scale at moderate to high temperatures, CaCO_3 control is a crucial part of

general treatment strategies to deal with deposits. Thus, the rate of precipitation will be influenced by the supersaturation level, temperature and the individual mineral ion characteristics.

1.2.1 Magnetic Fields as an Alternative Technique in Chemical Industry

Recently, magnetic field treatment to prevent scale formation in mineral aqueous solutions has found extensive use [27-30]. This treatment has a controversial history but has been reported to be effective in numerous cases [19, 31]. Until now, the effect of the magnetic fields on the dissolved constituents has not been confirmed. A number of theories have been postulated, such as the modification of the molecular structure of water, changes in the ion hydration, effects on the surface charge of the particulates, and altering proton spin and proton transfer rate [19, 22, 27, 28, 30-34]. These theories and mechanism, based on practical and computer simulation investigations [35-38], have been published in numerous leading journals and reports. The growth rate of traditional scientific publication has been illustrated in Figure 1-3 from 2014 to 2018 using available data from a number of scholarly databases at Curtin University. Peer-reviewed scientific journals are still growing and there are no indications that the publication rate has decreased in the last 4 years. This means that leading scientific journals are still paying serious attention to the applications of the magnetic field in water treatment.

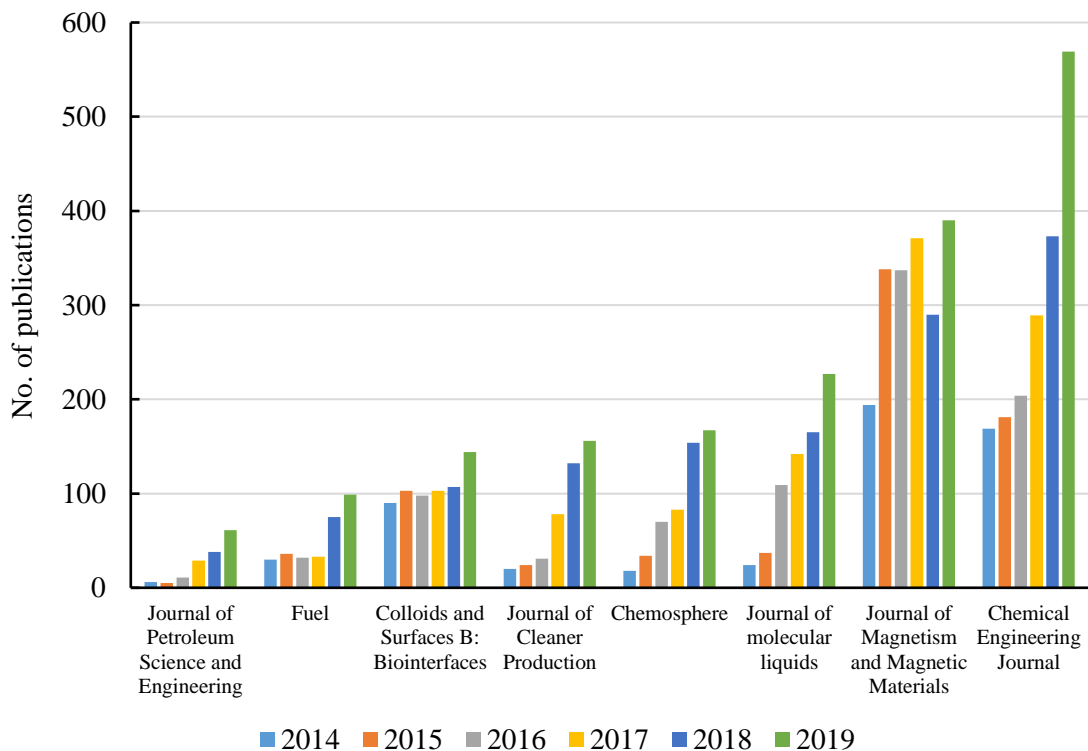


Figure 1-3 Cumulative number of magnetic water treatment articles in various leading scientific journals, from the beginning of 2014 to 2018.

The mechanism by which MF affects scale formation is still controversial, and a range of hypotheses and mechanisms have been reported. Some of these hypotheses conflict with each other while others lack interpretation and evidence. This is because most scientific studies are conducted in the laboratory under ideal conditions and do not consider the full effects of real conditions. The nucleation of metal ions can be considered as the basic principle for understanding how MFs affect scale formation, but this is not the whole story, and several factors contribute to the overall effect of MFs: the Lorentz force, magnetic gradient, magnetic memory, and magnetism. These factors can be used to understand how MFs affect molecules.

In many cases, the MF is produced by an alternating current and pulsed fields, whereas, in other cases, permanent magnets of different configurations and shapes have been used [19, 31, 39, 40]. Because of the feedback concerning the use of this device, MF utilization in industry sector has improved considerably. In 1890, Faunce and Cabell invented an electromagnetic device for hard water treatment in steam boilers [27, 41]; however, this device did not attract attention. Interestingly the first patent of a device for MF treatment was published and registered in 1945 by Theo Vermeiren in Belgium [42, 43]. In the 1960s and 1970s, Russian authors published many papers on this topic [41, 44-46]. The use of MFs was first reported in the United States in the 1970s [23, 47]. Numerous review articles on the effects of MFs and applications have been presented, including those by Chibowski and Szczes [31], Luo and Nguyen [48], Zaidi, Sohaili [32], Ambashta and Sillanpaa [49], and Baker and Judd [19], who discussed the influence of MF on chemical reactions (radical intermediates), which affects the reaction rate, yield, and product distribution. These effects could be interpreted via the radical pair mechanism (spin chemistry). Zaidi, Sohaili [32] considering four factors:

1. Magnetization and exhibition of a MF [31, 50];
2. Magnetic gradient [41, 51];
3. Lorentz force [19, 32];
4. Magnetic memory [52-54].

The commonly measured parameters include the zeta potential of the precipitated or dispersed particles, coagulation, nucleation and precipitation rates of calcium carbonate and other sparingly soluble salts, electrical conductivity, time of exposure to the MF, pH changes, polymorphism of the crystals, viscosity, surface tension, and diffusivity. However, two mechanisms of MF action that are generally recognized will be discussed briefly:

- i) The MF field effect on the ions and molecules in the solution, the so-called “ion mechanism” [55];
- ii) The effects of the MF on the nuclei and particles already present in the solution, the so-called “surface mechanism” [55, 56].

Other hypotheses have stated that the external magnetic fields promote the forward radical reaction rather than backward reaction leading to increase the yield of the reaction [57-59]. This is due to the alteration in recombination reaction that exposed to the external magnetic fields [57-59]. The practice of using magnetic fields within the MEG and water system is an important addition to previous studies, especially in the field of oil and gas processing.

One of the most common methods used for the evaluation of chemical scale inhibitors (CSIs) and scale formation behavior is dynamic scale loop (DSL) testing, see Figure 1-4 [21, 60]. DSL tests generally use a capillary coil made from stainless steel, carbon steel, or Teflon. The test is often performed by varying the pH, flow rate, temperature, and pressure [60, 61]. CSIs are commonly used to inhibit or prevent scaling in aqueous systems, and the performance of CSIs is evaluated and ranked by using the DSL test method [60, 62]. Magnetic field treatment is a controversial method that is used to prevent scaling in water systems as well. However, investigation of the effect of magnetic fields as a scale inhibitor treatment has not been carried out using the systematic DSL test method. Although several mechanisms have been proposed to explain the effect of MFs on scale formation, these mechanisms have not been tested with DSL. Furthermore, the effects of the magnetic field on scale formation at high temperatures and pressures are still controversial and require further investigations. This study provides an overview of the new technology associated with scale formation and focuses on the DSL apparatus that has been modified to develop a new technique for scale reduction that uses MFs. Different types of magnetic field generators have been studied and combined with the DSL test method. Moreover, a systematic procedure has been reported for studying the effects of MFs on the formation of scale under different operational conditions using the dynamic method.



Figure 1-4 Dynamic scale loop unit from PSL systemtechnik/Germany

1.3 Objective

The aim of this study is to develop a non-chemical method (MF treatment) for controlling the formation and growth of CaCO_3 scale in MEG solutions and to find the relationship between the degree of scale formation and the external MF. Furthermore, the influence of non-sulfite scavenger products on oxygen scavenging performance was studied to determine the scavenging mechanism in magnetized and non-magnetized MEG solutions, as well as to propose optimized conditions for industrial processes to control scaling and corrosion issues without the use of sulfite oxygen scavengers. In addition, a mathematical correlation has been developed between the volume fraction of MEG and physical parameters that can be readily measured using portable refractive index, and electrical conductivity measurements devices that is an alternative method for determining the MEG concentration.

The approach of this study can be summarized as follows:

1. The determination of whether the pretreatment process can be minimized without negatively influencing the MEG regeneration process, i.e., because of the formation of scale on the heater bundle in the presence of low concentrations of divalent cations in the rich MEG stream.
2. The influence of the MF produced by a permanent diametric magnet on the formation of calcium carbonate scale within aqueous and MEG solutions in a DSL system was investigated.
3. Sealed jar test was conducted to investigate the formation of different crystals of CaCO_3 at different MEG concentrations and temperatures.
4. The effect of the external MF on the microscopic properties of molecules was investigated by monitoring the pH and EC of ionic solutions using different MEG concentrations by the dynamic scale loop technique.
5. The effect of the external MF on the performance of CSIs in inhibiting calcium carbonate scale formation using MEG solutions and different CSI concentrations was investigated by the DSL technique.
6. The effects of different ionic strengths, pH values, organic acid concentration, magnetic memory effect and different oxygen scavenger dosages on the performance of erythorbic acid oxygen scavenger in MEG solutions (85 wt. %) was investigated using the jar cell technique at room temperature.
7. The influence of fresh, thermally aged, and degraded MEG on the scavenging performance of erythorbic acid for the removal of oxygen molecules to below 20 ppb was investigated.

8. The effect of different ionic strengths (0 - 1 mol/L of NaCl) upon the volume fraction of MEG solutions ranging from 0% to 100% vol./vol. using refractive index and electrical conductivity was evaluated.
9. The derivation of correlations between the volume fraction of MEG, refractive index, and electrical conductivity was established.

1.4 Thesis Outline

This thesis contains twelve chapters. Aside from the introductory chapter, each chapter starts with a brief introduction outlining the contents and closes with conclusions to illustrate the major points. Figure 1-5 gives a layout of the thesis objectives and structure. It describes the outline of the thesis objectives and relates them to the chapters.

Chapter 1: Introduction

This chapter is an overview, presenting the objectives of the project and the background of the study. The contributions of previous researchers in this area and the present knowledge about the topic are described. The chapter ends with an outline of the thesis chapters.

Chapter 2: Literature Review

This chapter reviews the literature related to the inhibition of calcium carbonate scale formation in pipelines and on hot surfaces. It discusses the principal theories of non-chemical scaling inhibition methods and recent achievements in aqueous solutions.

Chapter 3: Developed DSL Techniques

This chapter describes the use of DSL methods to evaluate the performance of non-chemical treatments. The low operational cost and lack of other requirements (it is a stand-alone technique) using MF, specifically for use in the oil and gas field [19], is reported. As a result, the adoption of DSL to examine and classify magnetic device performance is possible but some changes should be made to this technique.

Chapter 4: Effect of Pre-treatment Process on Scale Formation in the Reboiler Section of Mono Ethylene Glycol Regeneration Plant

In this part of the study, the DSL method was utilized to investigate how various factors, such as the total dissolved solids and pH, influence the concentration of the divalent ions in the rich MEG feed solution. This information is necessary to guarantee safe operation.

Chapter 5: Influence of Magnetic Fields on Calcium Carbonate Scaling in Aqueous Solutions at 150°C and 1 Bar

In this chapter, the use of the DSL technique in the presence of a MF (neodymium magnet N45SH) is evaluated and its impact on scale formation is reported. DSL technology has been

established as a novel method for evaluating chemical scaling inhibition inside capillary tubes but has yet to be applied in determining the effects of MF strength and magnetic direction (diametrically magnetized) upon scale formation.

Chapter 6: The Influence of Magnetic Fields on Calcium Carbonate Scale Formation within Mono Ethylene Glycol Solutions under Regeneration Conditions

This chapter evaluates the inhibitory performance of MFs on CaCO₃ growth at different MEG concentrations (50 and 80 vol. %). Additionally, the EC and pressure variation were monitored and recorded continuously to evaluate the scale formation performance following MF exposure. Jar tests were also conducted without magnetic treatment to observe the CaCO₃ scale morphology under static conditions.

Chapter 7: Evaluation of Thermodynamic Physical Properties of Aqueous Glycolic Solution under External Magnetic Fields

The objective of this chapter was to determine which ions are attracted to external MFs by measuring the physical characteristics (i.e., EC and pH) of synthetic brine–MEG solutions. The variation in the EC and pH was monitored versus time to evaluate the effect of MF exposure.

Chapter 8: Evaluation of Chemical Scale Inhibitor Performance under External Magnetic Fields using a Dynamic Scale Loop

In this chapter, the effect of an external MF on CSI performance in the prevention of CaCO₃ formation using 80 vol. % MEG solutions was evaluated. The DSL technique was used to evaluate the scale-inhibiting performance at 130 °C and 1.0 bar.

Chapter 9: Performance of Erythorbic Acid as an Oxygen Scavenger in Thermally Aged Lean MEG

The viability of using erythorbic acid in MEG systems is evaluated because of its strong oxygen removal performance, as observed in food industries. The aim of this chapter is to further study the performance of erythorbic acid (D-isoascorbic acid) to scavenge oxygen in lean MEG.

Chapter 10: The Performance of Erythorbic Acid Oxygen Scavenger within Salty Fresh and Degraded Mono Ethylene Glycol under Magnetic Memory Effect

The aim of this chapter is to study the performance of erythorbic acid (D-isoascorbic acid) under magnetized conditions to scavenge oxygen in fresh and degraded lean MEG. The Jar cell technique was used to evaluate the scavenging performance at salts-free and high salt content lean MEG solutions at 1000 ppb and saturation oxygen concentration.

Chapter 11: Measurement of the Mono Ethylene Glycol Volume Fraction at Varying Ionic Strengths and Temperatures

In this chapter, the generation of empirical relationships capable of predicting the correct volume fraction of MEG (F_{vc}) from different physical parameters that can be quickly measured in the field, such as the refractive index (n_D) and either the electrical conductivity (EC) or total dissolved salt (TDS), is reported.

Chapter 11: CONCLUSION

References

Nomenclature

Appendices

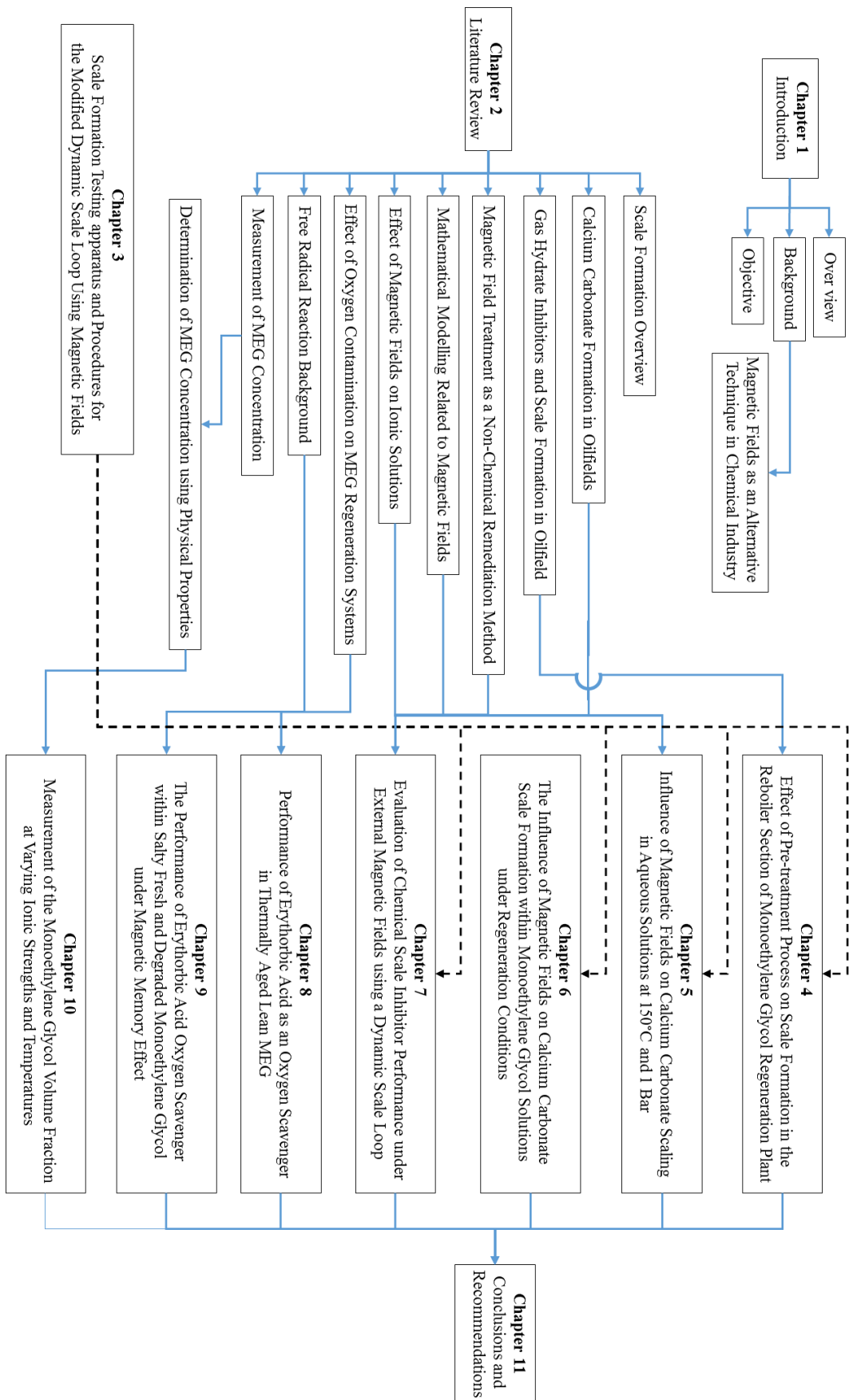


Figure 1-5 Layout of thesis objectives and structure

Chapter 2 Literature Review

This chapter presents the essential problems observed after using mono ethylene glycol (MEG) as a gas hydrate inhibitor during the transportation of oil and natural gas from the wellhead to onshore facilities and during the MEG regeneration process. These issues can be classified as scale formation, contamination with dissolved oxygen, gas hydrate formation, and corrosion. Simultaneously controlling these issues is challenging because they are linked to each other. In addition, the use of one technique to treat a problem may exacerbate or cause other problems in other aspects of the industrial process.

For instance, the change in the thermodynamic conditions in the oil and natural gas production wellheads contributes to the precipitation of dissolved mineral ions in the oil, gas, and brine mixture [63, 64], and the chemical composition of the water formation. H₂S and CO₂ partial pressure, oxygen contamination level, and temperature are considered key parameters that affect scale formation, and corrosion issues [65]. Some of the common scale deposits in downhole and topside processing facilities include calcium carbonate, barium sulfate, strontium sulfate, calcium sulfate dihydrate, lead sulfide, and magnesium carbonate [20]. The mineral scale can precipitate at any section that is in contact with the liquid phase, leading to flow assurance problems, such as flow restriction and complete pipeline blockage, over the well lifetime [66, 67]. In addition, the onshore MEG regeneration process could introduce oxygen molecules that promote the corrosion and pitting phenomena on the internal surface of carbon steel pipelines and equipment.

Negative consequences related to oil and natural gas production often require immediate mechanical maintenance. However, because of the high risk of mechanical damage and other difficulties, chemical scale inhibitors (CSIs), corrosion inhibitors (CIs), and oxygen scavengers (OS) are commonly used to control scale formation and corrosion inside the equipment [20, 68, 69]. Using CSIs, CIs, and OS strategies are a common practice in subsea fields [68]. They are often used at specific concentrations to slow or prevent the scale formation and corrosion at wellheads and flow pipelines [69]. Since these operational problems have been growing, CSIs, CIs, and OS performance have been successfully evaluated in the laboratory by using a dynamic scale loop (DSL) or jar test methods by following the techniques of leading researcher communities in oil and natural gas industry [70]. The best performance has been established by determining the minimum inhibitory concentration threshold (MIC) that minimizes the scale nucleation/growth and corrosion rate [60, 71]. Therefore, the MIC concept is a crucial factor in subsea oil and natural gas fields to ensure hydrocarbon production [63].

There are many challenges associated with the oil and natural gas production that demand new and innovative techniques to control scale formation. In particular, challenges include the high

temperature fluctuations, pumping pressures, and shear rates [20, 63]. Furthermore, CSIs, CIs, and OS agents must be stable, compatible, and perform well under subsea well conditions [68, 69]. In addition, several aspects should be considered before using CSIs, CIs, and OS agents in the subsea environment including toxicity, cost, influence on the aqueous system and environment and degradation rates [20]. These aspects could limit the utilization of these chemicals agents in industry. As a result, laboratory investigations are required to evaluate the performance of these agents in the subsea environment [72, 73]. This chapter reviews the literature in three research areas. The first area covers proposed non-chemical treatments (magnetic fields applications) that replicates the positive effects on scale formation reported for aqueous solutions. This is important because the review of traditional methods has, in the past, led to new applications in the oil and natural gas industry. The second area covers environmentally friendly alternative materials and conditions that rely on non-sulfite products through magnetic field treatment to remove oxygen dissolved in the fluid in the transportation pipelines. This is important because it prevents sulfate scale formation and corrosion, as well as associated health, environment, and safety risks related to the handling and transporting of large volumes of highly concentrated and harmful chemicals. The last area covers proposed methods that measure the concentrations of high ionic strength MEG solutions; these methods will contribute to replacing other traditional methods of analysis, which sometimes require the shipment of samples to external laboratories, operation at specific conditions and concentrations, or need continuous calibration, limiting their use.

2.1 Scale Formation Overview

The agglomeration of mineral ions is a major problem for cooling towers, power plants, reboilers, desalination facilities, and transportation pipelines. The insoluble materials are generally CaCO_3 , CaSO_4 , BaSO_4 , or FeCO_3 with impurities such as hydroxides, organic acids, and oxides. Scale formation restricts the flow of fluid, cause flow assurance problems, and fouls the surfaces of boilers and heat exchangers, which then requires chemical or mechanical maintenance and cleaning. These practices have environmental impacts, are expensive, and can cause sudden shutdowns. Furthermore, chemical treatments affect the chemical properties of the treated fluids.

Several factors affect the formation of deposits, but only some of these factors have been studied intensively. Briefly, these factors are the temperature and pressure, effects of other compounds and impurities, effect of pH and $\text{CO}_2/\text{H}_2\text{S}$ partial pressure, reaction kinetics, supersaturation, and mixing of incompatible solutions. To control scale formation, we must understand how it forms, its structure, and how it is bound together. This study focuses on CaCO_3 because it is a common scale forming factor in many industrial processes (not just oil and natural gas recovery) and is the most difficult to remove.

2.1.1 Polar and Non-Polar Solutions

Solutions can be classified as polar or non-polar [74, 75]. Polar solutions are composed of molecules with a dipole; that is, one end has a more negative charge and the other has a more positive charge [18, 32]. Otherwise, the solutions are called non-polar solutions [31, 76]. For instance, in water solutions, the hydrogen atoms have partially positive charges and the oxygen atoms have partially negative charges. This difference in charge is caused by the difference in electronegativity between these atoms, resulting in a polar solution [76, 77]. The polar nature of the water molecule, as a result of the covalent bonds between oxygen and hydrogen atoms, results in the formation of hydrogen bonds (H-bonds) with surrounding H₂O molecules.

2.1.1.1 Structure of Mono Ethylene Glycol and its Solutions

MEG, (CH₂OH)₂, is normally regarded as a non-electrolyte solvent [78]. It has an asymmetrical chemical structure as shown in Figure 2-1 [77, 79] and contains polar and non-polar bonds. Because of the different electronegativities of oxygen and hydrogen in the O-H bond, there is an internal dipole. However, the net dipole moment is zero because of its symmetrical chemical formula. These polar bonds make MEG miscible with water because “like dissolves like”, that is, polar compounds are miscible in other polar compounds [75, 80, 81]. Wu, Yang [75] reported that MEG has a boat-like structure rather than an asymmetric structure, which generates a dipole moment 2.75-Debye larger than that of ethanol. The boat-like minimum energy structure explains the lower miscibility of MEG in water compared to ethanol [75, 77].

Water dissolves many salts because it is polar [75]. When water molecules surround cations and anions they interact with the electric field and reorient with respect to the charge of ion [1]. This is due to the relative permittivity (dielectric constant) of the water solution, which is about 80 at room temperature [1]. This rearrangement reduces the force between the counterions [1]. MEG reduces the solubility of most salts in water, although to a lesser degree than other alcohols [82]. This is because of its low dielectric constant (MEG = 38), which is considerably lower than that of water [83, 84]. The low dielectric constant of MEG considerably reduces the degree of ion separation. The solubility of carbonate ions is, thus, affected by the addition of MEG solutions, which is troublesome because this affects the solubility and pH, as well as CO₂ gas dissociation [1]. Thus, the addition of MEG to water solutions may increase the precipitation of mineral ions compared to that from an aqueous solution.

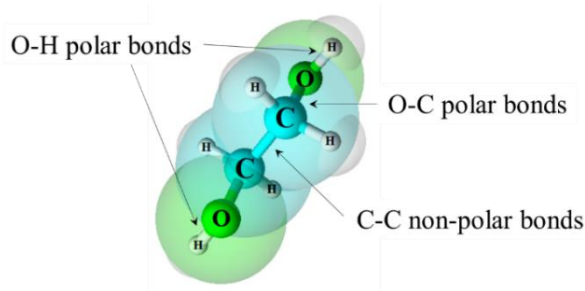


Figure 2-1 Three-dimensional view of MEG

2.1.2 Calcium Ions in Aqueous Solutions

When a solute dissolves in a solvent, the solute is surrounded by the solvent molecules with the polarized parts of the molecules oriented with respect to the charge of the solute; that is, the structure of the solvent later is affected by the surface charge of the solute, as shown in Figure 2-2 [85, 86]. A fully solvated solute is surrounded by solvent molecules, increasing the size of the solute particle because of the partially charged double layer [87]. This double layer comprises partially negative and positive layers. The solvation of a solute by water molecules is called hydration. Hydration defines the interaction of water molecules with dissolved cations and anions. H_2O molecules surround cations (calcium ions) with their positive hydrogen atoms ends pointing outward and negative oxygen atom end pointing inward.

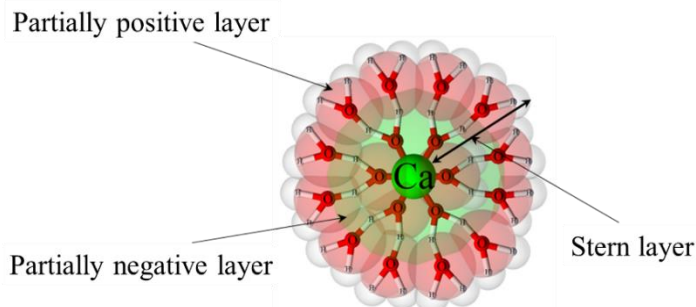


Figure 2-2 Simple demonstration of the stern layer around dissolved Ca^{2+} ions in aqueous solution

Ions interact strongly with water molecules, and the nature and strength of this interaction changes the characteristics of the ion, including the dissolution rate, activity, and reactivity with counterions [88]. Furthermore, this interaction affects the characteristics of the aqueous solution such as the refractive index, viscosity, evaporation rate, and density. In the process of hydration, a concentric shell of water molecules surrounds ions [76, 89]. Hydration is the process of reorganizing water and ion molecules into hydration systems; this affects the reactivity of Ca^{2+} ions in aqueous solutions. Hydration involves bond formation, hydrogen bonding, ion-dipole bonding, and van der Waals forces [77].

The formed double layer is also called the Stern layer [77, 90]. The number of water molecules in the Stern layer varies according to the size and charge density of the ion and can differ for the same ion in different conditions [91, 92]. For example, between six and nine water molecules can interact with a fully hydrated Ca^{2+} ion in aqueous solution [93, 94]. Ions and the surrounding water molecules form ion–dipole bonds in the hydration layer.

Several reports have claimed that the hydration of calcium ions in aqueous solutions show various coordination modes [37, 87, 94]. This is due to the slight changes in the binding energies between water molecules and ions as more water molecules are attracted to the ion [36, 95] (see Figure 2-3). Furthermore, when the number of water molecules in the Stern layer reaches eight, the competition between binding energies of the ion–water system and H-bonding energies within the coordination sphere of the calcium ion changes slightly. Using molecular dynamics simulations, Di Tommaso, Ruiz-Agudo [96] compared the interactions in water with Ca^{2+} only and aqueous solutions containing other electrolyte ions and calcium ions. They noticed a drastic reduction in the frequency of water exchange after the addition of an electrolyte, specifically in the first hydration shell around calcium ion. Other studies have claimed that many Stern layers can form, possibly involving many partial positive and negative layers [37, 38]. This is due to the wide hydration space around the calcium ions [35, 36]. However, the stable coordination environment of hydrated calcium ions is six-fold coordination, which prevents symmetry breaking, specifically when more water molecules are added. Thus, six-fold coordination creates an octahedral structure that is the most stable form in aqueous solutions. This conclusion has been achieved experimentally and computationally in several publications [31, 33, 36-38, 97].

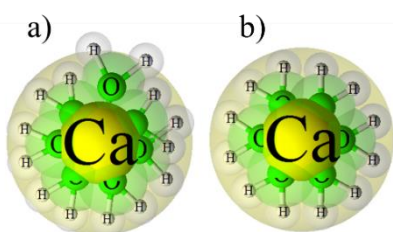


Figure 2-3 Hydration structure of Ca^{2+} ions: (a) Seven hydrating water molecules and (b) Six hydrating water molecules

2.1.3 Carbonate Ion Hydration in Aqueous Solutions

Carbonate ions have the chemical formula CO_3^{2-} , meaning that one carbonate ion contains three oxygen atoms and one carbon atom in a trigonal planar arrangement [98, 99]. This structure is inconsistent with the recognized symmetry of Ca^{2+} ions. The Lewis structure of CO_3^{2-} contains two types of bonds: a short double-bond and two single-bonds [77]. In addition, the free carbonate ion has three-fold symmetry, and the short and long bonds appear in the Lewis structure but not the experimental structure. The electron cloud tends to be distributed closer to the electronegative

atoms (oxygen) [90, 100]. Thus, the structure of the carbonate ion is perturbed in the presence of different cations. The difference in electronegativity is a result of the properties of carbon and oxygen rather than the geometry of the carbonate anion, where the carbonate ion has a total formal charge of CO_3^{2-} [80, 101]. The hydration of carbonate ions is more complex than that of Ca^{2+} ions. Computational simulations have indicated that, for long timescales, carbonate ions in aqueous solution attract six molecules of water, whereas, at short timescales, carbonate ions interact with one water molecule via a H-bond. The hydration of CO_3^{2-} ions is illustrated in Figure 2-4.

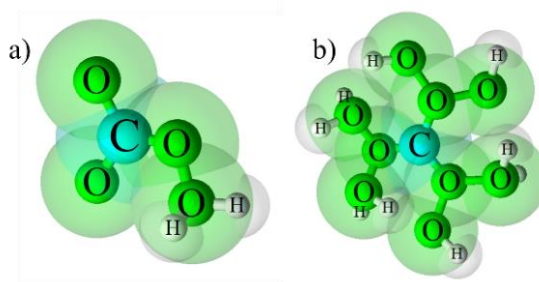


Figure 2-4 Hydration of carbonate ions: (a) One hydrating water molecule and (b) Six hydrating water molecules

In aqueous solutions, carbonate ions are formed by the dissociation of carbonic acid in highly alkaline conditions, whereas in weakly alkaline conditions the conjugate HCO_3^- ions are prevalent. In acidic conditions, aqueous CO_2 gas predominates, which is in a dynamic equilibrium with H_2CO_3 .

2.1.4 Calcium Carbonate Monomer Formation

The activity of calcium ions relies on the stability of the hydration shell thickness in aqueous solutions, becoming more stable when counterions (anions) are present. However, this stabilization can fluctuate because of the affinity for other alkali halides in solutions, which compete for placement in the second hydration shell of the Ca^{2+} ions [102]. This competition often affects the attraction between calcium ions and anions at the mineral–water interface [102]. In high ionic strength solutions, where the electrolyte solutions are very concentrated, there is no bulk water, and the majority of H_2O molecules are combined with one or more ions [103-105]. This has been investigated by different simulation approaches [35-38], and, in these concentrated solutions, no ion-specific changes to the kinetics of water exchange in the hydration shell of Ca^{2+} were observed. At the mineral ion–water interface, the ionic strength is most likely to be higher than in the bulk solution; thus, concentrated solutions could affect the hydration shell of Ca^{2+} and CO_3^{2-} ions to a significant extent, which plays a primary role in the first steps of the homogeneous nucleation of CaCO_3 [102, 103]. Calcium and carbonate ions can bind in a bidentate and mono-dentate form [77]. Bidentate bonding means two ionic bonds are formed between two oxygen atoms of CO_3 and the calcium ion, whereas mono-dentate bonding means one ionic bond links a

calcium ion with one oxygen atom (see Figure 2-5). The bidentate bond plays an essential role in generating the different polymorphs of CaCO_3 [77].

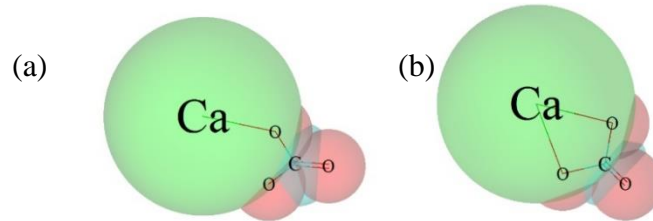


Figure 2-5 Monodentate and bidentate bonding in calcium carbonate [77]

Experimental studies have shown that the concentration of calcium ions within brine solutions thermodynamically influence the morphology and particle size of the calcium carbonate scale [9, 106-108]. For instance, below a calcium ion concentration of 6 mM, the formation of a multinucleated calcite morphology is dominant; in contrast to that, at a calcium ion concentration of 80 mM, perfect calcite particles form. However, at higher calcium ion concentrations (approximately 1 M), the formation of vaterite particles, in addition to rhombohedral calcite particles, is more likely [20, 77]. Vaterite particles can also be formed at low calcium ion concentrations and high CO_2 partial pressures [20, 77].

2.1.4.1 Calcium Carbonate Scale Formation

Calcium carbonate is a common mineral scale found in a wide range of industries including water treatment [20, 109], paper milling [110], cooling water systems [111], natural gas transportation pipelines, and MEG regeneration systems following the breakthrough of formation water [65, 83]. The formation of CaCO_3 occurs at the surface of heat transfer equipment operating at high temperatures, such as heat exchangers and reboilers, leading to reduced heat transfer efficiency [112] and potential blockages or the restriction of flow along the inner surfaces of the pipelines and tubing [16, 20]. Several studies have been conducted to investigate the scale formation behavior of CaCO_3 by examining various characteristics including crystalline phase, size distribution, and morphology [8, 106, 113]. The saturation index (SI) of calcium and carbonate ions has been the subject of extensive prior studies and represents a key factor in determining the tendency of CaCO_3 formation [109, 114].

Muryanto, Bayuseno [8] have reported that CaCO_3 crystals form as three anhydrous polymorphs: calcite, aragonite, and vaterite. Calcite is the most stable form of crystalline CaCO_3 , whereas aragonite and vaterite exhibit poor thermodynamic stability with the potential to convert to calcite after the readjustment of certain conditions, including solution pH, temperature, supersaturation, and the presence of additives [8, 115]. For instance, Hu, Wolthers [115] have reported that the anhydrous polymorph (vaterite) is more likely to form at pH 9.0 compared to the hydrated

polymorphs of CaCO_3 such as monohydrate and hexahydrate (ikaite), which form at high pH, approximately 13.4 and greater at low temperatures [115]. However, in the presence of phosphate additives, the ikaite polymorph is more likely to precipitate at a pH of 9.0 [115].

In the last decade, the morphology of CaCO_3 following the application of a magnetic field (MF) has been extensively investigated [19, 29, 116]. Silva, Neto [29] summarized the most significant results including the possibility of obtaining a particle morphology that has a lower tendency for attachment to the walls of water-conveying pipes or promoting the homogeneous precipitation of CaCO_3 . However, most of these studies have focused on aqueous solutions as part of attempts to modify scale formation in water systems. As such, little to no investigation has been conducted on the antiscaling potential of MFs for use in MEG systems containing mineral ions, an application relevant to the hydrocarbon and natural gas industries.

2.1.5 Morphology and Phases of Calcium Carbonate

2.1.5.1 Influence of pH and Temperature on Calcium Carbonate Morphology

In aqueous systems, inorganic scale formation is usually affected by pH changes to a greater degree than temperature because of the thermodynamic driving force for the precipitation of mineral ions with carbonic acid [117]. However, the presence of carbonate species in aqueous solutions is an indicator of the degree of calcium carbonate formation [118]. In Figure 2-6, the concentration of carbonate species is shown as a function of the pH gradient. As the pH of the solution increases, the concentration of carbonate species begins to increase as well. Although the solubility of calcium carbonate varies with pH, the solubility product of calcium carbonate is a function of temperature and pressure more than the pH [118, 119].

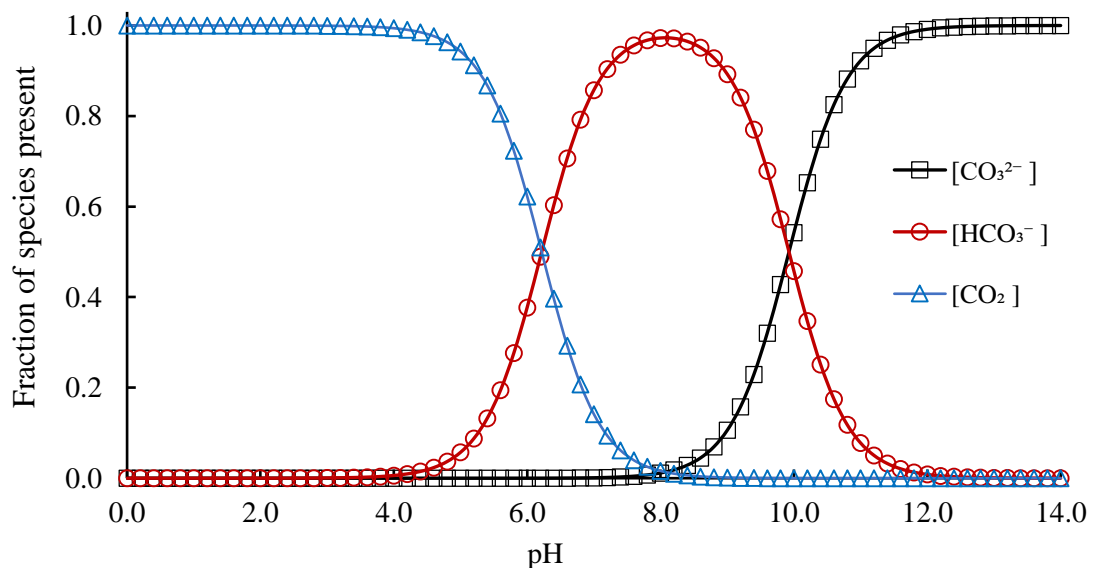


Figure 2-6 Relationship between the pH of solution and dissociation of carbonic acid in an aqueous solution [99]

In aqueous solutions, the solubility of mineral ions increases with increasing temperature, except for calcium carbonate (see Figure 2-7) [117, 120]. In contrast, the solubilities of calcium carbonate salts decrease as the temperature increases, except for the hexahydrate calcium carbonate (HCC) polymorph, which serves as an exception to the rules relating to shared physical properties. This behavior is important in the oil and natural gas industries, specifically in the pretreatment step of gas hydrate inhibitor regeneration plants, which are operated at 80°C.

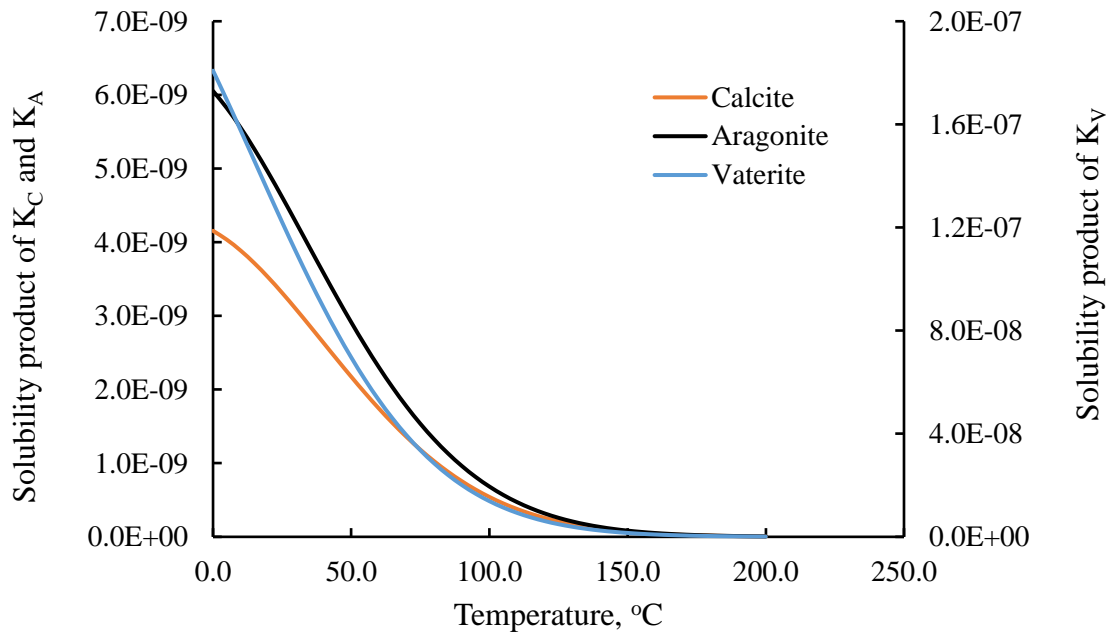


Figure 2-7 Solubility product of calcite, aragonite, and vaterite with temperature [120]

2.1.5.2 Polymorphs of Calcium Carbonate in Aqueous Solutions

Calcium carbonate crystallizes in different forms, polymorphs. In addition, polymorphs of calcium carbonate can crystallize as hydrous and anhydrous crystals. Hydrous polymorphs include monohydrate calcium carbonate (MCC), amorphous calcium carbonates (ACC), and hexahydrate calcium carbonate (HCC), and anhydrous polymorphs include calcite, vaterite, and aragonite. The anhydrous polymorphs can be interconverted by changing the reaction kinetics and temperature. The chemical properties of the anhydrous and hydrous polymorphs are the same, but the physical properties of each polymorph are different, specifically the shape and solubility. Aragonite and vaterite are thermodynamically unstable forms of the anhydrous polymorph, and calcite is the most thermodynamically stable form in aqueous solutions. The temperature of the mineral ion solution controls the formation of anhydrous polymorphs. For instance, high-temperature conditions tend to result in the formation of the aragonite structure, whereas low-temperature conditions tend to produce the calcite structure. The morphologies of the three hydrated crystals are completely different. Calcite crystals have a cubic-like shape, whereas

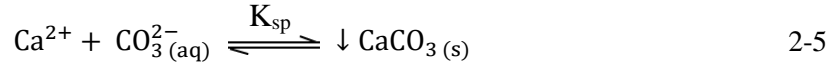
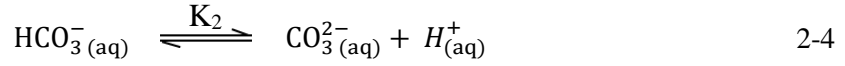
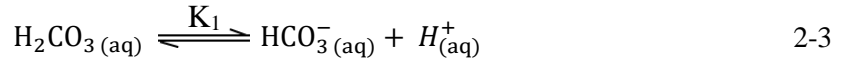
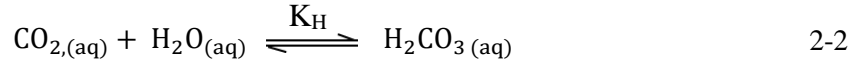
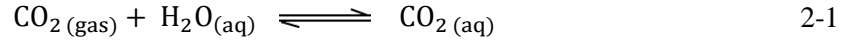
aragonite crystals have a needle-like shape. In contrast, vaterite crystals often have a hexagonal shape.

2.1.5.3 Polymorphs of Calcium Carbonate in Mono Ethylene Glycol Solutions

The study of the polymorphs of calcium carbonate within MEG and water co-solvents has attracted limited attention. However, the general behavior of mineral ions within co-solvents has been extensively studied and understood [106-108]. Several studies have examined the influence of MEG solutions on the ionic strength, ion activity, solubility, and, thus, the saturation index of different mineral ions in MEG–water mixtures with MEG contents between 0 and 90 wt. % at temperatures between 25 and 80°C [106, 107, 119, 121, 122]. These studies have concluded that the presence of MEG influences the morphology of calcium carbonate crystals and the transformation rates. Furthermore, high MEG ratios tend to favor the formation of vaterite particles [106], whereas the formation of aragonite is more likely at a higher temperature at the same MEG ratio. Moreover, the scale particles formed within the MEG–water system are smaller than those formed in pure water. Flaten, Seiersten [106] reported that the solubility of calcium carbonate decreases with increasing MEG ratio, leading to an increase in the supersaturation ratio. Evans [123] has reported that the percentage of metastable polymorphs is correlated with the ionic strength. This observation indicates that particles of metastable polymorphs of calcium carbonate are more likely to form within MEG and water systems because of the effect of the MEG ratio on the thermodynamic forces driving scale formation. Meanwhile, increasing the temperature affects the growth rate of calcium carbonate polymorphs. For instance, at 50°C in 95 wt. % MEG, aragonite transforms to vaterite. In contrast, aragonite crystals dominate at higher temperatures in solvent mixtures [106]. These results indicate that the use of MEG and water solutions affects the kinetics of scale formation under high-temperature conditions.

2.2 Calcium Carbonate Formation in Oilfields

The formation of scaling products affects the operation of natural gas transportation and production systems because of flow restriction, blockage, and fouling [1, 25]. Chemical analysis and laboratory studies have revealed that calcium carbonate, barium sulfate, and strontium sulfate are the most common inorganic compounds present in oil and gas facilities [124, 125], and calcium carbonate is considered as one of the most abundant inorganic deposits in deep saline wells [122, 126-128]. Because calcium carbonate has a low solubility in aqueous solutions, it is deposited in large quantities in pipelines and industrial units [83, 129, 130]. Furthermore, the solubility of calcium carbonate is inversely proportional to the temperature; thus, changes in temperature or pH are important factors having a direct effect on the overall equilibrium of calcium carbonate precipitation [8, 115]. The general equilibrium reactions, including CaCO_3 formation within the carbonate system [122], are summarized in reactions 2-1 to 2-5.



Here, $\text{CO}_{2(\text{gas})}$ is CO_2 in the gas phase, and $\text{CO}_{2(\text{aq})}$ is CO_2 dissolved in the aqueous phase. K_H , K_1 , K_2 and are the Henry's law, first and second dissociation constants, and K_{sp} is the equilibrium constant [122], respectively. The carbonate equilibrium model presents a challenge in the transportation of natural gas and condensate from offshore facilities.

Long subsea transportation pipelines must have a low risk of mineral scaling, as well as some hydrate formation prevention method (see Figure 2-8). During the production of natural gas in the deep water environment, there is a risk of gas hydrate formation in the pipelines [4, 131]. Gas hydrates are crystalline, ice-like solids made up of host molecules surrounded by water molecules [131]. As a result, gas hydrate inhibitors are used to ensure the flow of natural gas produced [131]. Mono ethylene glycol is among the most widely used gas hydrate inhibitor because it can be regenerated or reclaimed, thus minimizing operational costs [65, 132]. However, this gas hydrate inhibitor directly lowers the saturation concentrations of inorganic salts and, thus, increases the risk of scale formation [118, 121, 133]. The saturation index of calcium carbonate in the water/MEG system was determined by using the relationship between ion activity (calcium and carbonate) and the equilibrium constant, which can describe the influence of MEG on the activity coefficient of ions, as indicated in Equation 2-6 [122].

$$SI_{\text{calcite}} = \log_{10} \left(\frac{[\text{Ca}^{2+}] \cdot \gamma_{\text{Ca}^{2+}}^{\text{S}} \cdot \gamma_{\text{Ca}^{2+}}^{\text{N}} \cdot [\text{CO}_3^{2-}] \cdot \gamma_{\text{CO}_3^{2-}}^{\text{S}} \cdot \gamma_{\text{CO}_3^{2-}}^{\text{N}}}{K_{\text{sp}}} \right) \quad 2-6$$

Here, $\gamma_{\text{Ca}^{2+}}^{\text{N}}$ and $\gamma_{\text{CO}_3^{2-}}^{\text{N}}$ represent the effect of MEG on the activity coefficients, and $\gamma_{\text{Ca}^{2+}}^{\text{S}}$ and $\gamma_{\text{CO}_3^{2-}}^{\text{S}}$ represent the effect of salt on the activity coefficients.

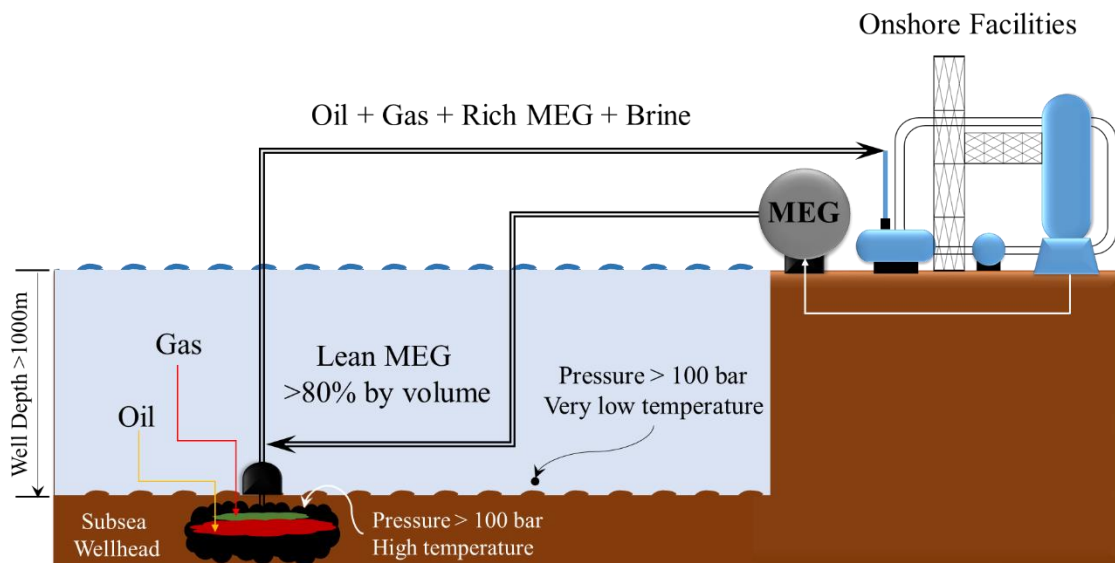


Figure 2-8 MEG loop injection in the pipelines

2.2.1 Mono Ethylene Glycol Regeneration during Oil and Gas Production

MEG regeneration involves a variety of industrial processes to ensure the reuse of the regenerated MEG: divalent ion precipitation (pretreatment), MEG re-concentration (distillation column), and reclamation units for monovalent ion removal [2, 64, 67]. The use of these units depends on the specifications of the MEG returning from the top of the well nozzle. Some wells have low salinity because of a low water flow rate, limiting the use of the pretreatment unit and the MEG regeneration unit [4]. In some other wells, however, the ion content of the water is especially high, requiring separation units for mono and divalent ions removal to ensure the purity of the recycled MEG [4]. Another factor to consider during MEG regeneration is the use of corrosion inhibitors, such as methyl diethanolamine (MDEA), also potassium hydroxide, and sodium hydroxide, which increase the pH, posing a long-term risk inside transportation pipelines in the case of divalent mineral ions [2, 4, 83, 134].

Often, MEG concentration reaching the MEG plant is less than 50 wt.% of that of the rich MEG solution; however, the lowest acceptable concentration for return to the top of the well is about 80 wt.% of the lean MEG concentration [4, 83]. Moreover, the presence of CO₂ during oil production causes the formation of carbonic acid, thus reducing the acidity (pH) of glycol solutions [119, 134, 135]. However, in the case of highly concentrated divalent ions in the rich MEG stream, it is necessary to use the pretreatment unit to accelerate the separation of these ions from the chemical solution. This process requires large amounts of alkaline base, which is used to increase the pH to higher than 8.0 because a low pH inhibits sedimentation [118, 120]. The temperature is also increased to 80°C to accelerate the reaction of divalent cations with anions. The high pH in the regenerated lean MEG contributes to the formation of sediments within the hydrocarbon transport lines because of the high concentration of divalent ions; therefore, the use

of chemical scale inhibitors is continuously required. These compounds are often acidic, meaning that the rich MEG stream pumped into the MEG regeneration plant will be acidic and will require a greater amount of alkaline base to induce precipitation in the pretreatment unit; this helps to ensure the flow of hydrocarbon products and to overcome the formation of gas hydrates and scale formation.

2.2.1.1 Corrosion Prevention in Oil and Gas Production

FeCO₃ mineral scale reduces corrosion to surfaces made of carbon steel in offshore and onshore equipment, which forms a protective lining inside the pipes by creating a barrier against the moving of the species involved in the corrosion reactions [134]. Unfortunately, this is not sufficient to prevent long-term corrosion in the acidic environment. Because most corrosion inhibitors are alkaline pH-based, operators have used different chemicals to overcome this problem. One of the most important compounds used is a film forming corrosion inhibitor (FFCI), which forms a thin lining on the internal surface of the pipes and equipment in direct contact with acidic solution, protecting them from corrosion and pitting. Organophosphates are the main FFCI components used in the natural gas and oil industry. However, the specific chemical formulation is typically confidential.

2.2.1.2 Possible other Problems during MEG Regeneration

During the MEG regeneration process, to boil-off excess water, the bulk temperature in the reboiler may be as high as 130–150°C; this heating is necessary to achieve the desired lean MEG concentration (>75%) [136, 137]. Meanwhile, the reboiler heater element skin (wall) temperatures may be even higher because the heating solution may be supplied to the unit at 177°C [138]. If divalent cations are present within the rich MEG feed, these high temperatures may cause the precipitation of solid particles, either causing fouling of the hot heat exchanger surfaces or suspended solids in the bulk liquid [138, 139]. This reduces heat transfer efficiency and may have adverse effects on the downstream system (e.g., blockage of the lean MEG filters). However, the extent of this impact is, at present, not well understood. As a conservative approach, some plants are targeting a low residual cation concentration (e.g., <1 ppm) in the feed to the reboiler. This will, in some cases, require somewhat acceptable quantities of a base (e.g., KOH or NaOH) to be injected into the MEG pretreatment system, resulting in high operating costs and associated health, environmental, and safety risks related to handling and transportation of large volumes of highly concentrated and harmful chemicals.

Several studies have indicated that the concentration of MEG has an effect on the deposition of inorganic salts [5, 121]. For example, with increasing MEG concentration, an increase in the calcium carbonate crystal formation induction time is observed [140]. This is attributed to the increase in the viscosity with increasing glycol concentration, which inhibits crystal formation

[140]. Another study conducted under gaseous treatment conditions has found that calcium carbonate crystals show a significant reduction in growth rates in experiments with more than 50 vol. % MEG (MEG rich) [132, 141]. The use of scale inhibitors is a common method used to reduce the extent of crystallization during the production of oil and natural gas [68, 128, 142]. Several studies have reported that MEG has an effect on the MIC performance [143-145], i.e., MEG reduces the performance of the scale inhibitors. These results led to evaluation of various chemical scale inhibitors or other techniques to reduce scale formation issue in the oil and gas industry.

2.2.2 Addition of Chemical Scale Inhibitors

Several investigations have been performed by researchers to evaluate suitable techniques that may reduce the scaling issues faced in the oil and gas industry [20, 61, 62, 69]. Typically, chemical scale inhibitors (CSIs) are effective methods to control inorganic deposition problems [9, 19, 128, 146]. However, the addition of CSIs has been shown to impact system chemistry and may also be expensive [19]. Furthermore, the applicability and the performance of CSIs is dependent on several parameters such as their toxicity, solubility, thermal stability, hydrolytic stability, degradation level, and minimum inhibitor concentration (MIC) [9, 62, 71]. As mentioned, the MIC is the minimum effective concentration of CSI required to prevent scaling in different industrial processes [9, 20, 62]. Despite some efforts to rank different scale inhibitors by evaluating their ability to inhibit scale formation under various conditions, a final comparison of their performance is difficult [20]. However, there are two main laboratory methods used for evaluation of the scale inhibitor performance. These have been defined by the National Association of Corrosion Engineers (NACE) standard testing method: DSL technique and the jar test technique (static) [60, 62, 147].

2.2.2.1 Laboratory Methods to Evaluate Chemical Scale Inhibitors

The differential DSL technique utilizes tube blocking as an industry standard method to determine the minimum chemical scale inhibitor concentration under dynamic conditions [9, 21, 60, 148]. The DSL device is used to examine the scale formation behavior under wellhead and transport pipeline conditions [9, 148]. The operating conditions of the DSL test such as temperature, pressure, flow rate, pH, anion dose, capillary coil material, and coil size can be adjusted throughout the experiment [9, 72, 148]. The differential pressure build-up can be monitored and recorded to determine the spike-time when full blockage occurs [60, 72]. Different operating conditions and initial mineral ions concentration result in different spike-times [60, 72]. The DSL method often gives rise to a different performance rankings compared to those obtained using the static jar test [62, 149, 150]. These differences in ranking are often attributed to the discrepancies in the response time of each technique [61, 148]. For instance, the efficiencies of scale inhibitors

evaluated using the DSL technique are determined by comparing the time required to impede flow through a thin steel tube in the presence of scale inhibitors to the time needed to obstruct the same narrow steel tube without scale inhibitors [151, 152]. Conversely, the efficiency of scale inhibitors in the jar technique is determined by comparing the time required to minimize the formation of scale in the presence of a scale inhibitor compared to that with the blank test [149, 151, 152]. To use these techniques to measure the effects of non-chemical treatment, the apparatus must be modified to determine the efficiency of MF methods in preventing the formation of calcium carbonate scales.

2.2.2.2 Limits of the Dynamic Scale Loop Technique

Previously, Bazin, Kohler [62] determined that the DSL test is reliable for evaluating antinucleation inhibitors, but crystallization inhibitors are often tested using the static method [150, 153, 154]. As a result, both techniques have limits concerning the assessment of the performance of different scale inhibitors [155]. Bazin, Kohler [62] also pointed out that the residence time in the static test is longer than that in the DSL test, which is advantageous for the latter technique [71]. Recent reports have indicated that the DSL technique could provide researchers with sufficient data to understand the kinetics and thermodynamic effects on mineral solubility under moderate conditions with varying flow rates, pH, temperatures, pressures, and total dissolved solids [61, 73, 148, 156].

2.2.3 Mechanisms of Chemical Scale Inhibitor Treatment

Injecting chemical inhibitors to treat scales formation in water systems is one of the most effective and common methods used in many industries [9, 128, 157]. These materials have high solubility in water solutions and therefore the possibility of a direct change in the environment of the scale formation [20]. The process of preventing or delaying the occurrence of scale formation is based on three main mechanisms. The first is known as the mechanism of the threshold effect [116, 155], the second is called the dispersion mechanism, while the third mechanism describes the process of distortion in the formed crystal [61]. Some other scale inhibitors may not follow the above mechanisms and may follow multiple patterns that could be occurring simultaneously. Phosphate compounds are often used as anti-scalents while aminocarboxylates are used as chelating agents [25, 115, 157, 158]. The chelating materials are characterized by their ability to change the function of calcium ions in the aqueous solution and thus mitigate of the process of scale formation [20, 157]. However, the use of these materials is directly proportional to the concentration of calcium ions in those solutions, which requires injection of large amounts of chelating agents to prevent the deposition of calcium ions. The phosphate compounds are limited to somewhat low concentrations, often up to 50 ppm. The least effective concentration of chemical inhibitors is an important factor in assessing their performance in practice. This factor

is usually called the minimum inhibitor concentration, which ranges in the standard temperature and pressure conditions between 0.5 and 20 ppm.

All scale inhibitors mechanisms are based on one concept: the absorption of those agents on the surface of the developing charged crystals. The particles of the scale inhibitor usually have negative charges to attack the surface of the mineral ions causing distortion in the formation of crystals. Furthermore, this contributes to the formation of small crystalline clusters, unstable and dissolved in their aqueous solutions. The forced distortion of the structure of the crystals by the growth inhibitors helps to prevent their deposition and adhesion on the surfaces of the equipment. It has been proven by the microscopic analysis that the result of this distortion is often vaterite crystals amorphous, which is dissolved and has low-adhesion nature when deposited over the contact surfaces.

Temperature, pH, calcium ion concentration and the presence of chemicals (such as corrosion inhibitors and hydrate inhibitors) determine the performance of chemical scale inhibitors. From an environmental viewpoint, most of the scale inhibitors contain phosphorus and/or nitrogen can be highly toxic to the environment through creating eutrophication via generating excessive nutrients. Furthermore, most of the chemical scale inhibitors experience low biodegradability rate and have adverse influences on the solution chemistry that they are treating. The most common anionic groups in chemical scale inhibitors and the equivalent scale inhibitors that have these groups have been summarized in Table 2-1:

Table 2-1 Important scale inhibition functional groups and corresponding main classes of inhibitors [157, 159]

Functional group	Classes of scale inhibitor
--SO ₃ --	Polysulfonates
--COO--	Phosphino polymers
--CO ₂ H--	Polycarboxylates
--PO ₃ H--	Polyphosphonates
--OPO ₃ H--	Small phosphonates and

2.2.4 Conventional Strategies for Scale Formation Remediation

Many different oil and natural gas field scale treatment strategies are known, and the majority are based on three basic methods [63, 158, 160]:

1. Sulfate ion separation from injected seawater;
2. Chemical or mechanical scale removal;
3. Pretreatment strategies based on the use of scale inhibitors.

For short-term treatment and mild-scaling conditions, the first two methods may be effective. However, continuous injection or chemical scale squeeze treatment with scale inhibitors have been proven over the years to be the most efficient preventative methods [72, 161].

Conventional strategies of scale control or hard water softening include the pretreatment of the scale former with caustic soda, the addition of chemical scale inhibiting substances, or the replacement of the scale former with soluble ions by ion exchange. Although all of these techniques are effective for scale control, they substantially change the solution chemistry [9, 20]. Additionally, these chemicals are highly toxic, unsustainable, and can be prohibitively expensive. Furthermore, in some other applications, there are very strict demands for water quality such as in the beverage and food industries and some oil and gas industries [20, 49, 161].

2.2.5 Non-Conventional Strategies for Scale Formation Remediation

Several non-chemical scale inhibition methods have been reported over the last decade [19, 31, 48, 77]. They cover physical and mechanical techniques that do not influence the water chemistry. These techniques can be divided into four groups [77, 162-164]:

1. Ultrasonic conditioning;
2. Turbulent conditioning;
3. Electrical conditioning;
4. Magnetic conditioning.

The ultrasonic conditioning method does not prevent scale formation, and reported results have shown an acceleration in scale precipitation without any effects on the particle morphology or size [77]. Thus, this method may be useful for pretreatment to promote the scale to precipitate before reaching (and harming) other equipment. The turbulent conditioning method has not been studied extensively yet. However, the few extant works studying this method have reported that the turbulence technique can increase the control over and prevention of scale formation. The theory behind this method is that turbulent hydrodynamic conditions prevent the formation of scale by washing the inorganic deposit away before it can attach to the internal surfaces of the pipeline. Electrical and magnetic conditioning are similar techniques, both applying MFs to flowing water to prevent scale formation. The electrical method relies on a coil wound around the pipeline [162, 164], whereas the non-electrical magnetic methods apply a MF via a permanent magnetic [19]. The reported results have shown that the electromagnetic method results in the formation of larger crystals, as well as the formation of calcite rather than aragonite particles. In contrast, permanent MFs result in the formation of aragonite crystals with small particle sizes. Furthermore, the conditioning effect of electromagnetic methods is achieved by the movement of electrons via the wound coil around the pipe rather than by water circulation through a field gradient; hence, turbulent flow is not required.

2.3 Gas Hydrate Inhibitors and Scale Formation in Oilfield

Gas hydrate formation has become a topic of interest in the oil and gas industry. In 1934, Hammerschmidt first observed the formation of hydrates in transport pipelines above the ice formation temperature. Hydrate formation in the oil and gas industry is problematic and requires effective inhibition methods; thus, several thermodynamic methods have been implemented to prevent gas hydrate formation by reducing the activity of water molecules in the forming gas hydrate [2, 131]. The inhibition of gas hydrate formation requires the use of alcohols, which depress the freezing point of the solution. However, when using large quantities of these compounds, careful material selection and specification is required because of the need for their recycling and reuse, which can have a significant effect on the economics of oil and gas extraction.

MEG is used extensively in natural gas transportation pipelines as an inhibitor to prevent the formation of natural gas hydrates [64, 136]. The use of MEG as a hydrate inhibitor rather than the use of other traditional hydrate inhibitors, such as methanol, has increased because of its ability to be regenerated and reused, thus reducing operational costs [131, 136]. However, in such applications, several problems may arise following the breakthrough of formation water and the subsequent introduction of mineral salts into the regeneration loop [64, 116]. The introduction of divalent cations, including calcium, magnesium, and barium, poses a scaling risks within critical systems including the subsea pipelines and MEG injection points [165], as well as within MEG regeneration systems operating at a high temperatures, such as reboilers [64, 136]. Scaling within the MEG loop and associated systems can be minimized by controlling the system pH or by the injection of suitable scaling inhibitors [1, 64].

Flaten, Seiersten [106] have claimed that the presence of MEG in water affects the supersaturation ratio because of changes in the activity coefficients and the solubility of the dissolved salts. Therefore, the presence of MEG within a brine solution may influence the morphology of CaCO_3 at the wellhead and within the pipeline under continuous flow conditions [6, 140]. There is ample precedent to suggest that an increase in MEG weight fraction can reduce the growth rate of CaCO_3 and influence the polymorphism, phase transformation, and crystal size distribution [5]. Moreover, Flaten, Seiersten [106] have reported that the morphology of the CaCO_3 changes at various MEG concentrations and temperatures, that is, from calcite to vaterite. The reason behind this behavior is that the activity-based supersaturation ratio represents the actual driving force for CaCO_3 precipitation within the MEG solution [82].

As is well known, the process of recycling and regeneration of gas hydrate inhibitors depends mainly on the solid separation and distillation processes. If the difference between the degrees of volatilization of two liquids in a mixture is significant, their separation is easy, resulting in lower

energy consumption at the reboiler stage. Because the boiling point of MEG is 197°C, almost twice that of water, the separation of these liquids is easy using a distillation tower at atmospheric pressure. Moreover, the use of MEG solutions reduce the corrosion rates of carbon steel significantly compared to the use of ethanol and methanol because of the lower solubility of CO₂ gas in the MEG liquid phase. Therefore, the solubility of salts in ethanol and methanol solutions is much lower than in the MEG solutions, thus giving an added advantage for the use of MEG, especially when combined with formation water. In the oil and gas industry, operators consider that the use of MEG as a gas hydrate inhibitor is better economically, environmentally, and operationally.

The production of natural gas and oil from offshore wellheads is often associated with varying degrees of water formation. The formed water often contains high concentrations of divalent mineral ions and different mole fractions of CO₂ or H₂S. Based on the main factors shown in Figure 1-2, it can be noticed that there are two main components that are always available in the gas and oil wellheads. Therefore, a tendency to form inorganic sediments is more likely if the pH of the saline solutions becomes alkaline; specifically, this affects the deposition of CaCO₃. Because of the presence of organic acids dissolved in the water, operators usually pump large amounts of basic agents, such as caustic soda, potassium hydroxide, or sodium carbonate, into the mixture to increase the pH and combat corrosion, which worsens over time, especially if there is a high concentration of oxygen molecules. Therefore, the anticorrosion process is a third factor contributing to the precipitation of inorganic scale from subsea pipelines to the purification units and separation units on the surface. Thus, the economical effects of both inhibition and removal of scale can be significant.

2.3.1 Effect of Mono Ethylene Glycol on Scale Formation

The limits to the maximum solubility of mineral salts in solutions are based on thermodynamic factors. These limits are affected by many external factors such as temperature of the liquid mixture, fluid viscosity, and fluid ratio in the mixed salt solution. However, when the upper limit of solubility of any salt is exceeded, the excess ions are exposed to the abundant counter ions, such as carbonate ions, forming scale. This is the supersaturation stage, which changes with the characteristics of salt solutions, as mentioned earlier.

In the oil and gas wellheads, organic compounds reduce the maximum solubility of dissolved inorganic salts in the formation water associated with hydrocarbon products, thus reducing the saturation limit and resulting in the presence of larger amounts of non-dissolved mineral ions in these solutions, which will be converted into inorganic scale later. It is well known that gas hydrate inhibitors, such as MEG solutions, act to reduce the solubility of mineral salts in the saline solution, and, thus, the saturation level is reached faster than normal. Therefore, even when the

concentration of mineral salts is low, the use of MEG solutions results in a significant interaction of the mineral ions with carbonate ions present in the same solutions. This phenomenon is important in the oil and gas industry because it determines the tendency of saline solutions to form sediments, which affects oil and gas production operations.

Oil wellheads are usually operated at very high pressures. This pressure gradually decreases following the extraction of hydrocarbon compounds, resulting in the release of gases dissolved in the saline solutions, such as carbon dioxide, which in turn causes a significant increase in the pH of the formation water. This increase in pH drives the remaining dissolved CO₂ gas to produce bicarbonate and carbonate, completing the last corner of inorganic deposit formation shown in Figure 1-2. However, other anions can coexist with bicarbonates and carbonates, such as sulfate ions. Sulfate ions often enter the saline system because of pumping of massive amounts of seawater into the wells to control the well pressure and increase the hydrocarbon productivity. Seawater contains high concentrations of SO₄²⁻ anions. Therefore, the combination of these anions with mineral cations (divalent ions) will lead to the formation of unwanted deposits, which are no less dangerous than those containing carbonate ions. Therefore, in the oil and gas industry, the removal of these anions is a priority, requiring the pretreatment of seawater before it is injected into the oil wells and, thus, additional economic costs.

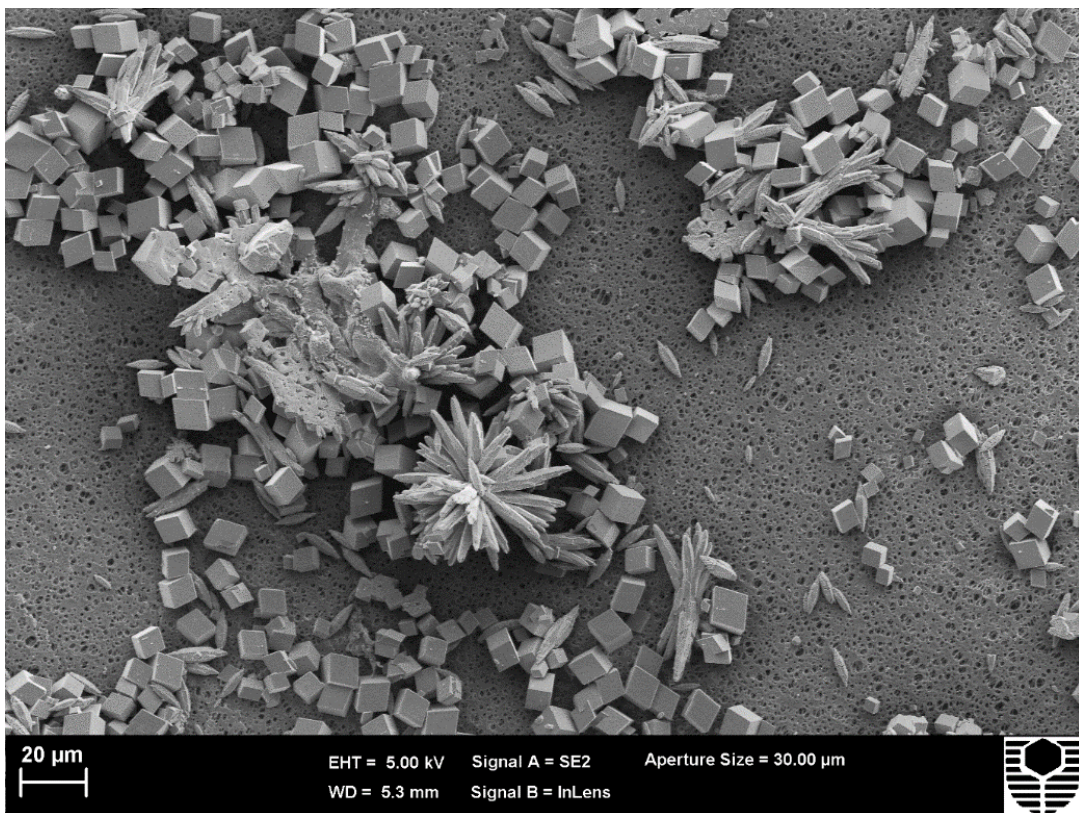


Figure 2-9 CaCO₃ crystals precipitated from a water + MEG solution (ca. 80% by volume of MEG) at ca. 125°C

2.3.2 Hydration Shell of Ions in Mono Ethylene Glycol

Rozhkova, Rozhkova [79] investigated the separation of MEG from saline solutions by ionic exchange membranes and found the separation was improved significantly when electrolytes were present. They attributed this improvement to the apparent changes in the strength of the hydrogen bonds between the OH groups of the MEG and the hydrogen atoms of the water molecules. In more detail, there is a clear reduction in the energy of hydrogen bonds between water and MEG, increasing the mobility of MEG molecules during the ionic separation process. Thus, the hydrogen bonds between water and MEG are interrupted by the presence of electrolyte ions, which form strong bonds with water molecules in the first hydration shell (refer to Figure 2-10). These bonds are often stronger than the hydrogen bonds formed between the water molecules and the OH group of MEG, where the large size of the MEG molecules usually causing hydrogen bonds to weaken and then rupture [79, 166]. Therefore, any changes to the hydration shell surrounding the electrolytes can distort the hydrogen bonds between water and the MEG molecules.

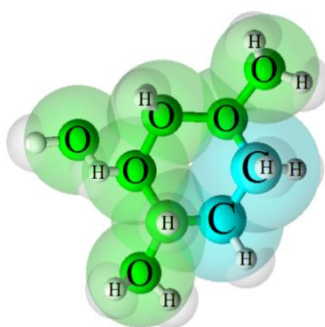


Figure 2-10 Hydrogen bonding and covalent bonding of a MEG - water system as proposed by Rozhkova, Rozhkova [79]. Images were generated using ACD/ChemSketch freeware [167]

Most fundamental studies have presented a precise description of the hydration shell in aqueous solutions, which has been defined as the layer of water molecules arranged around the cations and anions and linked to them by ion–dipole forces [85, 168]. The thickness of the hydration shell often varies according to the size of the ions and the density of the electronic charge, giving it spatial and dynamic properties in the liquid phase [85]. Several studies have indicated an inversely proportional relationship between the thickness of the hydration shell and the ionic mobility in aqueous solutions and a proportional relationship with the valence [169]. Previous reports have demonstrated the possibility of competition between MEG and water molecules for the formation of a solvation shell in saline solutions [79, 170]. Therefore, the use of external forces, such as a MF, may induce significant changes in the thickness of the hydration shell in MEG solutions.

2.4 Magnetic Field Treatment as a Non-Chemical Remediation Method

Having reviewed the literature concerning both static and dynamic techniques to evaluate the performance of chemical inhibitors, we have not observed their use to assess the performance of non-chemical methods to reduce scale formation. For example, one of the most important, although controversial, non-chemical methods is magnetic treatment. Unfortunately, this method has not been studied properly, and its effectiveness in preventing scale deposition has not been confirmed. However, recently, positive results generated using traditional antiscaling magnetic treatment (AMT) methods have been reported by various authors [29, 97, 171-174]. Zaidi, Sohaili [32] concluded that the use of a MF can enhance solid–liquid separation performance because of the improved gathering of colloidal particles through manipulation of the particle arrangement. Fathi, Mohamed [175] found that AMT can enhance the precipitation of CaCO_3 in aqueous solution by controlling the solution pH, flow rate, and time of exposure. Furthermore, Fathi, Mohamed [175] observed that AMT affects the mineral ions involved in the formation of CaCO_3 and suggested that its scale does not need to be present for the MF treatment to influence further scale formation. Baker and Judd [19] reviewed in detail the advantages and the disadvantages of AMT when applied to small-scale water treatment. They presented several positive results that indicate that the aggregation of particles was enhanced, and the size of hydrophilic crystals was observed to be larger than usual [19].

Baker and Judd [19] also found that the AMT technique was successful when applied to thermal circulating processes such as in reboilers and heat exchangers, showing reduced carbonate scaling during operation. It has also been established that AMT can lead to large savings in cleaning, power consumption, time, and maintenance cost, as well as preventing unexpected shutdowns within water-based applications such as water treatment, paper production processes, and within the oil and gas industry [19, 154, 176, 177].

In addition, Higashitani, Kage [174] found that the growth of CaCO_3 particles was accelerated at high MF densities after exposure to a MF for more than 10 min. Higashitani, Kage [174] attributed the effect of magnetic exposure upon CaCO_3 growth behavior to the effect of the applied MF upon the bicarbonate species before mixing with calcium ions. Their results highlight the different responses of the cationic (calcium) and anionic (bicarbonate) species to the MF. A similar conclusion was made by Baker and Judd [19], who stated that magnetic exposure primarily affects the anionic component of the scale forming compound.

2.4.1 Magnetic Field Concepts

To understand the effects of the application of MFs in water treatment, there are three main concepts that must be considered, as discussed by Zaidi, Sohaili [32], Okada, Ozaki [178], Oshitani, Yamada [51], and Higashitani, Iseri [179]. These concepts can be categorized as

follows: magnetism and the effects of MFs [180], the magnetic gradient [51], and magnetic memory [51]. The first factor describes the relationship between positive and negative particles, ions, and molecules and their responses to MFs [51]. Meanwhile, molecules can be divided into two categories, polar like water and non-polar like fats, oil, and petrol/gasoline [180-182]. The type of molecule, whether polar or non-polar, will dictate how the molecule responds when exposed to a high-intensity MF.

Göllei [76] and Zaidi, Sohaili [32] claimed that, in non-polar molecules, the proton and electron centers of gravity act around the same point. This results in continuous random movement in the absence of a MF, and, thus, the molecules are less susceptible to coagulation [178, 183, 184]. However, Zaidi, Sohaili [32] reported that if a non-polar molecule system is exposed to the MF generated by an electromagnet field, the molecules will adopt a less random movement pattern and reorient according to the direction of the magnetic flux, as shown in Figure 2-11. Because the non-polar molecules travel through the electromagnetic field, an induced dipole moment is generated. This rearrangement will promote the coagulation of molecules after MF exposure [178, 183]. However, in contrast to non-polar molecules, prior to MF exposure, polar molecules exhibit a more random arrangement. Because of the random arrangement of polar molecules in combination with the repulsion caused by the similarly charged ends of the surrounding particles, coagulation is unlikely to occur [178]. In a similar manner to non-polar molecules, the application of a strong MF can result in the rearrangement of polar molecules, thus promoting molecular coagulation [178, 184].

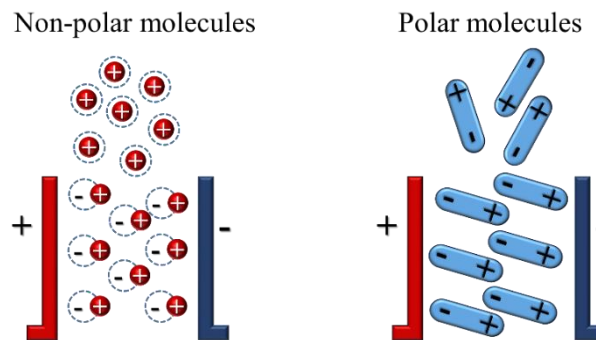


Figure 2-11 Structure of non-polar and polar molecules and their arrangement as they pass through an electromagnetic field

Furthermore, as the charged particle travels through a MF, it will experience a force (the Lorentz force). The Lorentz force acts upon a charged particle according to the “right hand rule”, meaning that a charged particle travelling through a MF will undergo a deviation in its trajectory perpendicular to the MF and axis of movement [185, 186]. The extent of the force exerted upon a charged particle can be estimated using Equation 2-7 and is dependent on the particle charge (positive or negative), its velocity as it travels through the MF, and the strength of the MF itself

[18]. A particle can be either negatively or positively charged, and the direction of the applied force produces a separation effect upon oppositely charged particles, as shown in Figure 2-12 [32].

$$\vec{F} = q \cdot \vec{v} \cdot \vec{B} \quad 2-7$$

Here, the \vec{F} represents the Lorentz force, which is a function of the electric charge of the particle q in coulomb units, instantaneous velocity, \vec{v} , in meters per second, and magnetic field, \vec{B} , in tesla.

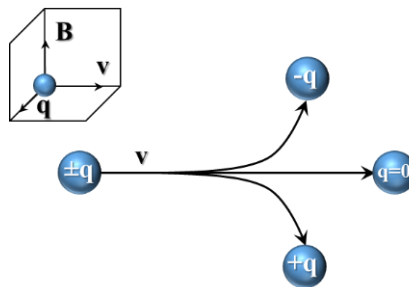


Figure 2-12 Lorentz force and the right-hand rule movement of charged molecules

The second concept required to understand the potential effects of MF exposure upon scale formation is magnetic flux density. The flux density of a magnet is dependent on several factors including, the type, shape, and the source of the MF, whether an electromagnet or a permanent magnet [32, 187]. In addition, the materials used to make the magnet, such as neodymium, samarium, alnico, or ceramic, represent a key factor in determining the magnetic flux intensity. For example, neodymium-type magnets have a higher flux density when compared to the other types of the same MF strength. As such, the magnetic flux density is often more important than its strength in determining how they will influence the particles.

Oshitani, Yamada [51] reported that when the flux density of a MF is uniform, the exposed molecules will tend to rearrange themselves according to the direction of the MF; hence, the separation of the molecules becomes more likely. They have reported that the influence of MFs on smaller molecules is greater than that on larger molecules. As a result, Vick [183] claimed that small molecules tend to orientate in the direction of the applied MF to a greater extent than larger molecules. Furthermore, when exposed to a MF of greater flux density, the resulting Lorentz force generated upon that particle will be greater than that produced by MFs of lesser flux density [185, 186]. The first and second concepts discussed are critical in understanding the relationship between MFs and the behavior of the exposed molecules. The final concept is related to the memory effect, which defines the relationship between the intensity of magnetic exposure and the retention time. In other words, to what extent the effects of magnetic exposure remain active

on the magnetized particles after exposure has ended [51]. It is important to maintain the influence of the MF upon the exposed particles for as long as possible to ensure the maximum impact.

2.4.2 Magnetic Field Treatment Mechanisms

Two mechanisms have been postulated to describe the effects of MFs on calcium carbonate precipitation. In the first mechanism, the dissolved ions are directly affected by the MF, influencing the growth and nucleation kinetics based on altering proton spin and proton transfer rate. In the second mechanism, there is a direct effect on particles based on surface charge modification. These mechanisms are contrary to each other. Concerning the dissolved ion mechanism, Higashitani, Kage [174] have reported that the rate of CaCO₃ particle growth increases but the nucleation rate is suppressed. Furthermore, Madsen [188] reported that the average size of the formed CaCO₃ crystals was reduced but a greater number of nuclei were formed when CaCl₂ and NaHCO₃ solutions were exposed to a MF because of the increasing proton transfer rate between bicarbonate ions and water molecules.

Concerning the second mechanism, Wang, Babchin [41] used turbidity measurements to investigate the effects of MFs on CaCO₃ and found that the formed crystals were smaller in size and greater in number; they also found that the precipitation rate was very high. Moreover, the MF affects the structure of the water-ion system at the colloid particle surface or the bulk fluid interface [189]. Both mechanisms indicate that the bonds of water molecules and the transfer of proton spin of H⁺ are restructured, hindering, and reorienting on exposure to MFs, affecting the thermodynamics and kinetics of ions in aqueous solutions. However, the response of the dissolved ions in glycolic solutions has not yet been extensively investigated in view of the ionic mechanism, which is believed to improve the control of scale formation in the oil and gas industry. Table 2-2 lists the results of previous studies using magnetic field devices for the treatment of aqueous solutions.

Table 2-2 Compilation of current experimental conclusions concerning MF treatment

Parameter	Observation	Additional Information
Clathrate formation	Enhanced	Checked by contact angle
Cluster size in liquid water	Increased	Checked by the infrared spectrum
Evaporation rate	Increased	Facile super cooling
Friction coefficient of water in thin films	Reduced	-
Hydration shell of ions	Fluctuated	Depending on the ion charge
Hydrogen bond strength	Reduced	-
Inter-cluster bond strengths	Reduced	-

Parameter	Observation	Additional Information
Intra-cluster bond strengths	Increased	-
Ion pair contact	Increased	-
Nucleation	Reduced	Nucleation rate of CaCO ₃
Number of monomers of water	Increased	By simulation
Particle morphology	Changed	Produces a stable phase morphology
Proton spin relaxation	Increased	-
Refractive index	Increased	Increased H-bond strength
Salt mobility	Increased	Disruption to H-bonds
Surface tension	Fluctuated	-
Tetrahedral geometry of water	Increased	By simulation
Magnetic susceptibility	-ve to +ve	-
Ordered structure of water formed	Increased	Around hydrophobic molecules
Solubility of gases	Increased	-
Van der Waals interactions	Weakened	-
Viscosity	Slightly increased	-
Water and ion interactions	Weakened	-
Water hydrogen bonding	Increased	At 5 M NaCl
Water hydrogen bonding	Reduced	At 1 M NaCl
Water molecule pairs	Reduced	-
Zeta potential	Reduced	Depending on the pH of the solution

2.4.3 Magnetic Field Orientation and Classification

Furthermore, Baker and Judd [19] stated that permanent magnets can be classified into four types, where each has a different orientation of the AMT (orthogonal or parallel) to the direction of flow, as shown in Figure 2-13 [19, 32, 101]. They further suggested that the different magnet orientations may result in different responses to how they influence scale formation. Zaidi, Sohaili [32] and Alimi, Tlili [190] have reported that it is preferable to use permanent magnets for water treatment because they are capable of generating a uniform MF. In addition, the manufacture of magnets with a high magnetic strength such as neodymium N45SH, which can thermally withstand temperatures of up to 150°C, is facile. In addition, permanent magnets can be formed in different shapes, dimensions, and orientations, for example, axially or diametrically magnetized [19].

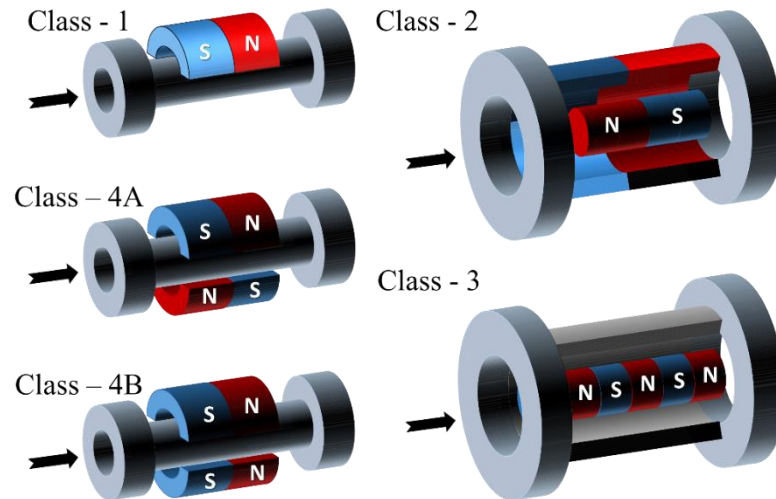


Figure 2-13 Recommended MF orientations across the fluid flow in pipelines: Class 4A is diametrically magnetized and class 4B is axially magnetized [19]

On the other hand, Busch and Busch [177] and Baker and Judd [19] have reported that the application of the AMT technique to industrial water treatment was ineffective. However, the reasons for this failure are unknown [191, 192]. Furthermore, other authors have criticized the AMT technique because of the lack of systematic evidence [154, 192]. Thus the efficiency of AMT in inhibiting scale formation is still disputed and a precise explanation of how AMT influences the formation of scale is unclear [175].

2.4.4 Why is Magnetic Field Application Important in Industry?

Most new theories and techniques, such as magnetic methods, receive criticisms and comments at the scientific, technical, and philosophical level. However, these criticisms drive the evaluation and study of the most important factors in these applications to make them more acceptable and convincing for use in industry. At the beginning of the last century, the use of MFs in medicine ⁵, water conditioning ⁶, agriculture ⁷, electrical power systems, and biology ^{8,9} was considered fantasy. Nevertheless, these technologies, supported by extensive studies, have become essential. Although magnetism is invisible without specialized equipment, the use of MFs has been demonstrated in magnetic resonance imaging (MRI), nuclear magnetic resonance (NMR), and power transformers. These applications have been explained by many theories based on logical relationships, which have contributed to their development.

The most important problem facing the use of magnetic fields in the chemical industry is understanding how magnetic fields affect chemical reactions, especially at the microscopic level. This requires careful investigation of the important variables that affect the thermodynamics and molecular systems. Therefore, researchers are currently studying and analyzing a number of variables and theories related to MFs to provide scientifically acceptable explanations. First, it is

necessary to understand what the magnetism concept is and its micro-molecular structure. As shown in Figure 2-14, there are two types of materials, magnetic materials and non-magnetic materials. In magnetic materials, the intensity of the magnetic flux is affected by the alignment of the magnetic domains. More structured magnetic materials generate stronger MFs. Neodymium is, thus, one of the most powerful magnets manufactured, generating energy up to 50 MGOe because of the highly oriented magnetic domains.

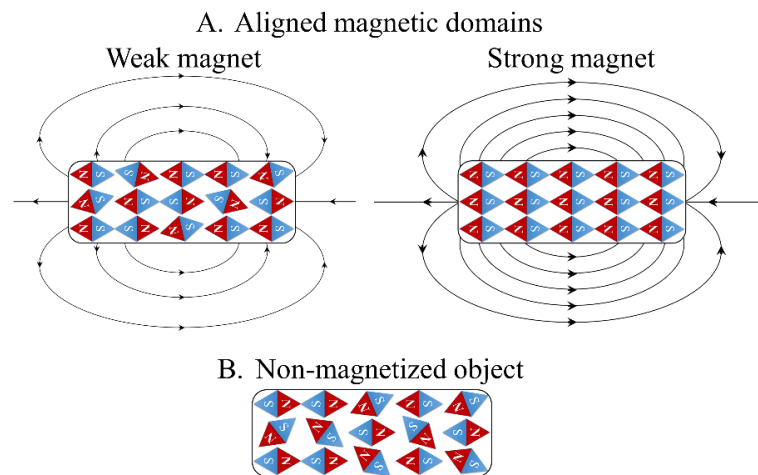


Figure 2-14 Ferromagnetism: (A) Magnetized material with corresponding MF lines shown and (B) Non-magnetized material

2.4.5 Effect of Magnetic Fields on the Physical Properties of Aqueous Saline Solutions

The effects of MFs on the characteristics of aqueous solutions have been intensively investigated for the last decade [169, 193-196]. The changes that occur in these characteristics are crucial to several applications and industries, such as cooling water systems, bio-treatment plants, heat exchangers, the oil and gas industry, and transportation processes [29, 30, 32, 193, 195, 197, 198]. Some studies have reported that physical characteristics, including pH, viscosity, refractive index, EC, water cluster size, and vaporization rate of aqueous solutions are affected by the application of a MF [38, 169, 179, 189, 199, 200]. For example, Holysz, Szczes [169] reported that the ECs of magnetized solutions decreased significantly after 5-min exposure, whereas a significant increase in the evaporation rates was observed. They hypothesized that the MFs could influence the thermodynamics of hydration. Thus, the solubility of mineral ions could be affected by the changes in the thermodynamic properties of the hydration shell, thus affecting scale formation behavior [174, 201, 202].

Some studies have reported that the electrical conductivity (EC) of electrolyte solutions is inversely proportional to the radii of the hydrated ions and proportional to their valence (see Table 2-3) [103, 169]. Therefore, this relationship has been used to evaluate the effect of MFs on

mineral ions in aqueous solutions. In addition, it has been reported that the solubility of oxygen and copper sulfate is considerably increased during exposure to MFs. Furthermore, a significant reduction in the corrosion rates of carbon steel has been reported after MF treatment for a short period [203].

Table 2-3 Ionic radius (r_i), hydrated radius (a_i), and ionic mobility of monovalent elements

Ion	Ionic radius, pm	Hydrated radius, pm	Ionic mobility, $\text{cm}^2 \text{ohm}^{-1} \text{mol}^{-1}$
Li^+	76	340	33.5
Na^+	102	276	43.5
K^+	138	232	64.5
Cs^+	152	228	67.5
Ca^{2+}	167	226	68

The application of an MF to an aqueous solution weakens the van der Waals interactions between water molecules, but the number and strength of hydrogen bonds increases significantly [38, 199]. Hosoda, Mori [200] and Ghauri and Ansari [199] reported that the increase in the number of hydrogen bonds led to a slight increase in the absolute viscosity of magnetized solutions. These changes in the absolute viscosity affect ion mobility rates and ion solubility in these solutions. For this reason, the EC of the solutions is affected by exposure to a MF. However, the extent of the changes to these parameters after long-term exposure of saline solutions to a very high magnetic flux density is still under investigation, especially concerning glycolic solutions.

Waluyo, Nordlund [105] reported that cations break the hydrogen-bonded structure of aqueous solutions. Furthermore, recent reports have stated that the presence of mineral ions in organic solvents such as MEG influences the hydrogen bond strength, thus altering scale formation in aqueous solutions [106, 107, 204]. For instance, Rozhkova, Rozhkova [79] reported that the presence of mineral ions in the aqueous glycolic mixture weakens the energy of hydrogen bonds, from 17.5 to 16.8 kJ/mol. As a result, in MEG solutions, a metastable CaCO_3 phase is formed [106-108]. It has been reported that increasing the number of MEG molecules in aqueous solution affects the nucleation rate of CaCO_3 [106]. However, the influence of MFs, mineral ions, and the MEG solution on hydrogen bonds has not yet been investigated by examining the changes in the thermodynamic properties.

Measuring the hydration shell thickness directly after treatment is challenging because of the influence of the analytical method on the structure of magnetized water molecules. Therefore, the dynamic flow method has been employed to obtain more details about the change in the physical properties, such as pH and EC. Although some studies have used weak magnetic fields to examine the effect of MFs on the physical properties of aqueous saline solutions, dynamic flow

experiments of a co-solvent system such as water–brine–MEG in a strong MF have yet to be carried out.

2.4.6 Magnetic Fields Treatments as Scale Formation Inhibitors with Gas Hydrate Inhibitors

The chemical performance of scale and gas hydrate inhibitors, which are injected into oilfields, is a critical factor for avoiding scaling and gas hydrate formation in water treatment equipment and pipelines [63, 70, 137]. Although MEG is remarkably successful in inhibiting gas hydrate formation [82], it aggravates scale formation [122]. Therefore, CSIs are frequently employed to overcome this problem [68]. On-shore analyses by scanning electron microscopy (SEM), X-ray diffraction (XRD), and chemical analysis have demonstrated that a significant component of scale deposit is CaCO_3 [65, 106, 126]. Chemical analysis of the water produced during the process has shown that the pH, concentration of divalent ions, particle morphology, and amount of suspended solid are affected by the addition of CSIs [9, 68].

Changing the oil recovery procedure to avoid the injection of seawater or the breakthrough of formation water to prevent scale formation is complicated. Additionally, mechanical removal of insoluble scale deposits is expensive, requiring process shutdown, and can damage the pipelines and equipment [9, 10]. Different strategies have been adopted to reduce the operating costs of the mechanical methods used for scale removal and reduce the non-operational period [73, 150]. For instance, CSIs are usually injected into the lean MEG solution after the regeneration process to prevent scale formation inside transportation pipelines [5, 6]. The most commonly used CSIs in the oil and gas industry are organic phosphonates, polyacrylates, phosphates and polyphosphates, phosphate esters, carboxylates, sulfonates, and various other polymers and copolymers of phosphonates [12, 20, 126, 205]. These chemical substances are chosen according to the environment of the oil reservoir and transportation pipelines [12, 205]. The concentration, dosage, and injection point of the CSI is assessed according to its performance in brine solutions in the laboratory [20, 126, 206]. However, because CSIs affect the solution chemistry and pose a risk to both users health and the environment, in addition to their inhibitory performance, they are often classified according to their health and environmental risks [20].

The threshold dose of a CSI for a defined level of inhibition is called the minimum effective dose or MIC, typically 0.5 to 20 ppm [206, 207]. Nevertheless, the MIC for high-temperature and high-pressure fields that suffer from severe scaling can be in the order of a few hundred parts per million [206, 208]. 1-Hydroxyethane-1,1-diphosphonic acid (HEDP) and its phosphate ester are extensively used in circulating cooling water processing and the chemical cleaning of hot surfaces [206, 209, 210]. However, only few investigations into the applications of HEDP and its phosphate ester for reboilers for MEG regeneration treatment have been carried out. In addition,

the remaining concentration of CSI in the intruded glycol solution reduces the pretreatment-process performance during the removal of divalent ions and MEG regeneration. This poor removal performance leads to the transfer of un-precipitated mineral ions to the reboiler section. To prevent the side effects of CSIs, magnetic treatment has been suggested by several researchers because it is a low-cost, stand-alone, and eco-friendly alternative scale treatment method [28, 31, 48]. Previous reports have described the strong potential of MFs in a variety of applications; however, the results are often difficult to reproduce [28, 31, 48]. Nevertheless, some results are impressive [40]; for example, Higashitani, Iseri [179] noted that the zeta potential (ζ) of the colloids was reduced after exposure to a MF. This reduction implies accelerated coagulation rates and, consequently, greater sedimentation. This finding highlights the fact that ionic particles are affected by the MF rather than the bulk solution.

On the other hand, Chang and Weng [38] have reported that the size of a water cluster could be controlled by the application of an external MF. Other studies have indicated that the CaCO_3 particles in scale have different morphologies and tend to form aragonite in magnetized water [196, 202, 211]. Moreover, it has been shown that MF treatment can significantly inhibit or promote CaCO_3 scale formation in aqueous solutions depending on the anionic and cationic concentration ratio in the brine solution [109]. Therefore, MF treatment could control the precipitation of CaCO_3 , thus serving as a scale formation inhibitor and reducing the precipitation of divalent ions in an aqueous solution. Consequently, both CSIs and MFs create favorable conditions for low scale growth and cause fewer severe scaling issues. However, the performance of external MF treatment for scale control has not been investigated in non-aqueous solutions in the presence of CSIs because of its lack of applicability in the oil and gas industry.

Chemical reactions that include radical intermediates can be affected by external magnetic fields [31], which appear to alter their rate of reaction, the yield of product, and chemical equilibrium [58, 59]. These results have been investigated extensively in aqueous and organic liquids phase [50, 77, 212], where these external effects may be described by using the radical pair mechanism [31, 57, 213]. Such results are the cornerstone to the area of spin chemistry. As the Electron Polarization and Chemically Induced Dynamic Nuclear Polarization have demonstrated the dependency of radical-pair reaction kinetics on the direction of magnetic fields [213]. Furthermore, The Zeeman interaction between the unpaired electron spins on each radical and the magnetic field obviously plays an essential role in the generation of magnetic field effects during calcium carbonate formation [101, 201, 212].

Most studies have assessed the performance of CSIs under different pressure and temperature conditions using the DSL method [11, 109, 156]. This method involves a tube-blocking system that is used to examine scale formation in capillary tubing coils such as oil and water pipelines

[20, 109, 214]. The system is recommended for determining inorganic scale formation under dynamic conditions [9, 63, 128]. However, there is a lack of literature concerning the effect of combined physicochemical treatments on scale formation, which has been established as the method of choice for understanding the behavior of CSIs when exposed to an external MF.

2.5 Mathematical Modelling Related to Magnetic Fields

Because of technological developments in the field of testing and measurement using electronic sensors, it is easy to measure the strength of an MF using a Hall effect sensor. This type of sensor generates a very weak voltage difference when exposed to an MF. In addition, many mathematical equations, such as the Maxwell model, have been derived to determine the energy and magnetic flux density, either from permanent magnetic objects or electrical fields (see Figure 2-15 and Equations 2-8 to 2-11). These relationships give a simplified understanding of how MFs correlate with elements and particles in electronic circuits. Therefore, it is possible to understand the changes in the behavior of ions and dissolved particles in electrolyte solutions. The Maxwell model symbols meaning are tabulated in Table 2-4.

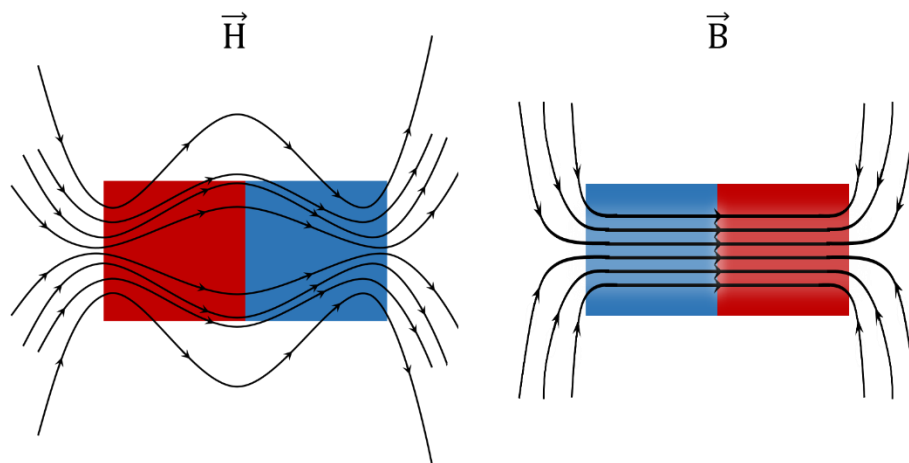


Figure 2-15 Diagram of induction and magnetic fields paths

$$\text{Gauss's Law } \nabla \cdot D = \rho_v \quad 2-8$$

$$\text{Gauss's Magnetism Law } \nabla \cdot B = 0 \quad 2-9$$

$$\text{Faraday's Law } \nabla \times E = -\frac{\partial B}{\partial t} \quad 2-10$$

$$\text{Ampere's Law } \nabla \times H = \frac{\partial D}{\partial t} + J \quad 2-11$$

Table 2-4 Description of each symbol and the corresponding SI-Unit of measure

Symbol	Meaning	SI Unit of Measure
E	Electric field	Volt per meter
v	Instantaneous velocity of the line element	Meters per second
H	Magnetic field strength	Ampere per meter
D	Electric displacement field	Coulomb per square meter
B	Magnetic flux density	Tesla or weber per square meter
ρ	Free electric charge density	Coulomb per cubic meter
J	Free current density	Ampere per square meter
t	Time	Second

2.5.1 Magnetic Susceptibility of Electrons

It is well known that the movement of electrons through a wire coil generates a MF. This MF can produce an electric current in another wire coil close to it. This theory is based on the concept of magnetic susceptibility (sensitivity), which indicates whether materials are attracted to or repelled by the MF, which is useful for practical applications. This phenomenon is the basis of the operation of electrical transformers. However, what is important about this phenomenon is the ability of MFs to induce electrons to move through a wired coil leading to power generation (voltage). Materials that are not affected by MFs are usually called diamagnetic, whereas those with a positive sensitivity (magnetized) are known as paramagnetic. Because all chemical elements containing a certain number of electrons in their outer orbitals, they are affected by MFs to varying degrees. The number of electrons in the outer orbitals of an element determines the valence and ion charge. According to Hund's rule, every orbital must be occupied by a single electron before it is doubly occupied [215, 216] (see Figure 2-16). Thus, some orbitals contain unpaired electrons, leading to single electron spin in either direction. The spin of a single electron means that it acts like a magnet but is oriented randomly [215, 216]. Thus, paramagnetic atoms are affected by external MFs, and paramagnetism is the magnetic state of elements with an electron configuration containing one or more unpaired electrons, such as some mineral ions (see Figure 2-17).

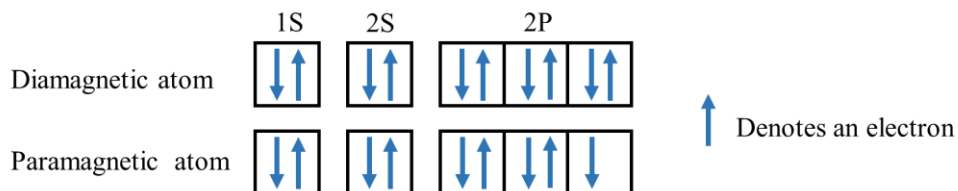


Figure 2-16 Electron configuration for diamagnetic and paramagnetic elements

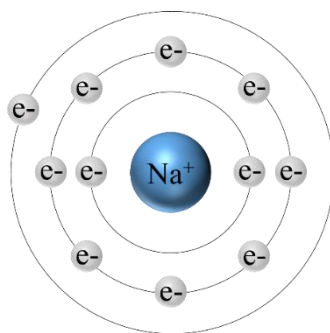


Figure 2-17 Electronic configuration of sodium atom

2.5.2 Magnetic Susceptibility of Substances

When organic and inorganic materials are subjected to a MF, a magnetic moment is induced. The generated magnetic momentum per unit volume is known as magnetization phenomenon (M), which is proportional to the MF strength (H) and volume susceptibility (k_v). Because MFs and magnetism have the same dimensions, k_v is dimensionless. The relationship between M , H , and k_v can be expressed by Equation 2-12.

$$M = k_v * H \quad 2-12$$

Here, k_v is in a proportional relationship with the molar susceptibility (χ_m) and molar volume (V_m) of the substance. Equation 2-13 expresses this relationship.

$$k_v = \chi_m * V_m \quad 2-13$$

Negative or positive magnetic susceptibility categorizes the magnetization of inorganic and organic materials. For instance, if a material is placed in a MF and it becomes weakly magnetized in the opposite direction to the MF, it has a negative magnetic susceptibility, i.e., it is diamagnetic. The opposite behavior indicates positive magnetic susceptibility or paramagnetism. Figure 2-18 shows the molar susceptibility of some common organic and inorganic compounds. It is clear that mineral ions in MEG tend to be paramagnetic whereas anions in water tend to be diamagnetic. This understanding of magnetism represents the cornerstone for understanding the relationship between MFs and scale formation in aqueous solutions. Whatever the effect on scale formation (inhibition or promotion), MF treatment provides the industry with an alternative eco-friendly method to avoid the use of conventional chemical scale inhibitors.

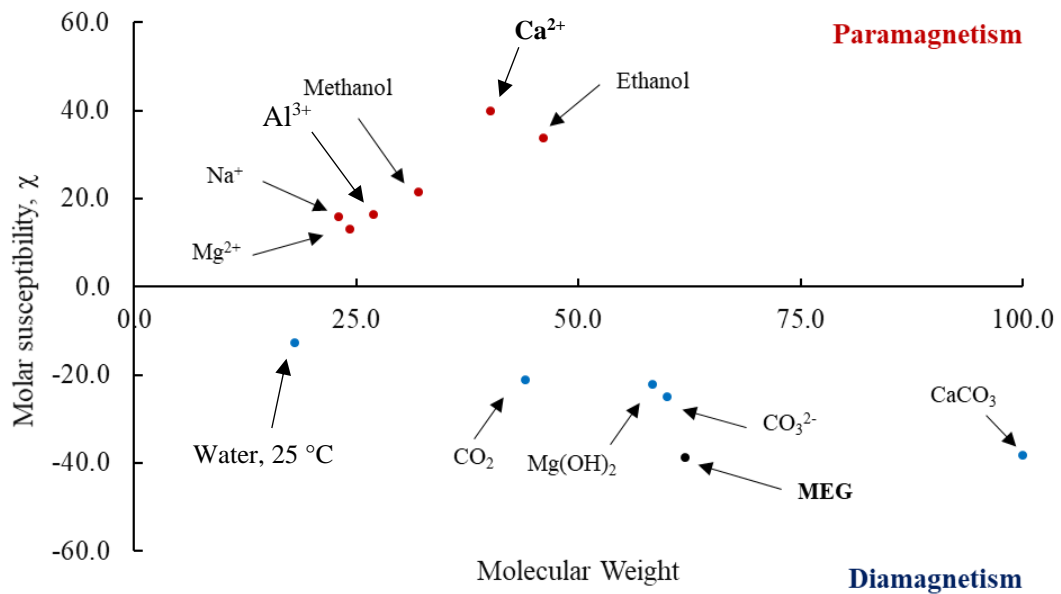


Figure 2-18 Molar susceptibility of the elements at room temperature (cgs units of 10^{-6} cm^3/mol) [217]

2.5.2.1 Effect of Magnetic Fields on the Properties of Ionic Species

Ionic mobility as a function of ionic radius, the viscosity of salt solutions, the ionic selectivity of membrane channels, and the sensitivity of particles to salting-in or salting-out are macroscopic examples of the competing interactions between dissolved ions, water, and larger molecules in solution. Thus, the extent of the influence of ions on the microscopic structure of water (as a solvent) and the structure of the ion hydration shell is highly specific to individual ions. Given the current vibrant debate about the mechanism by which descaling treatments are highly selective between cations and anions, along with the known MF effects, many of these phenomena are waiting for a microscopic interpretation beyond the simplistic definition of ions as structure makers/breakers. In particular, it should be noted that the classification of an ion as a structure maker or structure breaker also depends on its concentration.

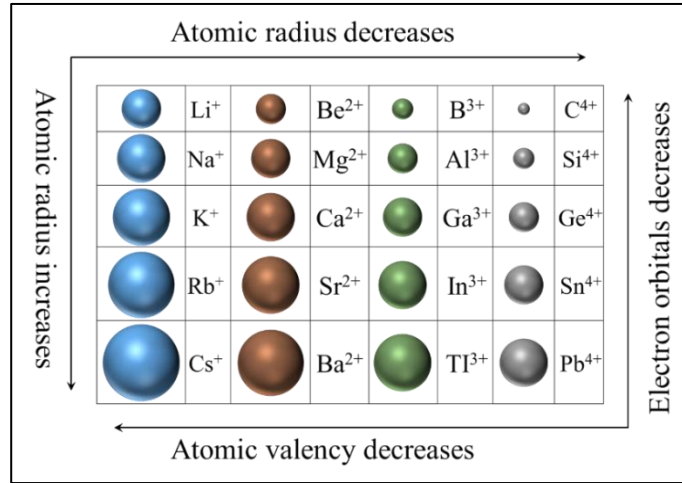
The experimental determination of the microscopic structure of aqueous salt solutions is the first step toward a detailed understanding of these properties. The ions in question have the ability to strongly reorient the local water structure, and in such case, help identify the extent to which the water structure is modified in the presence of ions.

2.5.2.2 Properties of Elements

The periodic table of elements can be used to obtain a simplified view of how MFs can affect atomic properties. The elements are arranged in the periodic table according to their atomic number and their valence. Each atom has a nucleus surrounded by electrons in different orbitals.

The number of electrons and orbitals determine the outer diameter of the element, which is considered spherical according to many hypotheses and studies.

Table 2-5 Radii of different ions in the periodic table



2.5.2.3 Trajectories of Ions under the Influence of a Magnetic Field

It is well known that ions have clear atomic structures in aqueous solutions. In addition, the intrinsic atomic properties classify atoms into superparamagnetic, mono-domain (singlet), and multi-domain (see Figure 2-19). These atomic properties are classified based on the MFs generated internally by electrons in an orbital. According to the magnetic domain theory, the critical size of a single domain is affected by several factors including the value of magnetic saturation, the strength of crystal anisotropy and exchange forces, surface or domain-wall energy, and the shape of the particles. Therefore, external MFs can distort the internal MFs, resulting in different properties in aqueous solutions containing ions. The state of the concentration of magnetizable rounded particles in an aqueous stream can be expressed as [50]:

$$\frac{F_m}{F_d} \geq 1 \quad 2-14$$

where F_m is the magnetic force on a particle [32, 48, 109, 185] and F_d is the Stokes force [29, 48, 77, 184]. These two forces influence the particle movement in an aqueous solution, where these forces can be expressed as:

$$F_m = q * v * B * \sin(\theta) \quad 2-15$$

$$F_{di} = 6 * \pi * \eta * v * r_i \quad 2-16$$

Here, r_i is the radius of a particle i , η is the dynamic viscosity of water, and v is the velocity of water flow. Equations 2-14, 2-15, and 2-16 describe the relationships between the liquid

momentum and the force of the external MF on the molecules resulting in the flocculation of magnetic particles. A reduction in liquid momentum increases the effect of the magnetic forces on the molecules and ions in the treated liquid. Thus, it is possible to control the properties of molecules and atoms after exposure to MFs by varying these factors.

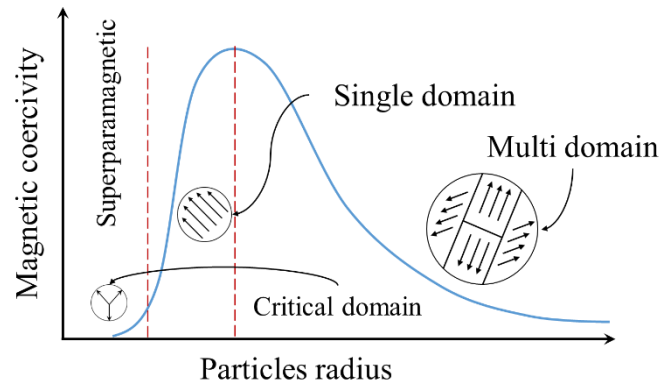


Figure 2-19 Relationship of particle size with MF coercivity [218]

The redistribution concept describes the interaction between protons and electrons according to the law of the conservation of impulse, where the impulse momentum results in electron spin. Water molecules are diamagnetic, and the spin state of water can be considered as singlet, which minimizes the electron vibrational energy of the water molecules regarding hydrogen bond formation. However, the proton spin does not depend on the singlet state of the molecule. Therefore, water molecules need not be in a paramagnetic state to show a positive interaction when exposed to an MF. However, a complete spin of a proton–electron system is required to compensate for the formation of hydrogen bonds.

2.5.2.4 Relationship of Ionic Activity and External Atomic Radius

Atoms have different radii, typically reported in angstroms or picometers. In Table 2-3, the atomic radii (r_i), hydration radius (α_i) and valences (z_i) of some ions are shown. These properties affect the ion mobility in solution because it is inversely proportional to the radius size and valence of the element. Therefore, the maximum atomic radius leads to minimum atomic mobility. The activity coefficient (γ_i) is directly proportional to the atomic radius, as shown by many mathematical relationships, such as those proposed by Debye and Hückel, MacInnes [219], and Davies [219], i.e., the Debye–Hückel and Extended Debye–Hückel models (Equation 2-17). Therefore, the activity of an element in a chemical reaction increases as the atomic radius increases; consequently, it has a higher reaction efficiency.

$$\log(\gamma_i) = -A^\circ * z_i^2 \left(\frac{\sqrt{I}}{1 + r_i * B^\circ \sqrt{I}} \right) \quad 2-17$$

Here, I , and z_i are the ionic strength (mole/kg) and the ion valence (i), respectively. The parameters A° and B° depend on the dielectric constant (ϵ) and temperature (T), as shown in Equations 2-18 and 2-19.

$$A^\circ = 1.82 * 10^6 (\epsilon * T)^{-\frac{3}{2}} \quad 2-18$$

$$B^\circ = 50.3 (\epsilon * T)^{-\frac{1}{2}} \quad 2-19$$

There are many factors affecting chemical interactions, but the most important are the size and radius of elements or particles [220, 221]. Concerning the effect of the size of elements and molecules on their interactions with each other, Glueckauf [88] and Kielland [222] have discussed how the extent of the symmetry of an element or particle involved in a chemical reaction is determined by the reaction potential. The process of a chemical reaction improves as the diameters of the interacting particles become similar in size and vice versa. However, a more comprehensive explanation is based on the diameter of the solvation shell [88, 222]. The solvation shell is defined as a layer of solvent molecules around a solute whose diameter is inversely proportional to the radius of the solute but proportional to its valence [219]. If the solvent is water, the solvation shell is often referred to as a hydration shell. The linked solvent molecules change the outer diameter of the solute and, thus, the activity coefficient [88, 220, 223]. In conclusion, if the MF can manipulate the thickness of the solvation shell, the chemical reactivity, conductivity, and solubility can be directly altered.

2.6 Effect of Magnetic Fields on Ionic Solutions

2.6.1 Hydrogen Bonds in Ionic Aqueous Solutions

The molar susceptibility of substances is crucial for evaluating the potential of MFs to affect organic or inorganic substances. Higashitani, Iseri [179] have reported that MFs affect the particles in solution rather than the bulk solution. However, the hydrogen bonds of bulk water molecules may be distorted if the external magnetic energy is sufficiently strong to influence the hydrogen bond energy. In fact, the values of hydrogen bond energies ($E_{\text{hydrogen bond}}$) for water molecules has been reported [50] to range from 5.43 to 25 kJ/mol. Because the energy generated by an external MF can be calculated using Equation 2-20, we can verify whether an external MF can influence hydrogen bonds of the water system. The below expression can be used to calculate the magnetic energy.

$$E_{\text{magnetic field}} = X_m * H * B \quad 2-20$$

Here, B is the magnetic flux density, H is the MF intensity, and X_m is the volume magnetic susceptibility.

Table 2-6 Structural parameters of water and MEG molecules

Parameter	H ₂ O Property	MEG Property
Bond length, r_b , pm	O-H = 0.96	C-O = 143, C-C = 154, C-H = 108
Bond angle, °	H-O-H = 104.52	C-C-O = 109.5
Dipole moment, D	1.8546	2.28
Polarizability, m ³	1.48×10^{-30}	5.7×10^{-30}
Force constant H-O direction, N/m	8.256×10^2	-
Bond energy, kJ/mol	O-H = 21–25 [224]	C-O = 358, C-C = 346, O-H = 467, C-H = 411
Volumetric magnetic susceptibility, cm ³ mol ⁻¹	-12.63×10^{-6}	-38.9×10^{-6}

2.6.1.1 Ion Hydration Shell in Aqueous Solution

A free water molecule has three nuclei, and the average distance between the molecules of liquid water is 276 pm, as shown by X-ray analysis. At this distance, the water molecules can hydrogen-bond with up to four molecules, forming O–H···OH₂ hydrogen bonds. The hydration shell is the solvent interface of cations and anions dissolved in water. The hydration number is the number of water molecules surrounding each of the counterions. The thickness of the water molecule shell depends on the number of involved water molecules, strength of hydrogen bonds, ion charge density, valence, size, and atomic number. In an ionic solution, ion-dipole bonds are considered as the bond between ions and water molecules, whereas hydrogen bonds can be considered as the main interaction between water molecules.

Several studies have reported that the hydration energy can be characterized by its sign, as shown in Table 2-7. According to these authors, positive hydration energies indicate the formation of strong hydrogen bonds, and negative values indicate the loss of molecules from the hydration sphere. Furthermore, it has been reported that the temperature parameter of the water–ion structure is proportional to the strengthening of H-bonds and inversely proportional to the weakening of H-bonds. Therefore, the processes occurring at the water molecule sorption boundary within the admixture can be explained as a result of the strengthening and rupturing of hydration bonds.

$$\text{Hydration shell thickness} \propto \frac{\text{Ion Electrical Charge (z)}}{\text{Ion radius (r}_i\text{)}} \quad 2-21$$

Table 2-7 Hydration energy of ions

Ion Species	ΔE_i , kcal/mol
Li ⁺	0.56

Ion Species	ΔE_i , kcal/mol
Na ⁺	0.14
K ⁺	-0.36
Cs ⁺	-0.31
Ca ²⁺	0.28
Mg ²⁺	0.8
Ba ²⁺	0.02
Cl ⁻	-0.21
SO ₄ ²⁻	0.15

Because the activity of electrolyte solutions is often far from ideal because of the effects of the ionic hydration shell, ion mobility, and ionic strength, the activity coefficient of ions can be affected by the number of surrounding water molecules. The activity coefficients of single ions cannot be experimentally measured because solution properties depend on the counterions. Theoretically, the Debye–Hückel equation can be used to calculate the single-ion activity coefficients. Therefore, the ionic activity coefficient is linked to the ionic hydration shell radius, α_i , using the correlation obtained from the Debye–Hückel theory of electrolyte systems.

2.6.2 Ionic Colloid Systems in Aqueous Solutions

It is essential to consider that the ions surrounded by a hydration sphere of solvent molecules when exposed to external MFs in aqueous solution have a spherical shape. Furthermore, the minimum particle radius should not be greater 0.5×10^{-8} m to avoid the loss of ferromagnetic properties. This hypothesis explains the effect of the MF on such ions in organic and inorganic solutions, especially under low hydrodynamic forces. In the course of an experiment, when an external MF is applied to spherical particles, their negative and positive ions are displaced in the opposite directions increasing the ionic separation until the bonding forces between these ions stop this process. At this stage, the dipole moment between opposite ions is increased. The whole process, starting from ion displacement until the end of the separation, is known as ionic polarization (see Figure 2-20). Thus, the magnetizable spherical ions in a liquid stream are subject to two types of force: the magnetic force (F_m) and the hydrodynamic force (F_d) (see Equations 2-15 and 2-16).

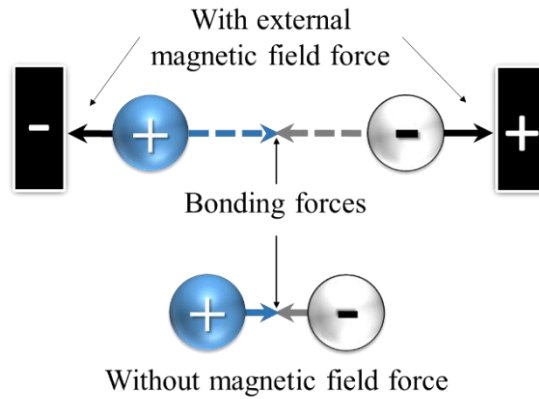


Figure 2-20 Ionic polarization under an external MF

2.6.3 Memory Effect

Magnetic memory can be described as the period in which particles can sustain their magnetization characteristics after being exposed to an MF of a certain intensity. Magnetic memory effects have been described by Higashitani, Kage [174], Ellingsen and Kristiansen [225], Tombacz, Ma [226], Higashitani, Okuhara [52], and Colic and Morse [53]. The effects of the magnetic memory on particles were recorded over time periods ranging from 10 min [225] to 150 h [52, 174]. Lychagin [227] proposed that the kinetic energy of water molecules is changed on the application of a MF. The MF affects the momentum of dipolar molecules and, thus, can induce particle aggregation [227]. After the magnetic field is removed, the generated aggregates are large and stable; thus, it is very difficult for them to return to their original shape. Similarly, Colic and Morse [54] claimed that further changes in the molecular structure of water molecules are caused by magnetic memory. This is because the magnetic memory effect can almost be permanent because of storage by aggregates [180]. The application of weak or strong magnetic fields could affect the magnetic memory of dissolved ions by increasing or reducing their activities, thus influencing the chemical interactions [34, 50]. This can be explained in terms of the magnetic susceptibility of elements in liquid phase. However, the mechanism of the memory effect in decreasing scale formation, eliminating existing scale, or producing less scale deposit is still controversial, and a clear scientific explanation does not exist yet.

2.7 Effect of Oxygen Contamination on MEG Regeneration Systems

2.7.1 Degradation of MEG Solutions

MEG regeneration plants are designed to re-concentrate and reuse the pre-injected MEG (rich MEG), to reduce dependence on fresh MEG [1, 228]. This process consists of three basic stages starting with the process of removing bicarbonate salts (pretreatment process), followed by re-concentrating the rich MEG (distillation is typically used), and finally removing the mono salts under vacuum conditions (reclamation process) [135]. These three stages operate under moderate

to relatively high temperature conditions and an oxidizing environment, affecting the quality of the recovered MEG, due to thermal oxidation [131, 229].

During the regeneration process, if MEG is exposed to high temperatures or excessive oxygen levels, degradation may occur [65, 131, 137, 230]. The thermal degradation of MEG may result in the formation of organic acids including glycolic, acetic, and formic acids (see Figure 2-21). The formation of these organic acids limits the number MEG regeneration cycles that can be performed before replacement is required [131, 139, 231] if the organic acids are not continuously removed from the closed glycol loop.

Rudenko, Gershuni [232] reported that the thermal degradation of MEG solutions may occur in the absence of oxygen molecules, specifically above 157°C. However, other reports have emphasized that thermal degradation in the oil field industry is more likely in the presence of oxygen molecules, up to 20 ppb [2, 230, 233-235]. To avoid thermally oxidized degradation products and corrosion during the regeneration processes or in the oil field, oxygen scavengers must be utilized to reduce the oxygen concentrations to less than 20 ppb. However, these oxygen scavengers should not cause further corrosion or scale formation issues such as sulfate products during oil and gas production. Although some research has been carried out using fresh MEG solutions under ideal laboratory conditions, actual oil fields or real industrial conditions have not been really simulated, stressing the need to conduct laboratory tests with the same properties of field solutions.

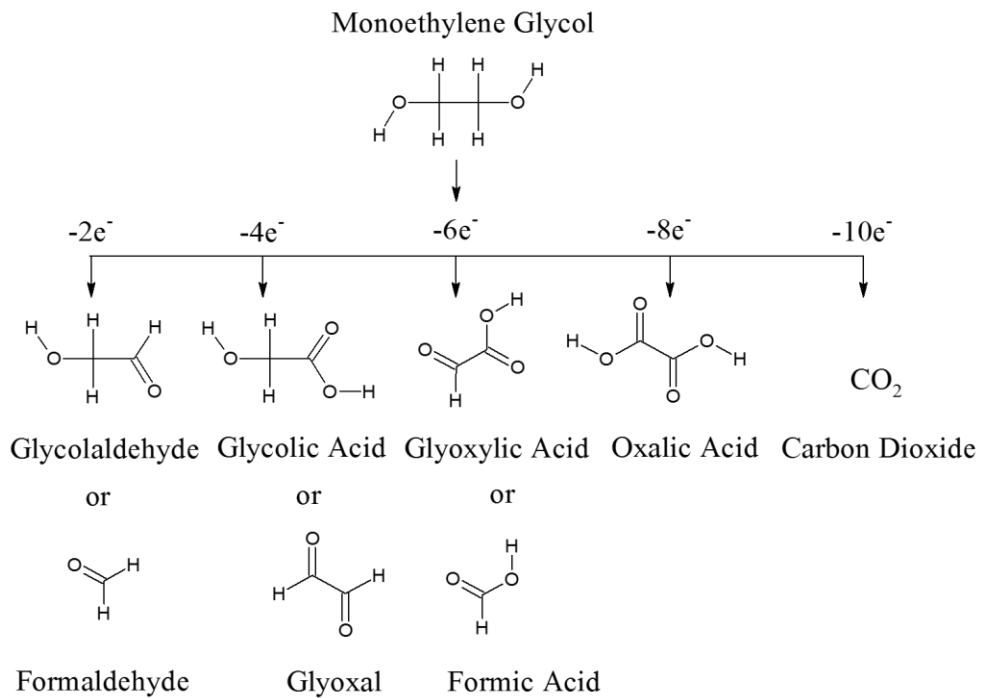


Figure 2-21 Multi-electron oxidation reactions of Mono Ethylene Glycol [236]

Numerous studies in the oil and gas industry have been conducted to evaluate the effects of the thermal aging of MEG on various operational parameters, such as the regeneration temperature [137, 237], pH [238, 239], organic acid formation [238, 239], corrosion rate [137, 239], gas hydrate thermodynamics [131], and oxidation of MEG in the presence of metals [239, 240]. However, the performance of oxygen scavengers in the presence of thermally aged lean mono ethylene glycol (TAL-MEG) solutions has received little to no attention.

Furthermore, during the production of natural gas, the breakthrough of formation water is expected, leading to the introduction of monovalent and divalent mineral ions into the MEG regeneration system [1, 64, 83, 131]. The ratio of divalent cations to bicarbonate or sulfate ions plays a crucial role in determining how scale forms inside pipelines and on hot surfaces [109, 122]. Moreover, the presence of mineral salts in large quantities can pose significant operational constraints during MEG regeneration because of their tendency to cause scaling at elevated pH values and temperatures [82, 83, 126]. Likewise, the introduction of organic acids, including acetic, propanoic, and butanoic acid, can occur in the condensed water phase if such acids are present within the reservoir [67, 235]. The presence of contaminants such as salts and organic acids has been found to influence the performance of certain oxygen scavengers, with sulfite-based oxygen scavengers being particularly affected by organic acids [234, 241]. According to several studies, organic acids including acetic acid may inhibit sulfite oxygen scavenger performance through interactions with transition metals such as the manganese that is used to catalyze the oxygen removal reaction [234, 242-244].

2.7.2 Carbon Steel Corrosion Risks

The prevention of corrosion in pipelines and process equipment is an important aspect of the continued operation of MEG regeneration facilities and transportation pipelines. Various methods of corrosion mitigation for natural gas pipelines can be applied depending upon the amount and kind of formation water within the system [64, 229, 234]. Where formation water breakthrough has not occurred, corrosion mitigation through pH stabilization is typically performed through addition of basic chemicals such as NaOH, KOH or MDEA, which promote the formation of a protective iron carbonate scale [64, 229, 233, 235, 245]. However, if formation water is produced and mineral salt ions are present, the use of film-forming corrosion inhibitors (FFCIs) is necessary to avoid issues associated with scaling at elevated pH [137, 229, 235]. Furthermore, the oxygen contamination, even in minute amounts, can also pose a corrosion risk to transportation pipelines and subsea systems constructed using corrosion resistant alloys [235, 246, 247].

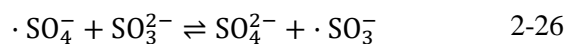
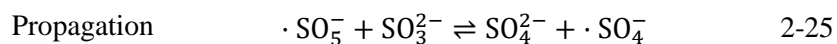
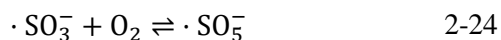
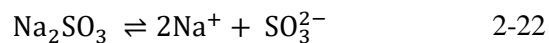
Kundu and Seiersten [230] stressed the importance of controlling the oxygen level in the injected MEG solutions to prevent problems such as the degradation of MEG and general corrosion. To prevent oxygen-based corrosion issues in MEG system, oxygen, even in minute amounts, must

be removed [234, 246]. The acceptable level of remaining oxygen in the MEG solution is less than 20 ppb; this eliminates the risk of oxygen corrosion of subsea equipment [131, 137, 230, 234, 235, 246]. Oxygen intrusion into MEG systems can occur via oxygen saturated chemicals and leakages in the units that operate under vacuum, such as the MEG reclaimers [137, 229, 230]. Additionally, industrial nitrogen may contain up to 3–5 mol. % oxygen, thus contaminating the lean MEG if it is used for storage tank blanketing [235, 248]. Oxygen-scavenging chemicals may then be added to reduce the possibility of corrosion by reducing the residual dissolved oxygen concentration to acceptable levels [230, 234, 235].

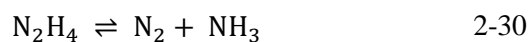
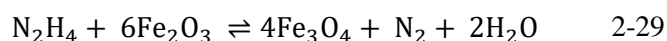
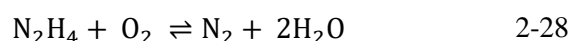
2.7.3 Typical Oxygen Scavenger Application in General Chemical Industries

The key to solving the corrosion and MEG degradation problems is to remove the oxygen. To avoid this issue, MEG solution in the MEG regeneration equipment is physically treated to deaerate the solution. Oxygen-scavenging chemicals are then added to reduce further the possibility of pitting. Chemicals commonly used for this purpose are sodium sulfite, catalysed sodium sulfite, hydrazine, and catalysed hydrazine, and amine neutralized erythorbic acid [249-252]. The authors reported that the amines substance have some catalytic effect on the erythorbic acid. Ascorbic acid has also been evaluated and discussed as an oxygen scavenger. Indeed, it is structurally very similar to erythorbic acid but has greater thermal stability.

Each of these oxygen scavengers has different problems. For instance, sodium sulfite (Na_2SO_3) reacts with O_2 to form sodium sulfate (Na_2SO_4). To scavenge oxygen effectively from the solutions, eight parts of sodium sulfite are required for each part of dissolved oxygen. The multi-step reaction mechanism of sodium sulfite with oxygen suggested by Backstrom [253], Snavely [254], and Hobson, Richardson [255] is given by Equations 2-22 to 2-27. Sodium sulfite provides efficient scavenging in moderate and low-pressure conditions with no harmful by-products [9, 234]. Its use, however, is prohibited in boilers operating at or above 124 bar where the high pressures cause the formation of sulfur dioxide and hydrogen sulfide by thermal decomposition of the chemical [9].



Theoretically, hydrazine (N₂H₄) reacts with equal parts of oxygen to produce inert nitrogen and water, but actually, 1.5 to 2.0 part of N₂H₄ are required for one part O₂ [256, 257] (refer to the equation 2-28). Since the by-products are neutral, this approach does not develop the dissolved solid concentrations in hot surface water. Furthermore, hydrazine reacts with Fe₂O₃ that is present in the hot surface to produce a passive magnitude film inside the pipelines surface, avoiding the corrosion phenomenon [258, 259] (refer to the equation 2-29). Hydrazine is an efficient scavenger at low levels of oxygen. Unfortunately, since hydrazine is volatile, its thermal decomposition takes place above 270°C to form ammonia and nitrogen (refer to the equation 2-30). Christensen and Steimel [256] reported that the development of ammonia might inhibit hydrazine activity to prevent corrosion.



Oxygen gas behaves as a depolarizer and has a direct influence on corrosion. It is necessary for the cathodic reaction to take place. However, other dissolved gases (NH₃, H₂S, and SO₂) affect corrosion indirectly.

A commonly used industrial oxygen scavenger (specifically for water treatment and in the food industry) is erythorbic acid [20, 230, 234, 249-252]. May [260] stated that erythorbic acid (D-isoascorbic acid) can scavenge oxygen rapidly at high temperatures and pressures (boiler conditions). Furthermore, ascorbic acid (L-ascorbic acid) has also been investigated and recommended as an antioxidant in the food industry because of its rapid reaction with oxygen [256, 261]. Obtaining a dissolved oxygen concentration below 20 ppb within a reasonable timeframe using an alternative oxygen scavenger would avoid the use of sulfite-based scavengers. Ascorbic acid is structurally similar to erythorbic acid but has greater thermal stability; thus, it is preferred in high-temperature industrial operations [262] (see Figure 2-22).

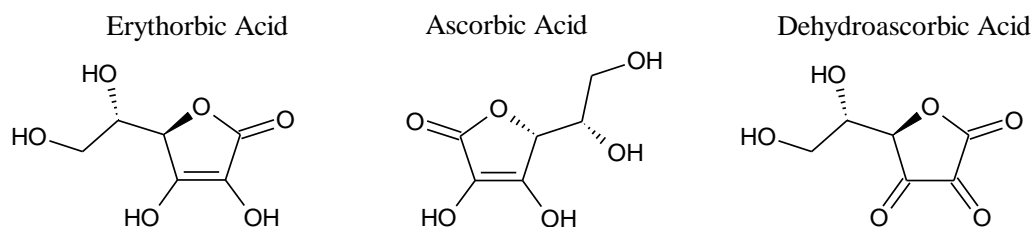


Figure 2-22 Chemical structure difference between erythorbic acid, ascorbic acid, and dehydroascorbic acid [262]

2.7.3.1 Erythorbic Acid as an Oxygen Scavenger

Erythorbic acid, a stereoisomer of ascorbic acid (vitamin C), plays a significant role in the human body and food industry. It is widely used as a supplement, additive, preservative, and an antioxidant in processed foods [251, 261, 263]. In food applications, many investigations have been carried out to evaluate the use of Erythorbic acid as an oxygen scavenger/antioxidant, including the use of different catalysts and reaction conditions [20, 252, 261, 264, 265]. Kramarenko, Hummel [261] have reported that the reaction of erythorbic acid with singlet oxygen is rapid, forming hydrogen peroxide. The general chemical reaction of erythorbic acid with oxygen molecules, as suggested by Nimse and Pal [262], is illustrated in Figure 2-23. The mechanism of oxygen consumption is typically initiated by neutralizing erythorbic acid using hydroxylamine compounds such as diethylhydroxylamine (DEHA), hydroquinone, and DEAE to form the ascorbate ion (AscH^-) [252, 256, 262, 266, 267].

The oxidation of the erythorbate/ascorbate ion is an electron transfer reaction. Therefore, the scavenging mechanism is expected to follow the same oxidation pathway as that of ascorbic acid [262]. Nimse and Pal [262] have demonstrated that ascorbate ions are capable of losing an electron to produce an ascorbate radical ($\dot{\text{A}}\text{ScH}$). This ascorbate radical initiates oxygen removal through a series of internal chemical reactions [230, 251, 262]. Furthermore, Christensen and Steimel [256] and Colton and Gilbert [268] have mentioned that the presence of transition metal ions such as Mn^{2+} , Ni^{2+} , and Cu^{2+} might improve the scavenging performance of ascorbic acid (hence, also erythorbic acid). In such systems, transition metals promote the formation of erythorbic acid radicals through improved electron transfer [230, 234, 269-271].

Various researchers have also concluded that the oxidized erythorbate/ascorbate converts to a more stable structure, dehydroascorbic/dehydroerythorbic acid, at the end of the reaction [89, 262-264]. To date, the performance of erythorbic acid as an oxygen scavenger in MEG solutions has not been investigated sufficiently. Furthermore, there is lack of literature concerning how oxygen scavengers perform within MEG regeneration plants under field conditions. This lack of information makes it difficult to evaluate the performance of erythorbic acid as an oxygen scavenger under field conditions and has, to date, limited its industrial use for MEG regeneration and in natural gas systems because of the lack of conclusive evidence of performance.

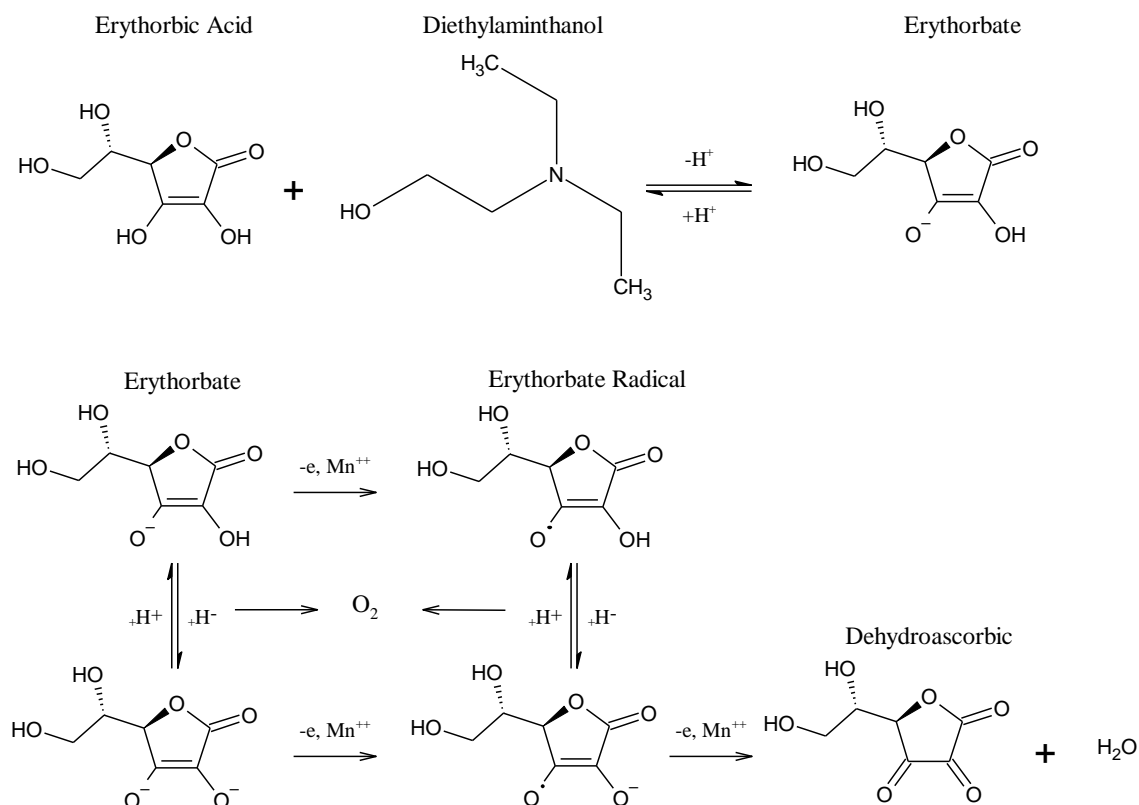


Figure 2-23 Proposed mechanism of radical scavenging activity of erythorbic acid [262]

2.7.3.2 Relationship between DEAE, Mineral Ions, and Erythorbic Acid

Several researchers have investigated the chemical reaction of DEAE with erythorbic acid [264, 266, 272]. Related to food industry, it has been reported that the interaction of DEAE with erythorbic acid can enhance oxygen removal [9, 251, 273]. Christensen and Steimel [256] stated that hydroxylamine compounds have a catalytic effect on the erythorbic acid reaction. Conversely, Crovetto, Murtagh [252] and Amjad [20] concluded that the use of DEAE in other industries is limited to combating corrosion in steam boilers by neutralizing the condensate pH. However, Kundu and Seiersten [230] and Christensen and Steimel [256] recommended the use of DEAE instead of NaOH or MDEA because of the significant improvement in oxygen scavenging performance of erythorbic acid via the scavenging reaction shown in Figure 2-23. Once added to the erythorbic acid solution, the DEAE neutralizes the erythorbic acid, forming the conjugate base, erythorbate [89, 230, 256].

However, it is still unclear how the erythorbate ion reacts with mono and divalent mineral salt ions introduced via formation water. Furthermore, erythorbic acid has been observed to undergo reactions with scale products, including calcium carbonate, thus forming calcium erythorbate [274, 275]. A wide range of minerals is typically present in the formation water, which may lead to the formation of scale such as calcium carbonate, calcium sulfate, and barium sulfate depending on the temperature and, in some instances, the pH [64, 151, 229].

2.7.4 Effect of Magnetic Field on Microscopic Properties of Aqueous System

The thermodynamic properties of water solutions are affected by several operational factors such as heat, pressure, and impurities [276-278]. Furthermore, the type and quantity of soluble substances within the liquid phase also control the responsiveness of these solutions to the external magnetic effect [18, 32, 52, 179]. Several publications have reported that an external MF can induce a significant change in the microscopic properties of the exposed aqueous solutions [169, 194, 212, 279]. For example, Otsuka and Ozeki [280] reported that strong MFs acting on a pure distilled water solution under vacuum conditions (0.0% O₂) did not change its properties. However, they observed a clear reduction in the wetting contact surface on a platinum plate, which was measured in a vacuum chamber from 65° to 57.5° after saturating the solution with 99.99% pure oxygen. Moreover, the MFs altered the interfacial water-platinum free energy by -15 mJ/cm². Researchers attributed these changes to an increase in hydration energy near the platinum surface [38, 280]. Furthermore, these treated water solutions were examined using a Raman device, and a clear strengthening was observed in the Raman spectra measurements due to oxygen clathrate-like hydrate formation. Another study has shown a clear rise in the electrochemical potential of oxygenated water from 2.34 to 2.63 V. Other research findings have also confirmed that no significant changes occur in saline solutions exposed to MFs because they are free of dissolved oxygen, contrary to the oxygenated solution results. Therefore, these studies have concluded that oxygen molecules should exist in these solutions if clear changes in the properties of water during MF treatments are to be observed. This is due to the possibility of the impact of oxygen molecules on water cluster structures via hydrogen bond interactions. Furthermore, the magnetic effects on the magnetized solutions can remain for two days due to the magnetic memory effect, according to many earlier studies [31, 52, 54, 225, 226]. Therefore, this phenomenon was the subject of interest in this study to evaluate the performance of the magnetic memory effect on solutions that have been removed from the generated MF regions.

Replacing sulfate product oxygen scavengers with erythorbic acid has been experimentally confirmed by Kundu and Seiersten [230] to be effective and applicable for oil field production. Moreover, a significant difference in the performance of erythorbic acid was reported for the F-MEG and aged-MEG solutions, specifically at alkaline conditions [230, 281]. However, the influence of external non-chemical factors on the performance of the kinetics of the microscopic reactions between oxygen molecules and an oxygen scavenger has not been investigated yet, specifically within glycolic solutions. The mechanism of oxygen scavengers has been reported and described in earlier publications [251, 256, 262]. They state that transition metals promote the formation of unstable erythorbate radicals through improved electron transfer that initiates the oxidation process [256, 262]. However, radical pairs are rarely created in steady states, but fluctuate coherently from spin-correlated electronic singlets to triplets [57, 213, 282].

Furthermore, the oscillation of radical pairs is affected by the equally nuclear hyperfine-weak electron interactions [57, 213, 282]. These specific properties of radical pairs lead to several interesting phenomena, including the alteration of reaction performance by a static magnetic field (MF).

Currently, the removal of oxygen molecules requires a highly active catalyst, to achieve an adequate removal rate for the scavenging of dissolved O₂ in glycolic solutions at ambient temperature, because it is impossible to improve the removal performance rate by heating the whole glycolic solutions. Furthermore, there has been no study on an efficient external physical catalyst to scavenge dissolved O₂ molecules in aqueous or non-aqueous solutions using an appropriate nonchemical reductant at ambient temperature. Hence, a study of the effect of MF treatment on scavenging performance following the memory effect was proposed. What is currently important is the extent to which the MF affects the performance of oxygen scavengers in F-MEG and D-MEG solutions with different saline contents and different dosages of erythorbic acid at a pH of 9.0. Therefore, this study focused on the follow-up of the decrease in oxygen concentration of these solutions before and after exposure to an MF, to determine the effectiveness of the process on the performance of the oxygen scavenger.

2.7.5 Jar Cell Technique for Oxygen Scavenger Test

The bench-scale oxygen scavenger testing conducted within this study was performed using glass testing cells fitted with airtight lids. The testing cells incorporated a pH probe and dissolved oxygen (DO) sensor supplied by Mettler Toledo. Oxygen and nitrogen gases were connected directly to the testing cells to allow continuous controlling of system conditions as well as a directly injecting of an oxygen scavenger to the glass cells via syringes. The lean MEG solution was examined under magnetized conditions as well to evaluate the scavenging performance of non-sulfite scavenger at different MEG regeneration conditions.

2.8 Free Radical Reaction Background

The chemistry of free radicals has been a matter of interest in many scientific studies to date. There have been numerous observations of the chemical and biologic reaction processes, both in aqueous and organic solutions [269, 283]. The presence of free radicals contributes to the interaction with the reactive oxygen species (ROS) which can also be stimulated in chemical or physical conditions [262, 269]. It is reported that most of the radical reactions follow the chain reaction mechanism which has three main steps; a chain initiation, a chain propagation and a chain termination. Some publications suggest that the formation of free radicals is subject to many determinants that characterize chemical reactions [57, 262, 284]. Some of these determinants were first described by Gomberg [285] and Paneth [286] when the formation of the triphenylmethyl radical was discovered [287]. Later studies were carried out to determine the

types and pathways of free radicals and to classify them to facilitate control of the reaction products [262, 283].

The most important reaction types including the free radicals are:

- Free-radical substitution reactions
- Free-radical addition reactions
- Intramolecular free radical reactions (substitution or addition)
- Free radical rearrangement reactions
- Fragmentation reactions or hemolysis
- Electron transfer
- Radical-nucleophilic aromatic substitution
- Carbon-carbon coupling reactions
- Elimination reactions

It is well known that most radical reactions often take place in the gas phase where the radical formation is formed by using UV-light or metal catalysts, redox reactions, ionizing radiation, heat, electrical discharges and electrolysis [262, 283, 288]. Other studies have stated that there is an abundance of free radicals found as intermediate substances in many organic chemical reactions [283]. For example, the practice of radical reaction in the chemical industry is a process of oxygen scavenging by using multi-hydroxyl groups that integrate with organic compounds such as formic acid, erythorbic acid, and ascorbic acid [284, 288]. This produces both free radicals and hydrogen ions, and the latter contributes to the removal of the free oxygen molecules in particular conditions [284]. Arguably, this type of process has been significantly influenced by the initial operating conditions such as the pH, temperature, and the type of transition metal catalyst, where these conditions determine the performance of the scavenging process by controlling the radical formation rate [283].

2.8.1 The Definition of a Radical Molecule

The definition of a radical is a single molecule, atom or ion with an odd number of electrons (unpaired valence electron), which make radicals highly chemically reactive compounds [213, 262]. Some molecules have multiple radical centers forming a di-radical or tri-radical molecule and so on [262]. It must be emphasized that two radicals in one molecule are not simply interpreted as a radical-pair or even as separate molecules due to the fact that radical-pairs are quantum complicated or entangled [289]. The term radical has a strong relationship with spin chemistry and its mechanism [59, 212]. It has been reported that the radical center has a spin electron within its orbital [212, 289]. Furthermore, the unpaired valence electrons have a spin

angular momentum which generates a magnetic moment and gives the spin chemistry a subject of interest during the application of the external force field [59]. In other words, the generating magnetic moment of the spinning state of unpaired electrons can be manipulated or distorted by applying an external magnetic field.

2.8.2 The Configuration of a Radical

According to Hund's rule, an opposite spin of two electrons can form interacting bonds during the chemical reactions [290]. This theory demonstrates the contribution of magnetic fields to preventing the backward chemical reaction rather than the forward reaction [289]. For instance, when the interacting bonds between the atoms are ruptured during the occurrence of chemical reactions each electron on both broken bond sides spins in the opposite direction and forms two radical pairs [289]. At this point, the promotion of the recombination mechanism occurs to reform the bond according to the chemical reaction equilibrium state of the backward reaction [289]. However, the interaction forces between the external magnetic field and spin are more likely to advance the products and break down the equilibrium. As a result, the external magnetic forces induce the occurrence of triplets rather than a singlet by flipping the electron spin of the anisotropic radical pair [57, 59, 212].

2.8.3 Radical Classification of Oxygen Molecules

Oxygen molecules typically exist as di-radicals in the atmospheric ground state as triplet oxygen, which is identified as form of low reactivities [268]. This is due to the spin-forbidden nature of the triplet-singlet transition expected for it to grab the un-paired electrons [268, 283]. However, this di-radical state produces a magnetic attraction behaviour known as paramagnetism [268, 291]. The radical-pair state is characterized as a triplet or singlet state by the coupled spin state of the two odd unpaired electrons [283, 289, 290]. The spin relationship may have opposite spin directions such as singlet (anti-spin direction) or triplet (the same spin direction) [89]. The singlet state involves one pattern of a coupled spin electron; while the triplet state exhibits three different patterns of spinning coupled electrons [89]. The radical-pair mechanism demonstrates how external magnetic fields can influence the interaction between the spin electron state and an external magnetic field [50, 58, 59, 212, 213]. It explains how a higher appearance of the triplet state stimulates radical reactions so that a triplets pattern can proceed to the products [58]. Where the singlets state is known to exist in equilibrium with the reactants and the products it cannot progress to the products [58]. Accordingly, chemical exposure to external magnetic fields can potentially transform the spinning state of the radical pair formation [50, 58, 59, 212]. As a result, radical pair theory is considered the most likely mechanism for interpreting the interaction between external magnetic fields and microstructure chemical reactions encountered in our environment and chemical systems [57, 58].

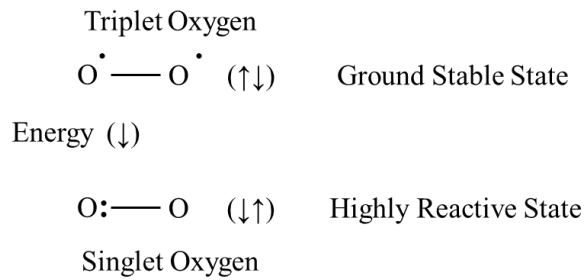


Figure 2-24 Configuration of triplet and singlet oxygen state

2.9 Measurement of MEG Concentration

The measurement of the MEG concentration is an important criterion during the regeneration process, allowing the evaluation of the efficiency of the distillation system and the control of the MEG concentration injected into the pipeline [1, 136, 292]. However, conventional methods of MEG concentration measurement during operation are challenging for plant operators [1, 292]. The main obstacles facing the plant operators is in accurately determining the concentration of MEG which can be summarized as: 1) the time required to determine the MEG concentration, which may involve shipping samples to an external laboratory for analysis, 2) the accuracy of the measurement of dilute solutions, which approach the limits of the testing devices, 3) the flexibility of the measurement process under different conditions, and, 4) the presence of mineral ions and impurities dissolved within the solution, which may cause measurement inaccuracy [292].

Numerous researchers have suggested the use of Karl Fischer titration for the determination of water content and, hence, the concentration of MEG [293-296]. In contrast, others have suggested using gas chromatography to measure the weight fraction of MEG [1, 292, 297, 298]. Recently, researchers have adopted a practical analytical method that uses different physical properties, such as the density, electrical conductivity, acoustic velocity, and refractive index, to measure the MEG concentration [1, 3, 292, 299-302].

Unfortunately, a common conclusion is that there is a deviation in accuracy when measuring the physical properties of a MEG/water mixture in the presence of impurities, and this is a fundamental limitation for accurate MEG measurement in the field [292]. The impurities, such as mineral ions, organic materials, and microbubbles, can cause a deviation in the measurement of different MEG solution parameters, such as the refractive index, density, color, and viscosity [1, 300, 303]. The measurement deviation may occur because of mineral ion interactions, which result in changes to the solution color, viscosity, or immiscibility of other compounds in the MEG/water mixture [1, 292]. In general, we can conclude that the refractive index, density, and electrical conductivity are functions of dissolved impurities in the aqueous solution and have a significant influence on the accuracy of analytical methods.

2.9.1 Determination of MEG Concentration using Physical Properties

The physical properties of MEG solutions have been investigated by several researchers who were interested in the influence of temperature on these parameters. For instance, Yang, Ma [304] studied the physical properties of water/MEG mixtures, such as the density, viscosity, and heat capacity, over the temperature range of 298.15 to 378.15 K. Furthermore, Moosavi, Motahari [300] investigated the thermophysical properties of polyethylene glycol at different temperatures. Similarly, Trimble and Potts [305] studied the relationship between the volume fractions of water/MEG versus the refractive index. However, previous studies did not investigate the impact of different salt contents on the physical properties of MEG/water solutions. In summary, the physical properties of ideal mixtures will not be representative of those of actual solutions produced by industrial processes.

To measure the volume fraction of MEG solutions in the presence of salt ions, different physical properties can be used in an alternative measurement method. For example, the refractive index is an essential physical property of a solution, describing how light propagates through the medium, and is determined by its composition [291, 306]. However, the refractive index of a solution may be influenced by the presence of salt ions, leading to inaccurate measurements, and this must be considered during measurement [1, 291, 301, 305, 307]. Commercial devices that have used the refractive index to measure the volume fraction of MEG, such as the ATAGO PAL-91S device, were not designed for accurate measurements in the presence of salts and are limited by instrument operating conditions. However, the total salinity of a solution can be reasonably predicted using portable measurement devices to estimate the electrical conductivity or total dissolved solids. As a result, these parameters can be fitted into a mathematical model to measure the corrected MEG volume fraction in regeneration plants at different degrees of salinity.

Furthermore, several commercially available in-line sensors and other devices have been developed to measure the concentration of ethylene glycol solutions [3, 308, 309]. However, in-line monitoring devices are often expensive and require regular calibration and maintenance to ensure accuracy. Common industrial contaminants, particularly mud and waxy materials, as well as inorganic scaling products, can limit the long-term accuracy of such systems if regular cleaning is not performed.

Chapter 3 Scale Formation Testing Apparatus and Procedures for the Modified Dynamic Scale Loop Using Magnetic Fields

3.1 Introduction

The positive results obtained from the use of MFs in the treatment of scale formation within aqueous solutions means that MFs are under serious consideration for industrial scale inhibition [31, 48, 55], as shown in Table 3-1. Therefore, using DSL method to evaluate the performance of non-chemical treatment is essential because of the low operational cost of the MF treatment method, in addition, it could be operated without any other requirements (i.e., it is a stand-alone technique), which is ideal for the oil and gas field conditions [19]. Hence, the adoption of DSL to examine and classify magnetic device performance should be carried out, but some modifications must be made to this technique.

Table 3-1 Parameters affected by MF treatment

Parameters	Magnetic Fields Effect
Zeta potential	Lowering zeta potential and changing sign depending on the pH of the solution [179]
Particle morphology	Produces a stable phase morphology [19, 55]
Nucleation	Decreases the nucleation rate of CaCO ₃ [55, 174]
Crystal size	Reduction in crystal size [52, 55, 172, 174]
Lorentz force	Ion-pair contact and mobility are increased but water molecule pairs are decreased. The interaction of water and ions in the admixture solution weakens [32, 97, 109]
Hydration shell thickness of ions	Hydration shell of ions decreases with increasing the mobility [29, 77, 194, 310]
Memory effect	The induction time after treatment is affected by the magnetic flux density, time of exposure, temperature of solution, charge, and type of colloidal system, and the flow rate [18, 19, 28, 52]
Mobility of ions	The mobility of counterions is increased, leading to increased electrical conductivity [28, 51, 311, 312]
Surface tension, viscosity and evaporation rate	Significant increases, except for surface tension, which fluctuates [171, 193, 202, 279]
Hydrogen bonds	Intra-cluster bonds strengths are improved, but inter-cluster bonds strengths are weakened [33, 36, 38, 313]

3.1.1 General Overview of the Modified DSL Apparatus

DSL is a known technology that has been used to evaluate the performance of chemical scale inhibitors (CSIs) in preventing the formation of inorganic scales such as calcium carbonate, calcium sulfate, and barium sulfate. The DSL apparatus consists of the following:

- Three glass bottles to feed the cation, anion, and cleaning solutions.
- High-pressure pumps (usually one pump for each solution).

- Stainless-steel capillary coils, one for scale testing and another for mixing and heating.
- Stainless-steel tubing to transfer solutions inside the DSL system.
- A temperature detector.
- A pressure detector.
- A heating chamber.
- Regulator pressure control.
- Back pressure valve.
- Temperature controller.
- Overload pressure safety sensor.
- Inline magnetic field generator.
- Inline pH probe.
- Inline electrical conductivity sensor.
- Inline ion selective electrode.
- Inline carbon steel holder for the sample to collect the scale formed in each test.
- Data recording equipment.
- PC and data control interface.

The DSL system is often fitted with an electronic circuit to control and transfer the signals between the pumps, heaters, detectors, sensors, valves, and PC interface.

3.1.2 Capillary Tube Coil Size, Dimensions, and Construction Material

Scale inhibition is usually achieved by introducing the CSI to the mixed solution line or by injecting it into the anion-containing brine or to both brine solutions. Good scale inhibition performance is considered to have been achieved when there is no increase in the differential pressure build up across the capillary tube coil. The minimum concentration that is needed to perform adequate inhibition is identified as the minimum scale inhibitor concentration (MSIC or MIC). The MIC concept could be converted to the minimum MF strength (MMFS) when using MF treatment to influence the scale formation reaction and particle morphology. The cornerstone of the DSL test apparatus is the capillary tube coil. It is made of stainless steel, carbon steel, copper, polytetrafluoroethylene (PTFE), or polyetheretherketone (PEEK). The inside diameter and length of the capillary tube vary according to the conditions of the experiment. It has been reported that the inside diameter of the capillary tube varies between 0.05 and 1.7 mm, and the length varies between 50 mm, 2 m, and 15 m, but a standard length of 1 m is commonly used.

3.1.3 Magnetic Field Generator Types, Materials, and Size

The magnetic devices used within the DSL apparatus are installed between the mixing tube and testing capillary tube. The reason for choosing this location is to allow for the magnetic device to

operate at optimum performance. Moreover, scale formation has not yet started at this point, and the brine solutions still have the initial reactants of the cations and anions. It is essential to leave a tiny gap between the magnetic poles for brine flow; this small gap results in maximum performance (see Figure 3-1). The strength of the generated MF varies according to the type, shape, and size of the magnetic device. For instance, the magnetic flux density of cylindrical type N45 (neodymium-45) magnet with a 3-inch diameter and 9-inch thickness is approximately 6500 gauss with a maximum energy product, BH_{\max} , of around 44.384 MGOe. This energy cannot be produced by other permanent magnets such as alnico, ceramic, or ferrite magnets. Therefore, it is possible to evaluate the effect of different magnetic devices on scale formation, and we can rank the magnetic devices on the basis of the field strength and inhibition performance.

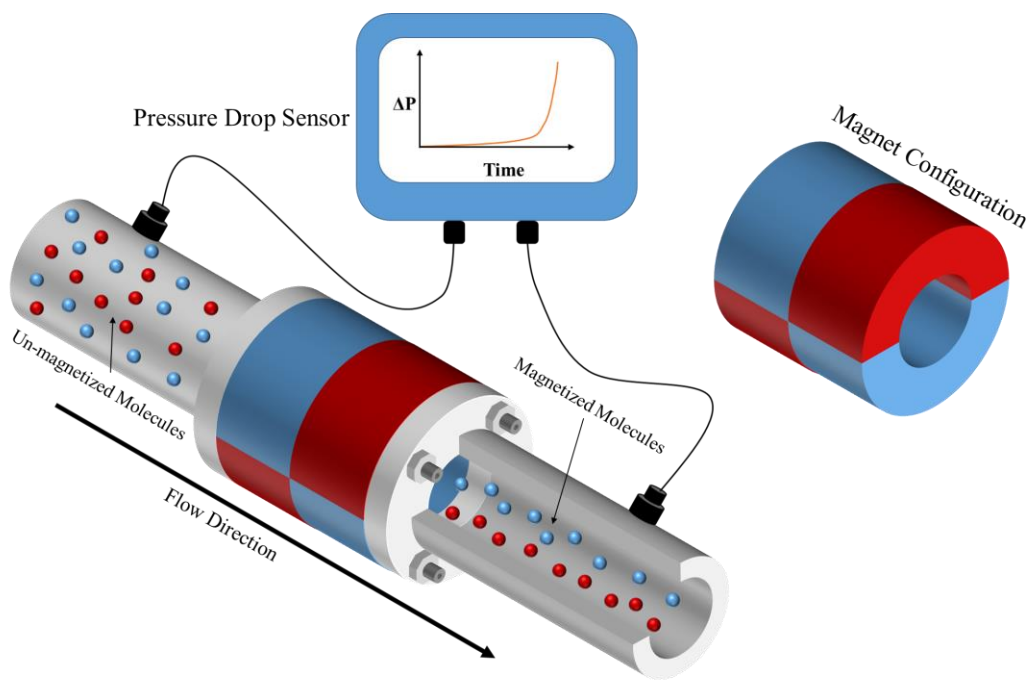


Figure 3-1 Permanent magnet shapes and configuration

To use these magnetic devices within the DSL system, they should be designed to fit the DSL requirements. For instance, permanent ferromagnetic materials such as neodymium are used to create permanent magnets. These magnets are C-shaped or mounted on C-shaped stands. Conventional steel is commonly used to create a C-shaped mount due to its high magnetic permeability. The C-form exposes the brine solution to the maximum MF (see Figure 3-1). Furthermore, permanent magnets are made in one piece of different shapes and sizes such as rectangles, cubes, and cylinders. The cylindrical shape is a robust design that suits the DSL experiments because a hole can be drilled in the center of the magnet for the passage of the brine solution in the tubing. In addition, MFs can be generated using a C-shaped ferromagnetic material with copper wire wrapped around the C-shaped metal (see Figure 3-2). The proposed design uses

a power source to convert the electric current to high strength MF across the air gap. The magnetic intensity is improved when the ferromagnetic material has a high magnetic permeability, and robust electromagnetic pulse devices that could be used in human therapy. The electromagnetic pulse device can generate up to 6000 gauss every 5 ms. The powerful MF intensity can affect ions within aqueous solutions, altering their reactivity and the formation of scale. The electronic circuit generating the magnetic pulse is illustrated in Figure 3-3. The electromagnetic pulse device has been tested for biological applications by several authors and has been shown to improve viable cell growth in organic solutions significantly compared to blank trials [314-317]. To link the magnetic pulse device to the DSL system, a stainless-steel holder instead of an inline magnetic device could be used to expose the brine solution to the MF as shown in Figure 3-4.

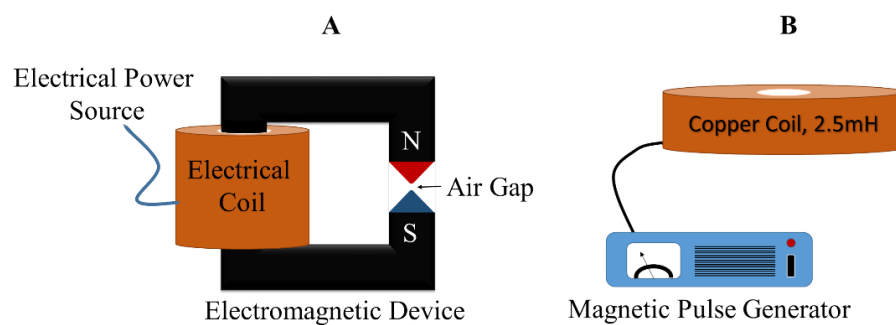


Figure 3-2 Electromagnetic devices: (A) Continuous MF and (B) Pulsed MF

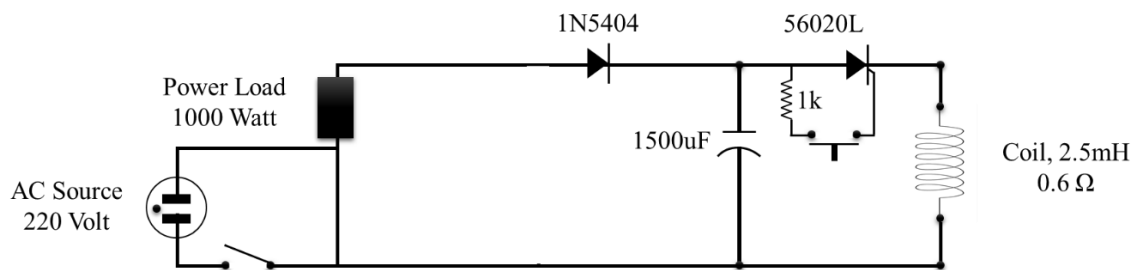


Figure 3-3 Electronic circuit diagram of a pulsed power generator, as shown in Figure 3-2-B

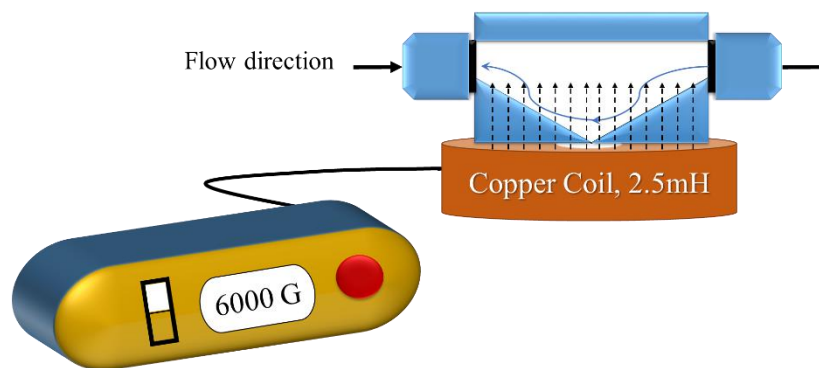


Figure 3-4 Fluid holder for the magnetic pulse technique

3.2 Test Methodologies for the Modified DSL Apparatus

3.2.1 Synthetic Brine Solutions and DSL Specifications

The concentrations of anions and cations were chosen based on the National Association of Corrosion Engineers (NACE) using a standard test method to evaluate the scale formation within the DSL [60, 147]. The cation and anion feed concentrations are listed in Table 3-2. The DSL apparatus configuration and operational conditions, as well as the probe, sensor, and detector specifications, are detailed in Table 3-3.

Table 3-2 Feed concentrations of cations and anions in the DSL test

Ion	Anion solution, mg/L	Cation solution, mg/L	Mixed solution, mg/L
Ca ²⁺	0	3313.8	1656.9
CO ₃ ²⁻	5256	0	2628
Na ⁺	15005.05	12990.8	13997.9
Cl ⁻	20033.37	25893.39	22963.4
*Ionic strength, mol/L at 25°C			0.761
*Electrical conductivity of the aqueous solution, mS/cm at 25°C			61.310

*Values were calculated using Aqion.

Table 3-3 Dynamic scale loop specifications

Component	Specifications	Notes
High-pressure liquid pumps	0.1–5 mL/min (± 0.01)	Data-logger
Back pressure valve	0–172 bar, ± 0.01 bar	Stainless steel 316
Capillary testing coil	1 m length	Stainless steel 316
	1.41 mm outside diameter	
	1.01 mm inside diameter	
Mixing coil	0.1–1.0 m length	Stainless steel 316
	3.17 mm outside diameter	
	1.01 mm inside diameter	
Pressure detector	1 bar to 172 bar	Data-logger
Heating chamber room	+30 to +250°C, ± 0.1 °C	Data-logger
pH meter and probe	1–14	Data-logger
Electrical conductivity meter	0 - 1000 mS/cm, ± 0.1 %	Data-logger
Ion selective electrode meter	0–4000 mg/L	Data-logger
PC interface	<i>winDSL</i> software	

Solutions were pre-prepared in two separate bottles, one containing the cations, such as Ca²⁺, Mg²⁺, Sr²⁺, Fe²⁺, and Ba²⁺ (as chloride salts), and the other containing the anions, such as CO₃²⁻, HCO₃⁻, and SO₃²⁻ (as sodium salts). It was essential to prepare each solution separately because of the possibility of scale formation on mixing. The initial pH is a crucial factor for initiating the reaction. For instance, it is recommended to adjust the pH of the brine solution to around 8.0 to 8.5 to initiate CaCO₃ scale formation. Real brine (seawater or formation water) could also be used as a feed solution during scale inhibitor evaluation. However, this could contaminate the system

because it contains hydrocarbons and mud, although the results obtained with these real solutions would be more accurate.

3.2.2 Dynamic Flow Loop Apparatus Operating Procedure

The brine solutions (cations and anions) are fed to the DSL system in equal amounts at specific flow rates using two high-pressure pumps. However, it is better to start the experiment with ultra-deionized water before injecting the brine solutions to stabilize the pressure and temperature sensors. The experimental pressure was maintained at a set point by using a back-pressure valve that hindered the progress of the injected solution, leading to increased pressure across the capillary coil. Before starting the test, the temperature of each test was set according to the conditions and requirements of the experiment. Once the differential pressure and temperature across the capillary coil reached the set point, the bypass valve between brine and the deionized solution was opened, and the experiment was started, either with or without the applied MF. When the mixed anion and cation solutions passed the heating coil section, scale started to form and accumulate as layers inside the capillary coil. At this stage, the pressure build-up started to increase gradually with time because of the precipitated layers of scale. Once the capillary coil was fully blocked, the overpressure detector stopped the pumps. At this moment, the brine valves for the cleaning solution line were switched off. Then, the sample holder was removed to take out the carbon steel samples for SEM analysis. After this, the pumps were turned on and the injection process was started to clean the whole system immediately. Three cases can lead to experiment failure: if the pressure built-up across the capillary tube is higher than the safety pressure point, if the cleaning solutions bottles are empty, or if the experimental period exceeds the preset duration time. The generated data after each experiment were recorded for further analyses. A schematic of the DSL apparatus is shown in

Figure 3-5.

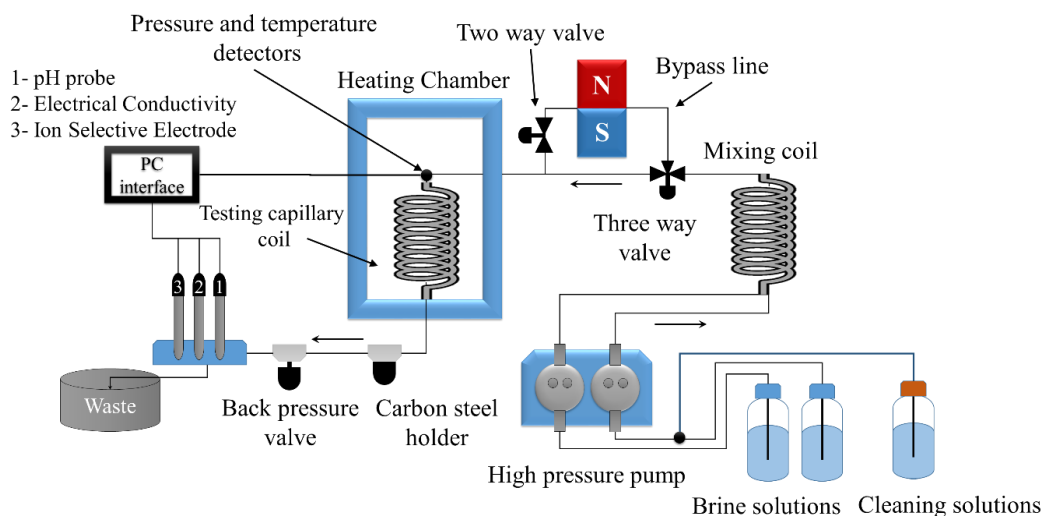


Figure 3-5 Schematic diagram of high-temperature and pressure DSL apparatus

3.3 Factors Influencing the Repeatability of DSL Tests

3.3.1 Cleaning Procedure

Cleaning after each test increases the accuracy of generated results, as well as increasing repeatability. The formation of scale that adheres to the inside of the tubing is common, so the scale should be removed before starting the next experiment. Several reports have recommended repeating each test at least three times to ensure accurate results and repeatabilities. To be more specific, remnants or scale formed on any section inside the DSL system can result in lack of repeatability. An appropriate chemical solution for cleaning the tubing is usually an acidic solution such as citric acid, maleic acid, or any weak acid. In addition, the use of an aqueous ethylenediaminetetraacetic acid (EDTA) solution can remove calcium and magnesium ions, followed by flushing with deionized water.

3.3.2 Operational Pressure and Temperature

It is essential to adjust the operating pressure for each experiment, including setting the maximum pressure offset at specific values, to obtain acceptable repeatability with the same operating condition and brine concentrations. The pressure set-point indicates the maximum pressure build-up across the capillary tube before the detector of safety pressure stops the test. For instance, when using different pressure offset, it is hard to achieve the same duration of each trial, which makes comparison difficult. However, if the offset is adjusted to one value, accurate results for each set will be achieved, thus yielding good repeatability.

Literature shows that DSL temperatures ranges from 30 to 200°C and pressures of 1 to 100 bar [61, 62, 148]. Temperatures and pressures in these ranges approximate wellhead conditions. Under the selected temperature and pressure conditions, it is possible to assess the performance of CSIs under practical conditions. Therefore, the inhibition time of different inhibitors over a range of concentrations could be evaluated by using DSL system under realistic conditions. Furthermore, different MF strengths, shapes, and poles could be investigated under different wellhead conditions.

3.3.3 Effect of Flow Rate

Fluid flow rate is usually chaotic, and changes in the velocity and tubing diameter could result in different Reynolds Numbers (Re). The Re is a critical factor in fluid mechanics, indicating whether flow conditions are turbulent or laminar. Re is inversely proportional to the kinematic viscosity (ν) of a fluid but proportional to the fluid velocity (u) and pipe diameter (d), as shown in Equation 3-1.

$$Re = \frac{u \cdot d}{\nu} \quad 3-1$$

For fluid flow in the DSL system, the internal diameter of capillary tube coil is small, ranging from 0.5 to 2 mm. Furthermore, the volumetric flow rate of the injected fluid, which is supplied by high-pressure pumps, ranges from 0 to 20 mL/min. These conditions lead to lower Reynolds numbers and, thus, laminar flow; that is, low flow rates lead to an increase in the contact time with the external magnetic device. Thus, the fluid residence time inside the capillary tube could increase, and the contact time between the solution and MF would be advantageously increased. However, a strong magnetic intensity could induce the desired reaction in seconds. This means, the flow rate parameter could be ignored when applying a high magnetic intensity. However, the flow rate is a crucial factor after exposure to low MF intensities. Therefore, the type of magnet and strength of intensity could determine the importance of the fluid flow rate factor on the magnetic performance. Moreover, the capacity of high-pressure fluid pumps and the dimensions of the capillary coils are limited to generating laminar flow patterns within the DSL system. However, trials should be conducted for the same fluid flow rates under the same operating conditions using the same magnetic intensity to generate accurate and repeatable results.

3.4 Experiment Duration

The duration required for the complete blockage of the capillary coil is the primary factor used to evaluate scale inhibitors in the DSL test method. It is also the basis for comparison of the performance of various scale inhibitors and MF treatment under the same operating conditions, for example, temperature, pressure, flow rate, and counter-ion concentration. The low MF strength used and long duration time without pressure built-up shows the efficiency of the MF in preventing scale formation within pipelines. The effectiveness of scale inhibitors for withstanding harsh conditions such as high pressure and high temperature is considered an essential performance indicator. Indeed, some inhibitors have failed to prevent scale formation in harsh conditions because of the decomposition or degradation of the chemicals at high operational temperatures. Thus, chemical inhibitors are being replaced with MF treatment because of its ability to withstand harsh operating conditions. The generated pressure build-up vs time within the capillary tube is illustrated in Figure 3-6 and Figure 3-7 respectively. They show how different magnetic field intensity and initial operating pressure could generate different time responses for pressure build-up in each test.

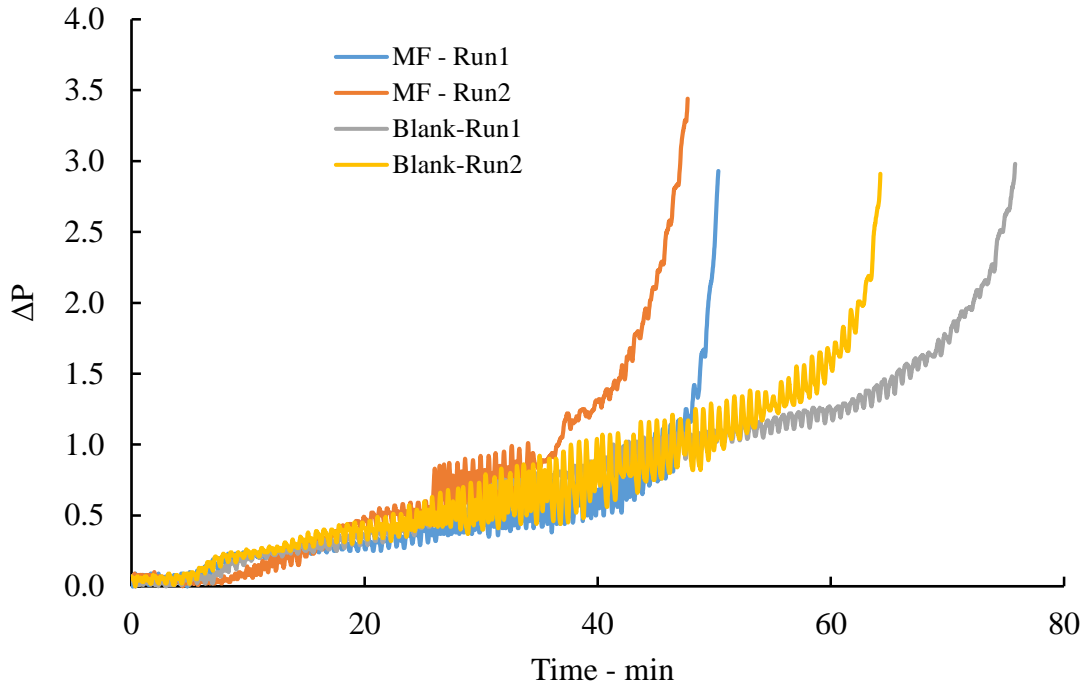


Figure 3-6 Differential pressure vs. time plot. The various curves indicate blank and different non-CSI trials at 1 bar and a flow rate of 5 mL/min

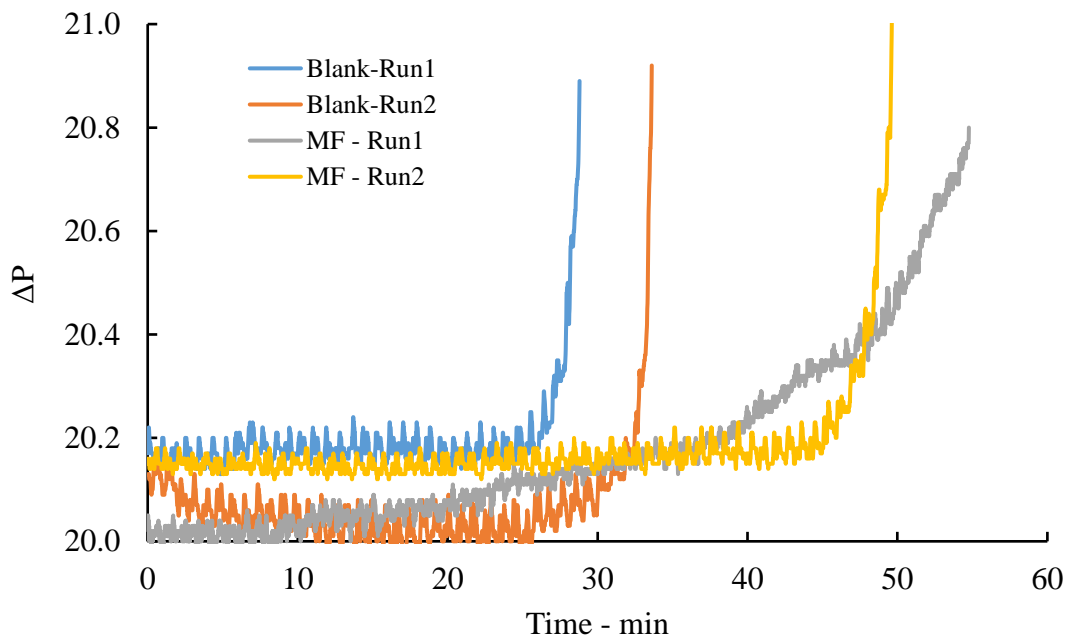


Figure 3-7 Differential pressure vs. time plot. The various curves are for blank and different non-CSI trials at 20 bar and a flow rate of 3.5 mL/min

3.5 Validation of Laboratory Tests with Actual Industrial Processes

Most domestic and industrial water treatment processes suffer from some kind of inorganic scale formation issues. These processes are often operated using continuous flow systems, wherein the

pumps and heat exchanger are used to keep the fluid moving from one section to another. To simulate the actual continuous flow process at the laboratory scale, we need to maintain circulation because it is a crucial factor for the evaluation of scale inhibitors.

There is another technique that may be used to evaluate scale inhibitors: the jar cell test method. However, the jar cell test method is a batch method, simulating units such as steam power plants and batch reactors. In this part of the study, which used the same brine concentration at the same operating conditions as in the DSL method, the morphology of the scale formed within the jar test was entirely different from that observed in the DSL tests. Therefore, the DSL technique is more likely to give a good evaluation of the scale inhibitors used in continuous industrial processes.

3.6 Location of Scale in the Capillary Tube Coil

It is hard to identify the location of scale formation within the capillary coil. The difficulty lies in the inability to open the capillary tube to see the location of the scale, as well as the absence of any technique capable of penetrating the metal capillary tube to examine the location of scale accurately. Most previous studies have been carried out using stainless-steel or carbon-steel capillary tube coils. However, other studies have used plastic or Teflon capillary coils. Plastic tubing cannot always be used to study the formation of scale by DSL because these kinds of tubing materials cannot be used at high-temperature and under high-pressure conditions.

A number of factors affect the deposition rates and growth within the capillary tubes at different locations in the capillary coil surfaces such as surface roughness, corrosion, and erosion. Several studies have reported that blockage consistently occurs in the first few centimeters of the capillary coil, whereas other reports have shown deposition extending to the middle of the capillary tube. In contrast, other studies have reported that obstructions persist to the end of the capillary tube. Therefore, the location of scale formation within the capillary tube coil is still controversial.

3.7 Effects of the MF on Thermodynamic Properties of Scale Formation

3.7.1 Effect on the Electrical Conductivity

As discussed in Section 2.5.2, there is a strong relationship between the ionic radii and the hydrodynamic force. Furthermore, the changing ionic strength may lead to different specific surface values. These relationships are vital in understanding the philosophy of MF treatment. However, another interesting factor that cannot be ignored when evaluating the effect of MFs on scale formation is the electrical conductivity. A number of studies have confirmed that there is an inverse relationship between the ionic size and electrical conductivity within a fluid. The reason for this relationship is the low ion transfer rate when the outer diameter of the ion is increased in solution, where a larger outer diameter of the ion leads to slower ionic movement. However, ions have a constant external diameter that cannot be changed. Therefore, the hydration

shell radius of the ions must be used instead of the ionic radius in this hypothesis. The hydration radius is more easily manipulated and modified depending on the thermodynamic conditions of the solutions and represents the number of participating water molecules around the ions within the fluid. According to the Nernst–Einstein equation, there is a relationship between the self-diffusion coefficient and the electrical conductivity, as shown by Equation 3-2 to 3-3.

$$EC = \left(\frac{F^2}{RT} \right) \sum_i D_i z_i^2 (\gamma_i)^\beta c_i \quad 3-2$$

$$\beta = \begin{cases} \frac{0.6}{|z_i|^{0.5}} \text{ if } I \leq 0.36 |z_i| \\ \frac{\sqrt{I}}{|z_i|} \end{cases} \quad 3-3$$

Here, F is Faraday’s constant (96485 °C/mol), T is the temperature in Kelvin, R is the gas constant (8.314 J/mol·K), z_i is the ionic species charge, and c_i is the molar concentration. D_i denotes the self-diffusion coefficient of ions, which can be calculated using the Stokes–Einstein equation. The Stokes–Einstein equation describes the relationship between the self-diffusion coefficient, D_i , of ions and the ionic radius including water molecules (a_i). This relationship can be expressed by Equation 3-4.

$$D_i = \frac{k_B T}{6 \pi \mu a_i} \quad 3-4$$

Although there is a significant relationship between self-diffusion coefficient and solution viscosity, it can be ignored after exposure to the external MF. The reason behind this assumption is that the MF has little influence on the viscosity of the solution. Therefore, the bonded interactions between the hydration shell its ions and the admixture must be considered within the solution to understand the effect of the MF. As described in Section 2.6.1, one can understand how the external MFs affect the hydrogen bonds in the water–water system and the dipole bonds in water–ion systems based on their weakening or strengthening. Therefore, the thickness of the hydration shells around ions can be predicted after exposure to a MF, making it the primary means of monitoring the influence of MFs on scale formation. Experimentally, the electrical conductivity of a solution can be measured before and after exposure to a MF. Therefore, we can easily compare the average electrical conductivity values of fluids before and after MF treatment.

According to Equation 3-4, the reduction in electrical conductivity could lead to an increase in the hydration shell thickness. This result has been proved experimentally after the exposure of different concentrations of cation and anion aqueous solutions to MFs. However, the cation/anion ratio plays an essential role in giving the opposite scale formation behaviors. It has been reported that at low and moderate calcium ion concentrations, the MF inhibits scale formation and vice

versa. Therefore, both the industrial processes and the brine concentration must be taken into consideration when evaluating the effects of external MFs on scale formation.

3.7.2 Effect on Zeta Potential

Two mechanisms describe the amount and sizes of the precipitated particles. According to the particle mechanism, although the size of precipitated particles increases, the quantity of particles decreases. However, the ionic mechanism suggests the opposite effect [55]. In addition, the particle mechanism indicates changes in the zeta potential under MF exposure. In aqueous solution studies, the zeta potential of nanosized colloids decreased after crossing a static MF, whereas the opposite results were observed with an alcoholic aqueous solution.

To describe the correlation between the potential and diffuse charge, the zeta potential in the diffuse part of the electrical double layer was assumed to have a spherical distribution. This relationship can be expressed by the following equation.

$$\frac{dy(t)}{dx(t)} \cdot \frac{dx(t)}{dt} = -0.25\varphi u_m F z c \text{Exp}\left(\frac{F z x(t)}{RT}\right) \mu B \quad 3-5$$

Here, y is the diffuse charge, x is the potential, φ is the ratio of the number of adsorbed counter-ions to the total number transferred to the Stern layer, u_m is the mobility of the counter-ions (electrophoretic mobility), z is the counter-ion charge, c is the molar concentration in the bulk, μ is the flow velocity, T is the absolute temperature, and B is the MF perpendicular to the fluid flow in the tubing lines. Equation 3-6, a first-order differential kinetic equation, can be solved numerically, and this was carried out with respect to the potential of the particle coagulation. The proposed model can predict the coagulation of aqueous solutions passing through the MF. According to the results generated from the use of Equation 3-6, the coagulation mechanism takes place, and crystallization occurs on the particle surfaces once the MF is applied, possibly because of lack of electrostatic barriers around colloid particles. However, the thermodynamic and electro-kinetic conditions could alter upon exposure to a MF, leading to different ζ and electrophoretic mobility values and hydration-shell thicknesses as shown by the following equation.

$$\zeta = \frac{\varepsilon \cdot u_m}{\mu} f(k_H \cdot R_s) \quad 3-6$$

Where, ε the dielectric constant, k_H Debye-Hückel parameter, and R_s particle radius respectively [318]. Electrophoretic mobility can be also calculated by stokes' law and force fields when the ion has reached its drift velocity as shown by the following equation [48, 85, 89, 189],

$$u_m = \frac{e \cdot z}{6 \cdot \pi \cdot \eta \cdot \alpha_i} \quad 3-7$$

where, e denotes elementary charge ($1.602176634 \times 10^{-19}$ coulomb) and r the hydrodynamic radius including water ligands.

3.7.3 Effect of MF on Scale Crystal Morphology

SEM and XRD measurements allow the changes in the morphology of the scale formed after exposure to a MF to be observed, showing shapes, size, and arrangements of the generated crystals under MF treatments. In studies of calcium carbonate, it has been reported that the aragonite morphology is formed after exposure to MFs. Aragonite is a metastable phase of CaCO_3 and is less likely to adhere to the pipeline walls. Thus, the formation of aragonite could help to overcome scale formation. However, it is necessary to study other parameters that may affect the scale morphology structure such as the pH, temperature, additives, testing mode (static or dynamic), and saturation index. Several studies have hypothesized that the temperature and the additives could determine the particle morphology and crystal phases, whereas others have stated that the temperature and testing mode are the dominant parameters affecting crystallization [9, 19]. By using carbon steel discs, the scale formed after exposure to MFs could be collected, and this would help determine which parameters affect the scale morphology under different operating conditions.

3.8 Conclusions

An experimental methodology has been proposed to minimize the cost and hazards of the conventional methods usually required to treat the scale formation commonly formed in the oil and gas industry. The methodology consists of sequential scale formation procedures that can be performed using an external MF and the DSL method. This approach reduces the chemical contamination and the total duration of the treatments.

By using this innovative DSL approach to evaluate scale formation and tendency, researchers can easily study the relationship between the MF, nucleation, crystallization, morphology, and blockage tendency in pipelines under different operating conditions. Furthermore, it would be possible to use eco-friendly treatments instead of chemical substances, which contaminate the chemical process and the environment. In addition, MF treatment is a simple, stand-alone, and low-cost method to overcome scale formation issues. The parameters that will be monitored could be easily evaluated and investigated, leading to the identification of suitable MF devices in terms of shape, size, and strength. Moreover, the mechanism of MF treatment could be understood using the DSL methods because this allows researchers to conduct more systematic investigations.

Chapter 4 Effect of Pre-treatment Process on Scale Formation in the Reboiler Section of Mono Ethylene Glycol Regeneration Plant

4.1 Introduction

MEG regeneration plants often use pretreatment vessels to precipitate divalent cations, such as Fe^{2+} , Ca^{2+} , and Mg^{2+} , to avoid and reduce fouling in the downstream reboilers and heat exchangers [2, 26, 65, 151]. The pretreatment process operates under alkaline conditions and moderate temperatures (ca. 80°C) to accelerate the formation of poorly soluble divalent salts [2, 26]. In this part of the study, we investigated whether the pretreatment process could be minimized without negatively influencing the MEG regeneration process by forming scale on the heater bundle in the presence of low concentrations of divalent cations in the rich MEG stream. The scale formation was analyzed under MEG regeneration processing conditions using a DSL, and verification experiments were carried out using a MEG regeneration and reclamation pilot plant. Various rich MEG–brine mixtures at various pretreatment pH levels and dissolved CO_2 concentrations were evaluated for their scaling tendency. An evaluation temperature of 180°C was chosen to match the skin temperature of the reboiler heater bundle during the MEG regeneration process.

4.2 Experimental Methodology

4.2.1 Test Conditions

The absolute pressure of the CO_2 gas reached in the facility was set at 44 bar, while its partial pressure was 0.5, 1.0, 2.0, or 5.0 mol. To simulate the dissolved CO_2 concentration in the pretreatment vessel and its subsequent conversion to bicarbonate and carbonate (see Figure 2-6), the concentrations of the carbonate species at specific CO_2 concentrations, and their associated pHs, were calculated using carbonate–gas/brine/water equilibrium models [119, 120, 122, 319]. The carbonate species were introduced via their respective sodium salts. Calcium chloride dihydrate powder (Scharlau, reagent grade ACS, > 99 wt. %), magnesium chloride hexahydrate powder (Chem-Supply, reagent grade, > 99 wt. %), barium chloride powder (Chem-Supply, reagent grade, 99.7 wt. %), sodium hydrogen carbonate powder (Chem-Supply, reagent grade, 99.7 wt. %), and iron chloride powder (Chem-Supply, reagent grade, 99.9 wt. %) were used to prepare the brine solutions. MEG (Chem-Supply, reagent grade, > 99 wt. %), hydrochloric acid (Chem-Supply, reagent grade, 32 wt. %), and KOH (Chem-Supply, reagent grade, 99.9 wt. %) were used to prepare the MEG solutions. Ethanol (Chem-Supply, reagent grade, > 99 wt. %), ethylenediaminetetraacetic acid disodium salt dihydrate (EDTA) solution (Chem-Supply, reagent grade, 0.1 M), and citric acid powder (Rowe Scientific Pty Ltd, reagent grade, > 98 wt. %) were used for cleaning to remove residual precipitations. Two rich MEG (61.4 wt. % MEG in water)

compositions were tested: case-1, which was high in calcium; and case-2, which was high in magnesium. In addition, we applied the following pretreatments: a) no pretreatment (pH < 5.0), b) pretreatment to >> 10 ppm TDS at pH 7.24, c) pretreatment to > 10 ppm TDS (pH > 8.85) and d) pretreatment to > 5 ppm TDS (pH > 9.40). All test cases are presented in Table 2-3. For each test involving a pretreatment step, we adjusted the pH by adding varying quantities of KOH to achieve the initial desired value. The removal of water from a rich MEG solution at a high temperature results in pH increase, since the remaining dissolved CO₂ also boils off during the process, thereby decreasing the concentration of dissolved carbonic acid Figure 4-1. In turn, this pH increase also increases the alkalinity of the aqueous glycolic system due to the accumulation of carbonate and bicarbonate ions [64, 136]. Since pH thus changes during the distillation process due to CO₂ removal, we adjusted the pH of the starting anion lean MEG solution to the value determined experimentally during lab-scale distillation (typically > 11.5) for each respective CO₂ concentration. For the experiments not involving a pretreatment, we used the pH of the initial rich MEG (typically 4.6) because any increase of pH during the regeneration process was found to be negligible.

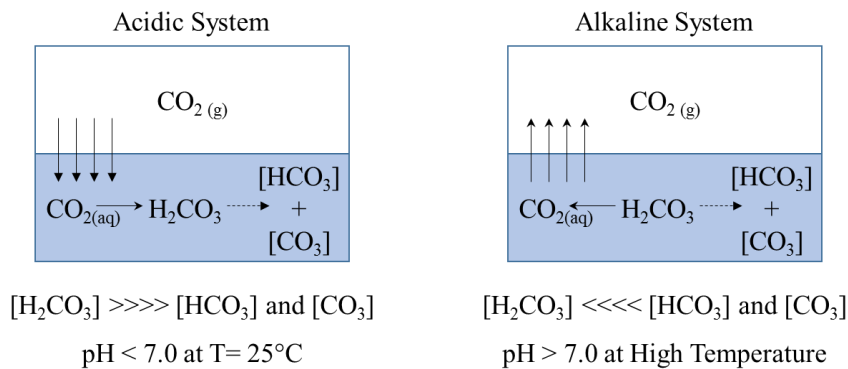


Figure 4-1 pH change in carbonate systems at different temperatures [320]

All pH measurements were recalibrated by using the Sandengen, Kaasa [321] model due to the influence of MEG on the liquid junction potential, refer to Equation 6, where w_G is the weight fraction of MEG.

$$pH_{MEG} = pH_{measured} + 0.41 w_G - 0.393 w_G^2 + 0.606 w_G^3 \quad 4-1$$

Using this method, we determined that the pH correction factor was 0.24 for 61.4 wt. % MEG solutions and 0.49 for 90 wt. % MEG solutions. The corrected pH values are presented Table 4-1 and Table 4-2. To evaluate the scaling tendency of each rich MEG solution as defined in Table 4-1 and Table 4-2, we converted the divalent ion concentrations to their corresponding 90 wt. % lean MEG concentrations. This simulated the removal of excess water that occurs during the distillation process. We also checked the prepared concentration of lean MEG solution using the

Al Helal, Soames [322] models, to ensure that the MEG concentration after water boil-off was within the suggested concentration range.

Table 4-1 Remaining divalent ions compositions in 61.4 wt. % rich MEG solution for different pretreatment (Case-1)

Ion Species	No Pretreatment	With Pretreatment		
	pH <5.0	pH 7.24	pH > 8.85	
	High TDS		TDS~10	TDS~5
0.5 mole% CO ₂				
pH _{at Rich Tank}	5.0	7.24	9.57	9.90
Ca ²⁺ , ppm	58.73	42.97	0.72	0.52
Fe ²⁺ , ppm	14.65	0.16	0.0	0.0
Mg ²⁺ , ppm	14.71	14.70	7.55	3.33
Ba ²⁺ , ppm	14.71	14.70	1.84	1.10
T _k [*] , mmol/kg	0	1.634	3.298	3.518
TDS, ppm	102.81	72.55	10.12	4.96
1.0 mole% CO ₂				
pH _{at Rich Tank}	4.91	7.24	9.23	9.56
Ca ²⁺ , ppm	58.73	18.88	0.87	0.48
Fe ²⁺ , ppm	14.65	0.07	0.0	0.0
Mg ²⁺ , ppm	14.71	14.70	6.03	3.44
Ba ²⁺ , ppm	14.71	14.70	2.98	0.95
T _k , mmol/kg	0	3.367	8.134	8.401
TDS, ppm	102.81	48.36	9.88	4.87
2.0 mole% CO ₂				
pH _{at Rich Tank}	4.80	7.24	8.85	9.40
Ca ²⁺ , ppm	58.76	14.70	0.59	0.48
Fe ²⁺ , ppm	14.65	0.04	0.0	0.0
Mg ²⁺ , ppm	14.71	14.70	6.74	2.89
Ba ²⁺ , ppm	14.71	14.70	2.63	1.52
T _k , mmol/kg	0	6.216	17.453	18.287
TDS, ppm	102.81	40.62	9.96	4.89
5.0 mole% CO ₂				
pH _{at Rich Tank}	4.70	7.24	8.85	9.40
Ca ²⁺ , ppm	58.80	6.43	0.45	0.39
Fe ²⁺ , ppm	14.65	0.02	0.0	0.0
Mg ²⁺ , ppm	14.72	14.70	8.11	3.72
Ba ²⁺ , ppm	14.72	14.70	1.32	0.87
T _k , mmol/kg	0	11.862	44.521	46.488
TDS, ppm	102.91	35.85	9.87	4.99

Table 4-2 Remaining divalent ions compositions in 61.4 wt. % rich MEG solution for different pretreatment (Case-2)

Ion Species	No Pretreatment	With Pretreatment		
	pH <5.0	pH 7.24	pH > 8.85	
	High TDS		TDS~10	TDS~5
0.5 mole% CO ₂				
pH _{at Rich Tank}	5.0	7.24	9.57	9.90
Ca ²⁺ , ppm	14.68	14.68	0.52	0.47
Fe ²⁺ , ppm	14.68	0.14	0.0	0.0
Mg ²⁺ , ppm	58.83	58.82	8.21	3.50
Ba ²⁺ , ppm	14.71	14.71	1.09	0.92
T _k , mmol/kg	0	1.832	4.255	4.538
TDS, ppm	102.81	88.34	9.82	4.89
1.0 mole% CO ₂				
pH _{at Rich Tank}	4.91	7.24	9.23	9.56
Ca ²⁺ , ppm	14.69	14.68	0.40	0.37
Fe ²⁺ , ppm	14.65	0.07	0.0	0.0
Mg ²⁺ , ppm	58.84	58.81	8.86	4.11
Ba ²⁺ , ppm	14.71	14.70	2.98	0.57
T _k , mmol/kg	0	3.594	8.88	9.338
TDS, ppm	102.88	88.27	9.90	5.05
2.0 mole% CO ₂				
pH _{at Rich Tank}	4.80	7.24	8.85	9.40
Ca ²⁺ , ppm	14.69	11.41	0.33	0.32
Fe ²⁺ , ppm	14.65	0.04	0.0	0.0
Mg ²⁺ , ppm	58.85	58.81	9.11	4.34
Ba ²⁺ , ppm	14.71	14.70	0.42	0.37
T _k , mmol/kg	0	6.372	18.083	18.921
TDS, ppm	102.91	84.97	9.87	5.04
5.0 mole% CO ₂				
pH _{at Rich Tank}	4.70	7.24	8.85	9.40
Ca ²⁺ , ppm	14.70	6.17	0.44	0.33
Fe ²⁺ , ppm	14.65	0.02	0.0	0.0
Mg ²⁺ , ppm	58.89	58.82	8.14	4.16
Ba ²⁺ , ppm	14.72	14.70	1.30	0.41
T _k , mmol/kg	0	12.289	45.524	47.280
TDS, ppm	102.98	79.72	9.89	4.89

* T_k is Total alkalinity

4.3 Dynamic Scale Loop

DSL is commonly used to test scale formation under controlled temperature, pressure, and flow rate conditions [152, 323]. Our experimental set-up is illustrated in Figure 4-2. Separate solutions containing the required cations and anions were mixed and then subjected to a temperature of 180°C (to replicate reboiler skin temperature) at atmospheric pressure. The formation of scale within the capillary tubing was monitored by measuring the differential pressure build-up across the capillary tube. A carbon steel disk (Figure 4-2) was also installed after the capillary tubing

chamber which was heated to evaluate the formation of scale crystals on a carbon steel surface. Following each experiment, we analyzed the scale formation on the carbon steel disk using SEM to determine the morphology of the deposits.

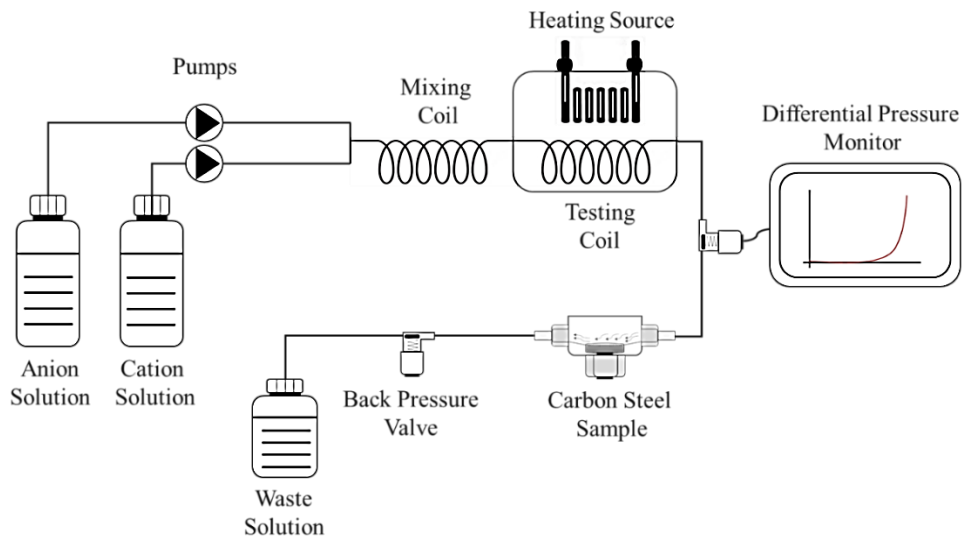


Figure 4-2 DSL configuration and in-line carbon steel disk holder

4.4 Pilot Plant Distillation

Next, we verified the experimental results generated from the DSL tests. MEG regeneration pilot plant (Figure 4-3) was used to investigate scale formation tendencies within the reboiler and heating bundle by applying two pretreatment conditions: at TDS \gg 10 ppm (pH 7.24), and at TDS \sim 10 (pH 8.85), both with 5.0 mol % CO₂ (Table 4-1). The reboiler was continually fed with the rich MEG solution (61.4 wt. %) to re-concentrate the solution in the reboiler to 90 wt. % (i.e., lean MEG). Prior to starting these tests, the rich MEG tank was sparged with 100% CO₂ gas to reach saturation. During the operation of the MEG pilot plant, the CO₂ gas that was boiled off in the distillation process was compensated for by sparging with CO₂ gas into the feed blender to ensure that the rich MEG tank solution remained at constant saturation in each cycle. The reboiler was operated at 145°C to achieve lean MEG (90 wt. %). A carbon steel sample was also installed in-line between the reboiler and lean MEG tank to assess the scaling tendency on carbon steel. A ten-micron filter was then installed to evaluate its ability to filtrate the lean MEG and remove suspended solids prior to being recycled to the lean MEG tank

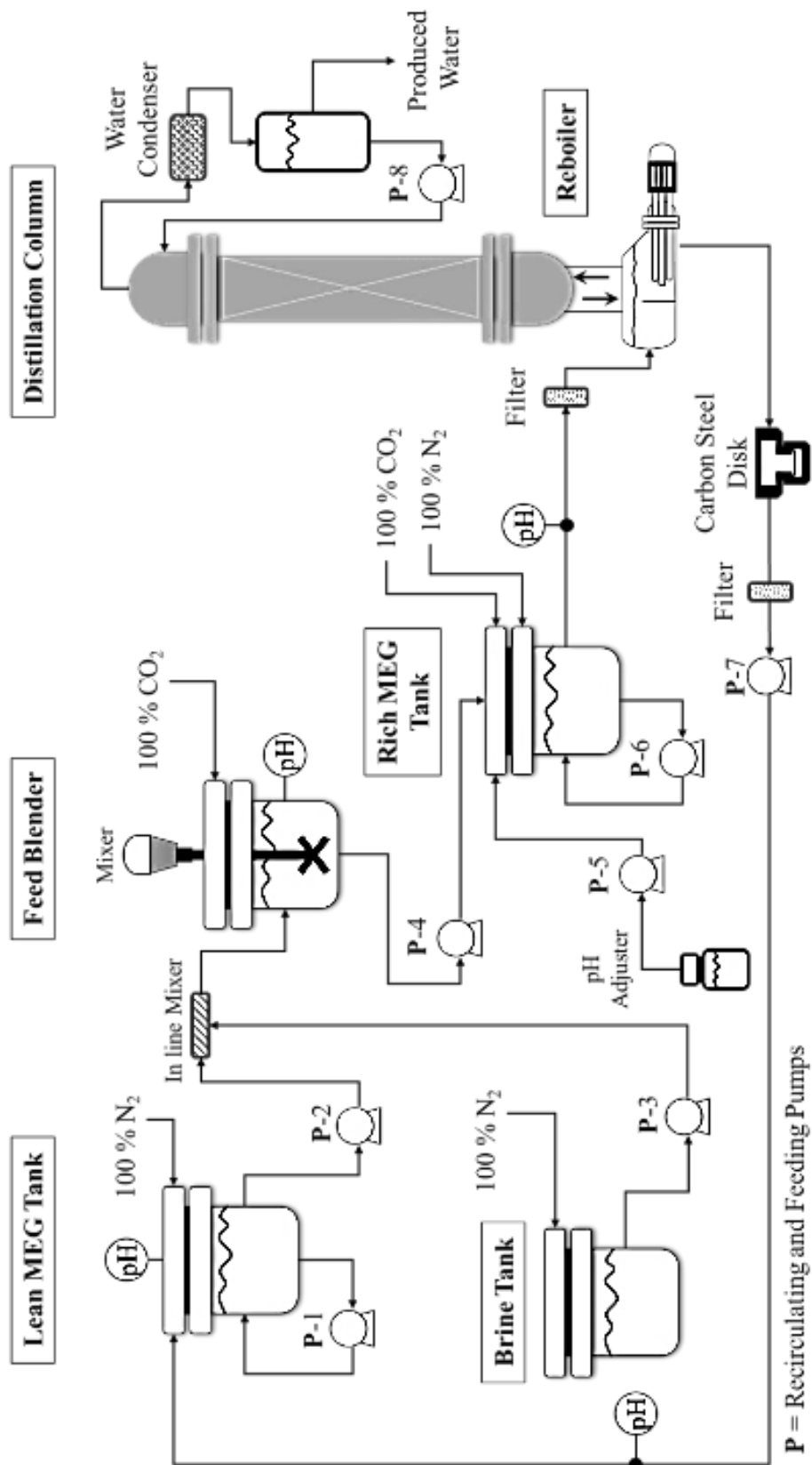


Figure 4-3 MEG pilot plant configuration

4.5 Experimental Results and Discussion

4.5.1 Alkalinity Measurements: Case-1 and Case-2 after and before DSL Testing

The total alkalinity in aqueous glycolic solutions plays an important role in controlling the rate of scale precipitation in both pretreatment vessels and reboilers [107, 119]. As shown in Figure 2-6, the number of carbonate and bicarbonate ions can be controlled by adjusting the pH value in the aqueous system. In addition, the total alkalinity can be increased by increasing the dissolved CO₂ mole% under alkaline conditions (Figure 4-1). Carbonate ions often react with sparingly soluble ions (e.g., Fe²⁺, Ca²⁺, Mg²⁺) when appropriate conditions prevail [5]. As shown in Table 4-1 and Table 4-2, in pretreatment trials with pH 7.24 at 0.5 mol % CO₂, Ferrous carbonate (FeCO₃) tended to be consumed faster than other divalent ions. This was due to the Fe²⁺ ions' greater ability to precipitate at low carbonate concentrations than other divalent ions. These results are in line with Esmaeely, et al. [7] findings, who have reported that the formation of FeCO₃ was more rapid in solutions containing low concentrations of calcium ions (10 and 100 ppm) than in solutions containing high calcium ion concentrations (> 100 ppm). When the pH of our experiment increased to > 8.85 at a constant CO₂ mole fraction, the precipitation of divalent compounds became greater. Similar responses were observed when the CO₂ mol fraction increased from 1.0 to 5.0 moles %.

4.5.2 Scale Formation Analysis

Theoretically, the pH 7.24 pretreatment level was expected to produce the worst results due to its higher concentrations of remaining divalent ions in its feed stream in comparison to the pH > 8.85 pretreatment trials (Table 4-1 and Table 4-2): the remaining high concentrations of divalent ions in the reboiler could precipitate after the CO₂ gas is boiled off, due to the significant increase in the bicarbonate and carbonate ion concentrations [2]. In contrast, we expected the pH > 8.85 pretreatment to be less risky because of the high pre-precipitation of divalent ions in its pretreatment process, which could potentially contribute to lower depositions in the reboiler [324]. We performed experimental DSL trials using the rich MEG compositions (Table 4-1 and Table 4-2) to confirm these hypotheses; Table 4-3 and Table 4-4 summarize the results. These tables show the tendency of blockage and semi blockage inside the capillary tubing which has occurred only within a pH of 7.24 for cases 1 and 2. Furthermore, they show that the calcium ion concentrations played a crucial factor to precipitate more scale layers inside the capillary tubing when abundance amounts of carbonate ions are available, specifically at CO₂ mole fraction below 2.0%. High CO₂ mole fraction (5.0 mole %) does not show blockage or semi blockage within capillary tubing due to low Calcium ions concentration in the feed stream, but it can be seen that a thin scale layer has been precipitated over the carbon steel sample.





The tendencies of the solutions to form scale are indicated by a) complete blockage of the capillary tube and scale formation on the in-line sample (red), b) formation of scale on in-line sample (orange), c) partial blockage of the capillary tubing and scale formation on the in-line sample (yellow), and d), no scale formation (green), respectively.

Table 4-3 Summary of lab-scale DSL results at high TDS, ppm

CO ₂ mole %		No Pretreatment				With Pretreatment					
		pH 5.0				pH 7.24*					
		Ca ²⁺	Red	Orange	Yellow	Green	Ca ²⁺	Red	Orange	Yellow	Green
Case-1	0.5	58.73				•	42.97		•		
	1.0	58.73				•	18.88	•			
	2.0	58.76				•	14.70	•			
	5.0	58.80				•	6.43			•	
Case-2	0.5	14.68				•	14.68		•		
	1.0	14.69				•	14.68	•			
	2.0	14.69				•	11.41	•			
	5.0	14.70				•	6.17			•	

Table 4-4 Summary of lab-scale DSL results at low TDS (10 to 5 ppm)

CO ₂ mole %		With Pretreatment									
		pH >8.85*									
		Ca ²⁺	Red	Orange	Yellow	Green	Ca ²⁺	Red	Orange	Yellow	Green
Case-1	0.5	0.72			•		0.52			•	
	1.0	0.87			•		0.48			•	
	2.0	0.59			•		0.48			•	
	5.0	0.45			•		0.39			•	
Case-2	0.5	0.52			•		9.66			•	
	1.0	0.40			•		9.32			•	
	2.0	0.33			•		9.15			•	
	5.0	0.44			•		9.15			•	

	Complete blockage of the capillary tube and scale formation on the in-line sample
	Partially blockage of the capillary tube due to low initial Ca ²⁺ concentrations
	Formation of scale on the in-line sample at very low Calcium ion concentrations
	No scale formation
*	The tests were re-adjusted to pH > 11.4 to match the reboiler pH

4.5.3 Dynamic Scale Loop Method

With no pretreatment (pH < 5.0), no scale formation was observed. With the pH 7.24 pretreatment, scale formation was primarily observed for cases 1 and 2, with complete blockage of the capillary tubing achieved at 2.0 mol CO₂ and 1.0 mol CO₂, and semi-blockage at 0.5 mol CO₂, as illustrated in Figure 4-4, Figure 4-5, 7 by a sharp increase in the pressure across the capillary tube. The feeding concentrations of the Ca²⁺ divalent ions were the highest of all the other evaluated cases at 2.0, 1.0, and 0.5 mole % CO₂. In contrast, lowered concentrations of divalent ions injected from the rich MEG tank reduced blockage (Table 4-3). As a result, the high

remaining concentration of divalent ions ultimately facilitated the significant growth of calcium carbonate scale within the capillary tube, leading to increasing differential pressure build-up across the capillary coil. We were also interested to observe the differential pressure build-up fluctuated between 0.5 bar and 2.2 bar, leading to a semi-blocked capillary (Figure 4-5 and 7). This was because the accumulated scale formation inside the capillary coil led to the acceleration of the blockage of the capillary coil, resulting in a pressure increase. The pressure build-up on the blocked area then caused a breakdown in the formed deposit layers, indicating that the amount of formed scale was insufficient to block the flow through the capillary coil. However, over the long term, this issue could lead to the accumulation of several scale layers, thereby creating a full blockage.

In addition, with the 7.24 pH pretreatment, scale was formed on the in-line carbon steel samples, which were exposed to solutions containing 5.0 mol % CO₂. We expected greater scale formation with the pH > 8.85 pretreatment; however, for cases 1 and 2 at 5.0 mol % CO₂ content, we observed no differential pressure build-up (complete or partial blockage) due to the low concentrations of calcium ions that were fed to the DSL capillary coil (Table 4-1 and Table 4-2). These low calcium ion concentrations were caused by the pretreatment process. Nonetheless, a thin layer of scale was still formed on the surface of carbon steel disk, confirming the tendency for scale deposition on hot surfaces and pipelines, which can affect the long-term performance of hot surfaces. Similar results were observed with the ~10 and ~5 ppm TDS pretreatment conditions. The formation of scale on the in-line carbon steel sample was observed in cases 1 and 2 for all CO₂ concentrations, but no blockage occurred (see Figure 4-7 and Figure 4-8). These results indicate that, at both pretreatment levels, the formation of scale on carbon steel surfaces at 180°C (i.e., the reboiler bundle temperature) is likely. However, due to the low initial concentrations of calcium ions that, which were fed to the DSL system, the rate of solid formation within the capillary tubing was insufficient to cause blockage under the continuous flow conditions.

We also sought to investigate the amorphous dispersion of scale formation that caused the blockage and non-blockage behaviors. SEM analysis conducted on the carbon steel samples primarily indicated the formation of different calcium carbonate polymorphs, including calcite, vaterite, and aragonite. Where significant levels of magnesium were present, the formation of dolomite (a combination of calcium, magnesium, and carbonate) also occurred. The SEM images of the carbon steel in-line samples are presented in Figure 4-8 and highlight the different types of scale; these were confirmed using Energy-Dispersive Spectroscopy (EDS). They indicate that CaCO₃ is aragonite amorphous at high temperatures and high MEG concentrations; this is in line with previously published results [5, 106].

Another interesting result was the presence of a high concentration of Mg^{2+} ions (Table 4-2), which could affect the MEG pilot plant flow assurance, particularly in highly alkaline conditions. This was due to the fact that at pH values higher than 10, the Mg^{2+} ions tended to interact with the hydroxide ions in the reboiler, forming gel-like Magnesium hydroxide ($Mg(OH)_2$), which can accumulate on the surface of filters and prevent flow. These results are discussed in greater detail in section 4.5.4.4.

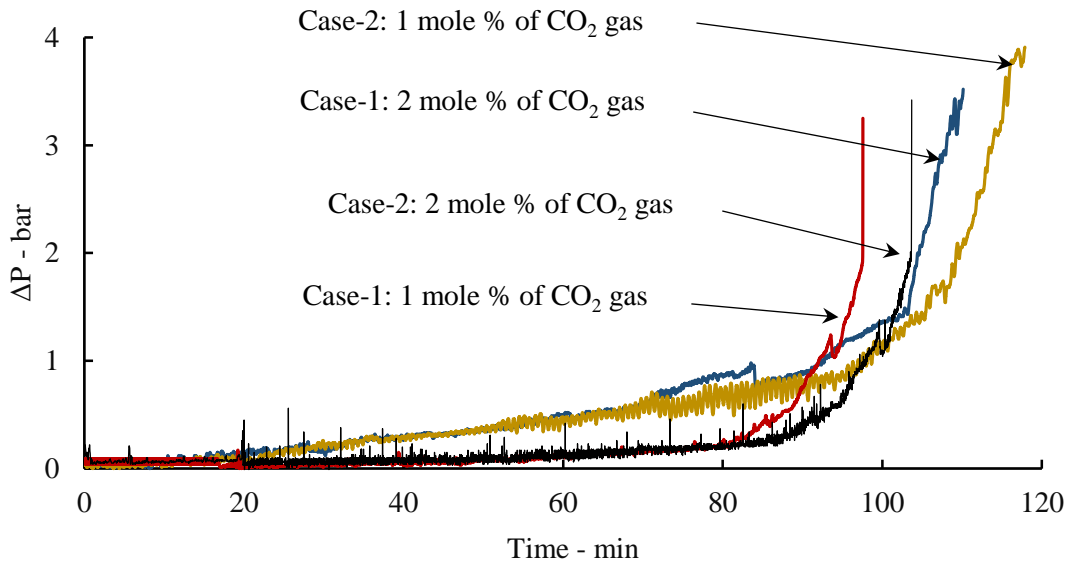


Figure 4-4 Differential pressure build-up over the capillary tube for case-1 and case-2 after pH adjustment to 7.24 (complete blockage)

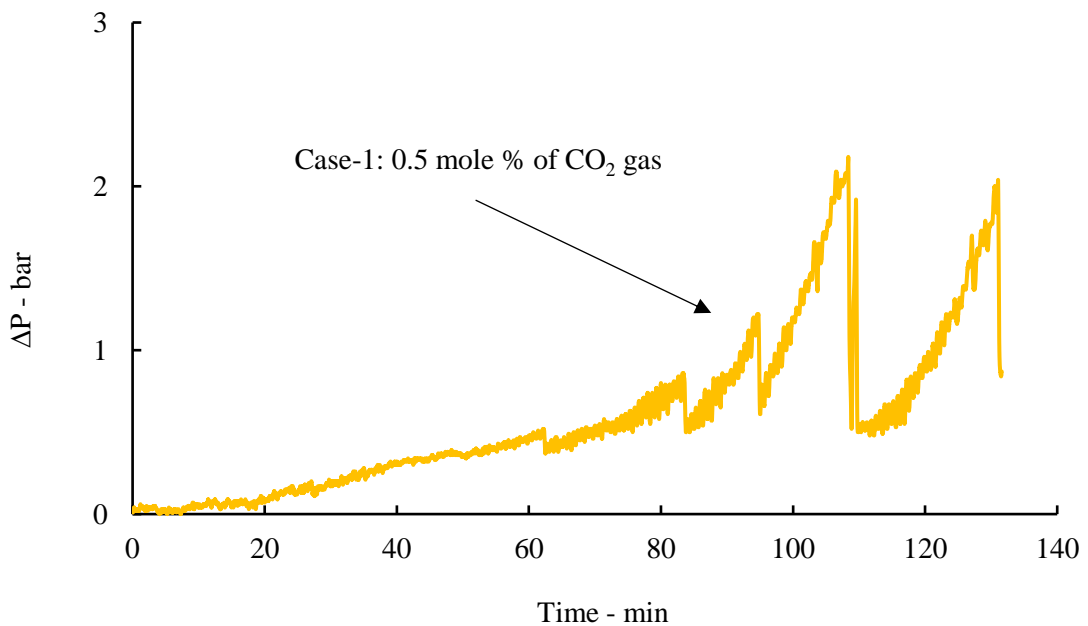


Figure 4-5 Differential pressure build-up over the capillary tube for case-1 0.5 mole % CO_2 after pH adjustment to 7.24 (semi-blockage)

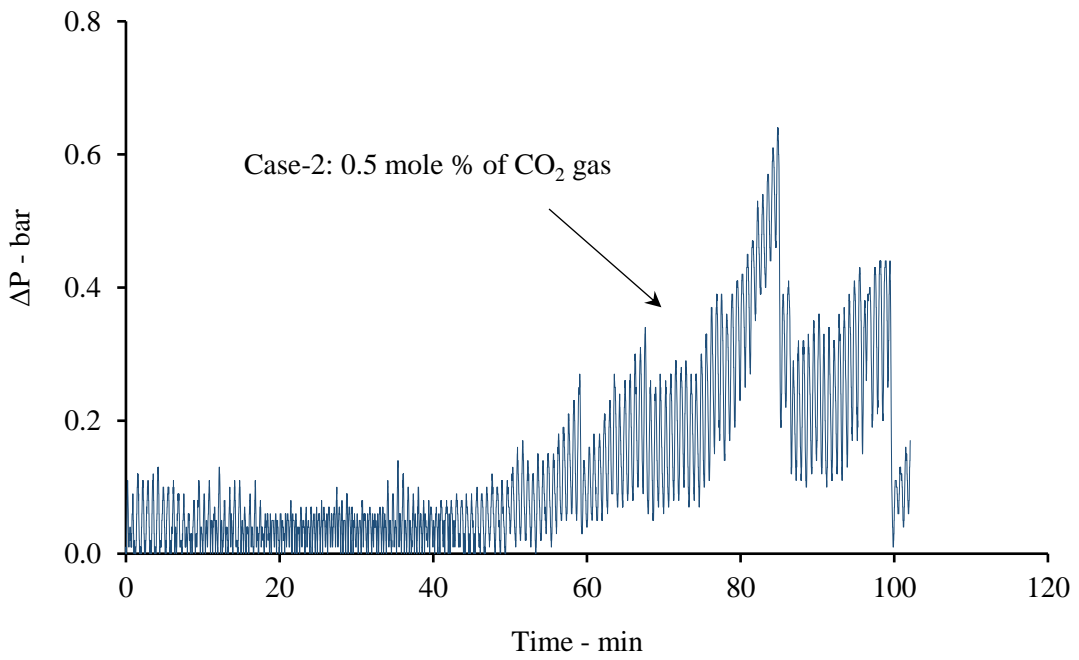


Figure 4-6 Differential pressure build-up over the capillary tube for case-2 0.5 mole % CO₂ after pH adjustment at 7.24 (semi-blockage)

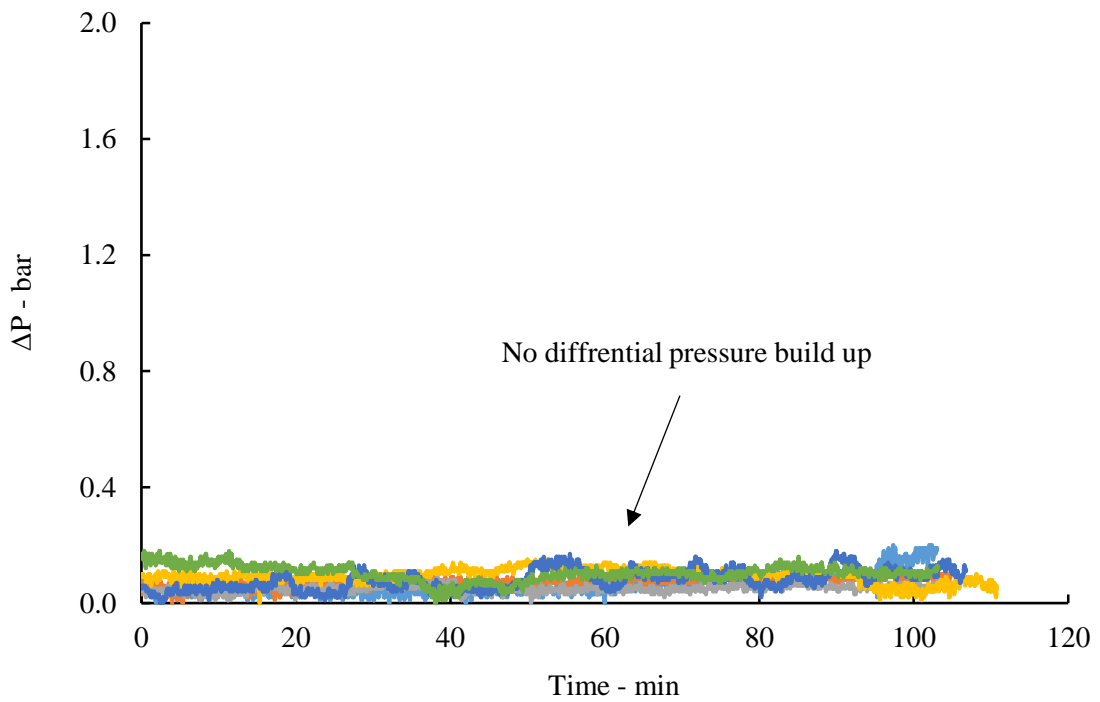


Figure 4-7 Differential pressure build-up over the capillary tube for case-1 and case-2 of some of the remaining red indicator trials as shown in Table 4-3 and Table 4-4 after pH adjustment

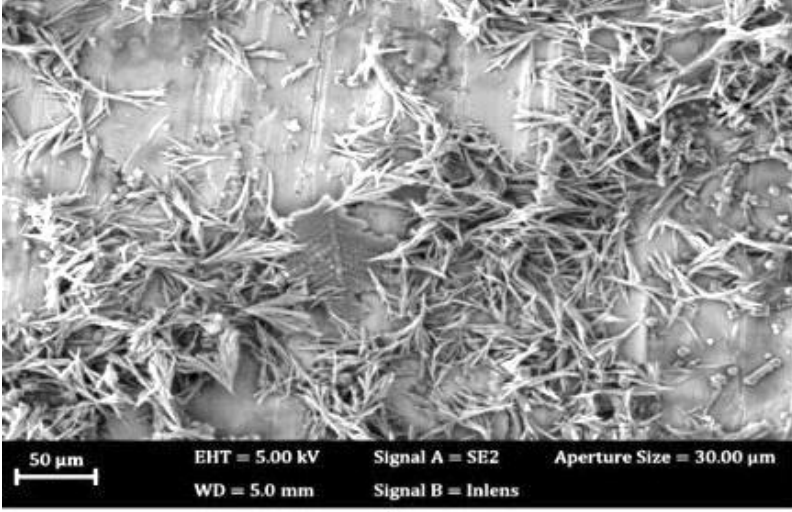

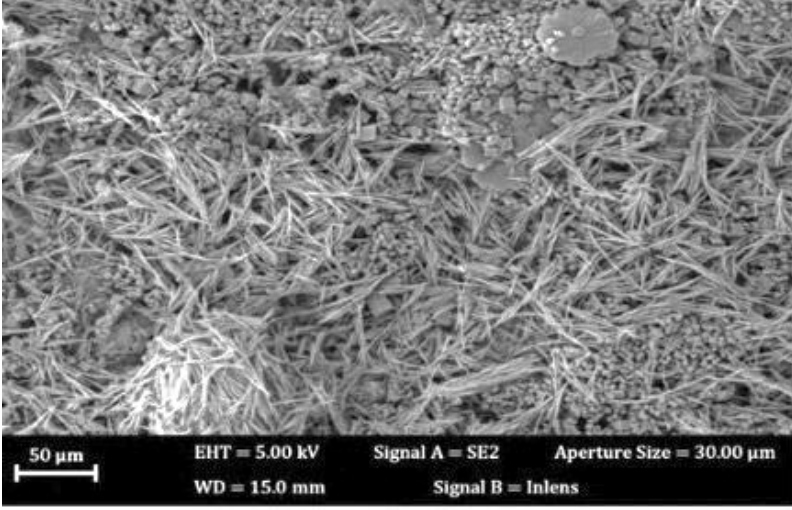
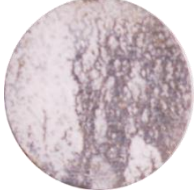

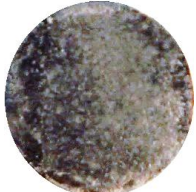
SEM analysis case-1, (DSL test) in-line sample 0.5% CO ₂ pretreatment pH of 7.24	
	 <p>Complete blockage</p>
SEM analysis case-1, (DSL test) in-line sample 2.0% CO ₂ pretreatment pH of 7.24	
	 <p>Complete blockage</p>
SEM analysis case-2, (DSL test) in-line sample 0.5% CO ₂ pretreatment 10 ppm	
	 <p>Semi-blockage</p>

Figure 4-8 Scale formation on carbon steel of selected MEG pilot plant trials of case-1

4.5.4 MEG Pilot Plant Distillation

To verify scale formation within the reboiler, two additional case-1 tests (pH 7.24 pretreatment and TDS ~ 10 ppm pretreatment) were conducted in MEG regeneration pilot plant to confirm the results generated by the DSL experiments.

4.5.4.1 Case-1: Pretreatment pH of 7.24 at 5.0 mole % CO₂

To maintain a pH of 7.24 within the rich MEG product, we continuously injected it with KOH to neutralize the incoming acidic CO₂-rich MEG mixture. The neutralized mixture was then pumped into the reboiler of the distillation column to re-concentrate the rich MEG solution into lean MEG. Consistent with our lab distillation test results, we noted a significant increase in the pH readings in the reboiler section when the rich MEG solution was concentrated and reached 90 wt. % MEG (Figure 4-9). We furthermore observed that the reboiler temperature caused the water content to be partially boiled off, including CO₂ gas, which affected the carbonate dissociation equilibria (reactions 1 and 2). The removal of CO₂ gas therefore concentrated the hydroxide and carbonate ions in the reboiler, promoting the formation of scale.

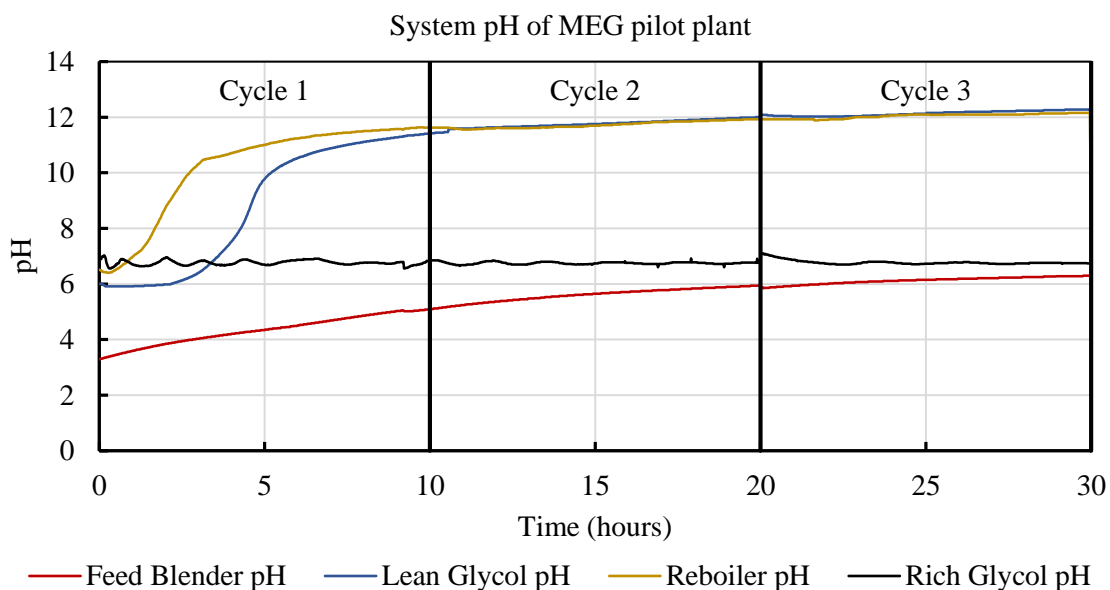


Figure 4-9 Effect of CO₂ removal and hydroxide concentration on system pH

4.5.4.2 Formation of Scale within the Reboiler System

After continually operating the MEG pilot plant for three inventory turnovers (cycles), significant scale formation in the reboiler was observed. As shown in Figure 4-10, scale accumulated along the inner wall of the reboiler. The in-line carbon steel disk also demonstrated strong scaling (Figure 4-11). Figure 4-12 also shows the similarity of the scale structures that formed in both the DSL and MEG pilot plant experiments. SEM analysis of the rough surface of the carbon steel disk indicated different CaCO₃ polymorph structures, including calcite, aragonite, and vaterite.

The results of the pilot plant were thus again consistent with the DSL results. Furthermore, as can be observed from Figure 4-11, the structure of the polymorph formed using both methods indicated to scaling issues. The scale formation on carbon steel disk highlights the high probability of scale formation along tubing lines and carbon steel reboiler bundles at high temperatures. However, a minimal amount of scale was observed along the reboiler's heating bundle. This can be attributed to the heating bundle's stainless steel material, which has a low surface roughness compared to typical industrial bundles manufactured from carbon steel. Overall, we concluded that a pH 7.24 for pretreatment process is not recommended due to its high probability of scale formation, which would require excessive reboiler cleanings to prevent the loss of heat transfer efficiency and tubing blockage.

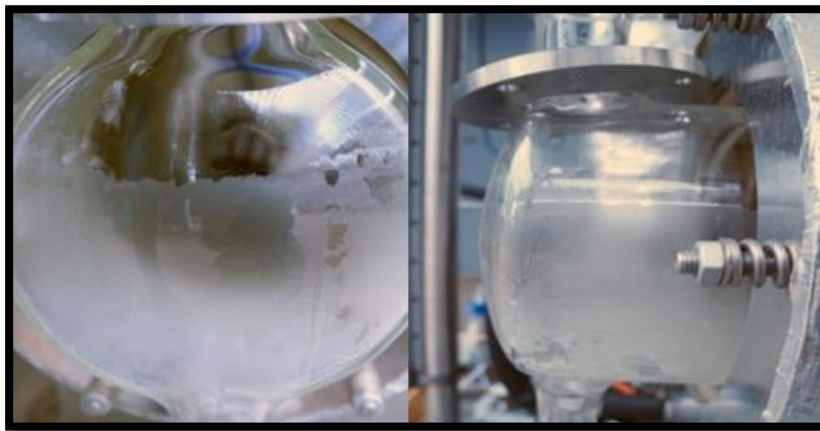
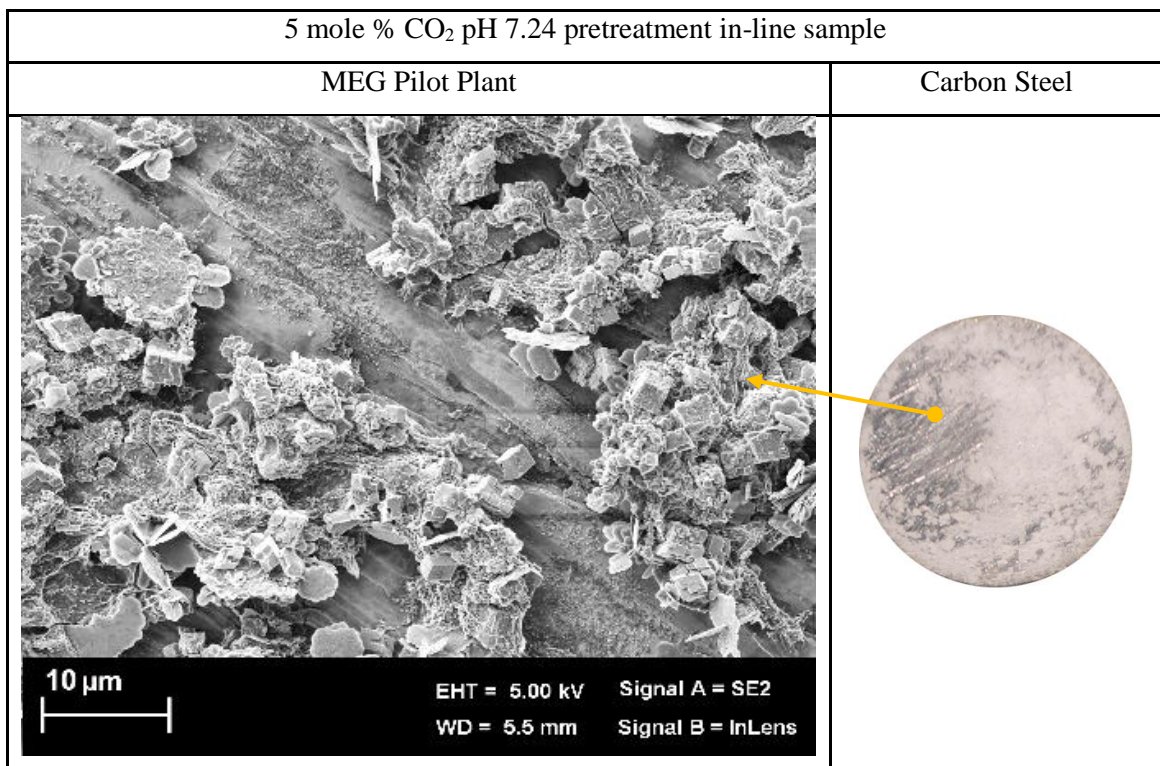
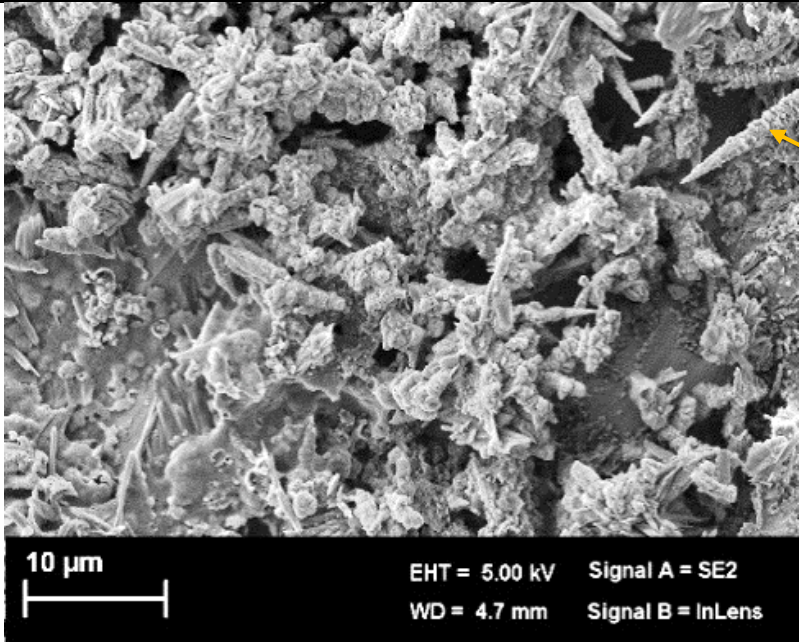
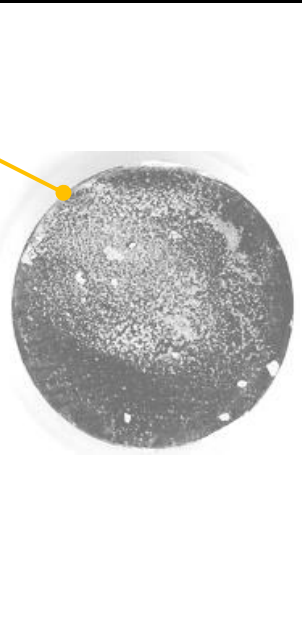
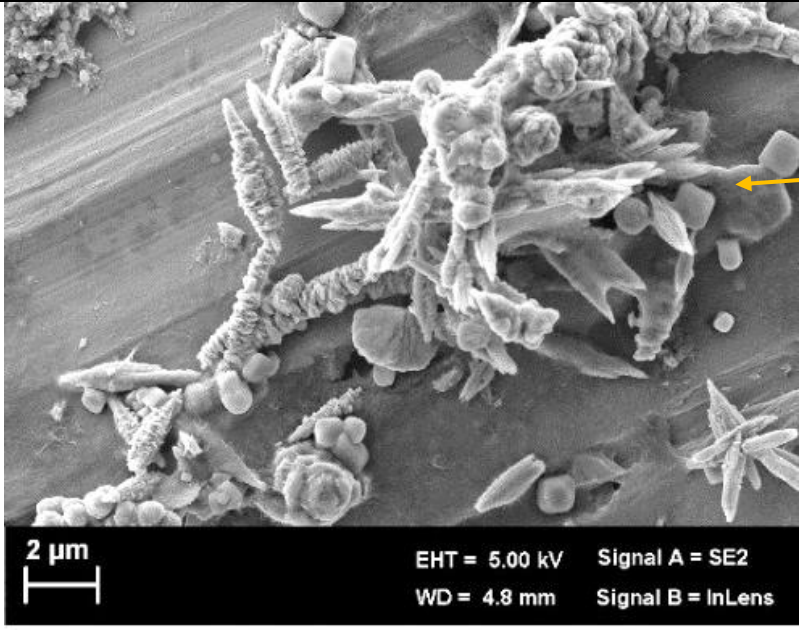
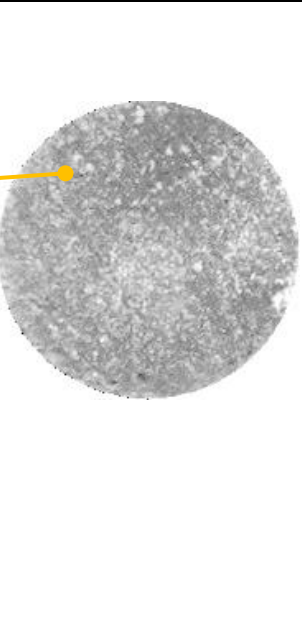


Figure 4-10 Scale formation on reboiler wall



5 mole% CO ₂ TDS 10ppm pretreatment in-line sample	
MEG Pilot Plant	Carbon Steel
	
5 mole% CO ₂ pH 7.24 pretreatment sample	
DSL Test	Carbon Steel
	
5 mole% CO ₂ TDS 10 ppm pretreatment sample	
DSL Test	Carbon Steel

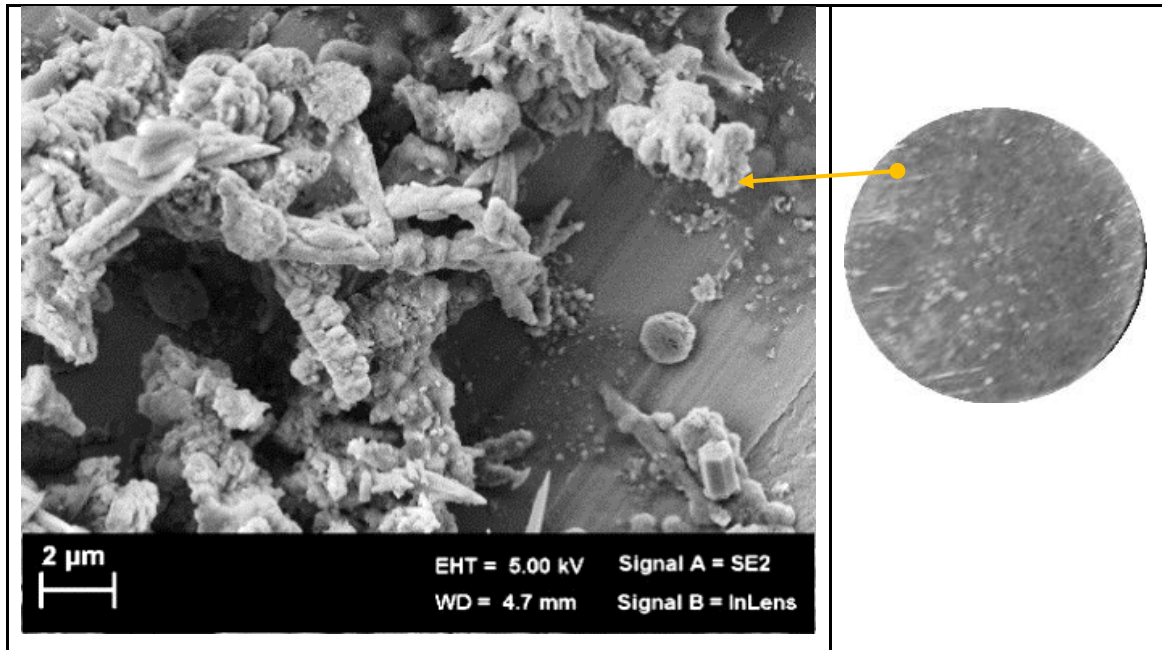


Figure 4-11 Scale formation on carbon steel of selected MEG pilot plant trials of case-1

4.5.4.3 Case-1: Pretreatment of TDS ~ 10ppm at 5.0 mole % CO₂

The entire regeneration system (including the reboiler walls and bundle, the in-line carbon steel sample, and the stainless steel level sensor submerged in the liquid) exhibited significant scale formation when using the ~ 10 ppm pretreatment divalent salt concentrations at 5.0 mol CO₂. A high pH (8.85) was maintained within the rich MEG tank to simulate the pretreatment and facilitate the conversion of bicarbonate to carbonate, which, once formed within the reboiler, ultimately promoted the formation of carbonate scale; this was also consistent with the DSL results. In addition, the rise in pH within the reboiler produced a lean MEG with a pH in excess of 11.5, thus increasing the potential for scale formation. SEM analysis indicated the formation of primarily calcium and magnesium carbonate scale, including calcite, vaterite, and dolomite; this was confirmed by EDS and X-ray diffraction tests for some samples. Figure 4-12 and 14 illustrate the formation of scale within the reboiler and highlight the forming of a scale layer on the glass wall as well as a thick coat of white scale on the heating bundle. The scale formed on the walls of the reboiler was of extremely fine nature, indicating primarily dolomite formation. In contrast, we judged that scale formed on the heating bundle consisted primarily of calcium carbonate (white color and ease of removal using citric acid).



Figure 4-12 Formation of scale on the reboiler wall



Figure 4-13 Formation of scale on reboiler bundle and pump head

4.5.4.4 Micro-Filters before and after Reboiler Process

Our findings also highlight the ability of magnesium ions to precipitate under highly alkaline conditions. The solutions containing brine were passed through the DSL mixing coil using a 2 μm filter, which was used to protect the capillary tubing from impurities (Figure 4-2). We found that a gel-like slurry started to accumulate on the surface of the micro-filter. A similar result was observed for a MEG pilot plant filter, as shown in Figure 4-14. We analyzed the gel-like slurry using EDS and found it to be $\text{Mg}(\text{OH})_2$, likely formed by the high alkalinity within the reboiler [20, 325]. The slurry increased the viscosity of the MEG-brine solution since a 50 wt. % $\text{Mg}(\text{OH})_2$ slurry has an approximate viscosity of 400 cp [326]. Furthermore, increased

viscosity influences scaling formation behavior on hot surfaces during shut-down and cool-down [4], and the diffusivity of CO_2 also drops with increasing viscosity [134]. The presence of $\text{Mg}(\text{OH})_2$ thus changes the physio-chemical properties of water-glycol solutions. However, several studies have reported that the solubility of $\text{Mg}(\text{OH})_2$ in water is very low and that it continues to decrease with increasing temperatures [20, 326]. These effects, particularly within a reboiler, would likely influence a MEG pilot plant operation.



After the commencement of operation

Before the commencement of operation

Figure 4-14 $\text{Mg}(\text{OH})_2$ material formed on the micro-filter surface of the MEG pilot plant

4.5.5 Proposed Scale Cleaning

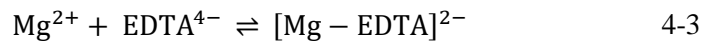
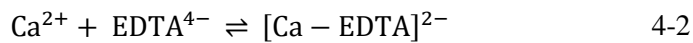
4.5.5.1 pH 7.24 Pretreatment at High Divalent Ion Concentrations

Following the formation of scale within the reboiler, a 5 wt. % citric acid solution was used to remove residual scale from both the wall of the round flask and the carbon steel samples. Citric acid solution easily removed the majority of scale from the walls and bottom of the carbon steel samples (using a squeeze-bottle application). To ensure that all scale had been removed from the samples, citric acid solution was then boiled and the carbon steel samples were re-washed using distilled water. However, some scale still remained, primarily on the top surface of the carbon steel samples. A variety of solvents were used to try and remove the remaining scale, including 10 wt. % citric acid, 1 wt. % HCl, ethanol, and acetate, but all were unsuccessful. Ultimately, to completely remove the scale from the carbon steel we had to physically remove it, as we did with the scale from the lab-scale distillation testing. It thus became apparent that using the pH 7.24 pretreatment resulted in the formation of scale that is extremely difficult to remove; this treatment should therefore be avoided in the field to prevent the need for excessive cleaning and reductions in reboiler efficiency.

4.5.5.2 pH > 8.85 Pretreatment at Low Divalent Concentrations

The initial cleaning of the reboiler was conducted with a 5 wt. % citric acid solution. The carbon steel sample was immersed in 5 wt. % citric acid and allowed to soak for approximately six hours

before being drained and subsequently cleaned with distilled water and ethanol. The initial cleaning with citric acid failed to remove all of the calcium carbonate scale from the carbon steel sample. To remove the remaining scale, we applied a solution of 5 wt. % citric acid and 2 wt. % EDTA. EDTA and citric acid act as chelating agents, directly reacting with heavy metal ions to form complexes and thus allowing their removal [327, 328]. To facilitate the removal of calcium and magnesium with EDTA, the pH of the cleaning solution was increased to approximately 9–10 [327]. The high pH allowed the EDTA to readily dissolve in water and this facilitated the reaction between the EDTA ions and the calcium and magnesium. The high pH also has the advantage of preventing the corrosion of carbon steel surfaces. We found that the EDTA was capable of removing a significant portion of the scale left on carbon steel after approximately two hours of soaking time. However, some scale still remained on the top surface of carbon steel. We recommend its complete removal using high-pressurized water.



The combination of EDTA followed by high-pressurized water cleaning procedure is recommended if heavy calcium and magnesium scaling occurs within the reboiler along both the reboiler bundle and the walls. If the scale consists primarily of calcium carbonate, cleaning with 5 wt. % citric acid is sufficient.

4.6 Conclusions

Our results will allow MEG regeneration plant operators to evaluate reboiler units under harsh conditions to prevent the occurrence of worst-case scenarios during field operations. Our primary findings indicate that low concentrations of divalent ions have a high likelihood of forming scale inside conveyer tubing and reboiler bundles even when using a pretreatment process in a MEG regeneration plant. The pretreatment vessel thus cannot be minimized without harming the MEG regeneration process.

The following conclusions can be drawn from these results:

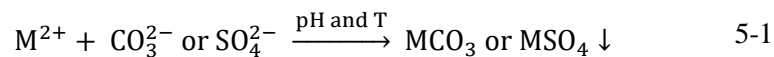
1. The primary scaling product identified for rich MEG solution (cases 1 and 2) was calcium carbonate in the form of calcite, vaterite, and dolomite.
2. In both cases 1 and 2, complete blockage of the capillary coil occurred during the DSL tests at a pretreatment pH of 7.24 at 1 and 2 mol CO₂, while partial blockage occurred at 0.5 mol CO₂.

3. The formation of calcium carbonate scale primarily occurred inside the DSL capillary tube at divalent cation concentrations of 10 and 5 ppm at 5 mol % CO₂, without any significant pressure build-up.
4. The DSL results were consistent with those from the MEG regeneration pilot plant.
5. The higher the concentration of CO₃²⁻ at the beginning of the experiment, the more likely the blocking of the capillary tubing.
6. Operating in highly alkaline conditions with a high concentration of magnesium ions led to the precipitation of magnesium hydroxide, which precipitated within the in-line filters and on hot surfaces.

Chapter 5 Influence of Magnetic Fields on Calcium Carbonate Scaling in Aqueous Solutions at 150°C and 1 Bar

5.1 Introduction

During the production of natural gas and oil, in most cases, some water is formed, known as formation water [2, 4]. This water contains dissolved mineral ions such as Calcium, Magnesium, Iron, Strontium, and Barium [5, 26]. Carbonate and bicarbonate ions can interact with existing salts to form inorganic scale [5, 10, 118]. Preventing scale formation requires the use of chemical scale inhibitors, which are often classified as acidic agents, to prevent the clogging of transportation pipelines and equipment [25, 62, 160, 214]. Nevertheless, these acidic treatments increase equipment corrosion [25, 153], reducing the effectiveness of these strategies. Other operational conditions such as the pressure, temperature, H₂S/CO₂ partial pressure ratio and pH are also crucial factors affecting mineral ion precipitation, as well as affecting the polymorphism of the formed scale [26, 106, 329]. Scaling is a severe problem in the natural gas and oil industry if not professionally controlled.



In this part of the study, experiments were conducted to evaluate the effect of magnetic field treatment upon the scale forming tendency of brine solutions containing, primarily, calcium bicarbonate. The results were generated using a DSL system where the brine solution was exposed to a magnetic field generated by a 6480-gauss grade N45SH magnet of in a diametrical orientation for 2.5 s. Following magnetic exposure, the brine solution was exposed to an elevated temperature, 150°C, at 1 bar to promote the formation of scale within a capillary tube. The extent of scaling was measured by recording the differential pressure across the tube as scaling proceeded.

5.2 Experimental Methodology

5.2.1 Chemicals and Equipment Used

5.2.1.1 Brine Solutions

Three water systems were utilized in these investigations. Each set contained a different initial concentration ratio of calcium to bicarbonate ions. Where set one contained high bicarbonate ion (high HCO₃⁻, approximately 3000 ppm) with low Calcium ion (Ca²⁺, approximately 110 ppm). Set two contained high Calcium ions (high Ca²⁺, approximately 8200 ppm) with low bicarbonate ion (HCO₃⁻, approximately 150 ppm), and lastly, set three contained equal amounts of calcium and bicarbonate ions (Ca²⁺ = HCO₃⁻, approximately 700 ppm). The ionic charges of all solutions

were balanced by addition of sodium chloride, and the ionic strengths were calculated for each solution, as shown in Table 5-1. These three sets were utilized in this study to simulate brine water at a different ionic strengths and different saturation index levels to investigate the influence of AMT upon the Ca^{2+} and HCO_3^- ions.

5.2.1.2 Chemicals Used

The chemical makeup of the brine solutions consisted of calcium chloride dihydrate powder (Scharlau reagent grade ACS, >99%), magnesium chloride hexahydrate powder (Chem-Supply reagent grade, >99%), sodium chloride powder (chem-supply reagent grade, 99.7%), sodium hydrogen carbonate powder Chem-Supply reagent grade, 99.7%), ethylene diamine tetraacetic acid disodium salt dihydrate (EDTA solution) (chem-supply reagent grade, 0.1 Molar), citric acid powder (ROWE Scientific PTY LTD reagent grade, >98%).

The relevant chemical compositions of the brine solutions are listed in Table 5-1.

Table 5-1 Brine water concentrations for sets 1, 2 and 3

Set-1: High bicarbonate low calcium

Ion	Bicarbonate, (mg/L)	Calcium, (mg/L)	Mixed Solution at DSL, (mg/L)
Na^+	12257	12257	12257
Mg^{2+}	-	100	50
Ca^{2+}	-	220	110
Cl^-	15416	19583	17499.5
HCO_3^-	6000	-	3000
pH	8.20	6.36	pH= 7.16*, pH= 6.88**
Ionic Strength, mole/L			0.54***

Set-2: Low bicarbonate high calcium

Ions	Bicarbonate, (mg/L)	Calcium, (mg/L)	Mixed Solution at DSL, (mg/L)
Na^+	2000	2000	2000
Mg^{2+}	-	100	50
Ca^{2+}	-	16400	8300
Cl^-	2910	32392	17651
HCO_3^-	300	-	150
pH	8.19	6.36	pH= 7.16*, pH= 5.85**
Ionic Strength, mole/L			0.707***

Set-3: Equal bicarbonate and calcium

Ions	Bicarbonate, (mg/L)	Calcium, (mg/L)	Mixed Solution at DSL, (mg/L)
Na^+	10600	10600	10600
Mg^{2+}	-	100	50
Ca^{2+}	-	1400	700
Cl^-	15533.4	19116	17325
HCO_3^-	1400	-	700

Ions	Bicarbonate, (mg/L)	Calcium, (mg/L)	Mixed Solution at DSL, (mg/L)
pH	8.20	6.34	pH= 7.16*, pH= 5.6**
Ionic Strength, mole/L			0.517***

* Initial pH of mixed solution before injection to DSL.

** Final pH of the mixed solution after injection to DSL.

*** Aqion software was used to calculate the required parameters such as ionic strength.

5.2.2 Cleaning Procedure

The cleaning method is an important step to keep the apparatus clean and to ensure accurate test results. Firstly, the capillary tubes and tubing lines were cleaned with citric acid 20 gm/L to dissolve any depositions followed by 8 gm/L of Ethylene Diamine Tetraacetic Acid Disodium salt Dihydrate (EDTA disodium, pH≈8.0) to react with the remaining divalent ions such as calcium and magnesium. Then the DSL tubes were flushed with deionized water before performing the proceeding tests. Furthermore, before starting any experiment, deionized water was injected into the DSL system for at least 30 minutes to stabilize all the sensors and detectors such as pH, electrical conductivity, thermocouples and the pressure sensor. The extensive cleaning procedure ensures minimal contamination therefore increasing the repeatability and accuracy of testing.

5.2.3 Magnet Field Unit

An Neodymium magnet of grade N45SH was utilized for the current study for its high residual flux density and potential to influence scale formation behavior. The class four-A magnet orientation with diametrically magnetized direction illustrated by Figure 2-13 was selected due to its flexibility in installation and was installed around the mixing tubing lines before exposing the calcium and bicarbonate fluids to the heating chamber as per Figure 5-1. The ring shape of the class four-A magnet orientation incorporates a small hole through the center generating a concentrated MF at the center of the magnet as shown in Figure 5-2. The field strength of the magnet was measured in the center of the magnet by using a Koshava Tesla meter supplied by wutronic/Germany, with the magnet specifications outlined Table 5-2.

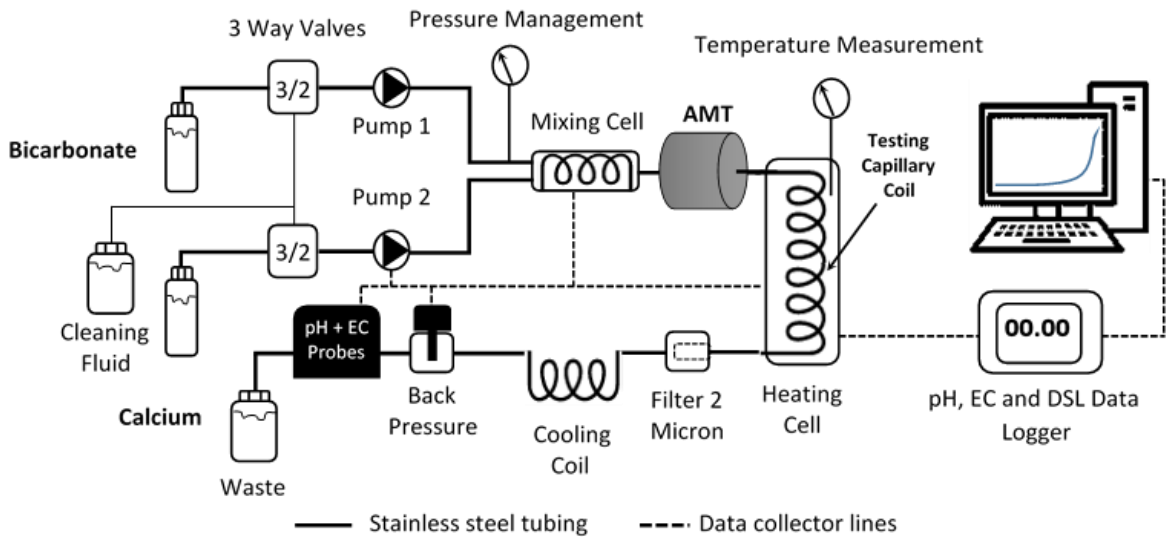


Figure 5-1 Schematic of the dynamic scale loop

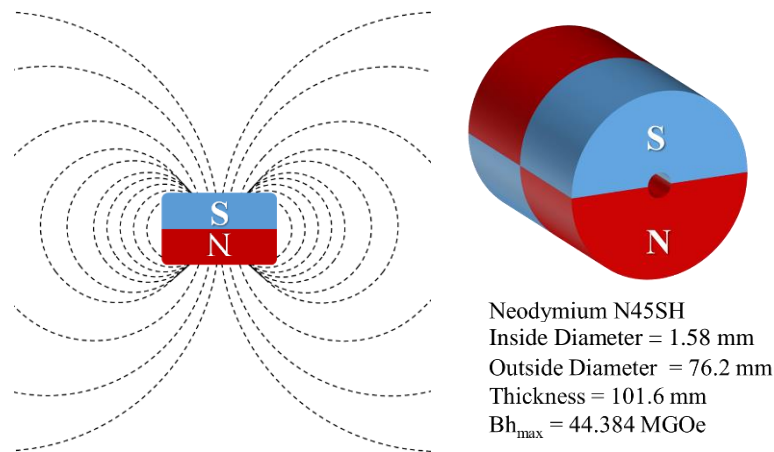


Figure 5-2 Dimensions and shape of the diametrically magnetize magnet and depiction of the diametrical MF

Table 5-2 Magnet specifications and dimensions

Property	Specification
Magnet Dimensions	76.2 mm OD, 1.58 mm ID, 101.6 mm Thickness
Materials	NdFeB
Grade	N45SH
Plating/Coating	Ni-Cu-Ni (Nickle)
Magnetization Direction	Diametrically magnetized
Gross weight	8 kg
Max operating temperature	150°C
Residual Flux Density $B_{r_{max}}$	13499 Gauss
The Maximum Energy Product	44.38 Megagauss Oersted (MGOe)
Magnetic field strength at the center	6480 Gauss at 15.4 mm inside the magnet

5.2.4 Experimental Setup

The experiments within this study were conducted to evaluate the scaling tendency of a solution containing bicarbonate and calcium in the presence of a diametrically MF (Figure 2-13 and Figure 5-2) using the DSL technique. To measure the influence of the applied MF upon the tendency of the solution to form scale, the DSL system measures the pressure increase across an internal capillary tube using pressure sensors located at the tubes inlet and outlet with accuracy of ± 0.01 bar. An increase in pressure across the capillary tube is indicative of scale formation as the flow of liquid is impeded.

To assess the effect of the MF on scale formation, the pressure across the tube was measured until complete blockage of the tube occurred as indicated by a sharp increase in pressure recorded by the DSL system. The time taken for each solution to achieve complete blockage of the capillary tube was used to measure the tendency of the solution to form scale. Overall, eight sets of blank (no magnetic exposure) and magnetically exposed trials were conducted for each brine composition to ensure accuracy and repeatability of results.

The calcium and bicarbonate solutions were injected into the DSL system by using two high-performance liquid chromatography pumps from PSL technology (one for the bicarbonate fluid and one for the calcium fluid). The total injection rate for the two solutions was maintained at 5 ml/min. The laboratory DSL apparatus is illustrated in detail in Figure 5-1 with specifications listed in Table 5-3. The DSL device contains two individual coils with the first used to provide mixing of the solution and the second exposed to a high temperature within a heat chamber to promote the growth of scale (refer to Table 5-3 for coil dimensions). Following mixing within the first coil, the solution is then passed through the centre of a neodymium magnet for a total of 2.5 seconds with a MF strength of approximately 6480 Gauss at the centre and maximum energy product BH_{\max} around 44.38 MGOe as shown in Figure 5-2 and Table 5-2.

After exposure to the MF, the solution enters the second coil located inside an electrical heating chamber controlled using a digital interface. The temperature of the heating chamber was maintained at 150°C ($\pm 1^{\circ}\text{C}$) throughout testing. Furthermore, the operating conditions such as flow rate and the temperature were controlled by using the *winDSL* software. A back pressure regulator was connected to the outlet line of the testing coil to maintain the pressure across the capillary tube. A GMH 5550 pH meter and GMH 5450 electrical conductivity (EC) meter were connected to the discharge line to monitor the change in pH and EC level after magnetic exposure, as per Table 5-3 and Figure 5-1.

Table 5-3 Dynamic scale loop specifications

Component	Specification	Notes
HPLC pumps	0.1 – 5 ml/min, ± 0.01 ml/min	Data-logger
Mixing Coil	1 m Length, 3.17 mm OD and 1.01 mm ID	Stainless steel 316
Test Coil	1 m Length, 1.41 mm OD and 0.76 mm ID	Stainless steel 316
Back Pressure Valve	0 – 172 bar, ± 0.01 bar	Data-logger
Pressure Range	1 bar to 172 bar	Regulating
Heating Chamber	+30 to +250°C, ± 0.1 °C	Regulating
pH meter	1-14	Data-logger
Electrical Conductivity meter	0 – 1000 mS/cm, $\pm 0.1\%$	Data-logger
Micro Filter	2 micron	Stainless steel

5.3 Results and Discussion

5.3.1 Concentrated HCO_3^- Solution

The results generated using the high concentration bicarbonate solution have demonstrated that exposure to a MF can inhibit the formation of calcium carbonate scale. These results were obtained after exposing the brine solution to the MF with a field strength of 6480 Gauss and diametrically magnetized magnet type for 2.5 seconds and comparing the results to a ‘blank’ test where no magnetic exposure occurred. From Figure 5-3, the responses of concentrated bicarbonate solution in terms of pressure change versus time has been plotted for the solutions exposed to a MF and the blank tests. In total, eight trials were conducted for both the exposed and blank trials with the average result plotted as shown in Figure 5-3, error bars have been included indicating one standard deviation of all eight trials away from the average result.

It can be clearly observed that the exposure to the MF has generated an inhibition effect upon the tendency of the bicarbonate solution to form scale in comparison to the non-exposed blank test solution. The sharp increase in pressure observed in both cases is indicative of the capillary tube becoming blocked due to the formation of scale. It can also be noted that the time required for a full capillary tube blockage under magnetic exposure was 8.5 minutes. On the other hand, the time needed to block the same capillary tube under the same conditions but without exposure to the MF was 6 minutes. This result means that MF treatment has effectively reduced the rate of scale formation of the bicarbonate solution.

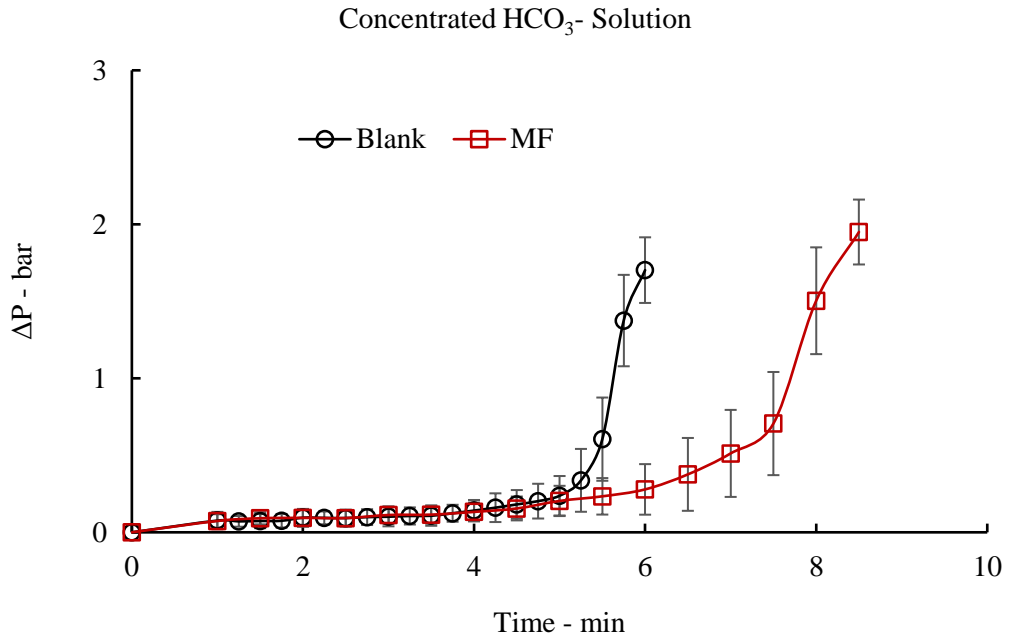


Figure 5-3 Effect of magnet field exposure upon the tendency of high bicarbonate solution to form scale

The reduced scaling tendency of the magnetically exposed solution illustrated by Figure 5-3 may be explained by the intermolecular separation of the calcium and bicarbonate ions generated by the Lorentz force as they travel through the MF. Figure 5-4 illustrates the applied MF within the capillary tube perpendicular to the fluid flow containing the calcium and bicarbonate ions. As the fluid passes through the MF, the positive and negatively charged ions are attracted to opposite sides of the capillary tube due to the equal, but opposite Lorentz force applied and are thus separated. As the separated ions (calcium and bicarbonate) enter the capillary tube under elevated temperature, the tendency of the solution to form scale is inhibited. The extent to which the oppositely charged ionic species remain separated is referred to as the memory effect [29, 53, 54, 77], with the extent of separation decreasing as time progresses following magnetic exposure.

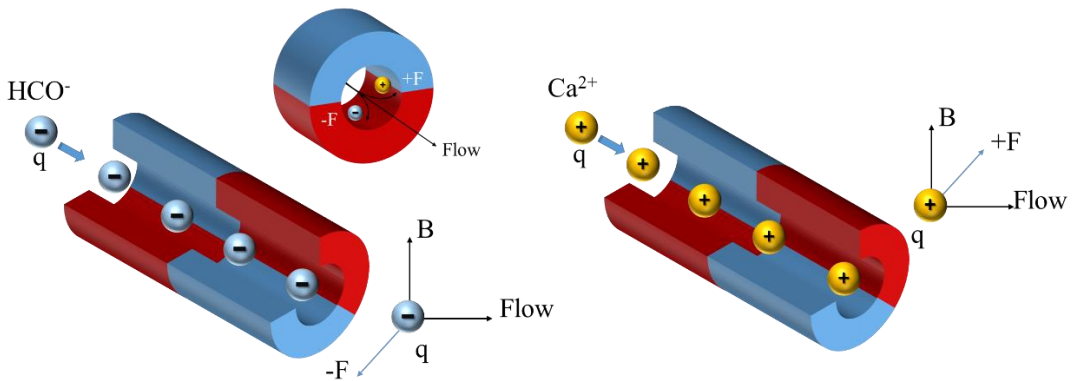


Figure 5-4 Influence of MFs on charged particles (see section 2.4.1)

Another interesting result has been observed as shown by Figure 5-5 where the measured electrical conductivity deviated between the control and exposed solutions. A slight change in the electrical conductivity readings were observed over the range of 0 to 5 minutes where the bicarbonate solution experienced a significant decrease in the conductivity when exposed to MF. This experimental result is in line with the findings of Hasaani, Hadi [30] who observed a similar reduction in electrical conductivity measurement in calcium-bicarbonate solution following exposure to a MF. Furthermore, whilst evaluating the effect of MF exposure on scale formation, Szczes, Chibowski [194], Holysz, Szczes [169] and Marcus [330] concluded that the hydration shell thickness of the bicarbonate and calcium ions are subject to manipulation by MFs leading to changes in electrical conductivity measurement. However, Waluyo, Huang [331] and Marcus [103] stated that there is competition between solute and solvent for the remaining H₂O molecules at a high salt concentration that might reduce the number of water molecules contributed within inner shell hydration. Overall, the exposure of the ions to the MF has increased the hydration shell thickness of the bicarbonate ions causing the reduced electrical conductivity measurements experienced within this test. The effects of MF exposure upon the hydration shell of the ionic species is further discussed in Section 0.

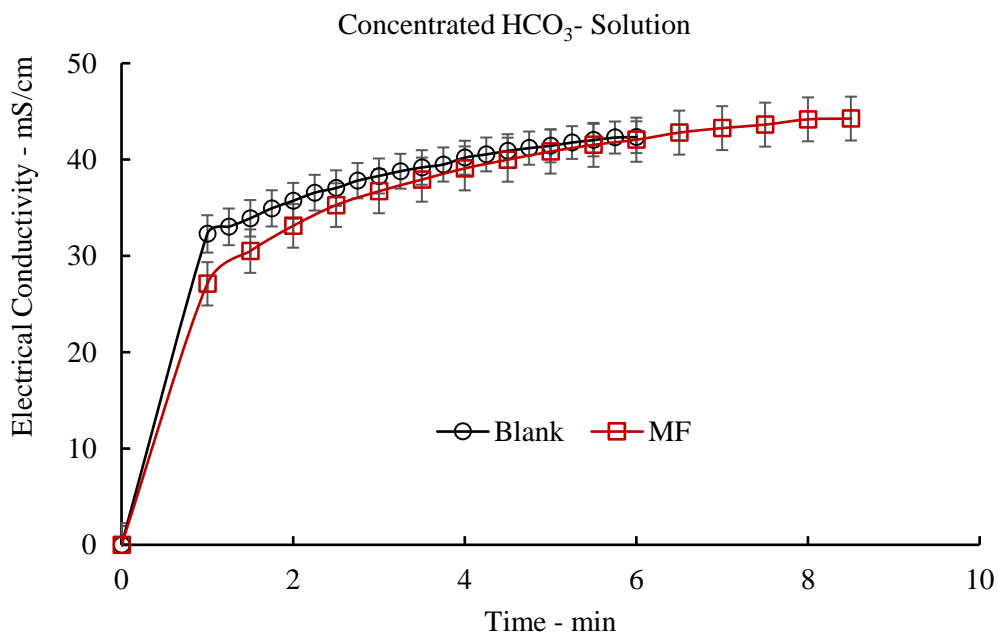


Figure 5-5 Effect of magnet field exposure upon electrical conductivity of high concentration bicarbonate solution

Additionally, if we compare the electrical conductivity response measured during the test with the change in pressure with time as illustrated in Figure 5-3, a clear relationship between the electrical conductivity and extent of scale formation is evident. As the formation of scale proceeds, the electrical conductivity measured at the outlet of the system gradually increases until

it reaches the maximum electrical conductivity at the point of blockage within the tube. The initial spike in electrical conductivity experienced over the first minute of the experiment represents the initial mixing within the system and response of the electrical conductivity meter as it is first exposed to the solution. It can therefore be concluded that electrical conductivity may provide a measure of scale formation within pipelines as a clear increase in electrical conductivity occurs in response to scale formation within the capillary tube [30, 169].

As the formation of CaCO_3 scale within the system proceeded during testing, a minor decrease in pH at the outlet of the system was observed as shown in Figure 5-6. The reaction of calcium and bicarbonate ions to form scale produces a free hydrogen ion and as such, a reduction in pH can be expected. Of the tests conducted, little to no difference in pH of the exposed and non-exposed solutions is evident indicating there is no impact upon pH due to magnetic exposure.

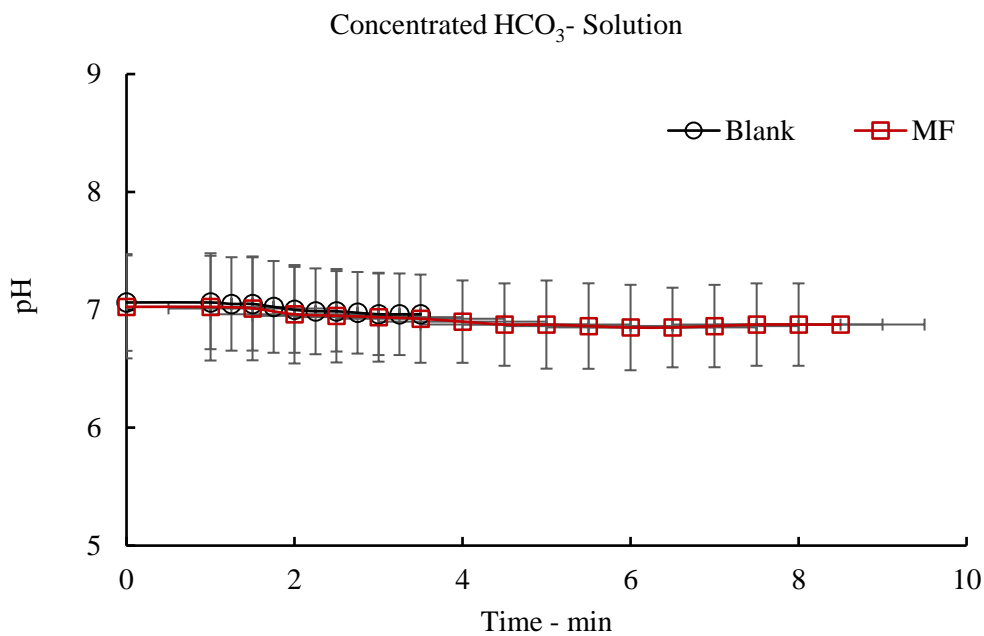


Figure 5-6 Effect of magnet field exposure upon the pH level of high concentration bicarbonate solution

5.3.2 Concentrated Ca^{2+} Solution

In a similar manner to the high concentration bicarbonate ion testing, the response of the brine solution containing high concentrations of calcium ions was evaluated by measuring the differential pressure build up across the capillary tube and the level of electrical conductivity with time. From Figure 5-7, the exposure to the MF appears to have the opposite effect upon the formation of scale in comparison to the bicarbonate solution leading to tube blockage faster than the corresponding blank trials. After the application of the MF demonstrated an inhibitory effect upon scale formation of high concentration bicarbonate solution, the opposite effect has been

observed for high concentration calcium solution with the MF instead promoting the formation of scale. On average, the time required to completely block the capillary tube under exposure to the MF was 87 minutes. However, the time required to block the same tube under the same conditions but without exposure to the MF was 103 minutes, corresponding to an increase in the scale formation rate of 15.5% on average.

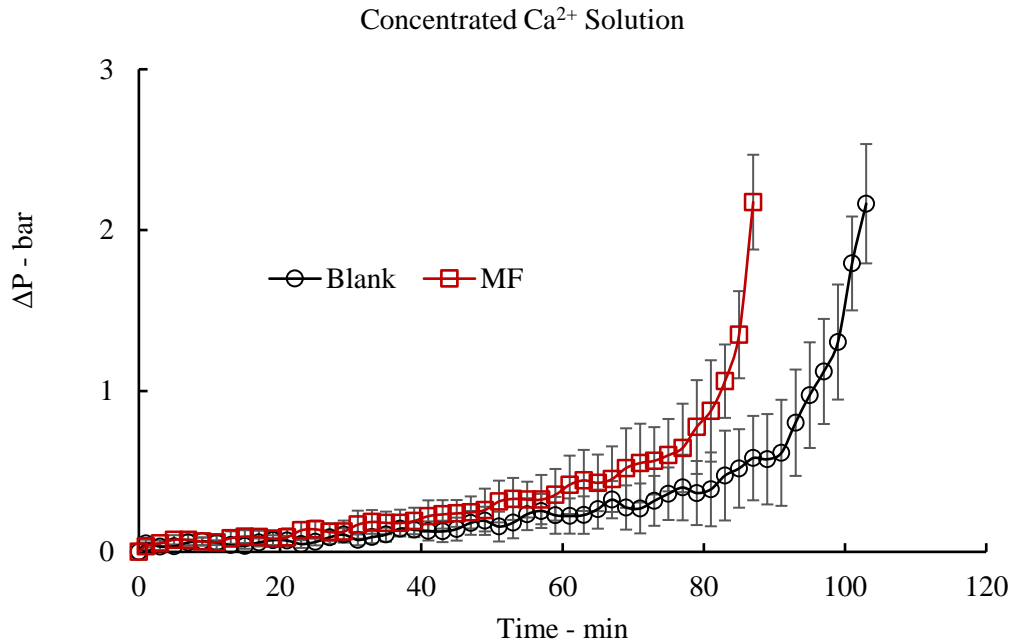


Figure 5-7 Effect of magnet field exposure upon the tendency of high concentration calcium solution to form scale

Therefore, it can be concluded that at the high calcium concentration tested within this study, the molecular separation of the ionic species did not occur to the same extent as the concentrated bicarbonate solution, instead promoting the formation of scale. It was theorized that due to a large amount of calcium ions present, an internal clot-like build-up of the calcium ions began to occur within the capillary tube leading to tube blockage. The generated results in Figure 5-7 are in line with the Marcus [103] conclusions. Whereas, Marcus [103], Marcus [104] and Waluyo, Huang [331] highlighted that for a high concentration of the salt solution, there might be competition between the solute and solvent for the remaining water molecules. Such competition leads to reduce the total number of water molecules around the salt ions. Therefore, the influence of magnetic fields treatment on the hydration shell thickness was ineffective. The accumulation scale is illustrated in Figure 5-8 where due to the poor separation of calcium by the MF, calcium is free to interact with the bicarbonate ions leading to scale formation. As scale formation proceeds, the scale restricts the area of flow through the capillary tube further negating the separation produced by the MF. A lower ratio of calcium to the bicarbonate species may provide a better scale inhibition response more in line with the results generated for test one.

The findings of this study also highlights the different potential responses of mineral ions when exposed to a MF. These responses are dependent on the concentration of ions and most importantly the type of ion whether a bicarbonate, or calcium within the brine solution at the time of magnetic exposure. Although, high bicarbonate findings are supported by the results of Higashitani, Kage [174] who observed a similar scale inhibition response of bicarbonate ions under the exposure of a MF but he could not replicate the same results for calcium ions. The findings may help to explain the uncertainty of magnet treatments in reducing the occurrence of scale formation and clarify the reasons for success or failure of the use of such treatments when applied in industry.

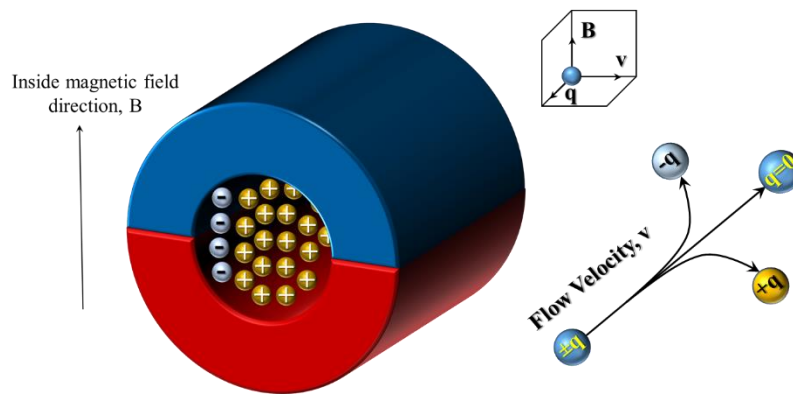


Figure 5-8 Theorized calcium accumulation following magnetic exposure

Furthermore, the electrical conductivity of the high concentration calcium solution to the applied MF demonstrated an opposite response to that of the bicarbonate solution. The application of the MF to the calcium solution instead resulted in increase in electrical conductivity when compared to the blank samples as shown in Figure 5-9. Ayrapetyan, Grigorian [332] reported that the increased electrical conductivity was dependent upon the high calcium concentration within the system. However, this does not fully explain the clear difference in electrical conductivity experienced between the exposed and non-exposed solutions. Instead, it may be considered that the application of the MF, in a similar manner to the bicarbonate solution, influenced the structure of the calcium ion leading to a change in electrical conductivity as discussed in Section 5.3.4.

The reduced hydration layer thickness of the calcium ions under magnet exposure may also play a further role in influencing the scale formation tendency of the high concentration calcium solution. The reduction in hydration layer thickness of the calcium ion when exposed to the MF may facilitate the interaction between the calcium and bicarbonate species resulting in the promoted scale formation experienced within this study for high concentration calcium solutions. In contrast, the increased hydration layer thickness experienced by the bicarbonate ions,

indicated by decreased conductivity measurements may have contributed to the inhibition of scale formation.

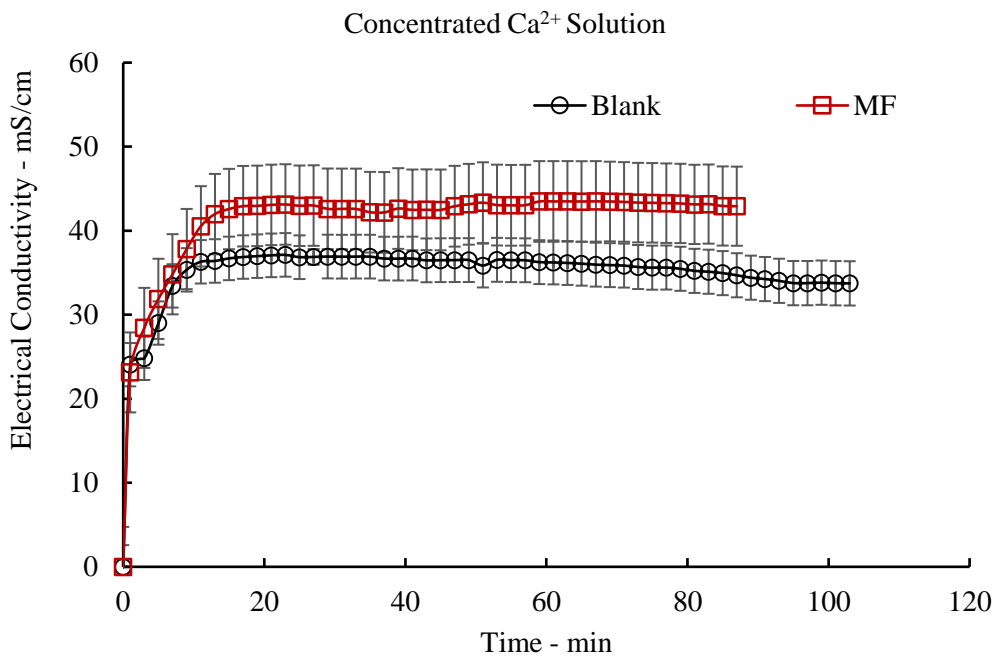


Figure 5-9 Effect of magnet field exposure upon the electrical conductivity of high concentration calcium solution

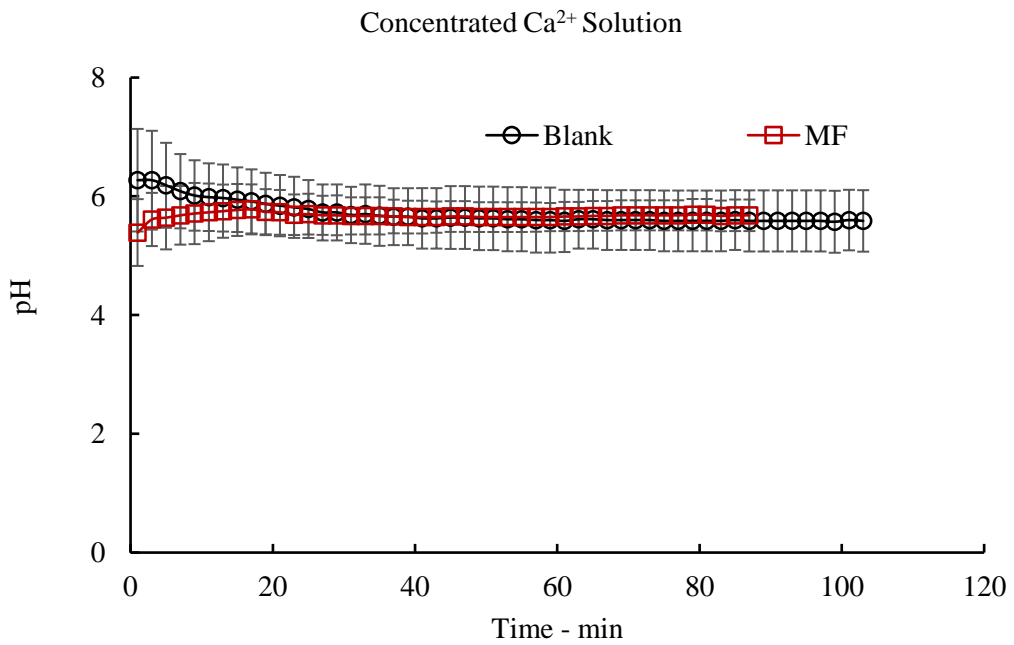


Figure 5-10 Effect of magnet field exposure upon pH level of high concentration calcium solution

5.3.3 Equal Concentration of Bicarbonate and Calcium Ions Solution

After observing interesting results whilst using opposing amounts of ionic species, a final test was conducted using a brine solution composed of equal amounts of calcium and bicarbonate. The brine solution used during tested was composed of approximately 700 ppm of the respective ions. The relationship between pressure changes over time is illustrated by Figure 5-11 where a similar trend to that observed for the high concentration bicarbonate solution was produced. However, the equal concentration brine solution required a longer time frame to achieve full blockage of the capillary tube than the high concentration bicarbonate solution. Furthermore, on average, the discrepancy between the time taken to achieve full tube blockage of the exposed and non-exposed tests is greatest for the bicarbonate-rich solution. Thus, it appears that the magnetic effect upon scale formation was greatest for the highly concentrated bicarbonate brine. Overall, it has been established that the exposure to the MF can provide a scale inhibiting effect for brine solutions containing equal amounts of calcium and bicarbonate, or where the solution contains greater amounts of the bicarbonate species.

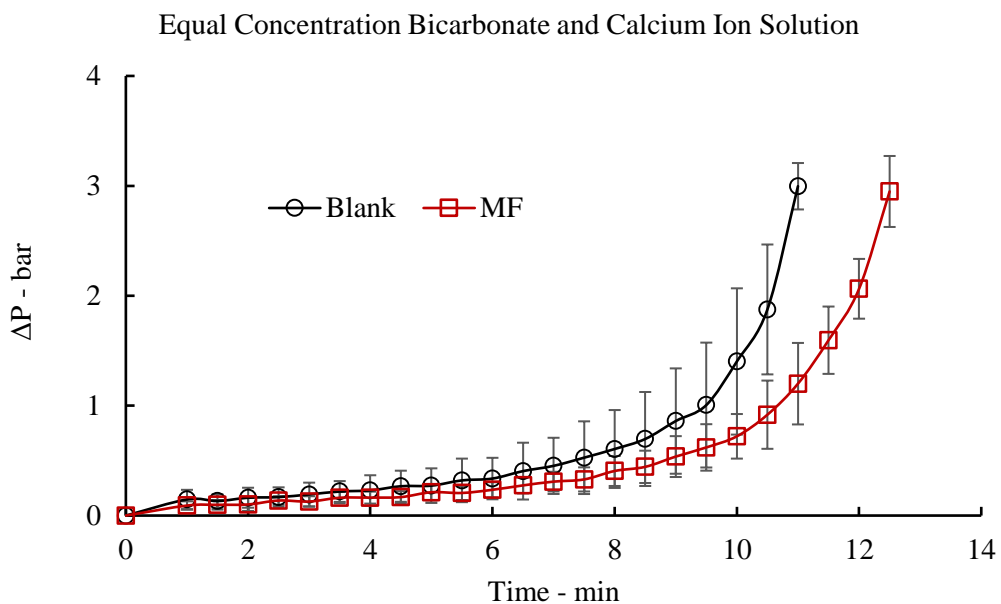


Figure 5-11 Effect of magnet field exposure upon the tendency of equal concentration solution to form scale

Furthermore, exposure of the equal-concentration ion calcium bicarbonate solution to the MF showed a significant influence upon the electrical conductivity measured. As shown in Figure 5-12, the electrical conductivity readings measured after exposure to the MF were on average noticeably less than the corresponding tests conducted without exposure. This outcome is in line with the previous results generated during the tests conducted with a high concentration of the bicarbonate species, however, to a greater extent. Furthermore, a little difference in pH response

within an equal concentration of bicarbonate and calcium ions solution was observed as shown in Figure 5-13.

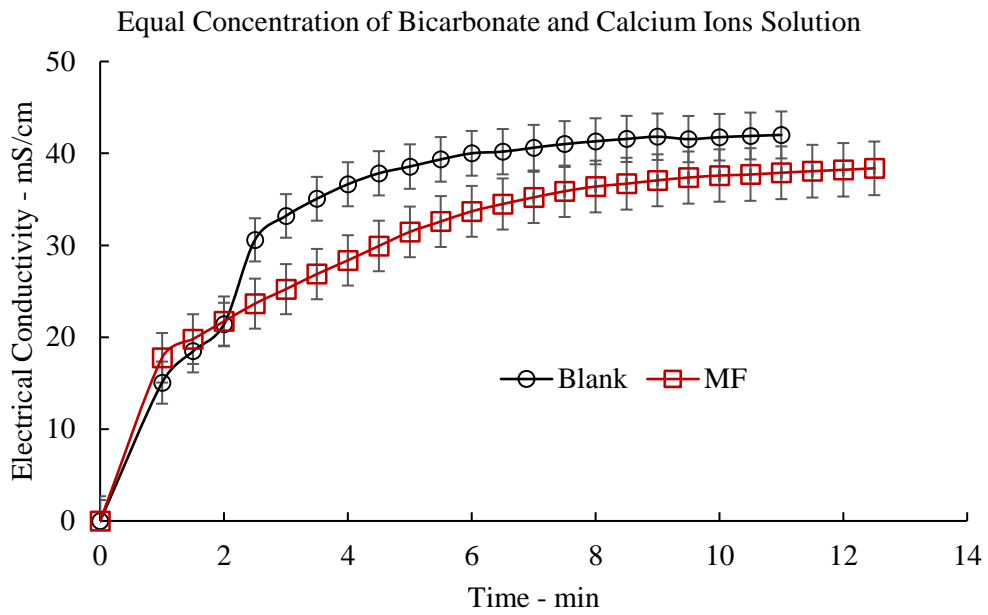


Figure 5-12 Effect of magnet field exposure upon the electrical conductivity of equal concentration solution

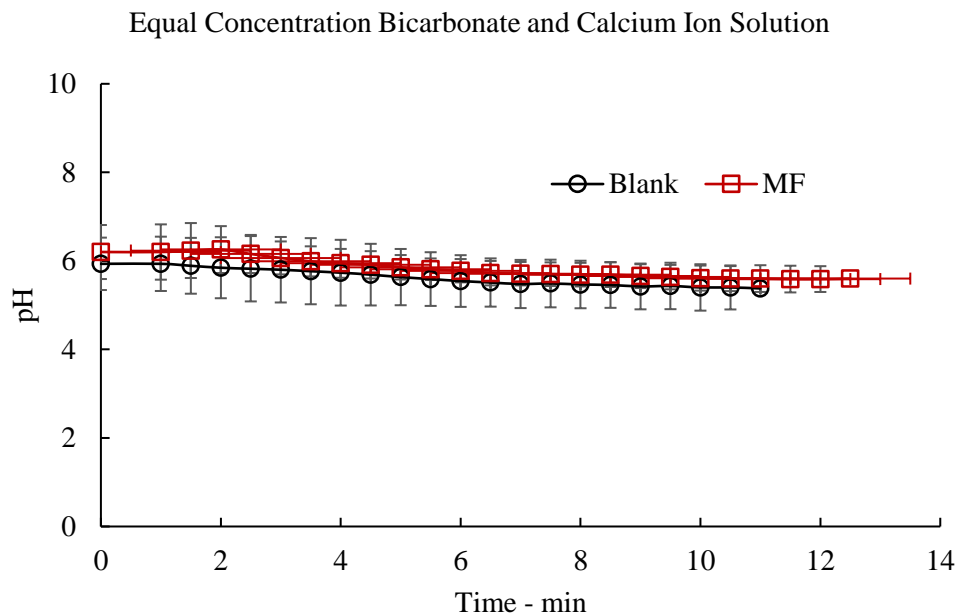


Figure 5-13 Effect of magnet field exposure upon pH level of equal concentration solution

5.3.4 Magnetic Field Influence upon the Hydration Shell of Ionic Species

It was observed during experimental testing that the solutions containing high concentrations of bicarbonate and calcium generated different responses when evaluated under a MF in terms of

electrical conductivity. The difference in response can be attributed to the structure and thickness of the respective ionic species' hydration shell and their response to magnetic exposure. Through the research conducted by Holysz, Szczes [169], it has been determined that there is an inversely proportional relationship between the hydration shell thickness of the ions and the electrical conductivity of solution. As such, the decrease in electrical conductivity observed for high bicarbonate testing (Figure 5-5) can be attributed to an increase in the hydration shell thickness of the bicarbonate ion due to manipulation by the MF. In contrast, the calcium ions experienced a reduction in hydration shell thickness after magnetic exposure causing an increase in electrical conductivity when compared to the blank test (Figure 5-9) a conclusion in line with the hypothesis of Higashitani, Kage [174], Oshitani, Yamada [51] and Holysz, Szczes [169].

In comparison to bicarbonate ions, as per Table 5-4, calcium ions have a much greater hydration shell thickness (Δr), and the number of water molecules in the shell (n). Figure 5-14 illustrates the difference in hydration shell thickness of calcium and bicarbonate ions within solution prior to magnetic exposure and the relationship between hydration shell thickness and electrical conductivity. Whilst Figure 5-14 illustrates the effect of magnetic exposure upon the hydration shell thickness of the calcium and bicarbonate ions. The hydration shell represents the accumulation of water molecules within the “ionic atmosphere” of an ion due to the attraction of either the positive and negatively charged poles of the polar water molecule to the ionic. Marcus [330] and Holysz, Szczes [169] reported that the smaller the ion, the greater the amount of water molecules that will interact around the ion species (Figure 5-16). Therefore, a small ion has a greater tendency to polarize the surrounding water molecules and will hence have a greater hydration shell radius in comparison to larger ions [168, 333, 334].

Table 5-4 Radius of ions, r_i , the thickness of ion hydration shell, Δr , and the number of water molecules in the shell, n [89, 169, 330]

Ion	r_i, nm	$\Delta r, nm$	n	Ionic mobility in water at 25°C, $u/m^2s^{-1}V^{-1}$
H ⁺	0.030	0.300	12.0	36.30*10 ⁻⁸
Mg ²⁺	0.072	0.227	10.0	5.50*10 ⁻⁸
Ca ²⁺	0.100	0.171	7.2	6.12*10 ⁻⁸
Na ⁺	0.102	0.116	3.5	5.19*10 ⁻⁸
OH ⁻	0.133	0.079	2.7	20.50*10 ⁻⁸
HCO ₃ ⁻	0.156	0.059	2.3	4.61*10 ⁻⁸
CO ₃ ⁻	0.178	0.076	4.0	7.18*10 ⁻⁸
Cl ⁻	0.181	0.043	2.0	7.91*10 ⁻⁸

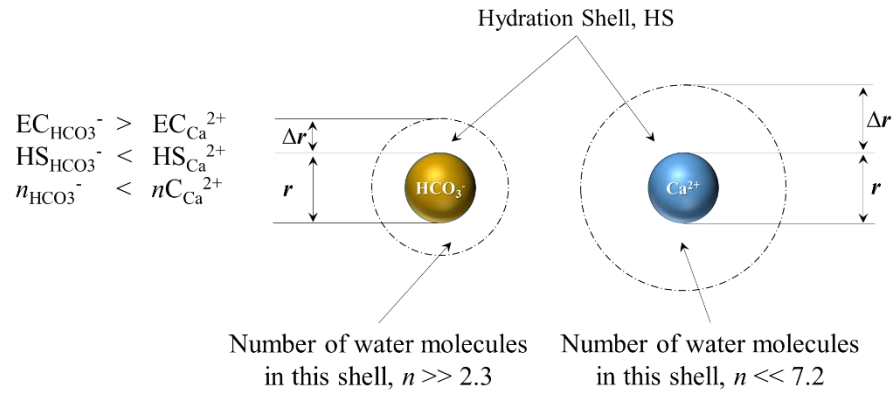


Figure 5-14 Relationship between hydration shell and electrical conductivity with respect to number of water molecules [89, 168, 169]

The inverse relationship between hydration shell thickness of the ionic species and the electrical conductivity of the solution occurs due to the accumulation of the water molecules around the ions. As the hydration shell thickness increases, the accumulation of water molecules effectively acts as an insulating barrier reducing the overall effective charge of the ion and hence a reduction in electrical conductivity, refer to Table 5-4. This relationship is illustrated within Figure 5-14 for the bicarbonate ion in a similar manner to that experienced within the high concentrated bicarbonate testing given by Figure 5-5. In contrast, the thickness of the calcium ion after magnetic exposure was theorized to have been reduced leading to the increased electrical conductivity measurements observed in Figure 5-9. Furthermore, as the hydration shell thickness grows, the ion will tend to react more slowly with surrounding ions due to the insulating effect of the water molecules [168, 333-335]. Therefore, the ability of the ionic species to interact with the opposing ion to form scale is inhibited an outcome in line with the high bicarbonate solution testing where scaling was inhibited.

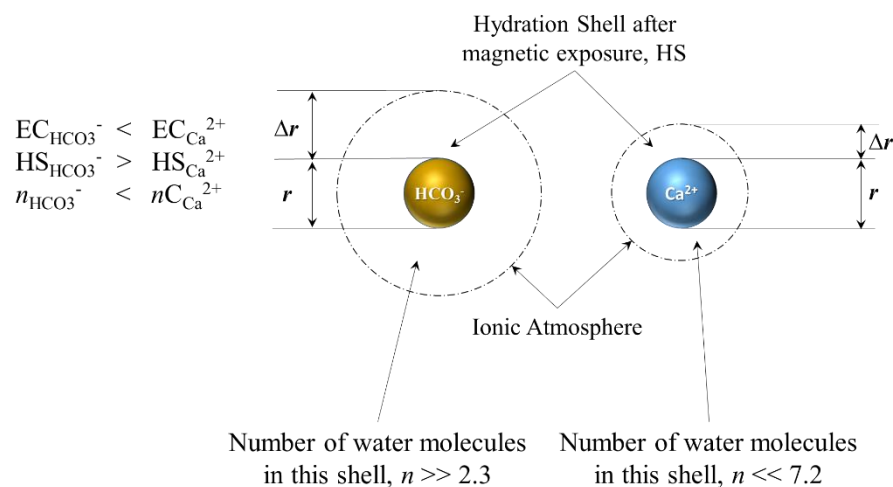


Figure 5-15 Hydration shell of calcium and bicarbonate ions after diametrically MF exposure [89, 168, 169]

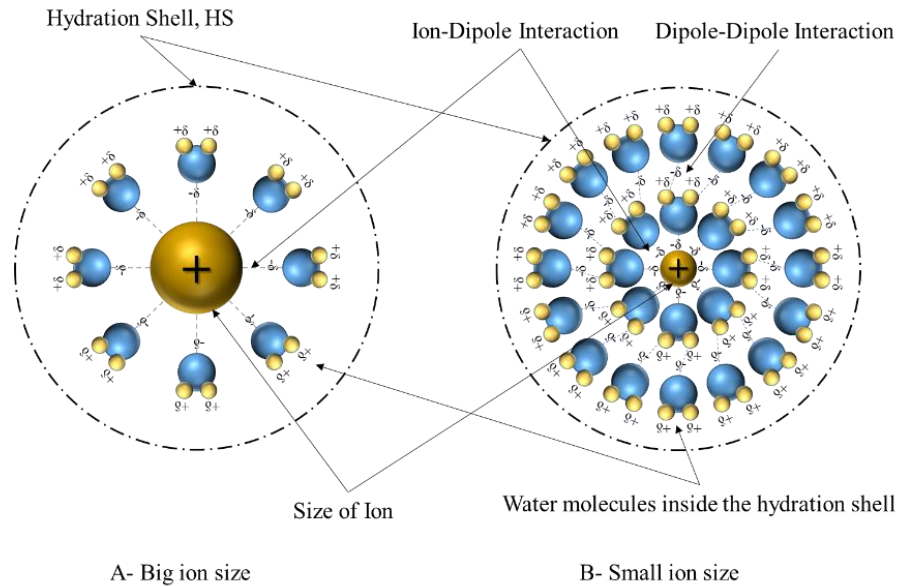


Figure 5-16 Comparison of hydration shells of large and small ions

The primary reason for the increase in hydration shell thickness around the bicarbonate ions is the rearrangement of water molecules (polar molecules) after MF exposure. As discussed previously, polar molecules such as water are influenced by the application of a MF causing them to adopt a more orderly arrangement, refer to Figure 2-11. This rearrangement leads to a more organized pattern of water molecules hence allowing a greater number of water molecules to fit within the hydration shell of the ion. However, it was observed experimentally that the opposite effect occurred when evaluating the effect of magnetic exposure upon high calcium concentration solution with respect to the calcium ion. Instead, the MF lead to a reduction in the hydration shell thickness of the calcium ion as evident through increased electrical conductivity measurements and tendency to form scale compared to blank tests, but does not seem to be fully applicable at high calcium ion concentrations. Overall, different responses of the cations and anions tested within this study to MF exposure was observed in terms of effect upon scaling and electrical conductivity.

5.4 Conclusions

Within this study, the application of MF treatment has been performed to evaluate its influence upon the scale formation tendency of sodium bicarbonate solutions of varying concentrations. The extent of scale formation was evaluated using a Dynamic Scale Loop system by measuring the increase in pressure across a capillary tube as the formation of scale proceeded. In contrast to similar studies performed to evaluate the effects of magnetic exposure upon the behavior of ionic species, an appreciable impact upon particle behavior in the form of inhibited scale formation and electrical conductivity was achieved using only brief magnetic exposure. Many studies use long term exposure to MFs to evaluate their impact, however, the results of this study have

conclusively demonstrated that only brief exposure (2.5 seconds) to a strong diametric MF can significantly influence particle behavior. Furthermore, prior studies performed to evaluate magnetic treatment tend to use singular or multiple rectangular magnetics arranged around the fluid flow using either Class 1 or 4 magnetic arrangement as shown in Figure 2-13. By comparison, the results of this study were generated using a Class 4-A magnetic arrangement utilizing a circular ringed shape with fluid flow occurring through the center of the magnet (Figure 5-4) making the results of this study unique.

Through the results generated using the DSL system, three conclusions were drawn regarding the use of MF treatment to inhibit the scale formation of calcium carbonate in water systems. Firstly, the extent of scale formation, whether inhibited or promoted, is dependent upon the ratio of bicarbonate to calcium. Through the tests conducted, it is apparent that the amount of bicarbonate present plays a key role in making the application of magnet treatment for preventing scale formation applicable to the brine solutions tested. Of the tests conducted, where bicarbonate was of greater or equal concentration to the calcium ions, appreciable inhibition of scale formation was achieved suggesting the bicarbonate are more responsive to the effects of the applied MF compared to the cations. The inhibition of scale formation was attributed to the intermolecular separation of the calcium and bicarbonate ionic species generated by the Lorentz force as the solution flowed through the MF.

Following exposure to the MF, the separated ions within the solution had sufficient magnetic memory to ensure the formation of scale was inhibited. However, due to the large amounts of calcium ions present during the high calcium concentration testing, the same behavior could not be repeated due to a theorized clot-like build upon within the capillary tube that lead to interaction between the calcium and bicarbonate forming scale deposition. A result in line with the conclusions of Marcus [104], Marcus [103] and Waluyo, Huang [331]. Furthermore, it should be noted that the separation of charged particles achieved through magnetic exposure can only be maintained during laminar flow. Turbulent flow of the solution would promote mixing of the separated charged particles effectively nullifying the effects of magnetic exposure.

Secondly, the exposure of the brine solutions to the applied MF had a significant impact upon the electrical conductivities measured. A considerable reduction in electrical conductivity of the high concentration bicarbonate and equal concentration solutions was observed during testing and was attributed to the influence of the MF on the structure of the ionic species. The results of the tests conducted were in line with previous testing performed by various authors who concluded that the hydration shell thickness of the bicarbonate and calcium ions are subject to manipulation by MFs leading to changes in electrical conductivity. Furthermore, it was observed that the electrical conductivity measured at the outlet of the DSL system steadily increased as scale formation

proceeded. It was therefore concluded that the measurement of electrical conductivity may provide an indirect measure of the extent of scale formation with a pipeline.

Finally, due to the successful inhibition of scale formation through the influence of the MF treatment applied during experimental testing, it can be suggested that MF treatment may provide an eco-friendly scale inhibition strategy in place of traditional chemical scale inhibitors. Furthermore, MF treatment for scale inhibition may provide a more cost effective method to prevent the formation of scale due to the one-time cost of a magnetic treatment system being outweighed by the continued cost of chemical scale inhibitor application with time. However, the applicability of MF treatment on large scale pipelines is yet to be fully evaluated.

Chapter 6 The Influence of Magnetic Fields on Calcium Carbonate Scale Formation within Mono Ethylene Glycol Solutions under Regeneration Conditions

6.1 Introduction

One of the most discussed topics related to the effects of external MFs on aqueous solutions is the influence on the formation of calcium carbonate scale [19, 22, 49, 190]. However, the extent of the effect of these forces on scale formation in non-aqueous solutions has not been investigated to date. Thus, MFs were applied to non-aqueous mixtures to identify the scale formation behavior. In this part of the study, inorganic scale formation in MEG solutions containing Ca^{2+} and HCO_3^- ions was investigated using both static and dynamic scale loop evaluation techniques. Furthermore, the influence of the MF on scale formation using the dynamic technique has also been studied. Results were obtained for brine/MEG solutions exposed to the MF produced by a 0.65 Tesla neodymium magnet for 2.5 second. The degree of scale formation was examined by measuring the pressure build-up across a capillary coil as scale developed. Moreover, differences in CaCO_3 morphologies were evaluated for the exposed and blank trials via the DSL technique and compared with the results obtained from the static scale evaluation method.

6.2 Experimental Methodology

6.2.1 Experimental Equipment and Chemicals

6.2.1.1 Brine Solutions

Two MEG solutions, typical for MEG regeneration plants (Table 6-1), were used in this study to evaluate the effects of MF treatment on scale formation at 50 and 80% by volume MEG fractions. Each experiment utilized equal concentrations of Ca^{2+} and HCO_3^- ions (750ppm) with keeping the divalent cationic and scale causing anionic species separately to prevent premature reaction. The MEG concentration returning from the pipeline is often 40 to 60% by volume [15, 67, 134], while post-regeneration concentrations often exceed 80% by volume of MEG [67, 134] before re-injection at the wellheads.

The cationic and anionic charges of all MEG-brine solutions were adjusted by addition of NaCl as per Table 6-2. The two MEG volume fractions were utilized to simulate aqueous glycolic solutions at various MEG to water volume fractions at the same ionic strength to assess the effect of MFs treatment on calcium and bicarb (Ca^{2+} and HCO_3^- ions) within the MEG solutions. Jar cell trials [147, 309] were conducted within this study to compare scale formation morphology of 0, 50 and 80% by volume of MEG solution with DSL technique but at 30 and 150°C. Jar cell trials could not be controlled at 150°C without using autoclaves due to the high evaporation rate, which changed the volume fraction of MEG. The mathematical model described by Al Helal,

Soames [322] was used to measure the volume fraction of the glycolic solutions after adding mineral salts to ensure that the initial volume fraction of MEG before each test was correct

Table 6-1 Experiments for the exposed and blank tests of DSL technique and non-exposed jar test technique at different conditions

Trial No.	Vol. % of MEG	Temperature, °C	Technique	Magnetic Fields
1	50	150	DSL	Yes
2	50	150	DSL	No
3	80	150	DSL	Yes
4	80	150	DSL	No
5	0	150	Jar	No
6	0	30	Jar	No
7	50	150	Jar	No
8	50	30	Jar	No
9	80	150	Jar	No
10	80	30	Jar	No

6.2.1.2 Chemicals Used

To produce the brine-MEG solutions, ultra-deionized water (18.2MΩ cm) was used for all experiments. The brine-MEG solutions used in this study are representative of worst conditions in real situations in the oil and gas industry. Prepared solutions were sparged with N₂ gas to avoid contamination by CO₂ gas. Brine-MEG solutions consisted of, MgCl₂·6H₂O powder (>99 wt. %), CaCl₂·2H₂O powder (>99 wt. %), NaHCO₃ powder (99.7 wt. %), NaCl powder (99.7 wt. %), MEG solution (99.9 wt. %) provided by Chem-Supply (reagent grade). The pH of injected solutions (i.e. cation and anion solutions) was adjusted by using few drops of 0.1 M of NaOH to maintain the initial pH conditions.

Table 6-2 Brine, MEG, and water concentrations for sets of 50% and 80% by volume of MEG

Ion	Anion Solution, mg/L	Cation Solution, mg/L	Mixed Solution, mg/L
Na ⁺	10600	10600	10600
Mg ²⁺	0	100	50
Cl ⁻	15475	19293	17384
Ca ²⁺	0	1500	750
HCO ₃ ⁻	1500	0	750
pH	8.2	6.34	

6.2.1 Experimental Design

The most common way to design a project in the laboratory is to divide the tests into two groups, a control group, and an experimental group. Changes in one or more operating variables are made to the experimental group but not to the control group. This type of lab experimental design is also known as “repeated measures” [336, 337]. However, the comparative variable (i.e. MF) of

the experiment includes one group of participants; while the other experiment does not include that variable and these experiments become a control group. For instance, trials would split into two groups A-MF and B-No MF (control). Group A-MF includes 50 and 80 vol. % of MEG with MF exposure; while group B-No-MF includes 50 and 80 vol. % of MEG without exposing to MF, this is to compare exposure effects. Even though temperature and brine effects occur for each group, because they exist equally in both groups, they balance each other out in the generated results

6.2.2 Magnetic Field Device

A N45SH magnet was used in this study due to its high maximum energy product to affect scale formation operation. The diametrically magnetized orientation was selected due to its flexibility to utilize and placed after the mixing tubing coil but the heating chamber, as shown in Figure 6-1. The cylindrical shape of the magnet orientation incorporates a small hole through the centre generating rich MFs. Due to the small gap between the magnetic poles of the cylindrical shape, which reached about 0.1588 cm, the magnetic field strength will reach its maximum strength. This intensive strength will contribute to the modification of some thermodynamic characteristics of the mixture passing through it. The MF intensity of the cylindrical magnet was measured by using a Gauss-meter provided by the Wutronic instrument from Germany. The N45SH magnet specifications and dimensions outlined in Table 6-3.

Table 6-3 Magnet specifications and dimensions

Property	Specification
Dimensions of Magnet, cm	7.62 OD, 0.15 ID, 10.16 Thickness
Materials and Grade	NdFeB and N45SH
Plating/Coating	Ni-Cu-Ni (Nickle)
Direction of Magnetization	Diametrically
Maximum operating temperature	150°C, ±5°C
Generated Residual Flux Density Brmax, Tesla	13.49 Tesla
The Maximum Energy Product, Megagauss Oersted	44.38
Magnetic susceptibility of water (χ), cm ³ /mol [217]	-12.63*10 ⁻⁶
Magnetic strength (H)	5.27*10 ⁵ A/m
Magnetic flux density (B)	0.65 T

6.2.2.1 Magnetic Fields Validation

Several hypotheses have been proposed to validate the effects of MFs on thermodynamic properties of hydration shells. For instance, the expression of volumetric density of magnetic energy (ρ_E) has been utilized to evaluate the direct potential of external MFs energy to break down the H-bonds of free water molecules[50]. This expression represents the relationship between magnetic susceptibility of water molecules (χ), Magnetic strength (H) and Magnetic flux density (B) of the applied magnetic device. The relationship can be expressed as such: -

$$\rho_E = \frac{\delta E_B}{\delta V} = \frac{\chi_{water} * H * B}{2} \quad 6-1$$

Where E_B denotes the generated energy from the MFs that is applied to the H-Bonds. By using the magnetic specification that is listed in Table 6-3, the generated energy (E_B) from the MFs was estimated at approx $4.33 * 10^{-9}$ kJ/mol. The calculated value of E_B was compared with the weakest H-bond energy of free water (5.43 kJ/mol[50]), which is found as such interval:

$$\frac{E_B}{E_{H-bonds}} = 4.43 * 10^{-5} \quad 6-2$$

The comparison leads to the conclusion that the effect of the external MF on the modification of the thickness of the hydration shell is not based on the generated magnetic energy effect. However, another explanation has been proposed by Madsen [188] which is related to the proton transfer from hydrogen carbonate to water molecules, due to proton spin inversion in the external MF. Moreover, MF effects were also described in terms of changes in the hydration of carbonate ions, which might directly alter the polymorph phase equilibrium throughout the precipitation. As a result, the external magnetic field can cause weakening, distorting and alteration in the number of H-bonds between water molecules and ions. Hence, MFs are affecting the water molecule structure and its reaction potential with dissolved ions to form hydration shells.

6.2.2.2 SEM Analyses

SEM analysis was used to identify the morphology of CaCO_3 of the exposed and the blank trials samples within different MEG concentration as described in Table 6-1 and Table 6-2. The discharge solution of each test was collected and filtered using a $0.22\mu\text{m}$ syringe filter. The filter papers were subsequently dried to remove any residual fluid. The filter papers were then coated with 5 nm platinum to allow analysis by SEM. SEM analysis of the dried samples was then generated using a Zeiss NEON, operating at 10 to 5 kV. Based on the energy dispersive spectroscopy (EDS) analyses, the scale formed seems to be of CaCO_3 polymorphs.

6.2.2.3 Experimental Setup of Dynamic Scale Loop Techniques

Trials were performed to investigate scaling tendencies of MEG-Brine solutions containing HCO_3^- and Ca^{2+} ions in the presence of an MF using the dynamic technique, model MinDSL 1725-M from PSL Systemtechnik Germany (refer to Figure 6-1). The DSL apparatus measures the differential pressure (ΔP) build-up across an inside capillary coil using a pressure detector placed at the inlet and outlet of the capillary coil with an accuracy of ± 0.009 bar. An increase in the ΔP across the capillary tube is indicative of the scale formation as the flow of solution is hindered. To investigate the influence of the MF on CaCO_3 formation, the ΔP across the capillary coil was monitored and measured until full blockage of the coil occurred as indicated by an

increase in the ΔP recorded by the pressure detector. The time recorded for each experiment to attain full blockage of the capillary coil was used to assess the tendency of the MEG-brine solution to form CaCO_3 .

The dynamic apparatus is illustrated in detail in Figure 6-1 with specifications outlined in Table 6-3. The DSL tubing and instruments were isolated to prevent changes in the operating temperature, brine solutions, and measurements of each trial. Cation and anion solutions were pumped separately into the dynamic apparatus through a Y shaped mixing stream by using two high-pressure pumps at room temperature. The combined flow rate for the cation and anion solutions was set at 300 ml/hr. At room temperature, the scale formation rate is slow that it allows mixing of the MEG-brine solution in the first coil and passing through the centre of a cylindrical magnet for a total time of 2.5 seconds with an MF flux density of approximately 0.65 Tesla at the centre, as shown in Figure 6-3 and Table 6-2. The second coil, which is placed inside a heating chamber, accelerating scale formation (refer to Table 3). The experimental conditions like temperature and flow rate were controlled and monitored by using the winDSL software. The heating chamber temperature was set to 150°C ($\pm 1^\circ\text{C}$) during testing using a digital interface controller, simulating skin temperature of the MEG regeneration column reboiler unit. A back-pressure regulator valve was placed on the outlet line of the testing capillary coil to set the ΔP across the capillary coil. EC and pH probes were installed to the discharge tubing to record variations in pH and conductivity after the MF exposure, as per Table 6-4 and Figure 6-1.

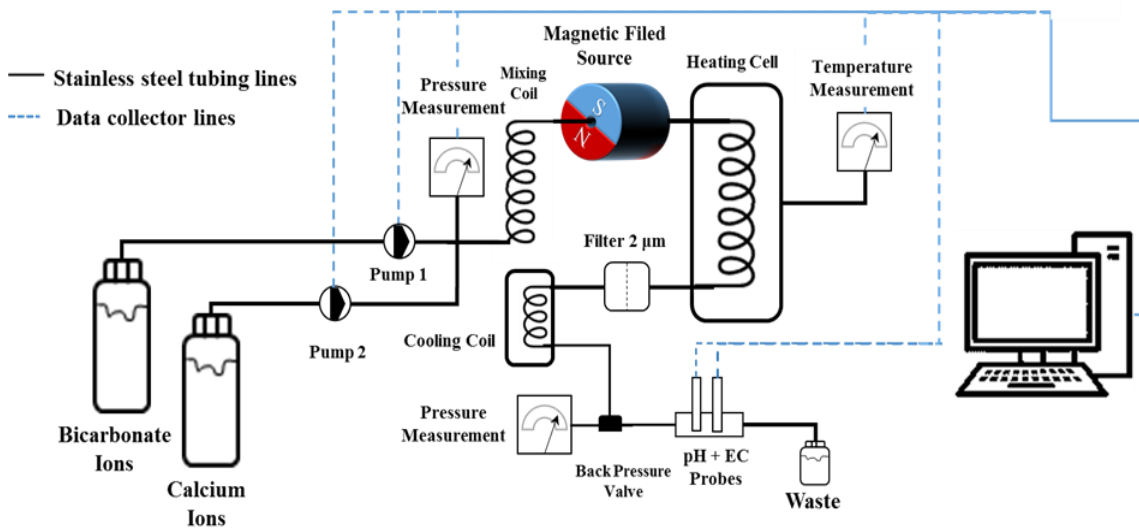


Figure 6-1 Schematic of the DSL system

Table 6-4 DSL specifications

Component	Specification	Notes
Higher pressure pumps	0 – 300 ml/hr, ± 0.6 ml/hr	Data-logger
Mixing Capillary Coil	10 cm Length, 3.17 mm OD	Stainless steel 316

Component	Specification	Notes
	and 1.01 mm ID	
Test Capillary Coil	100 cm Length, 1.41 mm OD and 0.76 mm ID	Stainless steel 316
Back Pressure Valve Range	0 – 172 bar, ± 0.01 bar	Data-logger
Operating Pressure Range	1 bar to 172 bar	Regulating
Operating Heating Chamber	+30 to +250°C, ± 0.1 °C	Regulating
pH-meter	1-14	Data-logger
Electrical Conductivity meter	0 – 1000 mS/cm, ± 0.1 %	Data-logger
Micro Filter	2 Microns	Stainless steel

6.2.2.4 Experimental Setup of Jar Cell Techniques

Closed jar testing [147, 309] was conducted to form different crystals of CaCO_3 at different MEG concentrations and temperature levels. The jar tests were conducted using the same brine solution compositions used for the DSL trials to evaluate the difference in scale formation morphology compared to that produced using the dynamic process of the DSL system. The experimental temperatures were set at 30°C, and 150°C to form different CaCO_3 structures and were exposed to the respective temperature for a period of one hour. The operating temperature was maintained by using an autoclave system having an accuracy of ± 2 °C, refer to Figure 6-2. Operation at 150°C was performed under a pressure of 3.0 bar to prevent boiling of the MEG solution. The CaCO_3 crystals formed were immediately filtered, dried and subsequently analyzed using SEM to distinguish the difference in the morphologies of the CaCO_3 .

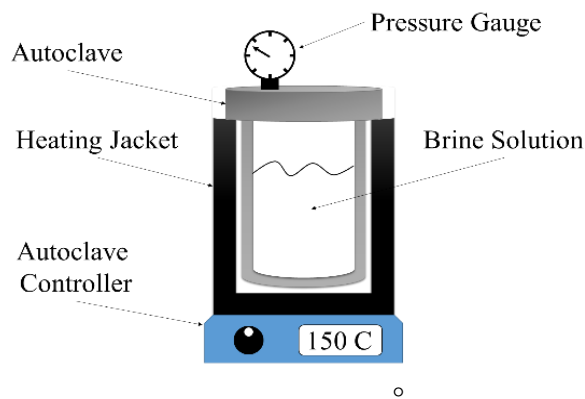


Figure 6-2 Schematic diagram of jar cell techniques (Autoclave)

6.3 Results and Discussion

6.3.1 Influence of Magnetic Fields on Scale Formation at 80 vol. % MEG Solution

To evaluate the impact of MF exposure on the scale formation tendency of CaCO_3 with MEG solution, 80 vol. % MEG solutions containing an equivalent concentration of Ca^{2+} and HCO_3^- ions was exposed to MFs as discussed in Section 6.2.2.3. For comparison purposes, blank trials were conducted using the same 80 vol. % MEG solutions with no exposure to the MF. The trials

exposed to the MF and corresponding blank tests have been plotted in Figure 6-3 with respect to the change in ΔP across the capillary coil with time. Overall, 8 trials were performed for each of both blank and exposed tests and the results average plotted and standard deviation error bars have been included.

A consistent sharp rise in ΔP across the capillary coil was observed for trials exposed to the MFs, whilst in comparison, a more gradual rise in ΔP followed by a sharp increase which occurred during blank tests. The sharp increase in ΔP is demonstrative of the capillary coil becoming fully blocked following the formation of scale. The duration time required for the blank tests to experience complete tube blockage was significantly longer than those trials exposed to the MF. As such, it is evident that MF exposure has promoted the formation of CaCO_3 scale within the 80 vol. % of MEG.

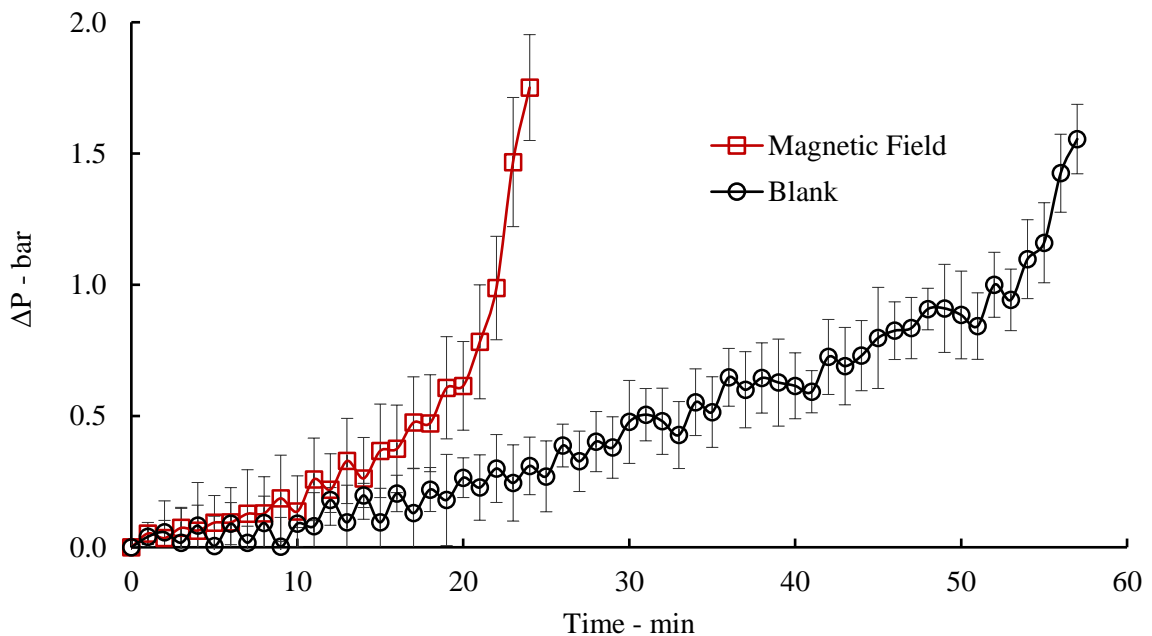


Figure 6-3 Effect of MF exposure on the tendency of equal concentration of Ca^{2+} and HCO_3^- solution within 80 vol. % MEG to form scale

Furthermore, the EC of equal concentrations of bicarbonate-calcium solutions established a similar behavior exhibited during the studies by Al Helal, Soames [109] and Szczes, Chibowski [194] following exposure to an MF. As shown in Figure 6-4, the application of the MF to equal bicarbonate-calcium concentration 80 vol. % MEG solution has directly decreased the EC readings when compared with the corresponding blank samples results. The results of the magnetically exposed trials are consistent with the conclusions of Hasaani, Hadi [30] who reported a similar change in EC of Ca^{2+} - HCO_3^- solution following experience to an MF. These changes were attributed to thermodynamic changes that altered the thickness of the hydration shell around those ions [29, 31, 174]. Therefore, the results could suggest that the hydrated layer

of the ions was influenced by exposure to the MF, and hence the electrophoretic activity of the electrolytes within 80 vol. % MEG decreased.

Such a decrease in EC may occur due to the bonding of MEG molecules with aqueous solution leading to weakening the H-bonds of water-water molecules [79] (refer to Figure 6-5). As a result, the weakening of hydrogen bonds tends to impact the hydration shell thickness around dissolved ions [38, 338]. Meanwhile, a number of publications stated that MFs led to an increase in EC of the aqueous solutions [103, 109, 194]. Furthermore, Silva, Neto [29] reported that less hydrated cations adhere more strongly to anions and vice versa after exposure to MFs within the aqueous solution. However, in the presence of MEG molecules, an opposite result was observed in terms of the EC reading following MF exposure.

The reduction in EC may have been caused by exchanging the water cluster typically around mineral ions with MEG molecules. Therefore, the hydration shell could be replaced with bulky MEG molecules that alter the thickness of the solvation shell around ions (less water content), refer to Figure 6-5. As a result, the low hydration thickness and low solubility rate within 80 vol. % MEG solution lead to a greater scale formation tendency after exposure to MFs. The proposed hypothesis was based on the conclusions of Rozhkova, Rozhkova [79] and Silva, Neto [29] as mentioned in the introductory section. As a result, the bulky ions generated a weaker EC measurement within 80 vol. % of MEG as shown in Figure 6-4. Moreover, exposure of the ionic species to the MF may not be the only factor influencing the hydration shell thickness due to the potential of MEG molecules to swap with the water molecules to form thicker solvation shell layers around ions.

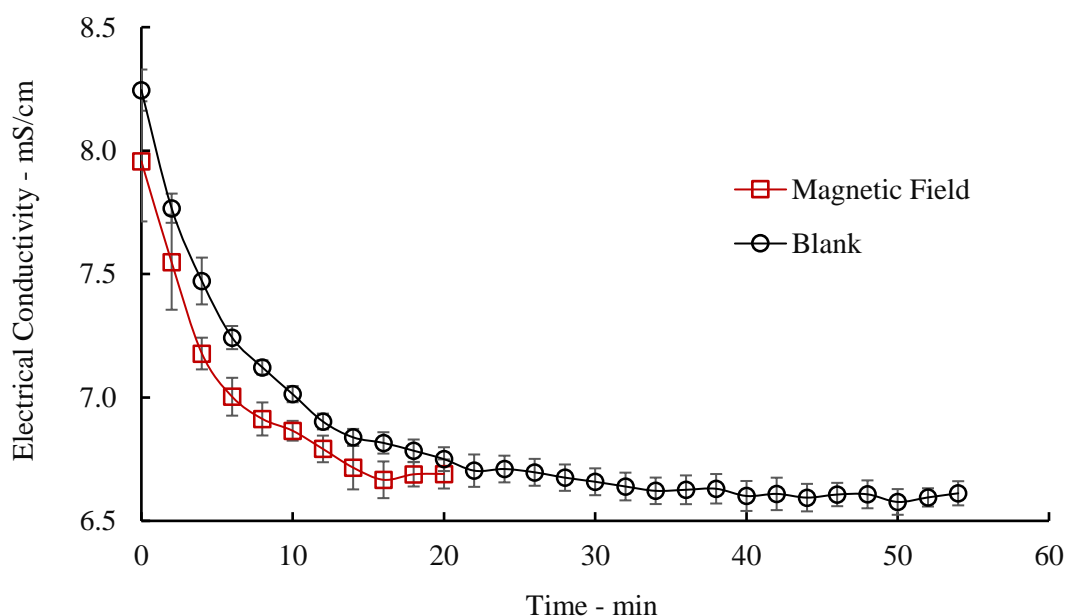


Figure 6-4 Effect of MF exposure upon EC of equal concentration of Ca^{2+} and HCO_3^- solution within 80 vol. % MEG

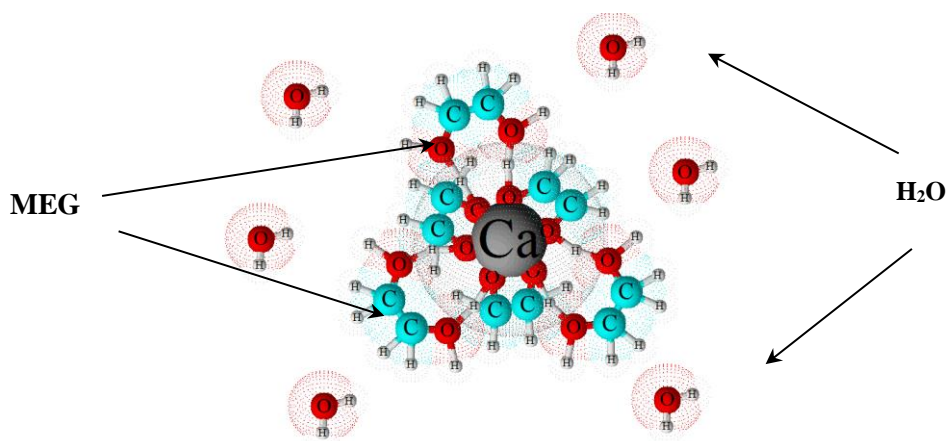


Figure 6-5 Structure of the solvation shell with MEG molecules after exposure to MFs. The images were generated using ACD/ChemSketch freeware software [167]

6.3.2 Influence of Magnetic Fields on Scale Formation at 50 vol. % MEG Solution

Similarly to the 80 vol. % MEG trials, the performance of MF treatment on equal concentration Ca^{2+} and HCO_3^- in 50 vol. % MEG solutions has been conducted by monitoring ΔP across the capillary coil. A contrary result was observed for CaCO_3 formation in comparison to the trials performed using 80 vol. % MEG solutions as given in Figure 6-6. Within the 50 vol. % MEG solutions, the MF inhibited scale formation in comparison to the blank trials leading to slower capillary tube blockage. The variation in scale formation behaviour following MF exposure has highlighted an important difference in the performance of the MF treatment at varying MEG concentration. Adhesion of the deposits on the inner surface of the capillary coil was less frequent compared to non-magnetized experiments. As such, it can be suggested that the inhibitory effect of MF treatment ultimately diminishes at higher MEG concentrations resulting in accelerated scale formation. The generated results are consistent with findings of Higashitani and Oshitani [189] who reported opposite effects of the MF when increasing methanol concentrations. Rozhkova, Rozhkova [79] and Crupi, Jannelli [166] reported that movement of MEG molecules within brine solution is higher compared to pure water. The increased movement of the MEG molecules was attributed to rupture of hydrogen bonds typically formed between the water and MEG molecules. The presence of MEG leads to a significant reduction of the solubility index of ions resulting in a decrease of the saturation level and overall increasing scaling potential. However, when the rich MEG solution (50 vol. %) was exposed to external MFs, the scale formation rate slowed, leading to a different scenario.

This scenario may have been caused by a decrease in solvation shell and an increase in the hydration shell thickness around the ionic species, therefore decreasing the potential for CaCO_3 scale formation [29]. Rozhkova, Rozhkova [79] further concluded that the addition of mineral ions to the MEG + water system may weaken but not rupture hydrogen bonds between OH-groups

of MEG molecules and H-groups of water molecules. Therefore, exposure to the MFs within the 50 vol. % MEG trials are further contributing to the weakening of said OH-H bonds, potentially leading to their rupture and reduction of the interaction of the MEG molecules and ionic species (refer to Figure 6-7). The potential weakening of OH-H bonds between water and MEG resulted in a significant increase in the measured EC readings following the MF exposure due to increase the ions solubility index.

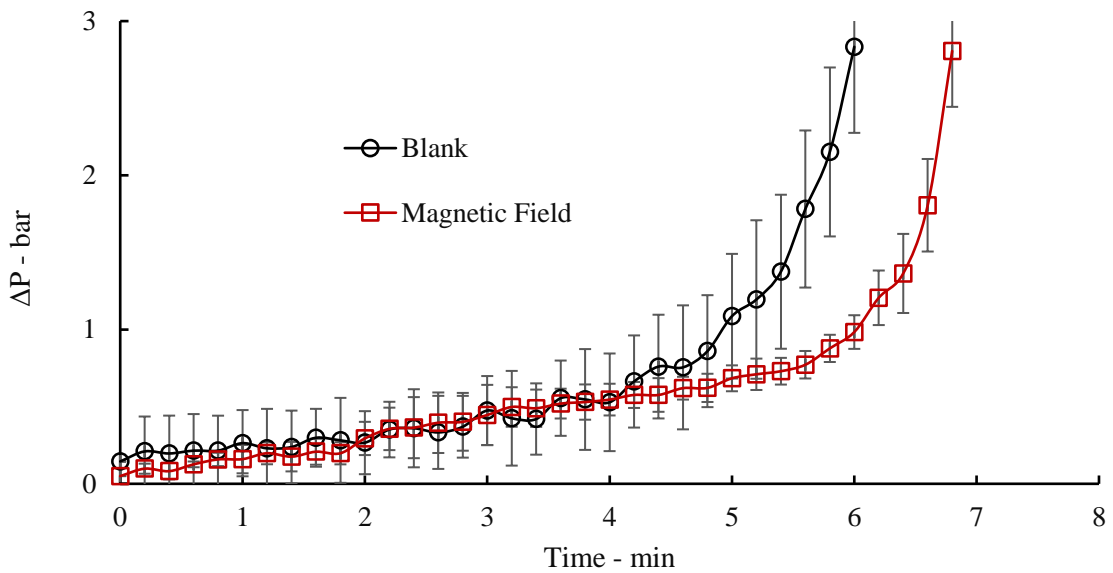


Figure 6-6 Effect of MF exposure upon the tendency of equal concentration of Ca^{2+} and HCO_3^- solution within 50 vol. % MEG to form scale

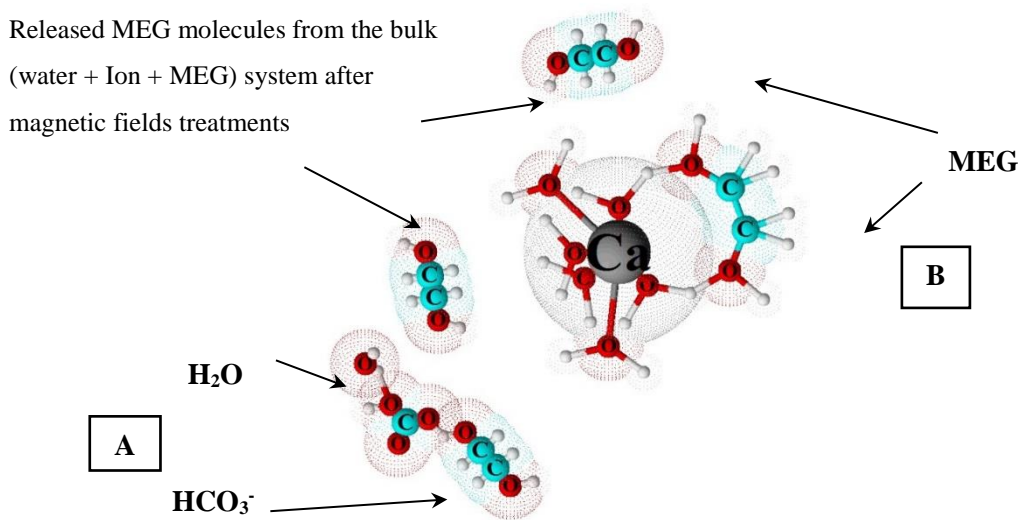


Figure 6-7 (A) Structure of MEG-bicarbonate ion-water system and (B) Structure of MEG-calcium ion-water system at 50 vol. % MEG after MFs treatment

Figure 6-8 illustrates differences in EC measurements of the exposed and blank trials within 50 vol. % MEG containing equal concentrations of Ca^{2+} and HCO_3^- ions. It is observed that exposure

to the MF has initiated an increase in EC when compared to corresponding blank tests. In other words, it is apparent that applied external MFs exert an opposite effect on the number of water molecules and it's inter-, and intramolecular attraction compared to 80% by volume of MEG trials. Furthermore, water–MEG molecules within the ions solvation shell followed a different arrangement pattern by keeping water molecules inside the solvation shell leading to weakening the effect of bulky MEG molecules [31, 189]. In other words, these results indicate that the number of water molecules involved in the solvation shell was increased in a way that minimized the effect of MEG molecules. As a result, the external MF had a positive impact on rich MEG solution by attracting more water molecules into the solvation shell. The reason behind this behaviour may be due to the smaller size of the water molecules compared to MEG molecules; this smaller size allows water molecules to create more ion-dipole bonds with ions in the solution leading to a change in hydration shell thickness. Since the EC measurement is dependent on the thermodynamic functions of hydration shell [194], this effect is generating the difference in EC measurements. As shown in Figure 6-8, it is observed that EC measurements, after exposure to MFs, confirm a decrease in thickness of the solvation shell around the ionic species due to their inversely proportional relationship [169] and, thus, the increase in the hydration shell [29]. Furthermore, the effect of MFs within the 50 vol. % MEG has shown an inhibitory effect on the scale formation due to increasing the number of water molecules within its hydration shell.

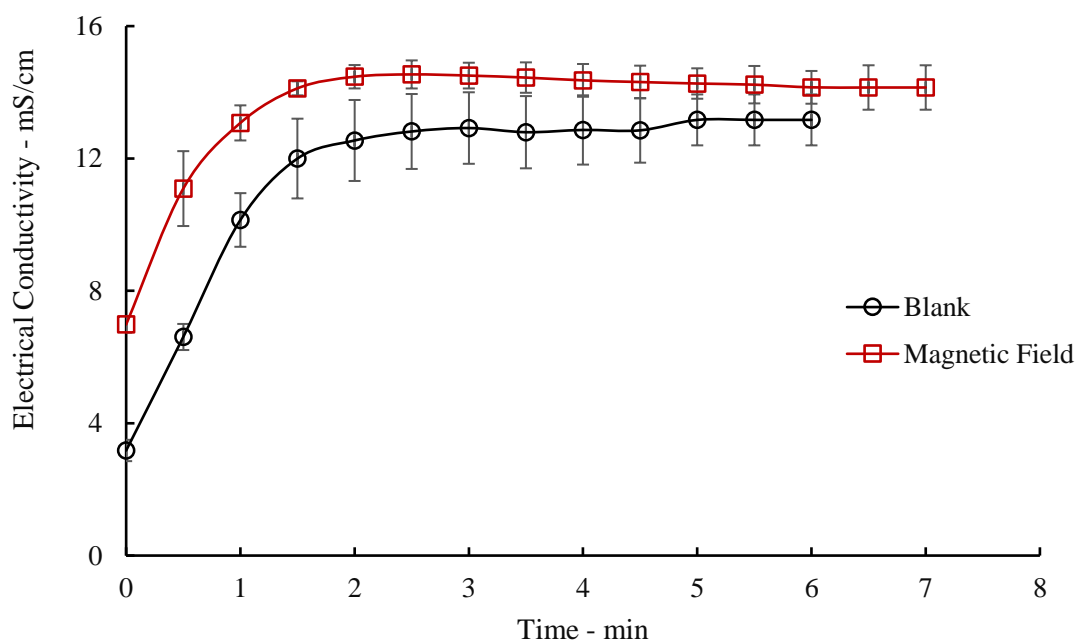


Figure 6-8 Effect of MF exposure upon EC of equal concentration of Ca^{2+} and HCO_3^- solution within 50 vol. % MEG

6.3.3 Morphology of the Precipitates Calcium Carbonate after Exposed to External Magnetic Field

After evaluating the influence of MFs exposure on the scale formation behaviour within 50 vol. % and 80 vol. % MEG solutions by using the DSL technique, as discussed in sections 6.3.1 and 6.3.2, the morphology of the formed CaCO_3 has been investigated for both the exposed and blank trials. Furthermore, additional tests were performed by using the static jar technique to compare the produced CaCO_3 morphology with the results of DSL testing.

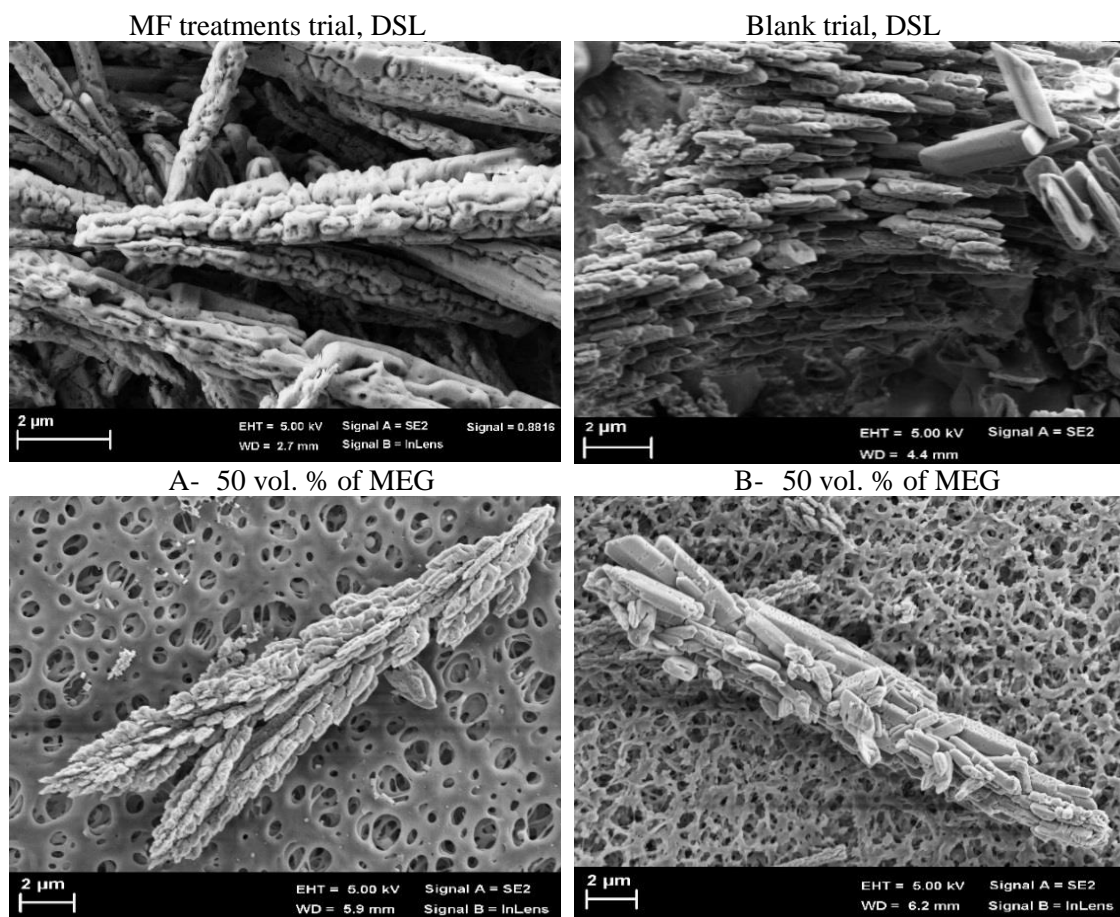
6.3.3.1 Crystal Structure of the Precipitates Calcium Carbonate at 50 and 80 vol. % MEG within DSL Technique

SEM images of exposed and blank trials within 50 percent by volume MEG at 150°C are illustrated in Figure 6-9 A and B and Figure 6-10, where needle-like aragonite morphology was formed under both conditions. The trials with MFs present generated a noticeably longer needle structure at low magnification that appeared to be more singular in nature. On the other hand, the blank trials formed shorter needle structures that agglomerated to form a cluster of scale particles. The formation of aragonite under these conditions is consistent with the findings of Flaten, Seiersten [106] who stated that at 80°C and above, aragonite is the dominant species within all MEG concentrations. Another interesting result observed is shown in Figure 6-10-A, where following MF treatment dendritic cluster aragonite with a snowflake shape have formed. Furthermore, the formation of the aragonite shape appeared to be non-stick and dry crystals. In contrast, images of blank tests highlight the formation of bulky aragonite spikes that are associated with other particles (refer to Figure 6-10-B). Additionally, it can be seen in image (B) that a thick fluid combined with generated crystals to form a non-regular surface, or liquid-like post-nucleation clusters, as was also reported by Coey [18]. Moreover, image (B) shows the impact of the MF treatment on the size of CaCO_3 crystals whereby larger bulky crystals were formed when no MF treatment was applied during DSL trials.

It is also important to consider the effect of varying MEG concentrations when evaluating the performance of MFs treatment to influence scale formation behaviour. The scale-formation products generated within 80 vol. % MEG solution utilizing the DSL testing technique (refer to Figure 6-11) did not show any noticeable difference to that of corresponding 50 vol. % DSL testing following magnetic exposure (Figure 6-9 A and B). Furthermore, no impact on the scale morphology was observed after treatment with MFs in terms of shape, size, and structure within 80 vol. % MEG as shown in Figure 6-9 C and D and Figure 6-11, a result contrary to the corresponding 50 vol. % experiments where a small difference in the morphology was observed. This result suggests that the effect of the MF treatment in terms of the morphology formed is limited to solutions with equal or higher concentrations of water than MEG. The reason behind

this difference may be explained by the effect of the MF on the MEG-water molecules within the solvation shell of the dissolved ions. The effect of the applied MF alters the arrangement of the bulky MEG molecules within the hydration shell of the ion (refer to Figure 6-7) whereby the ion's hydration shell thickness is more likely to be influenced by the number of water molecules [79, 170]. The bonding energy between water molecules and the dissolved ions is greater than that between the ions and MEG molecules [79, 170]. This greater bonding energy between water molecules and ions may facilitate their interaction leading to scale formation, as depicted in Figure 6-10 B. On the other hand, at higher MEG concentrations, where the potential interaction of ions and water molecules is limited, the drier singular dendritic clusters formed regardless of if a MF was applied or not.

The scale formation layers generated with an irregular surface play an essential role in the accumulation of scale within fluid transportation pipelines. Therefore, using the MF treatment within 50 vol. % of MEG and heat exchangers' skin temperature may provide a method to prevent the formation of thick fluid substances and, hence, scale, by creating a dry dendritic cluster aragonite structure of which is less likely to accumulate upon the surface of thermal units and pipelines. As such, applying MF treatment to rich MEG solutions containing brine solutions could provide an economical and eco-friendly method to achieve scale formation control but not at 80% by volume of MEG.



C- 80 vol. % of MEG

D- 80 vol. % of MEG

Figure 6-9 SEM images of different MEG concentrations at 150°C by using DSL technique.

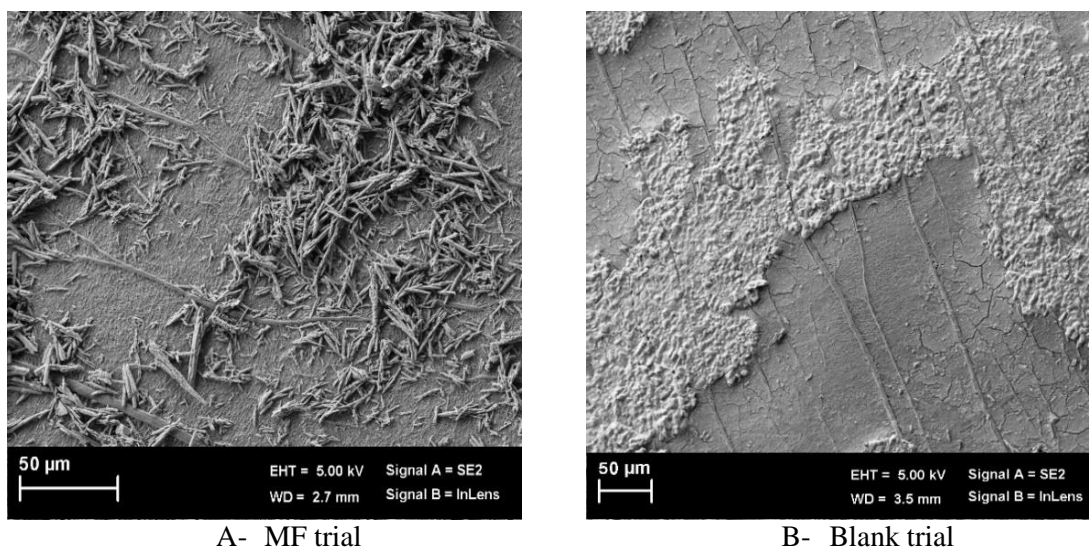


Figure 6-10 Low magnification SEM images of 50 % by volume of MEG concentrations at 150°C by using DSL

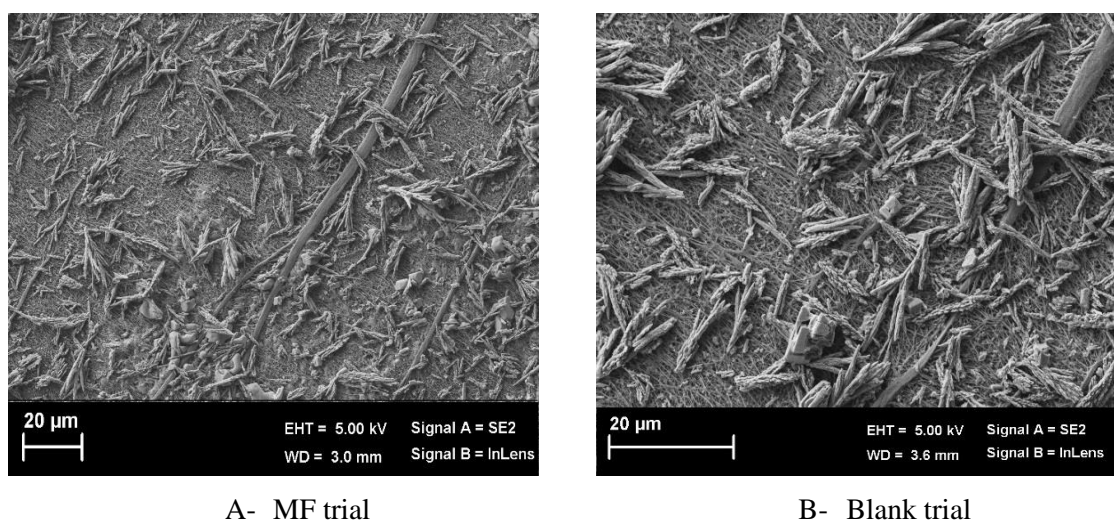


Figure 6-11 High magnification SEM images of 80 % by volume of MEG concentrations at 150°C by using DSL

6.3.3.2 Crystal Structure of Precipitated Calcium Carbonate at 50 and 80 vol. % MEG within Jar Cell Technique

Prior comparison of the jar test and DSL techniques for scaling evaluation have demonstrated that different CaCO_3 morphologies may be formed under the same conditions including temperature and composition [20, 25]. Furthermore, different nucleation rates and growth kinetics can also be expected during comparison of each analysis method [339]. It is well known that the nucleation rate and growth kinetics of CaCO_3 depends on both the system temperature and the

supersaturation of the solutions [340]. According to kinetic studies of CaCO_3 formation, the nucleation process is more sensitive to the supersaturation level than the growth process [120, 341, 342]. Therefore, the nucleation process may form smaller CaCO_3 particles within high supersaturation conditions [339, 340].

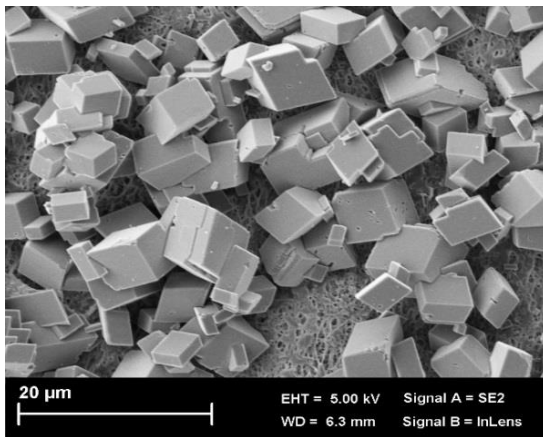
In such applications within aqueous solutions, Montazaud [26] has reported that the aragonite morphology is more likely to occur at a high temperature ($>90^\circ\text{C}$). On the other hand, Cowan and Weintritt [343] concluded that aragonite could be observed at temperatures above 30°C . However, within MEG applications, Flaten, Seiersten [106] stated that the morphology of CaCO_3 may be influenced by increasing MEG content at 50°C with the conversion of aragonite to vaterite. The increase in MEG concentration may influence the supersaturation ratio of CaCO_3 at high temperatures hence influencing the nucleation process.

To compare the differences in morphology formed when applying the jar and DSL test methodologies, jar test experiments were conducted at 30°C and 150°C ($\pm 1^\circ\text{C}$) for varying MEG concentrations (0, 50 and 80 vol. %) using the same brine composition outlined by Table 6-2. The CaCO_3 scale at 0 percent by volume MEG within the jar test formed an abundance of idiomorphic calcite rhombohedra structure, which was the structure prevalent at room temperature (refer to Figure 6-12-A). Additionally, Figure 6-12-B shows SEM images of CaCO_3 morphology formed from aqueous solution in jar tests at 150°C . The increase in temperature facilitated the formation of primarily idiomorphic calcite rhombohedral structures with non-smoothed surfaces. As a result, jar tests conducted as a part of this study were in line with the prior literature findings at 30 and 150°C [20, 140].

On the other hand, at 50 and 80% by volume of MEG, the morphologies of CaCO_3 produced during jar test experiments showed significantly different structures when compared to 0 vol. % of MEG trials, as shown in Figure 6-12C and E. The increase in MEG concentration had a significant impact on the type of crystal structure formed. It can be seen that vaterite crystals started to form at 30°C creating spherical shapes side by side with calcite within 50 vol. % of MEG as shown in Figure 6-12-C, while monoclinic and trigonal smooth surface shapes formed within 80 vol. % of MEG as shown in Figure 13-E. Upon raising the temperature to 150°C , a more complex assortment of crystals structures was found. Figure 6-12-D and F illustrate the formation of branched needle-like aragonite crystals in combination with idiomorphic calcite rhombohedra particles as identified by Flaten, Seiersten [106]. Moreover, Flaten, Seiersten [106] reported that vaterite particles would transition to aragonite crystals when the temperature was raised to approximately 80°C within 60% wt. of MEG solution; a result consistent with the findings of this study. Therefore, the generated results can be explained by the action of the MEG solution itself, which changes the kinetic control of morphology structure in jar tests.

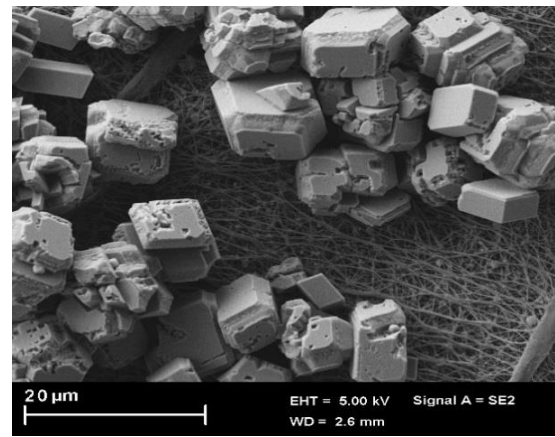
Overall, the jar test results are in line with the results of Flaten, Seiersten [106] with regards to the needle-like CaCO_3 structure formed at approximately > 50 vol. % of MEG. However, of the tests conducted, significant differences in morphology of the scale formation are evidently illustrating the joint impact of both MEG concentration and temperature on scale formation growth. Further impact on the type and size of CaCO_3 scale formed is also apparently due to the dynamic nature of the DSL testing whereby the crystal structures are exposed to continuous liquid flow. In contrast to the static jar testing performed, non-branching needle-like aragonite crystals formed during DSL testing at 150°C , which exhibited a different geometric structure with a lack of calcite particles present. Due to the dynamic nature, DSL testing more closely simulates actual pipeline conditions whereby continuous liquid flow occurs. As such, the DSL method presents a more realistic approach to investigate scale formation within industrial applications and evaluation of scale inhibitors.

Trials at 30°C

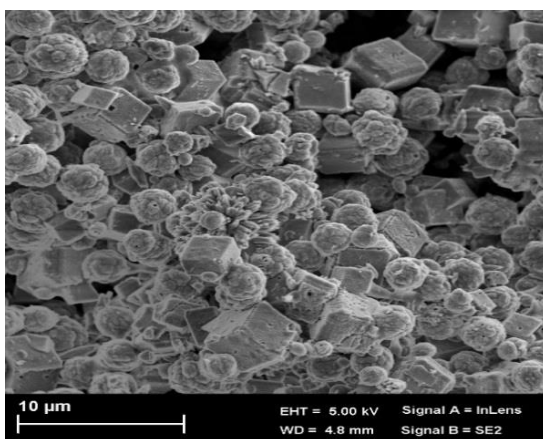


A- 0% by volume MEG, jar cell technique

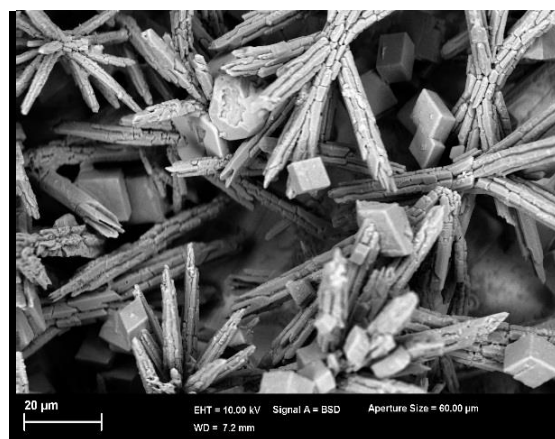
Trials at 150°C



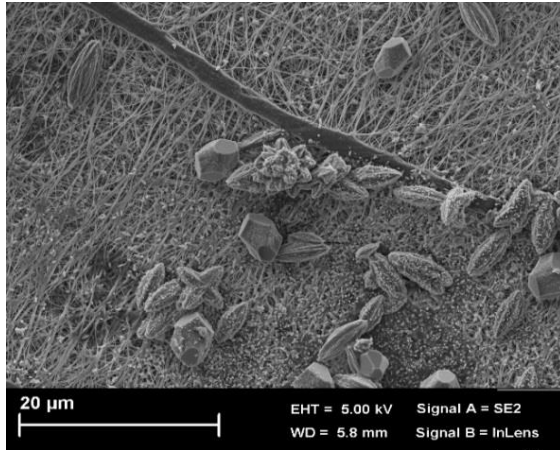
B- 0% by volume MEG, jar cell technique



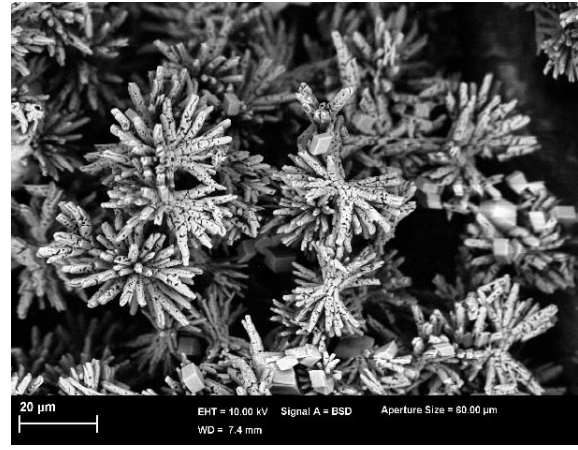
C- 50% by volume MEG, jar cell technique



D- 50% by volume MEG, jar cell technique



E- 80% by volume MEG, jar cell technique



F- 80% by volume MEG, jar cell technique

Figure 6-12 SEM images of different MEG concentrations at 30°C and 150°C by using jar cell

6.3.4 Discussion of Mechanism Caused after Exposure to Magnetic Fields

The influence of MFs on the strength of the intermolecular interactions in aqueous system impacts on hydration shell properties within the ionic solution [169, 174, 344, 345]. Furthermore, changes in hydration shell thickness results in a change in EC due to an alteration in the number of H₂O molecules in the first ion shell and ion mobility rate in watery system [109, 169, 194]. This hypothesis has been proven in several investigations within aqueous solutions, where the change in EC with hydration shell thickness was discussed [109, 169, 179].

Regarding the viscosity of MEG solutions, several studies have concluded that an increase in solution viscosity leads to lowered scale growth and nucleation rates [6, 107, 140]. This is due to the significantly slower diffusion of growing particles within high viscosity solutions[107, 140]. Furthermore, according to the Nernst-Einstein equation, there is a relationship between fluid viscosity and its EC [346].

$$EC = \left(\frac{F^2}{RT} \right) \sum_i D_i z_i^2 (\gamma_i)^a c_i \quad 6-3$$

Where, F denotes Faraday's constant (96485 °C/mol), T the temperature in Kelvin, R the gas constant (8.314 J/mol·K) and z_i and c_i the ionic species charge and molar concentration respectively. D_i denotes to the self-diffusion coefficient of ions, which can be calculated by the Stokes-Einstein equation.

$$D_i = \frac{k_B T}{6 \pi \mu r_i} \quad 6-4$$

Where k_B denotes the Boltzmann's constant ($1.38064852 \times 10^{-23}$ m².kg/s².K) and r_i the solvation radius of ions. A clear correlation is thus evident between EC and the viscosity of solution due to

its influence on the diffusion of ionic species through the solution (see Figure 6-13). As such, it can be expected that for higher MEG concentrations, a decrease in the measured EC would occur, consistent with Figure 6-13 for a range of 10 to 100 vol. % MEG concentration. However, further reduction in the EC occurred within the 80 vol. % MEG solutions following exposure to the MF in comparison to the blank tests (refer to Figure 6-4). The results can be further explained by a change in the radius of hydration and/or solvation shells around ions after exposure to the MFs as stated in the previous section.

According to Equations 6-3 and 6-4, the solvation shell radius of ions is inversely proportional to the electrical conductivity, and self-diffusion coefficient. However, the activity coefficient of ions is proportional to the solvation shell ion radius. The best mathematical model to describe the relationship between the activity coefficient and solvation shell radius is the extended Debye-Hückel model [347], as discussed in section 2.5.2.4.

Therefore, the increase of the solvation shell radius (decreases the hydration shell) would result in the increase of ion pair formation would thus affect supersaturation with respect to calcium carbonate, as shown for the 80 vol. % MEG experiments. In contrast, the 50 vol. % MEG experiments showed a reduction in the scale formation rate due to a reduction of the solvation shell radius as indicated by the increased electrical conductivity, especially after exposure to the applied MF. Therefore, any change in the solvation shell radius influences the self-diffusion coefficient and the activity coefficient of ions and thus changes the scale formation rate. The influence of ions hydrated radius on the activity coefficient is illustrated in Figure 6-15 and Figure 6-15.

Finally, it is essential to mention the dielectric constant that could be manipulated by external MFs thus impacting upon the Extended Debye-Hückel model (see the Equations 4 through 6). To be more precise in this hypothesis, Shen [348] reported that the dielectric constant of the electromagnetic field-treated water is 3.7% greater than the non-magnetized solutions, specifically under the extremely low electromagnetic field. While Pang and Shen [349] stated that the dielectric constant of the magnetized solution decreases with increasing the frequency of the applied electromagnetic field and exposure time.

These proposed results indicate that the dielectric parameter can be affected by controlling the intensity of the MFs and the exposure time. The Extended Debye-Hückel model can estimate the ionic activity coefficient (γ_i) of ions by taking into consideration the radius of ions (a_i) and the dielectric constant of the solution [219, 220, 319]. However, the dielectric constant of water is higher than the dielectric constant of MEG, by approximately a factor of two[1]. Therefore, the presence of external MFs could increase the dielectric constant of MEG-water solution, which in

turn influences the ion activity and scaling potential. This phenomenon suggests the possible advantage of using MFs within scale formation treatments if it is used correctly.

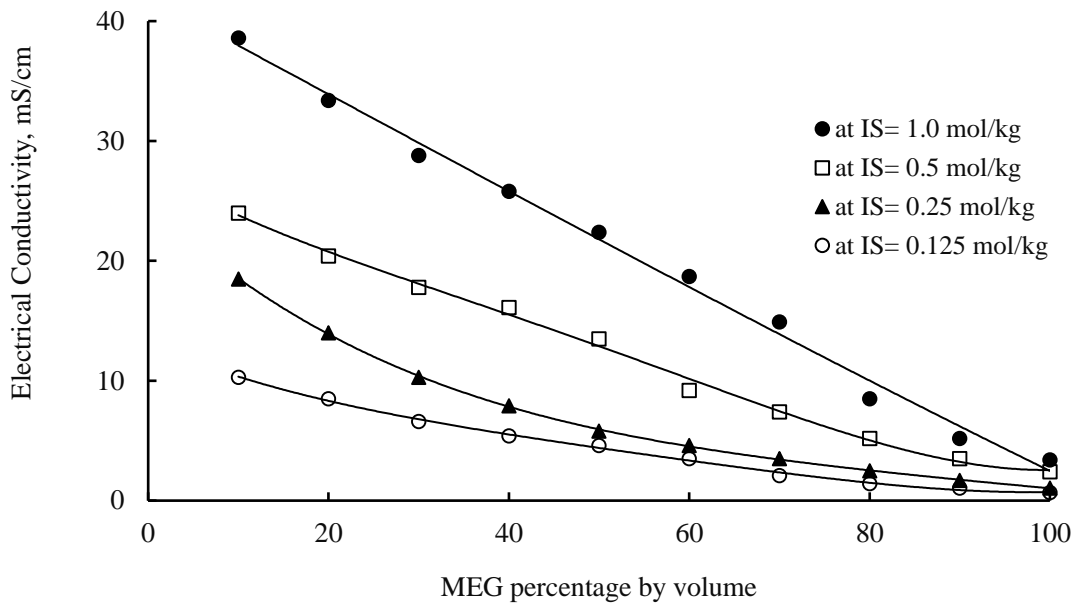


Figure 6-13 Electrical conductivity of different MEG concentrations of varying ionic strength at 20°C

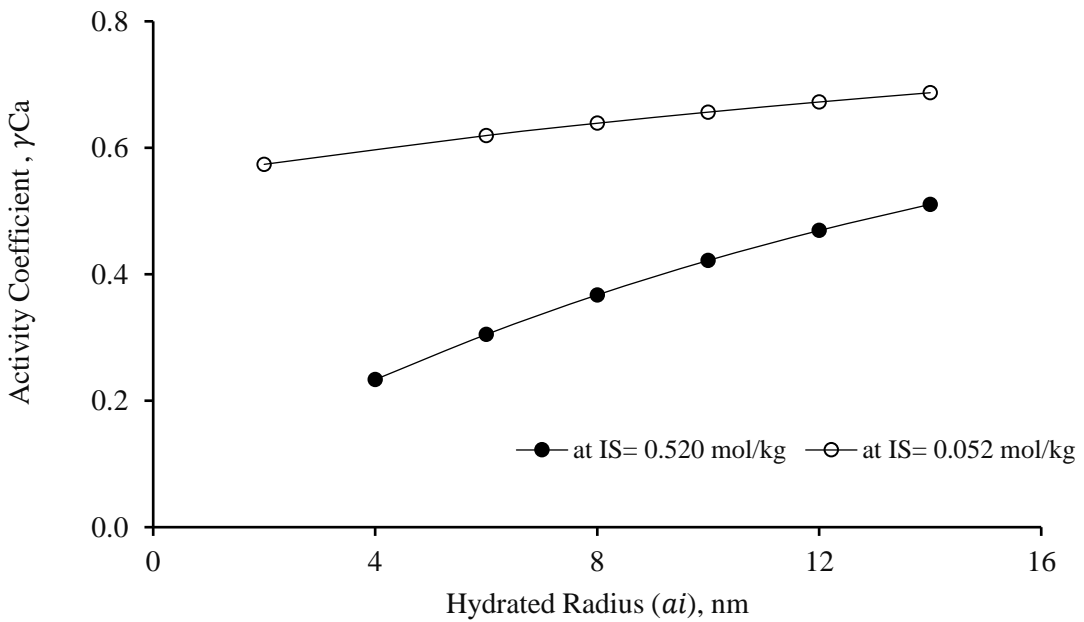


Figure 6-14 Estimated activity coefficient of calcium ions as a function of ionic strength using the extended Debye-Hückel model

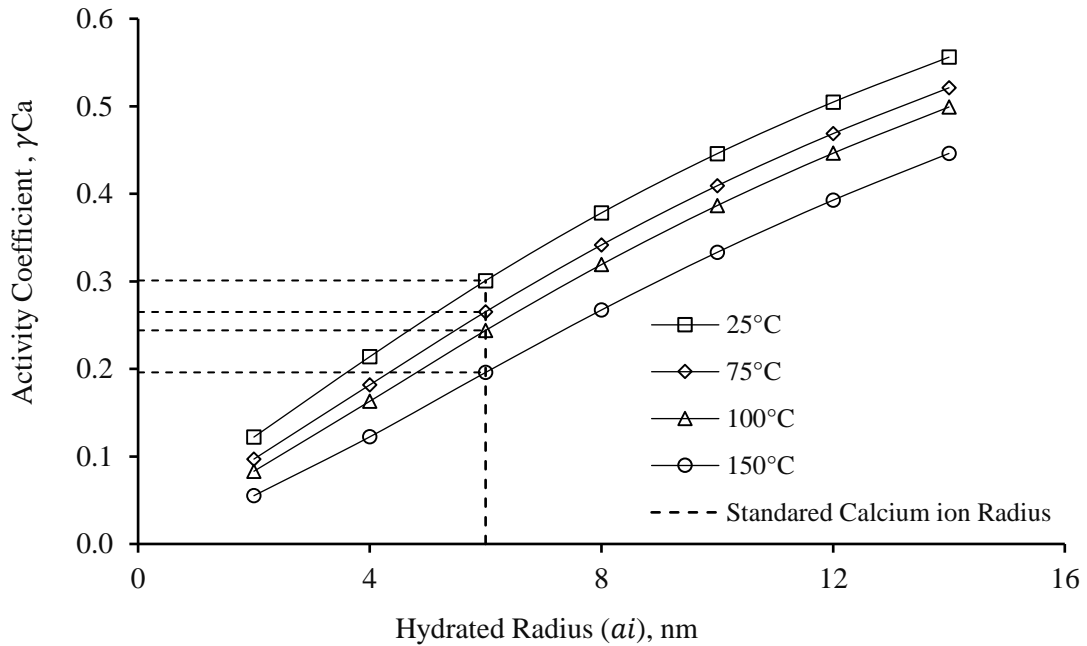


Figure 6-15 Estimated activity coefficient of calcium ions as a function of temperature using the extended Debye-Hückel model

6.4 Conclusions

It was intended to use a high concentration of both calcium and carbonate ions in this study to make the deposition process inside the capillary faster so that we can observe the effects of magnetic fields on scale formation. Five conclusions were reached concerning the applications of MF treatment in inhibiting the scale formation of CaCO_3 in aqueous solutions at different MEG concentrations. Firstly, the degree of scale formation, whether inhibited or promoted, is conditional on MEG content. Secondly, the exposure of the MEG and brine solutions to the applied MF had a significant impact on the EC measured. The results were consistent with previous studies of aqueous solutions where it was concluded that the solvation shell thickness of the Ca^{2+} and HCO_3^- ions were subject to manipulation by MFs leading to variations in EC [109, 169, 194]. Thirdly, following trials at 50 vol. % MEG concentration, bulky, and rough crystals were formed that may enhance a hypothesized clot-like build-up inside the transportation pipelines [109]. Similarly, jar tests highlighted the shift in crystallization processes that may occur at high MEG concentrations and high temperatures, although the jar test results cannot explain the morphology of real crystals in pipelines they can clarify the kinetic parameters that control crystals formed under different conditions.

Fourthly, previous studies suggested the external radius of ions to be the outer radius of hydration shells, not the actual ion radius in calculating the ionic activity coefficient [219, 220, 342]. This hypothesis has been reinforced after an improvement in the activity coefficient of ions occurring following exposure to MFs. Finally, due to the effective inhibition of scale formation produced

by the external MF treatment within 50% by volume of MEG, it can be proposed that MF treatment could provide an environmentally friendly scale inhibition approach that could replace/reduce the use of traditional chemical inhibitors in industry. In this regard, it is believed that research into the thermodynamic properties of an aqueous and non-aqueous solution in MFs is more promising.

Chapter 7 Evaluating Chemical-Scale-Inhibitor Performance in External Magnetic Fields Using a Dynamic Scale Loop System

7.1 Introduction

MEG is extensively used in oil and gas pipelines to prevent gas hydrate formation [3, 4, 131]. However, it also contributes to mineral ion precipitation under alkaline conditions [26, 350] and, thus, necessitates the use of CSIs to reduce scaling [121, 145, 146, 165]. Non-chemical inhibitors, such as an external magnetic field, can successfully inhibit scaling in aqueous solutions [19, 39, 174, 177]. Therefore, the combined application of MEG and MFs in mineral deposit treatment was investigated to understand the effect of the latter on CSI performance. Two commercial CSIs (HEDP and Phosphate ester) were examined with and without an external MF of 0.65 Tesla using a dynamic scale loop device. The CSIs were injected into ionic solutions containing 1656.9 ppm calcium ions and 2628 ppm carbonate ions in an aqueous MEG solution (80 vol. %), and the tests were performed at 130°C and pH 9.5.

7.2 Materials and Methods

7.2.1 Brine Solutions

The MEG-brine solutions used in this study resemble the compositions of those used in real oil-field situations, as recommended by NACE laboratory screening tests and PSL Systemtechnik [147, 309]. The aqueous glycolic solutions consisted of calcium chloride dihydrate (Scharlau reagent grade ACS, >99 wt%), sodium chloride (Chem-Supply reagent grade, >99 wt%), sodium carbonate (Chem-Supply reagent grade, 99.7 wt%), MEG solution (Chem-Supply reagent grade, >99 wt%), etidronic acid (Sigma-Aldrich, 60 wt%), and organophosphates (commercial brand, 30 wt%). An aqueous glycolic solution was used in this study to simulate the oil and gas pipeline brine solutions. The mineral ion compositions and their concentrations within the MEG-brine solution are listed in Table 7-1.

Table 7-1 Feed concentration of cations and anions for the DSL test

Ion	Anion Solution, mg/L	Cation Solution, mg/L	Mixed Solution, mg/L
Ca ²⁺	0	3313.8	1656.9
CO ₃ ²⁻	5256	0	2628
Na ⁺	15005.05	12990.8	13997.9
Cl ⁻	20033.37	25893.39	22963.4
Vol. % MEG	80	80	80
*Ionic Strength, Molar at 25°C			0.761
*Total Alkalinity, mg/L			10137
pH of mixed brine solutions			9.5

*These values were calculated by using Aqion software.

The performances of the two types of CSIs were evaluated in the laboratory in an external MF using the DSL system at 130°C and 1 bar. The concentrations of CSIs are shown in Table 7-2.

Table 7-2 CSI concentrations used in the DSL test

CSIs		Dosage Concentration, ppm		
Code	Chemical Name	Low	High	Extremely High
CSI-A	HEDP	20	100	200
CSI-B	Phosphate ester	20	100	200

7.2.2 Dynamic Tube Blockage Test

Figure 7-1 shows a schematic diagram of the DSL system (PSL Systemtechnik, Germany) with the magnetic treatment device. The specifications of the DSL system are listed in Table 7-3. Commercially available permanent magnets (NdFeB grade SHN45) from Oasis Materials Technology Limited were used in these experiments, and the magnetic flux density was measured using a teslameter (Wutronic, Germany). A permanent magnet was placed around the stainless steel tubing through which the solutions flowed prior to the capillary test coil inside the DSL device. The external magnetic device was designed as a cylinder with an outer diameter of 7.62 cm and a length of 22.86 cm in order to generate a field of approximately 0.65 Tesla with a maximum produced energy (BHMax) of 44.38 MGOe. The cylindrical magnet had a 0.32 cm hole in the center to allow the brine solution to flow through the MF. Magnetic induction was perpendicular to the flow of the brine solution in this configuration.

The DSL method was used to simulate real conditions within a distillation column when re-concentrating a mixture of brine, CSI, and MEG-rich solutions in the reboiler section. The MEG-rich solution was replaced with a MEG-lean solution during DSL experiments in order to approach the composition of the reboiler solution. CSI performance was evaluated before and after exposure to the external MF at different dosages. The experiments were conducted at 130°C and 1.0 bar, with 1656.9 ppm of calcium ions as the cationic solution and 2628 ppm of carbonate ions as the anionic solution. The two solutions were prepared separately in two bottles following the standard NACE procedure [351], filtered, and adjusted to a pH of 9.5 to enhance scale formation following mixing of cations and anions.

The stainless steel capillary tubing coil was preheated and set at 130°C before the commencement of any experiment. The cation and anion solutions were then injected into the DSL system at a constant flow rate of 5 mL/min. The formation of inorganic scale was monitored by PC-interface software that recorded the pressure built up across the capillary tube with time. The maximum pressure across the capillary tube was set to 5.5 bar; the DSL detector terminated the experiment once the pressure sensor detected this value. A two-way valve connected the injection pump lines and the mixing capillary tube coils in order to perform the experiments in magnetic

and non-magnetic modes. The data were compared in terms of CSI scale-formation-inhibition performance in a 1-m-long stainless steel coil with an internal diameter (ID) of 1.01 mm.

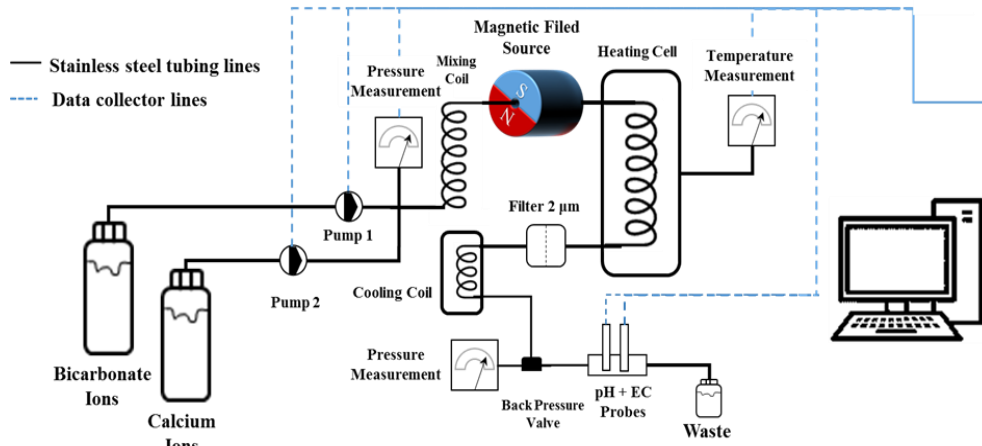


Figure 7-1 Schematic diagram of the DSL system

Table 7-3 DSL specifications

Component	Specification	Notes
High-pressure liquid pumps	0.1–5 mL/min, ± 0.01	Data-logger
Back pressure valve	0–172 bar, ± 0.01	Stainless steel 316
Capillary testing coil	1 m length	Stainless steel 316
	1.41 mm outer diameter	
	1.01 mm inner diameter	
Mixing coil	1.0 m length	Stainless steel 316
	3.17 mm outer diameter	
	2.01 mm inner diameter	
Pressure detector	1 bar to 172 bar	Data-logger
Heating chamber room	+30 to +250°C, $\pm 0.1^\circ\text{C}$	Data-logger
pH meter and the probe	1–14	Data-logger
Electrical conductivity	0–1000 mS/cm, $\pm 0.1\%$	Data-logger
PC interface	<i>winDSL</i> software, Windows 10	

CSIs were mixed with the anionic solution at twice the specified concentrations because subsequent addition of the cation solution (in a 1:1 volume ratio, as recommended by NACE laboratory screening tests and PSL Systemtechnik) leads to dilution, resulting in adjustment of the CSI concentration to the specified value (see Figure 7-2). The CSI concentration for each set was increased gradually, as shown in Table 7-2. Each experiment was repeated four times to validate the results. All experiments performed without exposure to the MF were repeated using the MF device. The non-CSI experiments were exposed to the MF and the results compared to those from blank experiments. The change in duration time of each experiment is representative of the performance of that CSI in preventing scale formation within the DSL device before and after exposure to the MF. In addition, the CaCO_3 solution in the outlet stream was collected for further analysis.

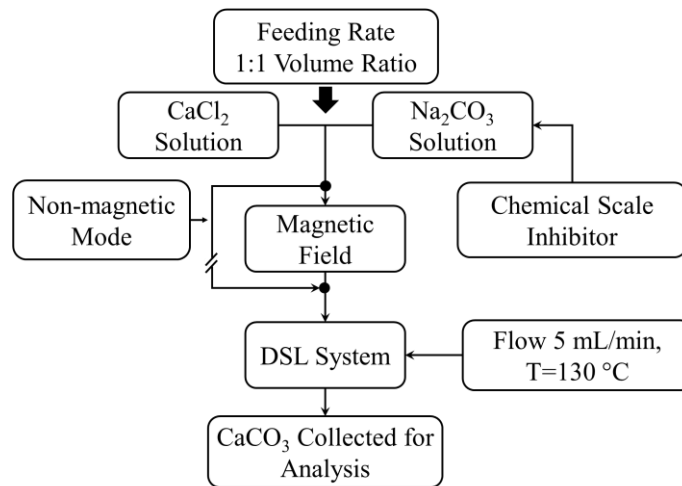


Figure 7-2 Flowchart of experimental procedure

7.2.3 Analytical Method

In this study, the discharge liquid from the DSL was collected for particle-size-distribution and other analyses. The liquid phase was separated from the solid phase by centrifugation of the entire resulting solution. Liquid-phase solutions were subsequently used to measure EC and turbidity, while the solid phases were used to determine ζ potential values; they were also subjected to scanning electron microscopy (SEM; NEON 40EsB FIBSEM, ZEISS NEON) (Figure 7-3). The turbidities of the aqueous solutions were measured using a portable turbidity meter (model HI98703-01, HANNA Instruments). Particle-size distributions and ζ potentials were measured following the formation of the CaCO_3 scale using a Malvern Panalytical Zetasizer (model ZSP). The CaCO_3 morphology was investigated by SEM; samples were coated with a 10-nm-thick platinum layer prior to SEM in order to obtain high-resolution images.

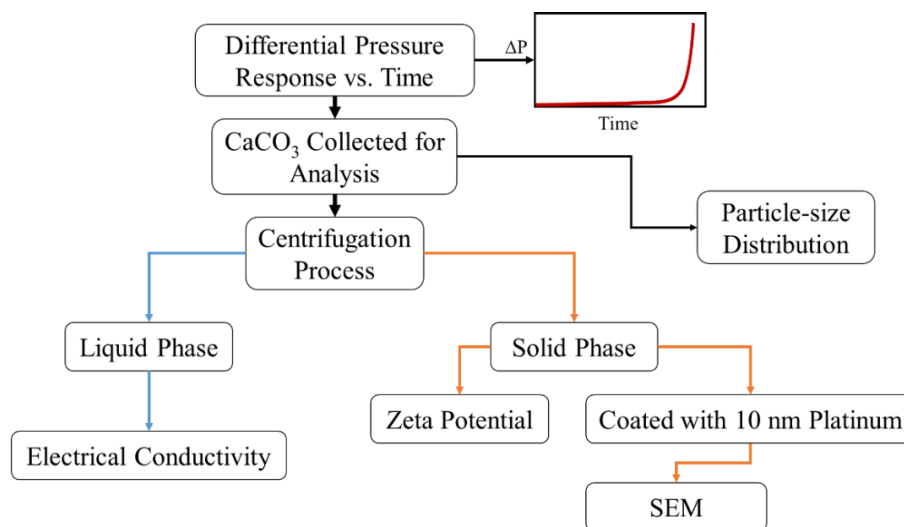


Figure 7-3 Flowchart of scale formation analyses for exposed and non-exposed trials

7.3 Results and Discussion

7.3.1 Effect of Magnetic Field on Brine Solution without CSIs

The responses of scale formation in terms of differential pressure change versus time are plotted in Figure 7-4, which shows the effect of MF on scale formation time after the brine solution was passed through the cylindrical magnetic device generating 0.65 Tesla of magnetic intensity compared to the ordinary brine solution (blank test). It is evident from Figure 7-4 that the magnetized solution showed an increased scale formation rate compared to the blank test as well as a significant increase of approximately 45% in scale formation time than that of the blank test. These results are consistent with those of Higashitani and Oshitani [189], who reported that an opposite effect of MF on scale formation may occur in methanolic solution (water-alcohol). Furthermore, the results are consistent with the findings of Higashitani, Kage [174], who pointed out that the nucleation frequency of molecules could be suppressed after exposure to MF while the growth of the nucleated crystal was accelerated. Another interesting observation from our study is that the applied MF promoted the formation of scale within 80 vol. % MEG solution which implies that the magnetic force was active even after the sample was exposed to a temperature of 130°C. These outcomes refute the prevailing idea that the MF-memory effect is destroyed by high temperatures [29]. Moreover, the maximum energy produced by the MF was shown to be more important than the MF strength itself [31].

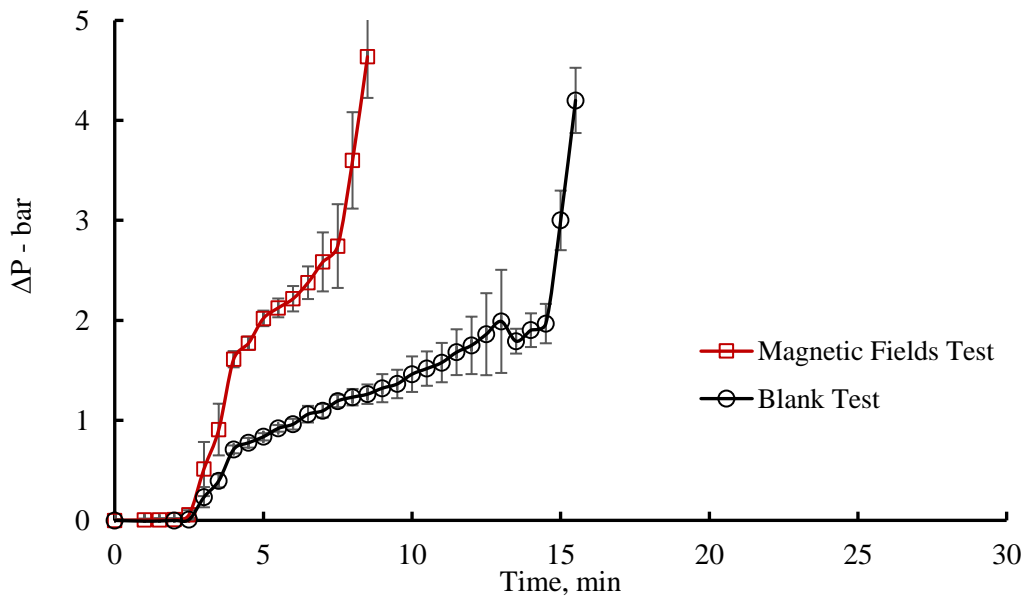


Figure 7-4 Changes in pressure (scale formation) as functions of time for calcium carbonate solutions following exposure, or not, to an applied magnetic field

7.3.2 Effect of Magnetic Field on CSI-A

Experiments were conducted with different CSI-A concentrations where the solution was exposed to a constant external magnetic strength for 5 seconds to determine the effect of the field

on CSI performance. It should be noted that in order to obtain rapid responses, the initial concentrations of anions and cations were relatively high in these experiments. Furthermore, CSIs have been ranked against scale formation in extensive studies in previous years; consequently, such a study was not repeated here, rather, the assessment of overall performance under MF conditions was our focus. The effect of MF strength on the ability of CSI-A, at concentrations of 20, 100, and 200 ppm, to inhibit scale formation is shown in Figure 7-5 to Figure 7-7. In the absence of the MF, CSI-A exhibited poor performance at 20 ppm; it failed to impede scale formation (Figure 7-5). However, the performance of CSI-A consistently improved at 100 and 200 ppm, with the scale-formation rate reduced by 50 % (Figure 7-6 and Figure 7-7). Furthermore, a noticeable difference in the CSI-A performance was observed at all dosages when exposed to the MF; these experiments revealed the inhibiting effect of MF on CSI-A performance, which varied from 33.3% at 20 ppm, to 37% at 100 ppm, and 4% at 200 ppm. At 200 ppm, CSI-A exhibited an excellent response under the external MF; however, this dosage is very high for industrial use and beyond the limits indicated for this kind of inhibitor [12]. When the effects of different CSI-A concentrations were compared at a constant flow rate of 5 mL/min, a significant reduction in CSI-A performance was observed under the applied external MF, which indicates that CSI-A is restricted in preventing scale formation in pipelines when exposed to a MF.

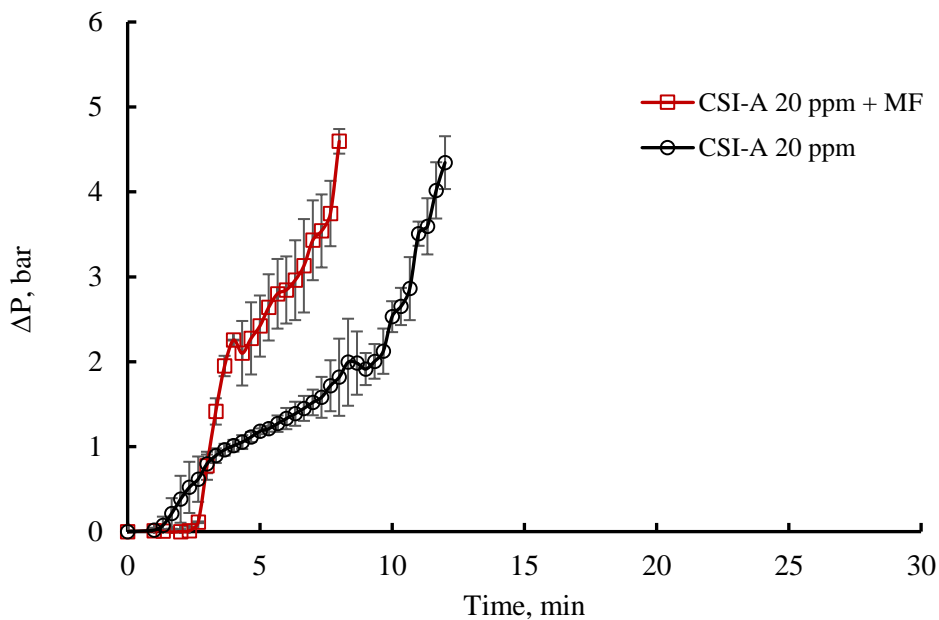


Figure 7-5 Changes in pressure (scale formation) as functions of time for calcium carbonate solutions in the presence of CSI-A at 20 ppm concentrations following exposure, or not, to an applied magnetic field

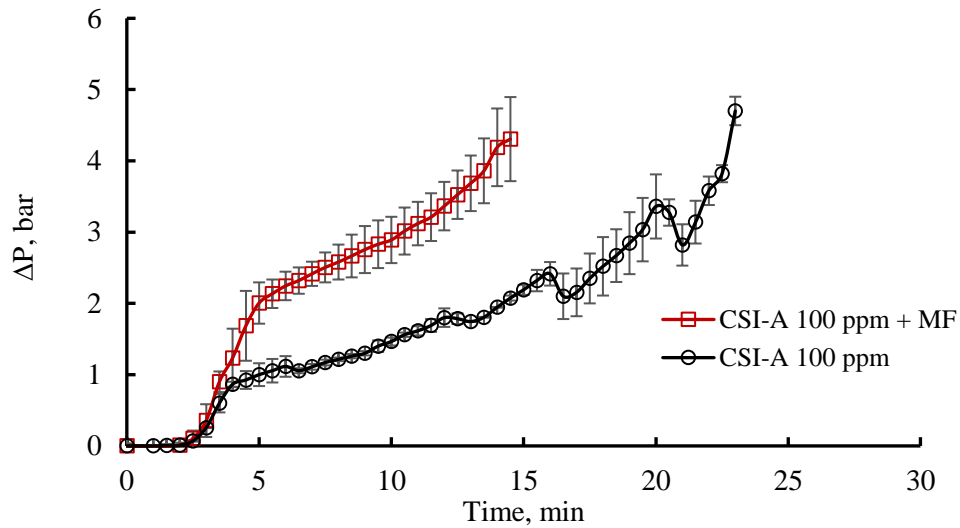


Figure 7-6 Changes in pressure (scale formation) as functions of time for calcium carbonate solutions in the presence of CSI-A at 100 ppm concentrations following exposure, or not, to an applied magnetic field

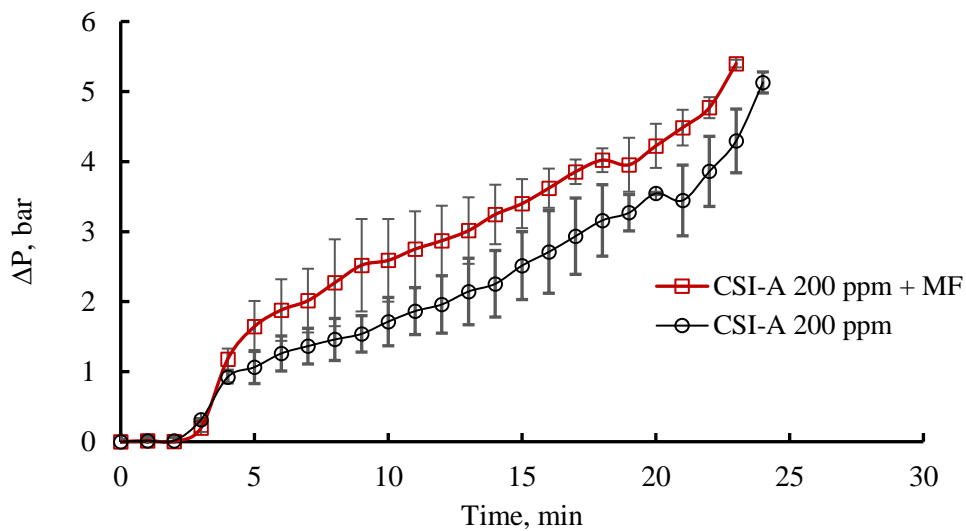


Figure 7-7 Changes in pressure (scale formation) as functions of time for calcium carbonate solutions in the presence of CSI-A at 200 ppm concentrations following exposure, or not, to an applied magnetic field

7.3.3 Effect of Magnetic Field on CSI-B

The effect of MF strength on the ability of CSI-B, at concentrations of 20, 100, and 200 ppm, to inhibit scale formation is shown in Figure 7-8 to Figure 7-10. Irrespective of the inadequate performance of the CSI in inhibiting scale formation, which is evident from Figure 7-8 to Figure 7-10, the results under the external MF are consistent with those obtained for CSI-A; the MF accelerated scale formation at all CSI-B concentrations. On the other hand, compared to the CSI-A results, those from the MF-exposed and non-exposed trials showed that CSI-B failed to inhibit

scale formation. Furthermore, the results discussed in Section 7.3.1 (in the absence of CSI treatment) and those presented in this section confirmed that CSI-B was inadequate for use as a CSI at such high MEG concentrations and high temperatures. Moreover, a comparison of the blocking times of the blank experiment described in Section 7.3.1 and the CSI-B experiments presented in this section, which are similar, reveal no changes in scale-formation time before and after the use of CSI-B. In addition, these results show that MF treatment with 80 vol. % solutions of MEG significantly advanced scale formation.

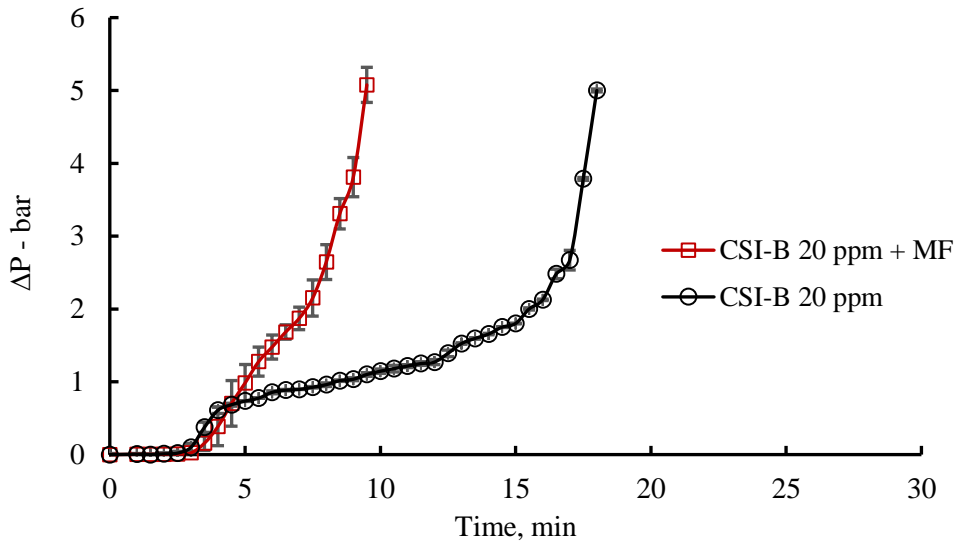


Figure 7-8 Changes in pressure (scale formation) as functions of time for calcium carbonate solutions in the presence of CSI-B at 20 ppm concentrations following exposure, or not, to an applied magnetic field

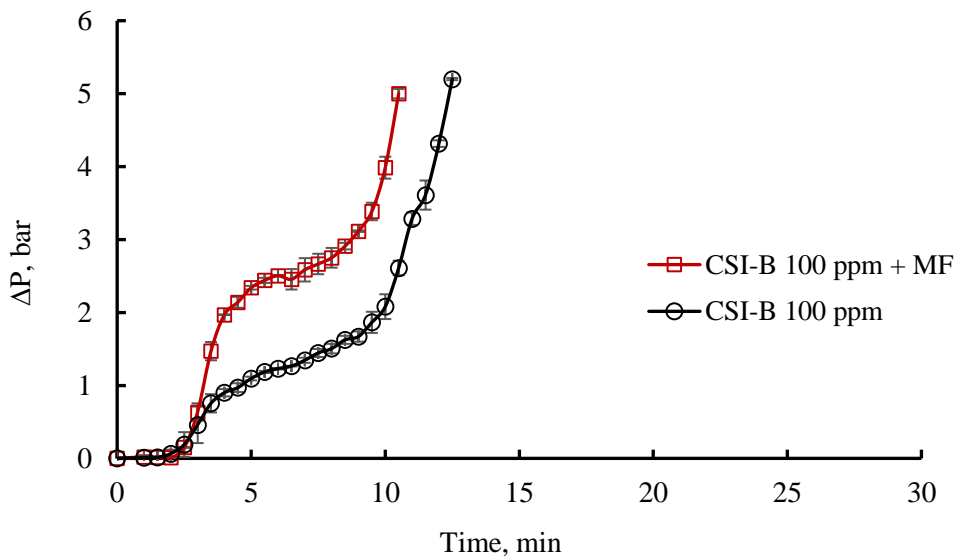


Figure 7-9 Changes in pressure (scale formation) as functions of time for calcium carbonate solutions in the presence of CSI-B at 100 ppm concentrations following exposure, or not, to an applied magnetic field

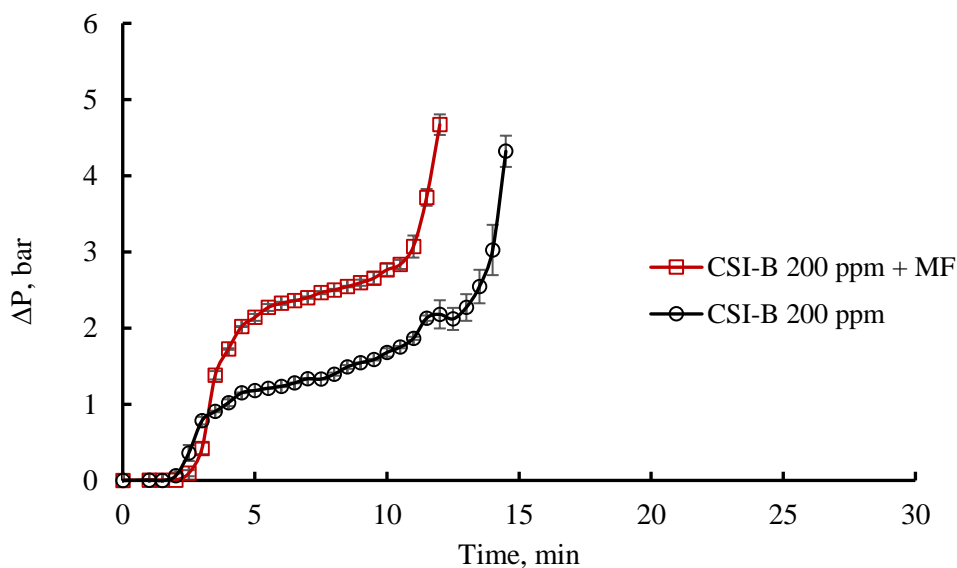


Figure 7-10 Changes in pressure (scale formation) as functions of time for calcium carbonate solutions in the presence of CSI-B at 200 ppm concentrations following exposure, or not, to an applied magnetic field

7.3.4 Effect of Magnetic Field on Electrical Conductivity

The ECs of CSI-A and CSI-B solutions that were collected before and after exposure to the MF were measured following centrifugation, the results of which are displayed in Figure 7-11 for various conditions. These plots reveal that the ECs of the solutions obtained from the magnetized experiments were lower than those obtained from the non-magnetized experiments. Furthermore, a significant reduction in EC was observed for samples from CSI-B concentrations of 100 and 200 ppm, as well 200 ppm of CSI-A. These observations are attributable to differences in the thermodynamic properties of the solutions, leading to changes in the thicknesses of the hydration shells that surround the mineral ions after exposure to the MF. Therefore, the ionic hydration layer was altered, which weakened the electrophoretic effect of the ionic solution. These results are consistent with previous reports; i.e., that the EC of an electrolyte solution is inversely proportional to the thickness of the hydration shell [169, 189, 194].

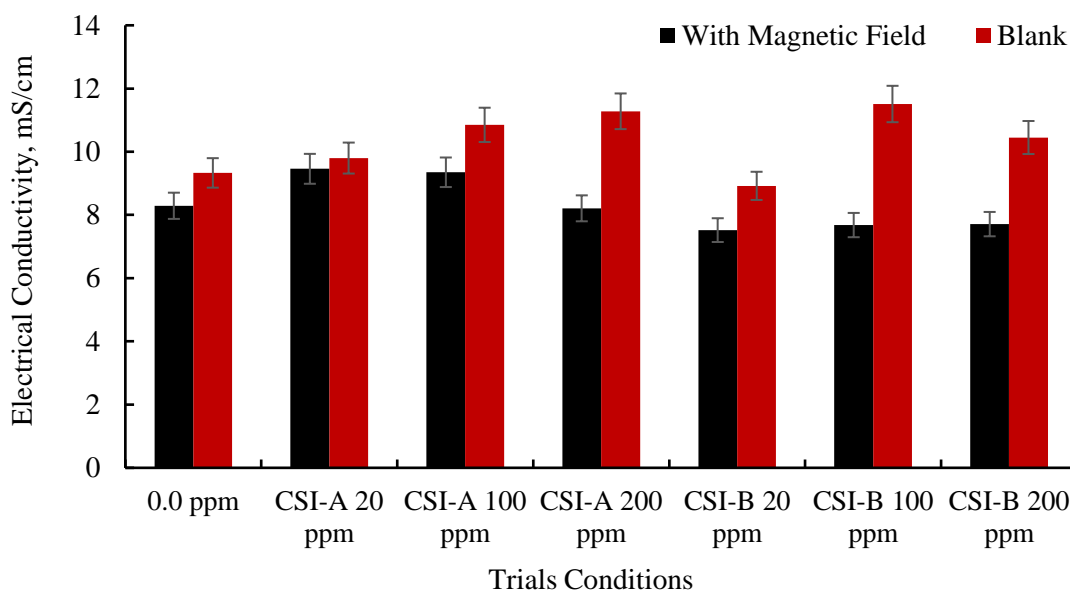


Figure 7-11 Electrical conductivities of solutions with various concentrations of CSI-A and CSI-B following exposure, or not, to an applied magnetic field

7.3.5 Effect of Magnetic Field on Turbidity

An interesting relationship between turbidity and magnetization can be observed in Figure 7-12. In the magnetization-free trials, a gradual and slight increase in turbidity was observed for all the proposed concentrations of both CSI-A and CSI-B compared with the non-CSI trials, suggesting that the formation of CaCO_3 particles was higher in the presence of CSIs. In contrast, the turbidities obtained for MF-exposed trials (~5 NTU) were lower than those obtained for non-exposed experiments. However, the trials with 100 and 200 ppm CSI-B showed higher turbidities than those observed in other tests even for the magnetization-free trials. This is possibly due to the hydrolysis reactions at higher temperatures, which may have changed the chemistry of the phosphate ester solutions. This hypothesis is in agreement with the findings of Valiakhmetova, Sorbie [158], who reported that phosphate esters could function up to 80°C. The turbidity measurements also showed that high concentrations of CSI-B caused an apparent change in the level of transparency of the treated solutions even when centrifugation was performed before or after exposure to the MF (Figure 7-12, 13, and 14). Thus, the use of this type of CSIs leads to a change in the physical properties of saline solutions because of the production of suspended solid

matter consisting of particles of many different sizes that likely affect the readings of inline sensors and detectors.

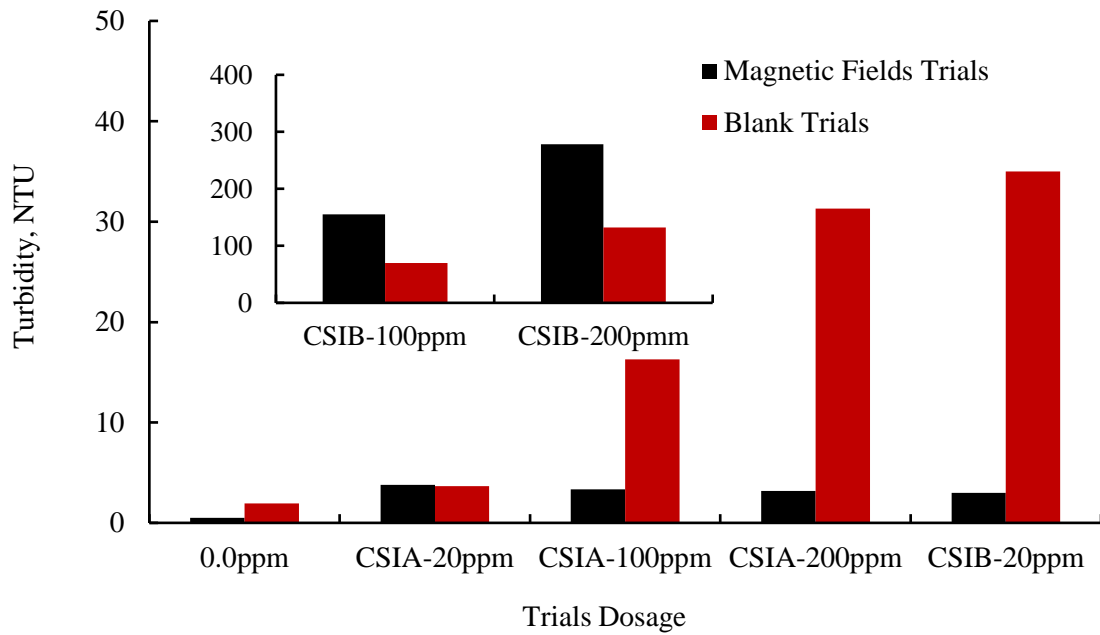


Figure 7-12 Turbidity of solutions with various CSI-A and CSI-B concentrations under an applied MF

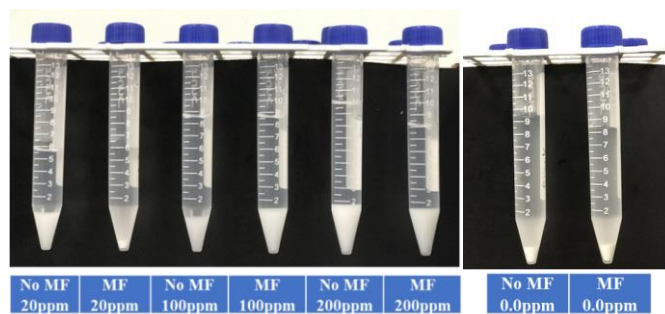


Figure 7-13 Liquid phase samples of CSI-A and without CSI-A after centrifugation

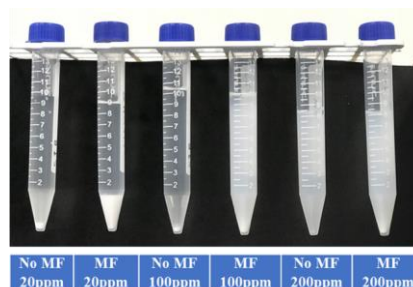


Figure 7-14 Liquid phase samples of CSI-B after centrifugation

7.3.6 Morphology of the Formed CaCO_3 Scale

The mineral deposits produced after each non-exposed experiment were examined by SEM in order to assess changes in morphology. The obtained SEM images were then compared with those

of brine solutions prepared at the same concentrations, but subjected to MF. In addition, non-inhibitory solutions were analyzed before and after exposure to the MF for comparison. The majority of scale particles formed in the non-exposed experiments had semi-spherical morphologies with flattened shapes, along with smooth cube-like structures, as shown in

Figure 7-15-A. These semi-spherical and cubic shapes were identified by XRD as vaterite and calcite, respectively (Figure 7-16), which is consistent with the results of Ryu, Ahn [352] and Flaten, Seiersten [106], who reported that the morphology of CaCO_3 changes into a meta-stable phase when MEG is used as the solvent. In addition, they claimed that higher temperatures induce the meta-stable morphology in MEG solution. Furthermore, the morphology of CaCO_3 is altered at higher initial calcium-ion concentrations and high aqueous glycolic-brine-solution pH [353]. Therefore, we conclude that the CaCO_3 morphology is very sensitive to the nature of the solvent, the ion concentration, and the reaction conditions in an aqueous solution. The geometrical features of the scale particles were seemingly affected by the external MF.

Figure 7-15-B reveals the formation of cube-like structures with rough surfaces following exposure to the MF at 130°C ; this morphology under these dynamic conditions is unique to this study. Furthermore, the cube-like particles generated in the MF-exposed experiments were larger than those generated in the non-exposed experiments, but slightly smaller than the spherical particles. Unfortunately, the roughened edges of the generated particles led to rapid blockage of the DSL capillary tube, which is consistent with the particle mechanism reported by Saksono, Gozan [55]. Therefore, the formation of a stable morphology is attributed to the effect of the magnetic field on the thermodynamic conditions during the reactions of calcium and carbonate ions, leading to the generation of more particles with rough cube-like surfaces.

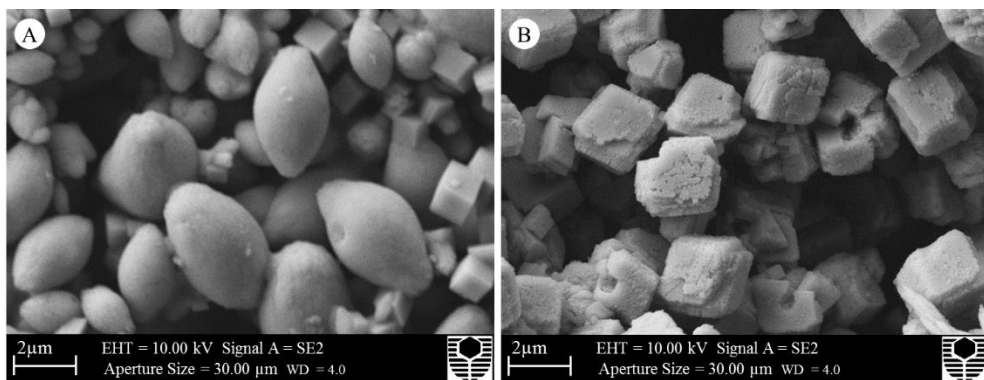


Figure 7-15 High-magnification SEM images (scale bar: $2\ \mu\text{m}$) of scales particles formed in magnetized and non-magnetized conditions in the absence of a CSIs: (A) non-magnetized and (B) magnetized

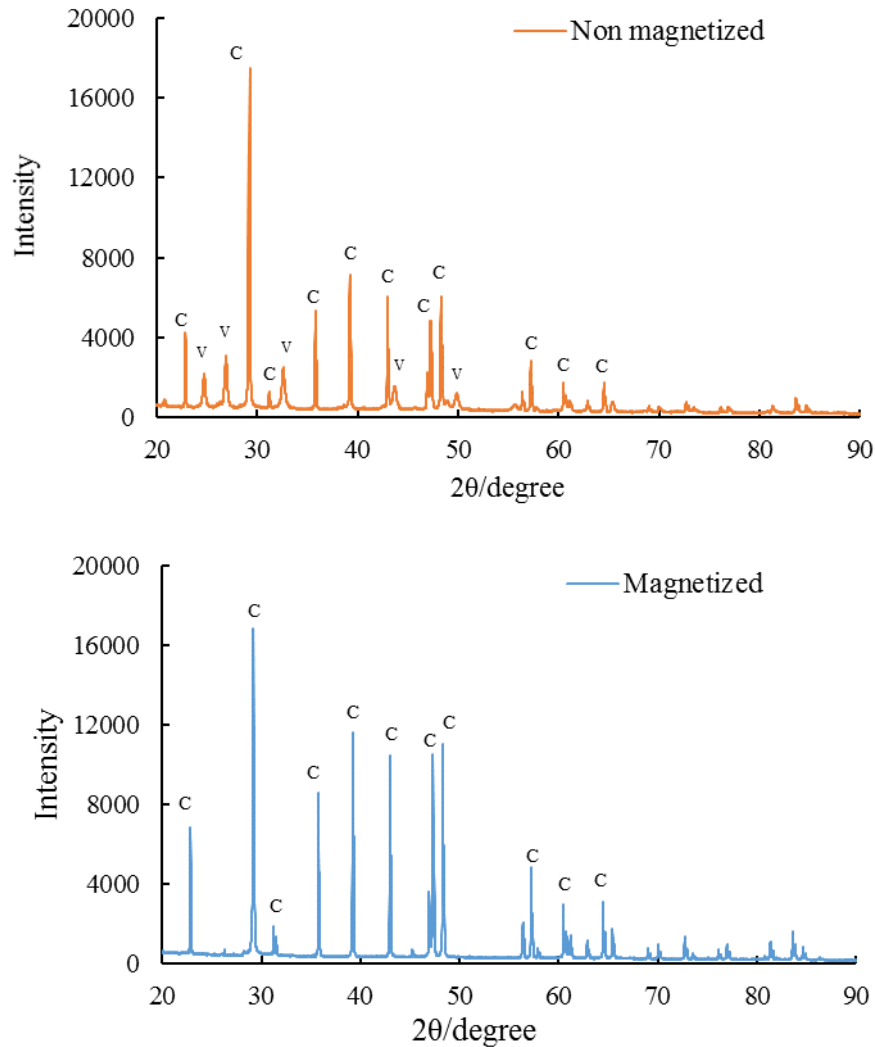


Figure 7-16 XRD profiles of (A) Vaterite “V” and Calcite “C” formed during the non-magnetized experiment, and (B) Calcite “C” formed during the magnetized experiment

7.3.6.1 Morphology of Scales Formed at Different CSI-A Concentrations

The formed scale was collected from the outlet solution of the capillary coil after commencement of the experiment and examined by SEM, the results of which are displayed in Figure 7-17. The non-exposed sample dosed with 20 ppm CSI-A shows smooth spherical structures along with needle-like and bulk crystalline clusters; the spherical structures were large, distinct, uniform in size, and aggregated. These results demonstrate the effect of MEG and CSI-A on CaCO_3 morphology, which results in an apparent deceleration of the rate of precipitate formation. However, after exposure to the external MF, intertwined and interconnected cubic structures were observed; these structures are more likely to accelerate occlusion of the capillary tube because of the small sizes of these deposits that tend to stick to the insides of the pipelines.

As the concentration of CSI-A was increased to 100 ppm in the non-exposed experiment, spherical shapes similar to those observed at the 20-ppm concentration were observed; however,

they were smaller and tended to be attracted to each other and overlap, as shown in Figure 7-17; this change generated micro-sized crystals that were somewhat differentiated. The crystalline arrangements of the obtained particles reflect the consequences of non-exposed experiments performed at concentrations of 20 and 100 ppm, and differential pressure variations. Accordingly, the time required to block the laboratory capillary tube in both experiments was reasonably close to 12–14 min. Hence, the same morphological form took approximately the same amount of time to block the tubing coil. In contrast, a cube-like morphology was observed after exposure to the MF at 100 ppm CSI-A, which is the same morphology as that observed for experiments performed with 20 ppm CSI-A; however, these cubic particles were less intertwined, and their surfaces were smooth and more distinct.

Increasing the concentration of the CSI-A injected into the brine solution to 200 ppm in the absence of the MF resulted in longitudinal rod-shaped aragonite that formed from smaller groups of longitudinal crystals; SEM revealed that these crystals were $\sim 4.5 \mu\text{m}$ in size (Figure 7-17). The generation of needle-like clusters at a high CSI-A concentration explains the good inhibitory behavior discussed in Section 7.3.2. We conclude that this concentration of CSI-A inhibitor in glycolic solutions of high concentration, and at a relatively high temperature, reduces the time required to block the flow tubes of high-salinity solutions. However, it is interesting to note that the resulting morphology for the same concentration of CSI-A after exposure to the MF was completely different, and distinctly unintertwined cube-like crystals were formed. Despite this difference in crystallization, the capillary occlusion rates were approximately equal, as described in Sections 7.3.1 to 7.3.3, which is possibly ascribable to the generation of similarly sized crystals with similar nucleation rates due of the same zeta potential values, as discussed in Section 7.3.8, which promotes cluster formation within the capillary tubes (similar to coagulation or clot formation).

In summary, the glycolic solution affects CaCO_3 morphology even in the presence of a CSI. Despite the apparent change in the CaCO_3 morphology observed at a CSI-A concentration of 200 ppm, MEG dominated the scale-formation process below 130°C . Furthermore, these results show that high concentrations of CSI-A alter the morphology of CaCO_3 during the inhibition process. Furthermore, in addition to acting as a chelating agent, CSI-A decelerated the rate of CaCO_3 formation somewhat. In contrast, scale formation could be reversed by the application of a MF, even after the addition of a CSI.

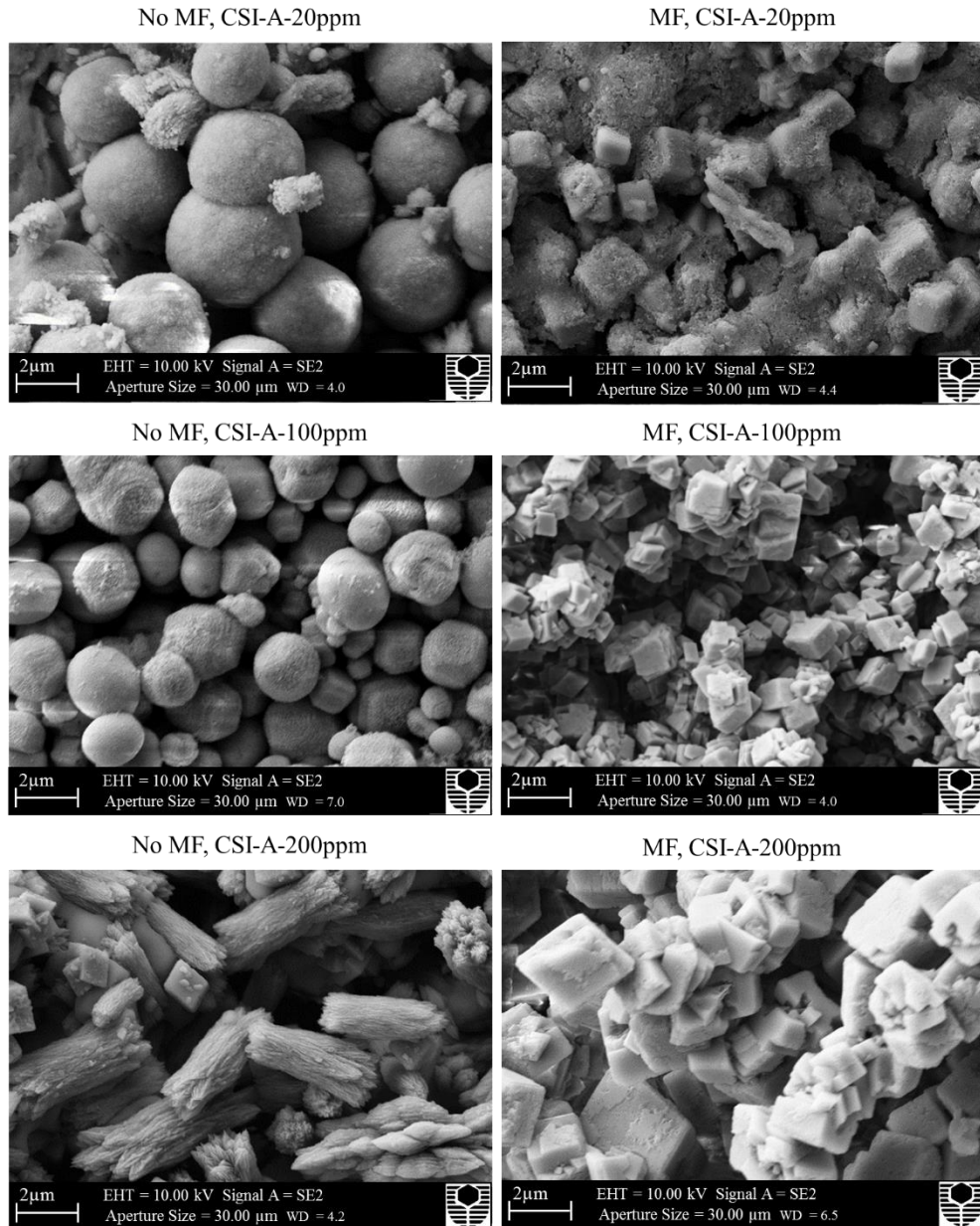


Figure 7-17 High-magnification SEM images (scale bar: 2 μm) of scales formed in magnetized and non-magnetized experiments involving CSI-A

7.3.6.2 Morphology of Scales Formed with Different CSI-B Concentrations

The morphologies of the crystals formed before and after exposure to MF at different concentrations of CSI-B were examined in a similar manner to that used in experiments involving CSI-A (Figure 7-18). As can be seen, the scale morphologies were very distinct at CSI-B concentrations of 20, 100, and 200 ppm, and exhibited a variety of structures when not exposed to the MF. Cubic and monolithic crystals with rough and distinct surfaces were observed, along with some longitudinal structures that were smaller than these cubic crystals. In contrast, no significant differences were observed in the crystals generated after exposure to the MF; the obtained crystals had cubic and rectangular shapes with lower surface roughnesses. In addition,

these crystals overlapped to generate a somewhat thick surface. These results indicate that MF treatment created stable CaCO_3 morphologies at all CSI-B concentrations. Furthermore, CSI-B failed to inhibit scale formation within the MEG solution at 130°C , but contributed to the formation of calcium carbonate with a similar, stable phase morphology. These results are unique in that they show that MEG can be prevented from promoting the formation of the meta-stable morphology.

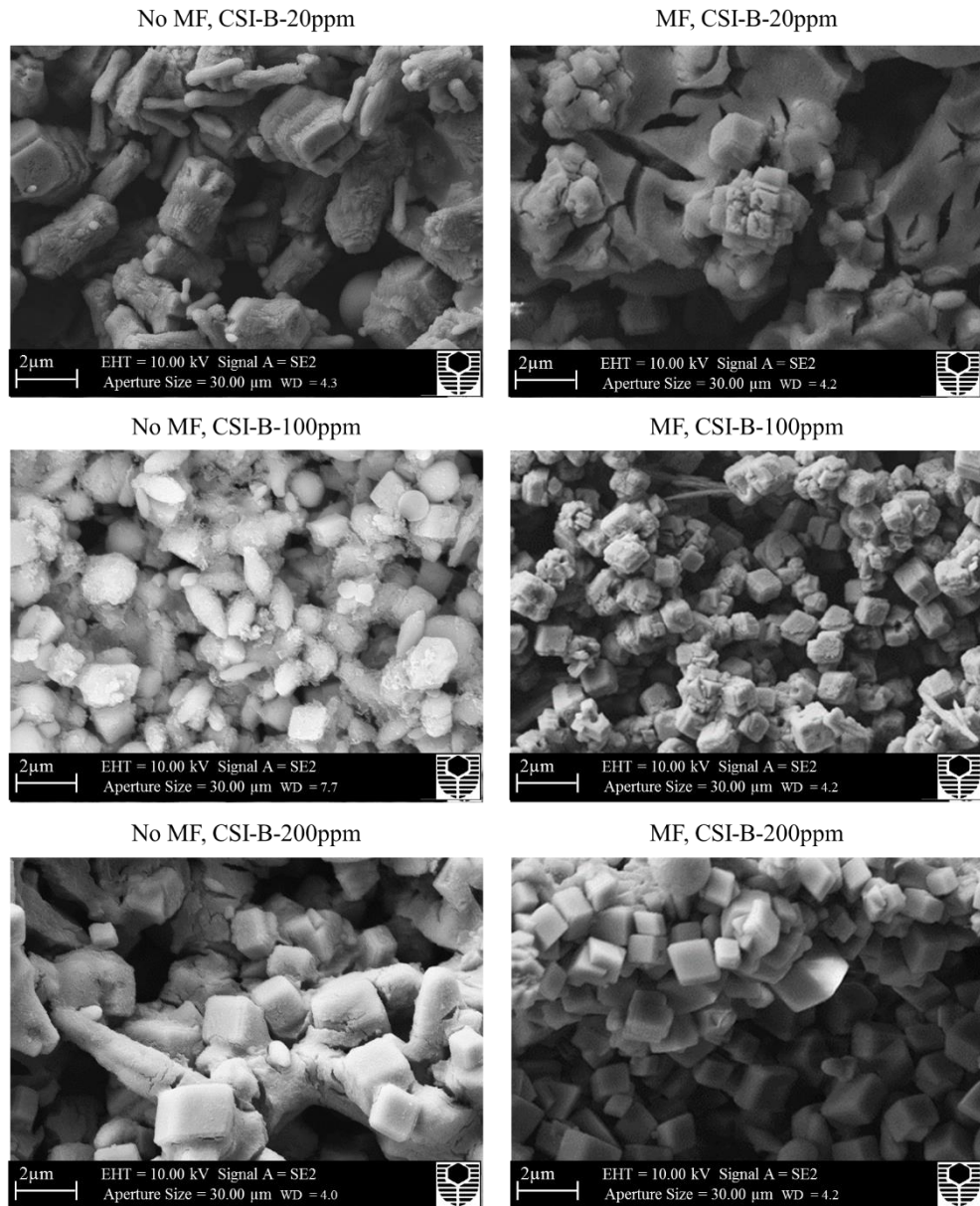


Figure 7-18 High-magnification SEM images (scale bar: 2 µm) of scales formed in magnetized and non-magnetized experiments involving CSI-B

7.3.7 Particle-size Analysis

Particle-size analysis determines the proportion of particles distributed within a colloidal system. Figure 7-19 and Figure 7-20 compare the particle-size distributions of magnetically treated and

non-treated solutions at various scale-inhibitor dosages. Obvious differences in the particle-size distributions were observed between the treated and non-treated samples. The scale particles dispersed in the colloidal system were observed to be more random in size under non-magnetic conditions; this scale also exhibited a wide particles-size distribution. On the other hand, particles 1.0–2.0 μm in size were observed following treatment with CSI-A and CSI-B solutions, at all dosages (Figure 7-20). These results show that the magnetized solution induces a significantly smaller particle-size distribution, although the distribution pattern fluctuates with time as larger particles form through aggregation. However, these smaller particles possess higher surface charges and therefore display superior tendencies to stick to hot surfaces or pipe walls, thereby increasing the risk of blockage. On the basis of crystallization theory, the MF also affects crystal nucleation and growth. The experimental results reveal that a strong magnetic field (0.65 T) and high-energy products can increase the nucleation rate leading to the formation of smaller crystals. These results are particularly interesting as they explain both the crystallization and coagulation mechanism, and reveal that the ζ potential is a quantifiable performance parameter.

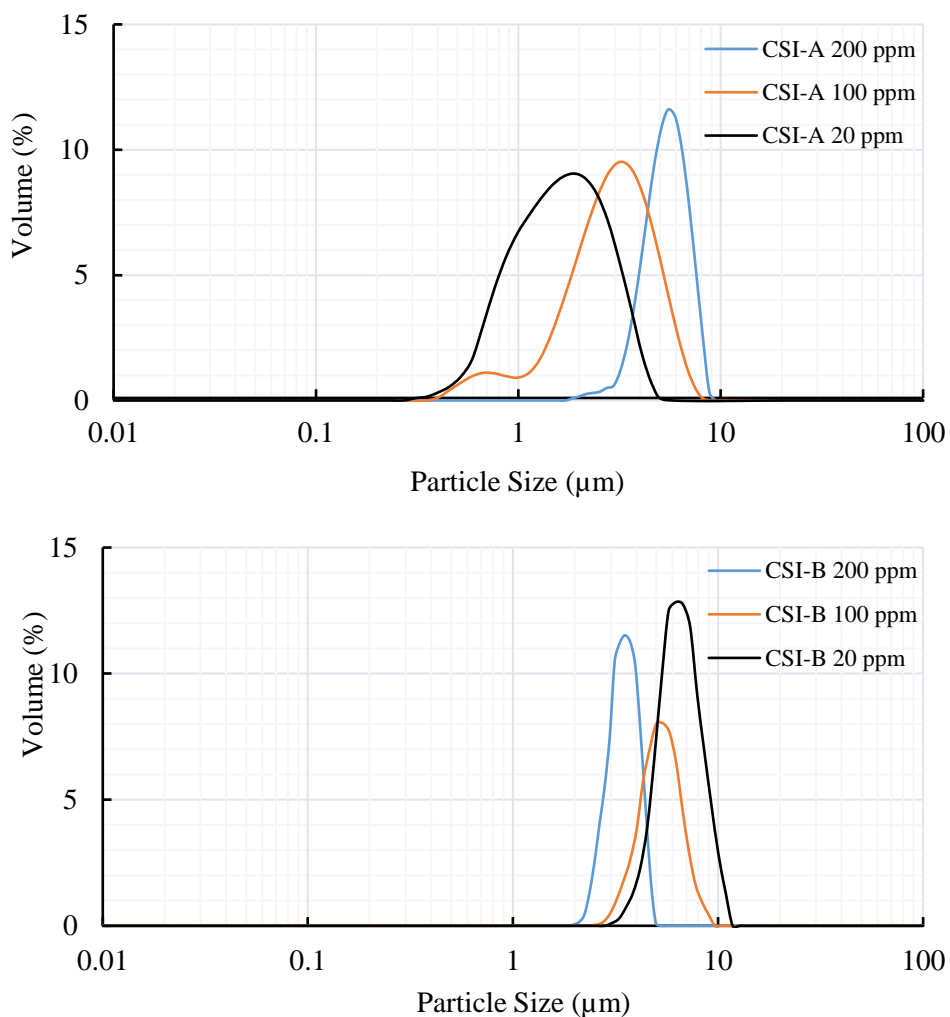


Figure 7-19 Particle-size distribution patterns from non-magnetized experiments

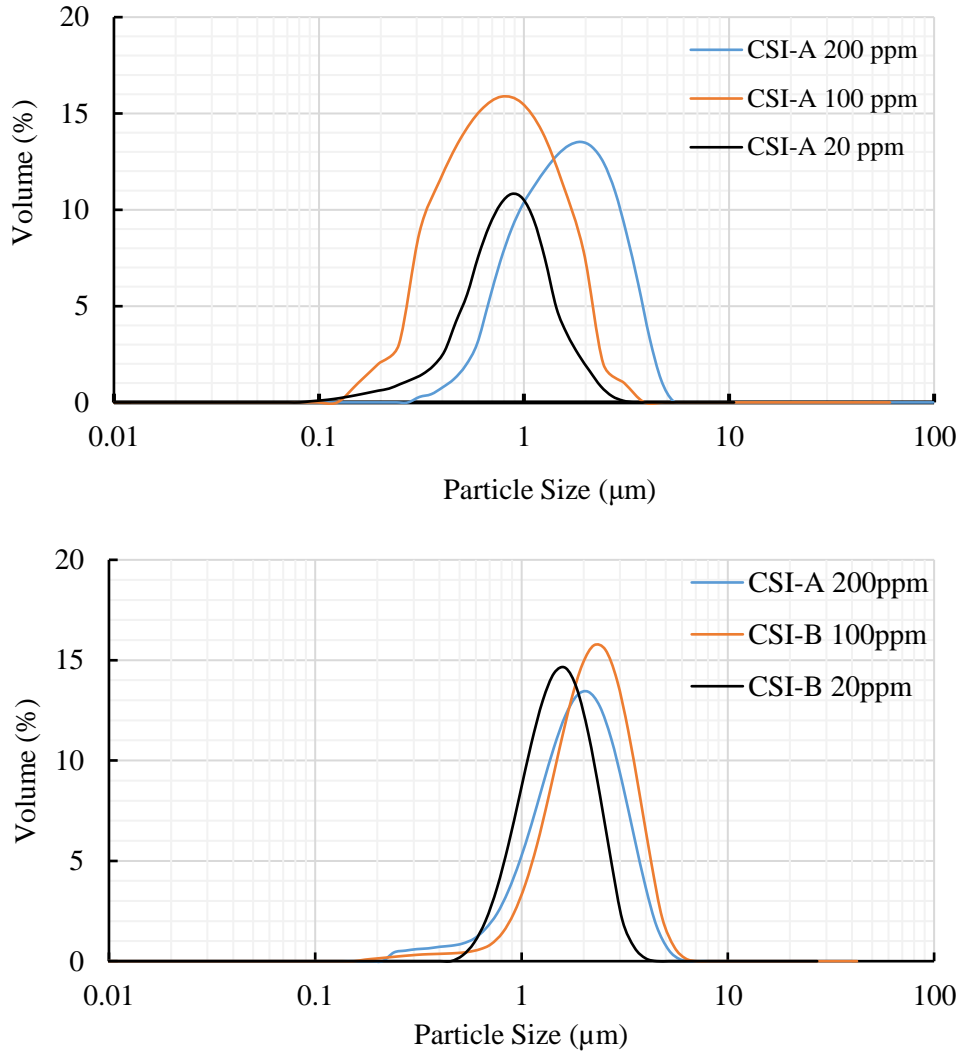


Figure 7-20 Particle-size distribution patterns from magnetized experiments

7.3.8 Zeta Potential

The zeta potential (ζ) provides an indication of interactions between particles and is an essential aggregate-forming factor. The measured zeta potentials were negative in all experiments because of the high operating pH values. Consequently, the absolute values of the measured zeta potentials were adopted in this study. Figure 7-21 compares the absolute ζ values of the magnetized (ζ_m) and non-magnetized (ζ_u) solutions as functions of CSI concentration for samples containing 80 vol% MEG, with the values tabulated in Table 7-4. Furthermore, the results from exposed and non-exposed blank (no CSI) experiments are also included in Figure 7-21. The ζ_m values for the magnetized MEG-brine solutions were always found to be lower in magnitude than those ζ_u of the non-magnetized solutions indicating a greater potential for particle agglomeration and hence scale formation.

The ratio between corresponding magnetized and non-magnetized zeta potentials ($1 - \zeta_m/\zeta_u$) is also reported in Table 7-4 to further illustrate the reduced effect of MF exposure with increasing CSI

concentration. As the concentration of the CSI increased, the MF appeared to have a reduced effect on the formed particles zeta potential almost reaching parity at 200 ppm CSI dosage rate. The reduced effect of MF as CSI concentration increased is in line with the experimental DSL results where the difference in scale formation rate between magnetized and non-magnetized experiments also decreased. Ultimately, this result may indicate that in the higher CSI concentration tests, the effect of CSIs on the scale formation is dominant over the potential effect of the MF.

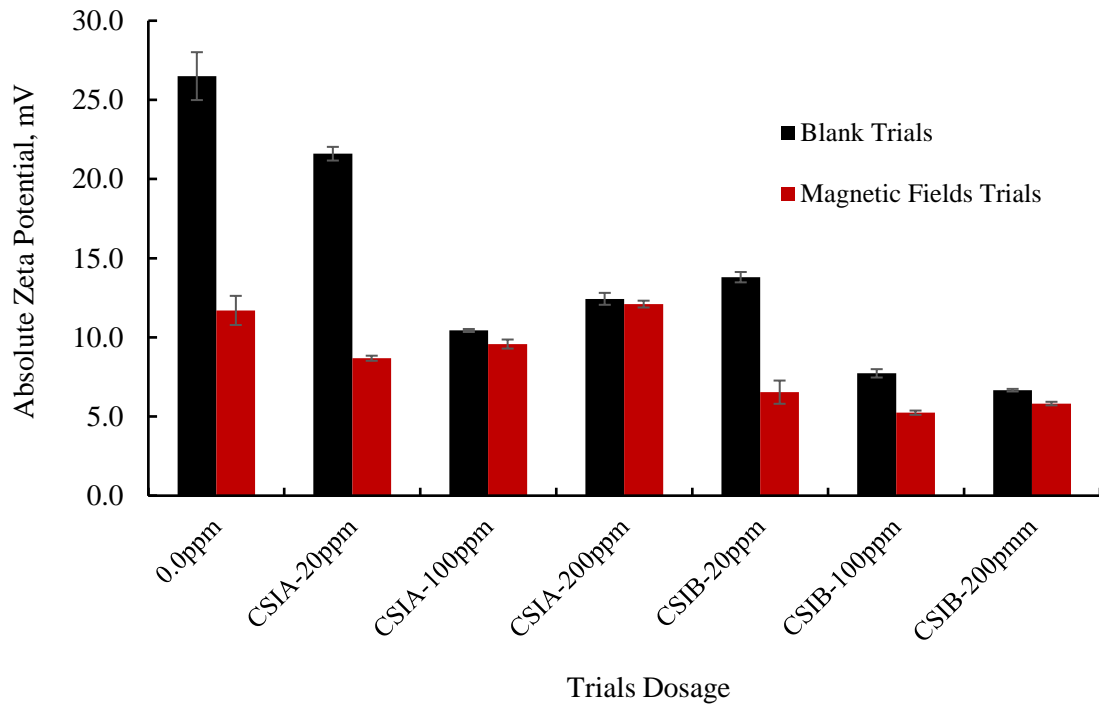


Figure 7-21 Absolute zeta potentials of solutions with various CSI-A and CSI-B concentrations before and after exposure to MF

Table 7-4 Absolute zeta potentials of various chemical scale inhibitors for magnetized and non-magnetized solutions

Trial Dosage	ζ_m	ζ	$(1 - \zeta_m/\zeta)$
0ppm	11.70	26.50	0.56
CSI-A-20ppm	8.68	21.60	0.60
CSI-A-100ppm	9.58	10.43	0.09
CSI-A-200ppm	12.10	12.43	0.03
CSI-B-20ppm	6.54	13.80	0.53
CSI-B-100ppm	5.24	7.73	0.33
CSI-B-200ppm	5.82	6.66	0.13

Higashitani, Iseri [179] reported that well-mixed solutions composed of colloids and electrolytes exposed to a MF exhibited lower ζ values than the same solutions that were not exposed to the

MF, which is consistent with the results obtained in this study. Furthermore, [201] and Alabi, Chiesa [22] concluded that a MF does affect colloidal stability, thereby modifying the charge density in the vicinity of the Stern layer. Also, synergism between the high magnetic energy produced and the high pH within the glycolic solution may appropriately explain the observed decrease in absolute ζ value when an external MF is applied. Ellingsen and Kristiansen [225] reported that MF treatment is affected by solution pH as CaCO_3 precipitation is inhibited at pH greater than 9.3 and enhanced at pH below 9.0. Hence, the operating pH in this study explains the reduction in ζ potential under MF conditions. The differences in the transmission rates of ions in the medium and altered double-layer properties of the glycolic environment also affected the ζ value (Figure 7-22); hence, the interaction rates for the formation of scale before and after exposure to MF were different.

In addition, magnetic treatment promotes the susceptibilities of the molecules in the suspension to coagulate by decreasing double-layer repulsion, which results in a reduction in particle surface area. This facilitates the penetration of ions into the liquid phase, which leads to a reduction in the density of the diffuse layer and a proportional reduction in the surface charge. This proposal is consistent with the reports of Krylov, Vikulova [354] and Parsons, Wang [201]. Furthermore, occlusion in the capillary coil, as discussed in Sections 3.1–3.3, is a result of changes in the CaCO_3 morphology resulting from exposure to the MF. These changes lead to the formation of deposits with stable morphologies that accelerated blockage of the conveyor tubes because of the small ζ values resulting from the applied MF. These results are consistent with the findings of Higashitani, Kage [174], who reported that although the nucleation of calcium carbonate was delayed, its growth was accelerated by high external magnetic-flux density. Hence, the presence of MEG and mineral ions altered the electro-kinetic potential in the ionic-dispersion system when the MF was applied.

The accelerated scale formation can be also described by the spin-chemistry mechanism, in which a weak internal magnetic field is generated by the electron spin within an atomic orbital [31, 58, 77]. This weak internal magnetic field manages the reactions of calcium and bicarbonate ions leading to increased scale formation in the presence of a powerful external magnetic effect [31, 58]. This promotion is attributed to the ability of the magnetic field to accelerate the forward reaction by decreasing the frequency of the reverse reaction. In other words, the magnetic field prevents the products from returning back to their original states [57, 213]. This result is consistent with the radical-pair mechanism in the presence of an external magnetic field as reported in several publications [31, 58, 77]. Therefore, the effects of magnetic fields on scale-formation reactions can be described by spin-chemistry theory.

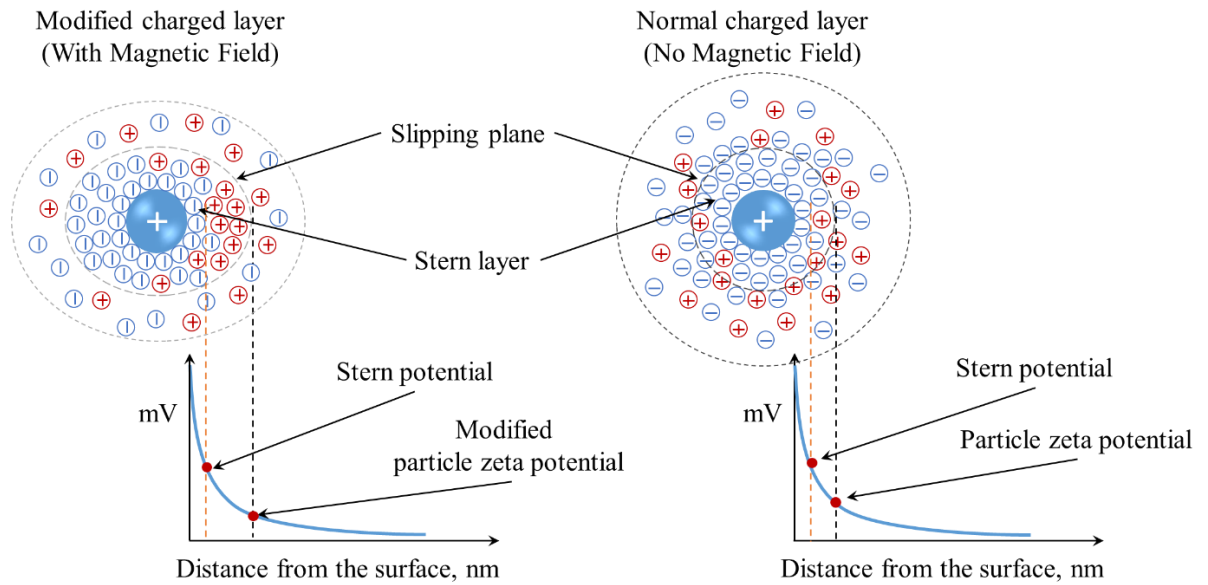


Figure 7-22 Depicting a possible mechanism for the effect of a magnetic field based on zeta-potential difference [22]

7.3.9 Effects of Magnetic Field on Individual Parameters

7.3.9.1 Ionic Hydration Shell

Mineral ions tend to interact with water or solvent molecules to form encapsulating hydration or solvation shells [204], whose thicknesses vary according to the thermodynamic conditions [33]. Furthermore, it has been reported that EC and hydration-shell thickness are inversely related [169]. Therefore, observed reductions in EC values are attributable to the weak bonding of ions with water molecules that increase the thicknesses of their solvation shells. Furthermore, exposure to the MF contributes to a lower ζ value that changes the thickness of the slipping-plane layers of the particles, which also lowers the EC value as described by the Henry Equation (see Equation 7-1). These results are consistent with those of previously published reports, in which similar relationships between the hydration shell and zeta potential were observed [31, 355]. Therefore, the closed-loop relationship between the hydration shell, EC, and ζ provides a theoretical explanation for the effects of MFs on saline solutions (see Equation 7-2). An increase in ζ value is usually an indication of repulsion between molecules; the higher the ζ value, the greater the repulsion, which leads to a reduced coagulation rate [356]. However, the thermodynamic and electro-kinetic conditions alter upon exposure to a MF, leading to different ζ and electrophoretic-mobility values and hydration-shell thicknesses.

$$\zeta = \frac{\epsilon \cdot u_m}{\mu} f(k \cdot R_s) \quad 7-1$$

where, u_m denotes electrophoretic mobility ($\mu\text{m}\cdot\text{cm}/\text{Volt}\cdot\text{s}$), ϵ is the dielectric constant, μ is the viscosity, k is the Debye–Hückel parameter, and R_s is the particle radius [318]. Electrophoretic

mobility and ionic conductivity (σ) can be also calculated by Stokes' law and the force fields associated with the ion at drift velocity, and Nernst-Einstein as shown by the following equations [48, 85, 89, 189, 357]:

$$u_m = \frac{e \cdot z}{6 \cdot \pi \cdot \mu \cdot r} = \frac{e \cdot z \cdot D}{k_B \cdot T} \quad 7-2$$

$$\sigma = \frac{(e \cdot z)^2 \cdot c \cdot D}{k_B \cdot T} \quad 7-3$$

Combining Equations 7-2 and 7-3 leads to the following relationship:

$$\sigma = e \cdot z \cdot c \cdot u_m \quad 7-4$$

where, e denotes the elementary charge, z is the number of ionic charges, r is the hydrodynamic radius including water ligands, D is the diffusion coefficient, T is the temperature in Kelvin, and c is the volume concentration of the ions.

The thermodynamic conditions also change in the presence of a CSI, high alkalinity, and other organic additives such as MEG. Such changes can lead to different results for ionic water binding systems exposed to a MF. In all experiments carried out in this study, we observed that the MF contributed to the accelerated blockage of laboratory capillary coils, even when a CSI was used. This acceleration was due to the presence of high concentrations of MEG that increase the viscosity of the solution and reduce the solubilities of the mineral ions, as well as pH values above 9.3 [225]. It is well-known that MEG molecules form hydrogen bonds with water molecules, thereby altering the thermodynamic behaviour of water molecules toward bonding with dissolved ions and the formation of hydration shells [79]. In addition, previous reports have indicated that MEG molecules directly decrease the saturation and ionizing levels of species in aqueous solutions, rendering the formation of inorganic scale more likely [26, 358]. These thermodynamic conditions, when combined with MF treatment, promote the formation of mineral deposits in the presence of a CSI.

7.3.9.2 Molecules Susceptibilities

Magnetic susceptibility is a critical factor that determines the responses of ions and molecules to external MFs [31]. MEG, water, and carbonate ions are diamagnetic substances; i.e., they are repelled by magnets in a temperature-independent manner [78, 273]. However, the magnetic susceptibility of water is reportedly three times lower than that of MEG and two times lower than that of carbonate ions [78]. Therefore, the magnetizations (M) of molecular MEG and CO_3^{2-} are much stronger than that of water, as indicated by the following equation:

$$M_i = k_i \times \vec{H}_i$$

7-5

where, χ_m is the molar susceptibility ($\times 10^{-6} \text{ cm}^3 \text{ mol}^{-1}$), V_m is the molar volume (cm^3/mol), and \vec{H}_i is the magnetic-field strength [78]. In contrast, calcium ions are known to be paramagnetic and consequently interact with an external MF (see Figure 7-23) [78, 273]. Therefore, calcium and carbonate ions can be separated from water molecules in aqueous solutions, as shown in Figure 2-18 in chapter 2. This separation inhibits scale formation after exposure to the MF. However, the molecular arrangements of MEG and water are modified by the MF [1]; the MEG molecules are expected to be located away from both the calcium and carbonate ions, leading to increased supersaturation; in other words, both ions are more likely to interact with each, particularly when the concentration of water molecules is reduced by increasing the amount of MEG present [1, 5]. Therefore, the formed ion hydration shell remains the determining factor that inhibits or promotes scale formation [29, 109].

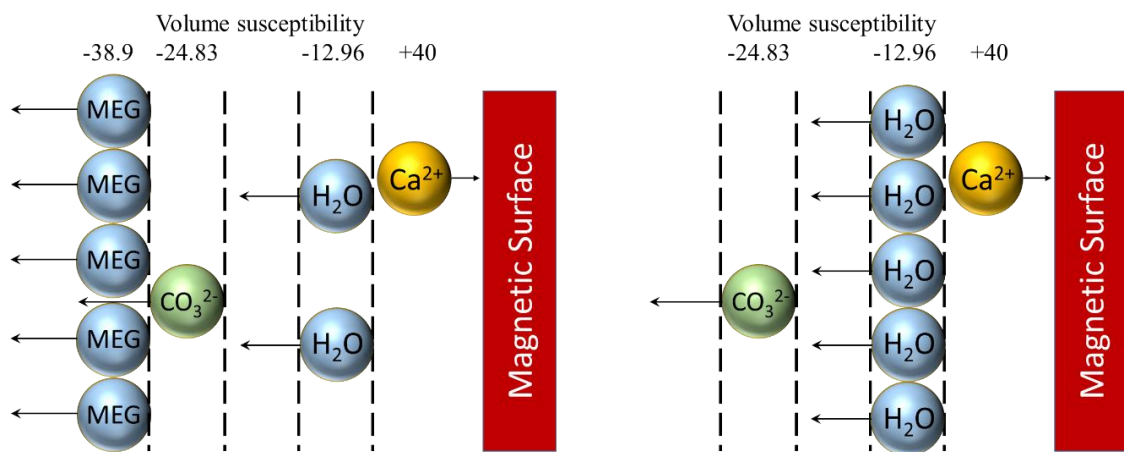


Figure 7-23 Magnetic volume susceptibility of admixtures of substances in the MEG system and water system after exposure to a MF

7.4 Conclusions

This study was undertaken to study the effect of magnetic fields on the performance of chemical scale inhibitors within MEG solutions. Prior studies have shown that the application of magnetic field treatment can inhibit the formation of mineral-ion scale in both water and rich MEG systems [109, 359], however, the combined effect of MFs with CSIs is uncertain. With this in mind, two commercially available CSIs were examined in the presence of a 0.65 Tesla external MF field under conditions potentially found within an industrial MEG regeneration system reboiler (130°C, pH 9.5). Overall, the results showed that inorganic deposits such as CaCO_3 form more rapidly within high MEG concentration solution when exposed to a MF under the conditions tested. The accelerated rate of deposit formation due to the applied MF, also negatively affected

the performance of the chemical inhibitors used in this study, irrespective of their concentrations. The application of the MF resulted in several key effects on the scale formation process including:

- Exposure to the MF produced a stable calcium carbonate (calcite) phase morphology, even when CSIs were used.
- Exposure to the MF resulted generated small sized particles compared to those of non-magnetized solutions in the presence of the CSIs.
- The absolute zeta potential of particles formed in the presence of the applied MF and MEG was lower than that in the absence of the MF. The relationship between the thickness of the hydration shell and the EC value is consistent with previously reported results for MF exposure.
- The results indicate that the effect of the applied magnetic field is retained even after heating the solution to high temperatures, a result contrary the findings of Silva, Neto [29].

The findings summarized above are significant in terms of understanding the effect of an applied MF on scale formation. The most significant finding was the apparent differences in ζ potential values. Although the measured values were not particularly high, the consistently observed differences in ζ potential before and after exposure to the MF highlight the ability of the MF to change the external charges on the surfaces of molecules present in solution, thereby changing the thicknesses of the hydration shells that encapsulates these ions. These results provide significant insight into the effect of a MF on scale formation, irrespective of whether or not a CSI is used, and helps to interpret the effects of various treatments for scale removal or the prevention of scale formation. Investigations into the abilities of MFs to fundamentally change scale formation during various operations including the MEG regeneration process are still in their early stages and require further intensive study.

Although it was consistently observed that application of a MF ultimately increased the rate of scale formation, something undesirable in most industrial operations, the application of MF treatment may have potential benefits during the MEG regeneration process. In some MEG systems, pre-treatment is performed in order to removal divalent cationic species that would otherwise scale and foul the down-stream regeneration column operating at high temperature [2, 4, 360]. The application of a MF inside the pre-treatment system may promote the formation of divalent salt products even in the presence of CSIs, allowing their separation and removal in down-stream precipitation vessels before entering the regeneration system. Overall, this study provides a reasonable assessment of the effects of the various treatments employed for preventing scale formation or scale removal in the reboiler section during the MEG regeneration process.

Chapter 8 Performance of Erythorbic Acid as an Oxygen Scavenger in Thermally Aged Lean MEG

8.1 Introduction

The oxygen dissolved in MEG solutions causes the corrosion of components in different sections of the MEG plant and transportation pipelines [230, 234, 235, 256]. Therefore, extensive studies have been devoted to developing strategies to substantially scavenge the oxygen content in MEG solutions [137, 230, 234, 235, 329]. Although the conventional practices of thermal deaeration and degasification are commonly used in chemical industries, these processes consume a lot of energy for operation [16, 20, 238]. Alternatively, dissolved O₂ can be reduced using oxygen scavengers such as erythorbic acid, which have managed and utilized to control oxygen levels in chemical industries effectively.

The objective of this chapter was to further evaluate the performance of the erythorbic acid oxygen scavenger designed by Kundu and Seiersten [230] in 85 wt.% thermally aged lean mono ethylene glycol (TAL-MEG). Experiments were performed at two levels of dissolved oxygen concentrations including 1000 ppb and > 7500 ppb at pH values of 6.0, 9.0, and 11.0. Furthermore, the erythorbic acid oxygen scavenger was evaluated under conditions representative of an industrial MEG regeneration system in terms of salt and organic acid concentrations to replicate in-field usage. The strong performance of erythorbic acid in combination with manganese and DEAE was observed under field conditions of food industries [20, 251, 263], suggesting that erythorbic acid is an attractive alternative oxygen scavenger for use in the oil and gas industry in place of traditional sulfite-based oxygen scavengers.

8.2 Equipment and Chemicals Used

The bench-scale oxygen scavenger testing conducted within this study was performed using four custom-made glass testing cells fitted with airtight lids as depicted by Figure 8-1. The testing cells incorporated an InPro 4800i pH probe and InPro 6850i polarographic dissolved oxygen (DO) sensor supplied by Mettler Toledo. The Mettler Toledo InPro 6850i DO sensor has an oxygen detection range of 6.0 ppb to saturation with an accuracy of ± 0.01 . The pH and DO sensors were connected directly to a Mettler Toledo M800 process measurement system to allow continuous monitoring of system conditions as well as a direct recording of all process data to a computer via USB connection.

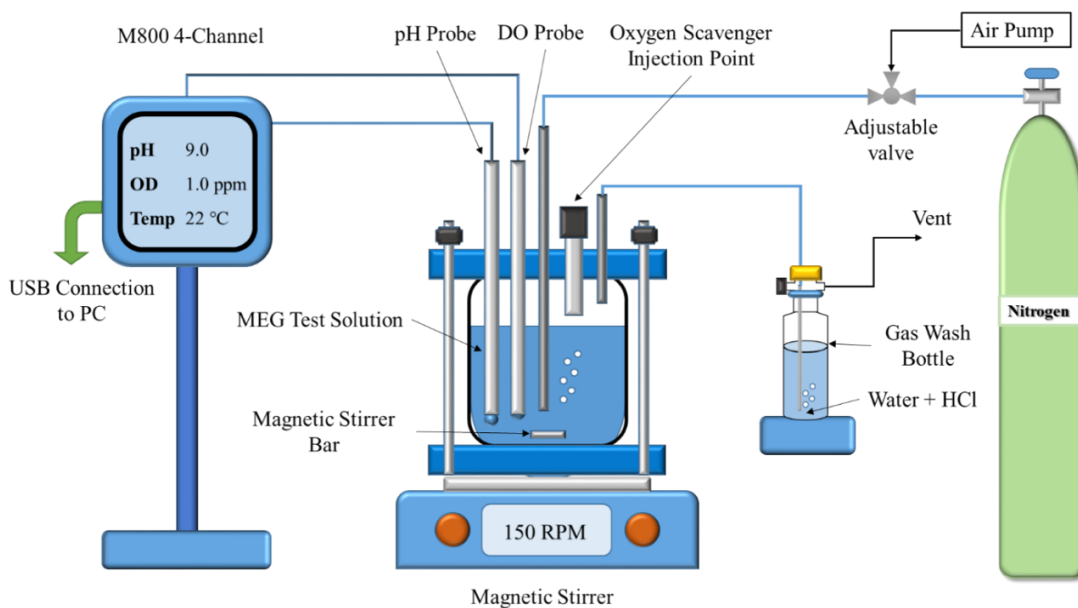


Figure 8-1 Bench scale oxygen scavenger experimental apparatus

Furthermore, each testing cell was fitted with a rubber injection port to allow the injection of the oxygen scavenger solution via a syringe while preventing oxygen intrusion during experimental trials. A retractable stainless steel tube was implemented into the test cell to allow sparging of the test solution with nitrogen or air to achieve the desired starting DO concentration. In addition, the retractable design of the tube enabled continuous sparging of ultra-high purity nitrogen (>99.999 mol%, supplied by BOC) to be applied within the headspace of the testing cell during operation to minimize oxygen intrusion. To prevent over pressurization of the test system, a gas outlet tube was attached to each cell and connected to a gas wash bottle to avoid flow reversal back into the test cell.

The erythorbic acid oxygen scavenger evaluated within this study was supplied by Sigma Aldrich at a purity greater than 99.0%. The specific erythorbic acid oxygen scavenger composition was developed by IFE [230] for its potential use within MEG regeneration systems and is outlined in Table 8-1. The diethylaminoethanol (DEAE) component of the oxygen scavenger was sourced from Sigma Aldrich at a purity greater than 99.5% and was used to neutralize the erythorbic acid to make erythorbate. Manganese chloride was used to catalyze the oxygen scavenger reaction and was supplied by Sigma Aldrich as $MnCl_2 \cdot 4H_2O$ at a purity greater than 99.0%. All testing was conducted within MEG solution supplied by Chem-Supply. Where the oxygen scavenger was tested within TAL-MEG, the MEG was thermally aged for 10 cycles using a MEG regeneration pilot plant operated by the Curtin Corrosion Engineering Industry Centre (CCIEC) [2, 136]. The MEG was cycled through the distillation system and exposed to temperatures between 125-135°C to produce TAL-MEG and subsequently reclaimed to remove any salt content.

Table 8-1 Evaluated erythorbic acid based oxygen scavenger [230]

Component	Concentration, (wt. %)	Component Purity, (%)
Erythorbic Acid	17	99.0
Diethylaminoethanol	25	99.5
MnCl ₂ ·4H ₂ O	0.5	99.0
Water	57.5	Distilled water Deoxygenated with N ₂

8.2.1 pH calibration procedure of TAL-MEG solutions

The pH measured in each test was corrected continuously by adding a deviation factor that appeared due to the interference of the liquid junction potential of the pH electrode with the presence of MEG and brine solution [321]. This bias was calibrated by the model developed by Sandengen, Kaasa [321].

$$\Delta\text{pH}_{\text{MEG}} = 0.416\text{wt} - 0.393\text{wt}^2 + 0.606\text{wt}^3 \quad 8-1$$

$$\text{pH}_{\text{corrected}} = \text{pH}_{\text{measured}} + \Delta\text{pH}_{\text{MEG}} \quad 8-2$$

Where wt. denotes the weight fraction of TAL-MEG solution.

8.3 Experimental Methodology

Bench-scale oxygen scavenger evaluation was performed using the experimental set-up depicted in Figure 8-1. Evaluation of oxygen scavenger performance was conducted within 85% wt. TAL-MEG solution to simulate its performance within downstream MEG injection systems following the regeneration process. The primary tests outlined within this study were conducted using TAL-MEG to replicate operational conditions found during field operation. To assess the performance of erythorbic acid as a potential oxygen scavenger for MEG service, its performance was evaluated under a range of conditions including varying pH, starting oxygen concentration, salinity, and oxygen scavenger dosage rate. Testing was conducted using three pH levels: 6.0, 9.0 and 11.0, to identify the influence of solution pH upon oxygen removal efficiency. The two starting oxygen concentrations studied included 1000 ppb and saturation (~7500 ppb), which represents varying degrees of oxygen content that may be experienced in field operations. To evaluate the efficacy of the erythorbic acid oxygen scavenger solution, two different oxygen scavenger dosage rates (refer to Table 8-2) were utilized to aid in optimization of dosage requirements in the field. The dosage rate utilized within this study is based upon the weight concentration (ppm) of the erythorbic acid ion (erythorbate) after dissociation within the solution has occurred. Full dissociation of the erythorbic acid was expected during testing through the neutralization reaction with diethylaminoethanol (DEAE) [256].

Additionally, four typical MEG solutions with varying contamination levels of mineral salts and organic acid were used in the oxygen scavenger trials, to assess erythorbic acid performance

under real field conditions. These four solutions included fresh MEG, TAL-MEG without mineral salt or organic acids (representing initial operation with uncontaminated fluids), TAL-MEG without mineral salt but with a low content of organic acids (representing operation prior to formation water breakthrough), and TAL-MEG with high content of mineral salt as well as presence of organic acids (representing operation following formation water breakthrough). Furthermore, weight fraction of TAL-MEG solution was measured by using Al Helal, Soames [322] models to ensure the concentration of TAL-MEG mixture was within the proposed concentrations. The compositions of the fresh MEG and three TAL-MEG solutions are outlined in Table 8-3.

Prior to the lean MEG solution tests, the solution was sparged with either nitrogen or air to reach the required starting oxygen concentration of 1000 ppb or >7500 ppb. Simultaneously during the sparging process, the solution pH was adjusted using either sodium hydroxide or hydrochloric acid solution to adjust the pH to the desired starting point of 6.0, 9.0 or 11.0. Once the required starting oxygen concentration and pH were reached, the retractable sparging tube was repositioned into the headspace of the testing cell and a nitrogen blanket produced to prevent oxygen ingress. The erythorbic acid oxygen scavenger solution was then injected into the MEG solution through the rubber injection port, and the recording function of the M800 system commenced using the DO and pH probes discussed in Section 8.2. Recording of the oxygen removal response of the erythorbic acid was conducted over a four-hour period to assess its ability to reach an oxygen concentration below 20 ppb. An oxygen concentration below 20 ppb within a four-hour time frame was set as the target by a third-party oil and gas company for whom the tests were conducted for based upon their system requirements.

Table 8-2 Erythorbic acid dosage rate

High Dosage Rate	Low Dosage Rate
200 ppm*	100 ppm*

*Dosage rate based upon erythorbate ion (by weight)

Table 8-3 MEG salinity levels*

Salt/Organic Acid, ppm	Fresh MEG	Aged MEG		
		No Salt (Initial operation)	Low Organic Acids (Condensed Water)	High Salt (Formation Water)
Na ⁺	0	0	0	7724.72
K ⁺	0	0	0	28.35
Ca ²⁺	0	0	0	43.65
Mg ²⁺	0	0	0	1.95
Fe ²⁺	0	0	0	0.72
Sr ²⁺	0	0	0	3.65
Ba ⁺	0	0	0	3.11
Li ⁺	0	0	0	0
Cl ⁻	0	0	0	11641.75

Salt/Organic Acid, ppm	Fresh MEG	Aged MEG		
		No Salt (Initial operation)	Salt/Organic Acid, ppm	Fresh MEG
HCO ₃ ⁻	0	0	0	87
SO ₄ ²⁻	0	0	0	23.55
Formic Acid	0	0	0	0
Acetic acid	0	2	25.5	462.90
Propanoic acid	0	0.1	1.98	44.25
Butanoic acid	0	0.5	3.345	54.30
Total Salinity	0	2.6	30.825	20119.90

*The salinity level were analyzed by using inductively coupled plasma mass spectrometry

8.4 Results and Discussion

8.4.1 Effect of MEG Thermal Aging upon Erythorbic Acid Oxygen Scavenging Performance

Four sets of experiments were carried out at pH 9.0 by using two solutions of fresh and TAL-MEG (No salts) and the low and high dosage rates of the erythorbic acid oxygen scavenger listed in Table 8-3. The testing was conducted to assess the influence of TAL-MEG upon erythorbic acid oxygen scavenger performance. For each test, the initial oxygen concentration in the MEG solution was adjusted to approximately 1000 ppb to simulate industrial field conditions due to oxygen contamination [230, 252]. The performance of the erythorbic acid oxygen scavenger was significantly affected by the thermal aging of MEG (when compared to fresh MEG) as shown by Figure 8-2. For both the high and low dosage rates of erythorbic acid, it was observed that TAL-MEG reduced the oxygen removal rate. The time required to reduce the oxygen content to below 20 ppb was 170 minutes (Figure 8-2); while in fresh MEG O₂ levels reduced to below 20 ppb within 100 minutes.

The results of the tests performed suggest that to attain comparable oxygen scavenger performance under field conditions where TAL-MEG is commonly used, a much longer residence time of the oxygen scavenger is required for TAL-MEG leading to increased corrosion potential inside transport pipelines if sufficient time is not provided. It was concluded that the effects of aged MEG products might lower the performance of the erythorbic acid oxygen scavenger. Therefore, it is recommended that future testing of oxygen scavengers for use in MEG systems be implemented in TAL-MEG and not fresh MEG to provide a more accurate representation of their assessment under realistic field conditions.

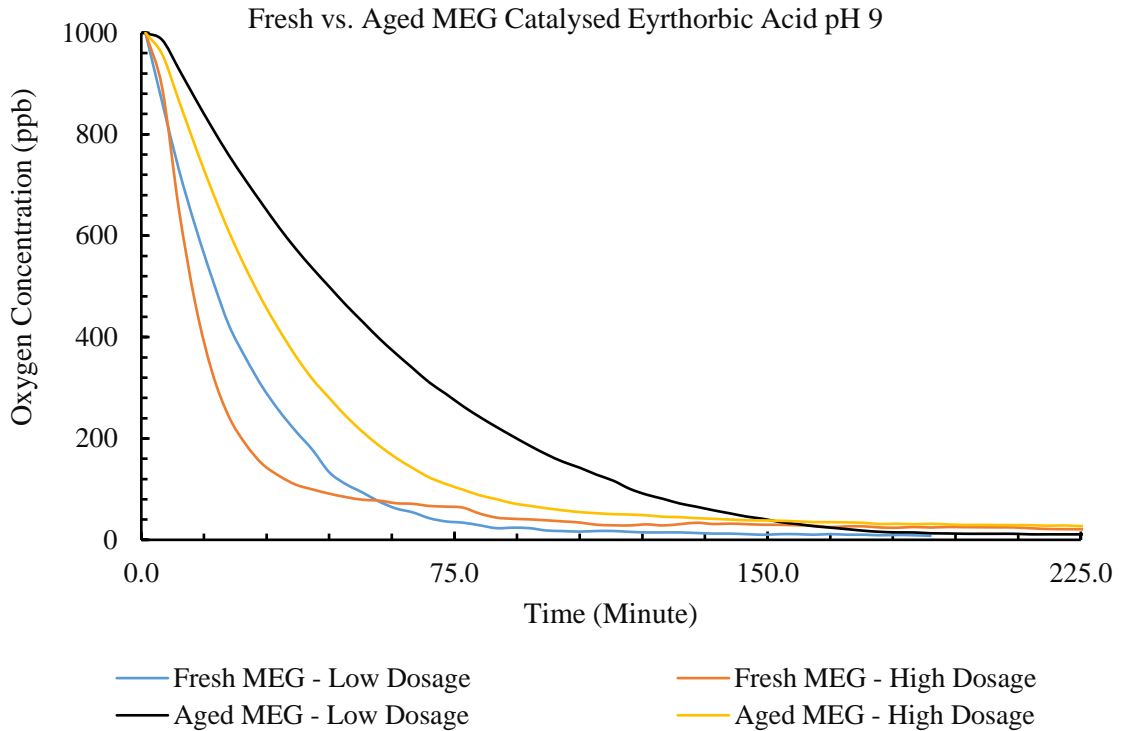


Figure 8-2 Effect of MEG thermal aging upon oxygen scavenger performance

8.4.2 Effect of Organic Acids on Erythorbic Acid Oxygen Scavenging Performance

Thermally degraded MEG and produced water contain acidic products such as formic acid, acetic acid, oxalic acid, and glycolic acid [137, 239]. These acids tend to accumulate in the closed glycol loop over time. To evaluate the influence of organic acids on the performance of erythorbic acid as an oxygen scavenger, four sets of tests using fresh MEG were conducted with various acetic acid concentrations ranging from 0 to 1000 ppm, where the pH level was maintained at 9.0. Acetic acid was used to investigate the effects of organic acids as it represents the majority of organic acids experienced in formation water [64, 128, 229, 361]. The results illustrated in Figure 8-3 showed no significant effect of acetic acid on the erythorbic acid oxygen scavenger performance at pH 9.0 up to 1000ppm. As shown in Figure 8-4, The majority of acetic acid will be present as its conjugate base, acetate at a pH of 9.0, therefore it can be concluded that the presence of acetate did not negatively influence the performance of erythorbic acid as an oxygen scavenger [362].

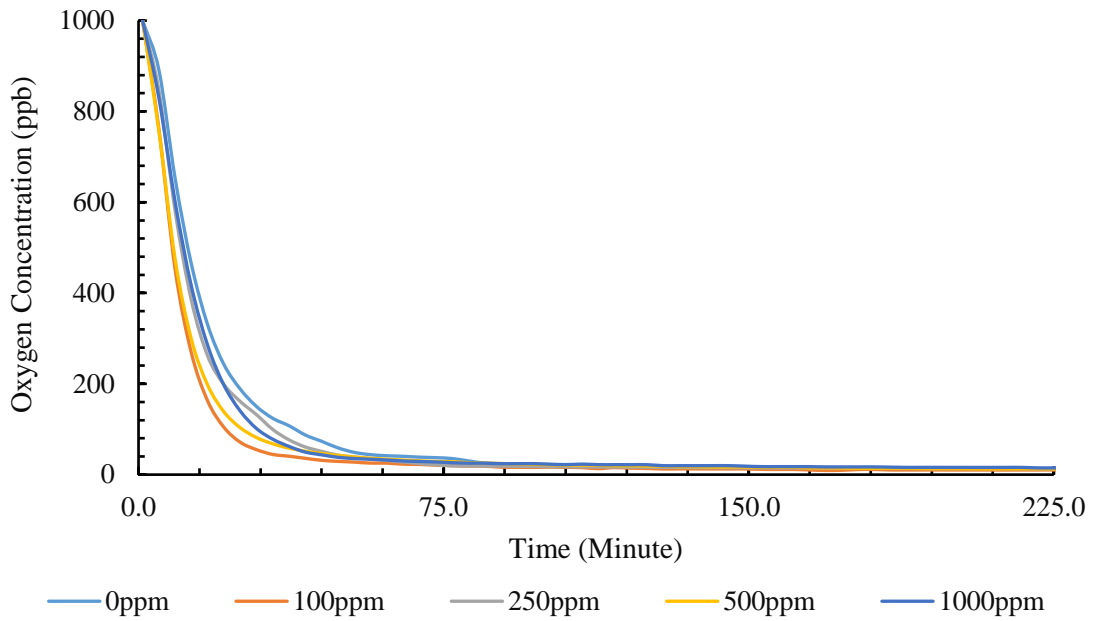


Figure 8-3 Effect of acetic acid concentration on erythorbic acid oxygen scavenger performance (at pH = 9) within fresh MEG

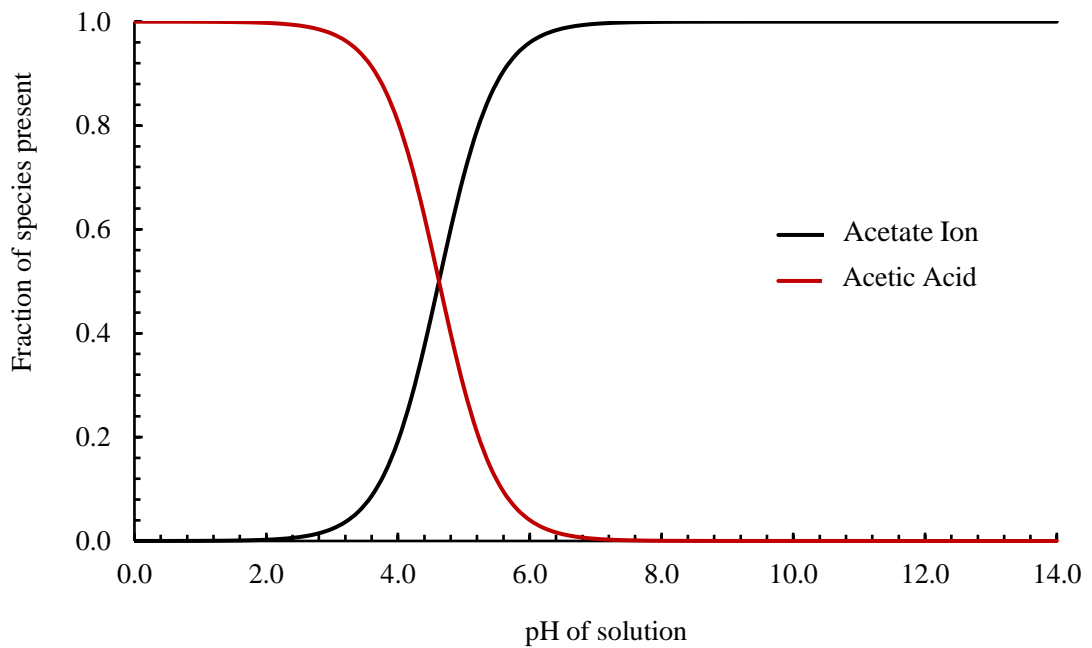


Figure 8-4 Relationship between pH of solution and dissociation status of acetic acid [362]

8.4.3 Evaluation of Erythorbic Acid Performance under Field Conditions (1000 ppb and Saturation)

The influence of pH was investigated to evaluate the performance of erythorbic acid oxygen scavengers within TAL-MEG using the three MEG solution compositions tested: MEG-low salts,

MEG-low organic acids (condensed water only) and MEG-high salts (with formation water). Three sets of experiments were conducted using the low and high dosage rates of erythorbic acid at pH of 6.0, 9.0 and 11.0 as outlined in Table 8-3. Furthermore, each set of experiments was conducted using both ~7500 ppb (saturation) oxygen concentration to evaluate the effect of erythorbic acid at high oxygen contents and 1000 ppb representing typical oxygen contamination levels in the industry.

The increase in pH from 6.0 to 11.0 (MEG-low salts) improved the oxygen scavenging performance of erythorbic acid within TAL-MEG. The results generated align with literature data which suggests that the performance of erythorbic acid is improved at high pH [9, 256, 260]. Under all salinity conditions tested, the poor performance of erythorbic acid was observed at pH 6.0 with erythorbic acid failing to reach the desired 20 ppb oxygen concentration from both saturation and 1000 ppb (refer to Figure 8-5 to Figure 8-10). The generated results are in line with the conclusions of Kundu and Seiersten [230] for pH 6.0 within fresh MEG. The poor performance of erythorbic acid at low pH is due to the initial step of the oxygen scavenging reaction where erythorbic acid is neutralized to erythorbate being either inhibited or reversed (refer to Figure 2-23). The different salt levels and low or high dosage rates had no significant effects on the final performance, as shown in Figure 8-8 to Figure 8-10.

In contrast to pH 6.0, erythorbic acid demonstrated consistently strong performance at pH 9.0 and was capable of successfully reducing the oxygen concentration from both saturation and 1000 ppb to below 20 ppb (refer to Figure 8-8 to Figure 8-10). However, a noticeable difference in oxygen removal rate was observed between the high and low dosage rates, with the low rate typically requiring an additional hour to achieve parity with the high dosage rate. The dependency on dosage rate for oxygen removal within MEG solution has been previously demonstrated by Salasi, Pojtanabuntoeng [234], where a greater dosage rate is often required within MEG compared to water systems. Furthermore, minimal to no impact due to the presence of organic acids and mineral salt ions was observed when compared to low salt trials (refer to Figure 8-6 and Figure 8-9) with the minimal impact due to high organic acid concentrations in line with the results in Section 8.4.2.

At a pH of 11.0 the erythorbic acid oxygen scavenger exhibited strong performance and was capable of reducing the dissolved oxygen concentration from both saturation and from 1000 ppb to below 10 ppb in less than one hour within TAL-MEG, with no influence of mineral ions and organic acid on performance exhibited (refer to Figure 8-5 to Figure 8-10). In addition, whilst tested at a pH of 11.0, due to the fast reaction time the erythorbic acid oxygen scavenger demonstrated near equal performance between the high and low dosage rates tested. As such, whilst operating at high pH the dosage rate of the oxygen scavenger can be effectively halved with no major implication on oxygen removal performance with a further reduction in dosage

rate possible. However during the processing of natural gas, it may not be desirable to operate under such high pH conditions for the injected lean MEG due to the potential for scale formation if salt-containing formation water is being produced [15, 67, 230, 363]. Therefore, the application of erythorbic acid for oxygen removal at pH 11.0 is only suitable where no formation water is produced or where an appropriate scale inhibitor is used in conjunction to manage the scale risk.

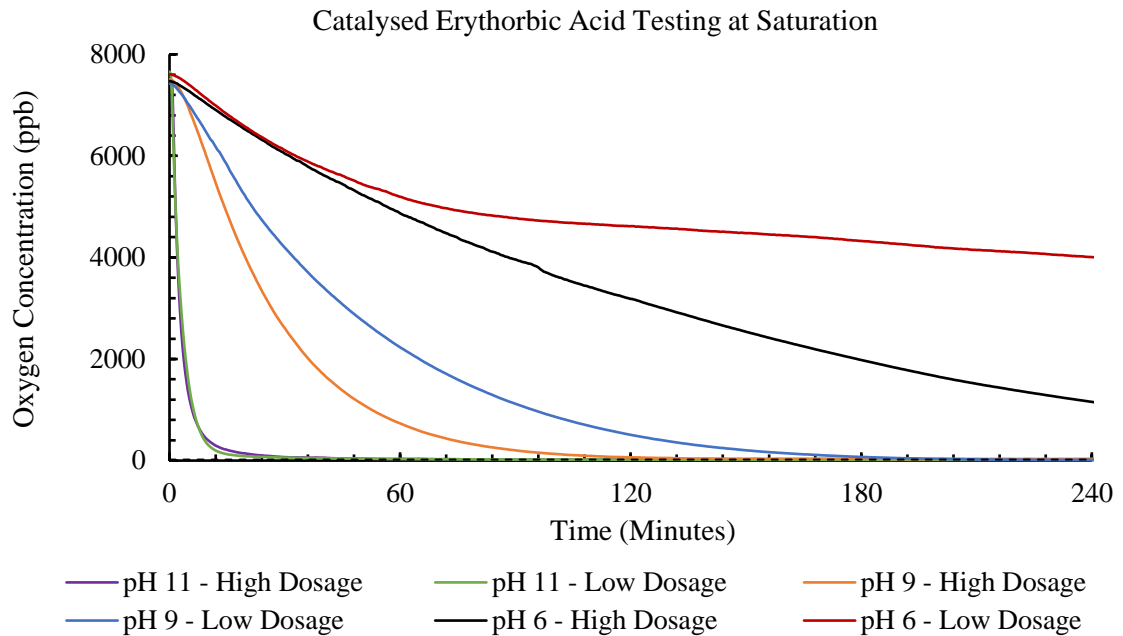


Figure 8-5 Effect of pH upon erythorbic acid performance in MEG no salts TAL-MEG

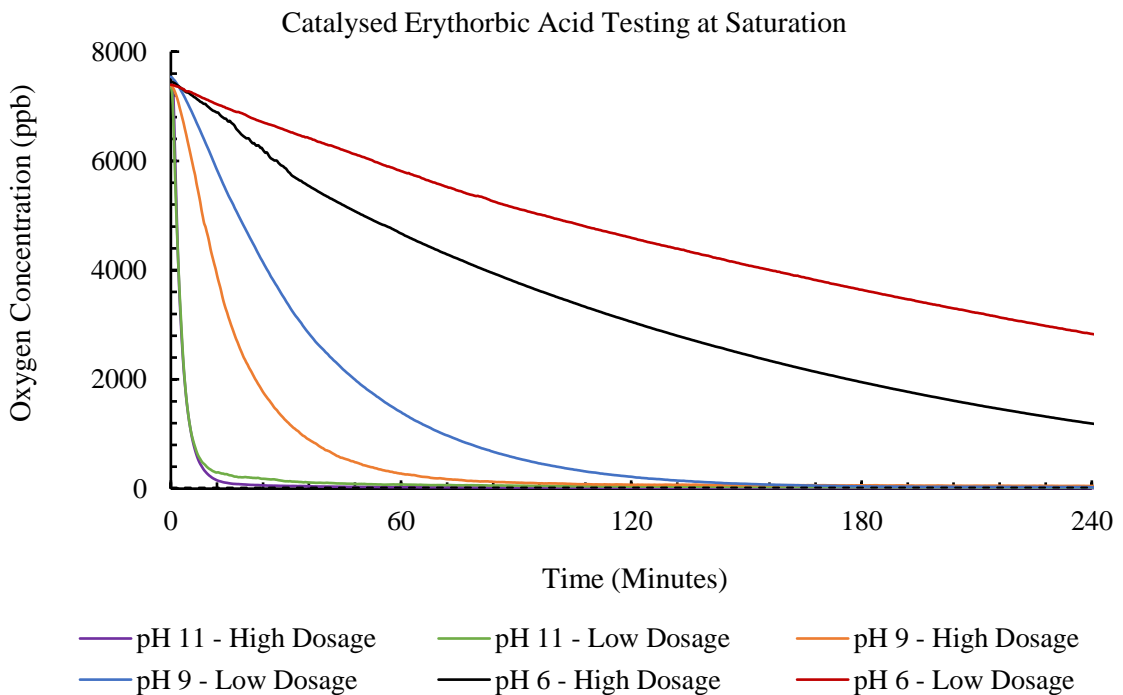


Figure 8-6 Effect of pH upon erythorbic acid performance in low organic acid TAL-MEG

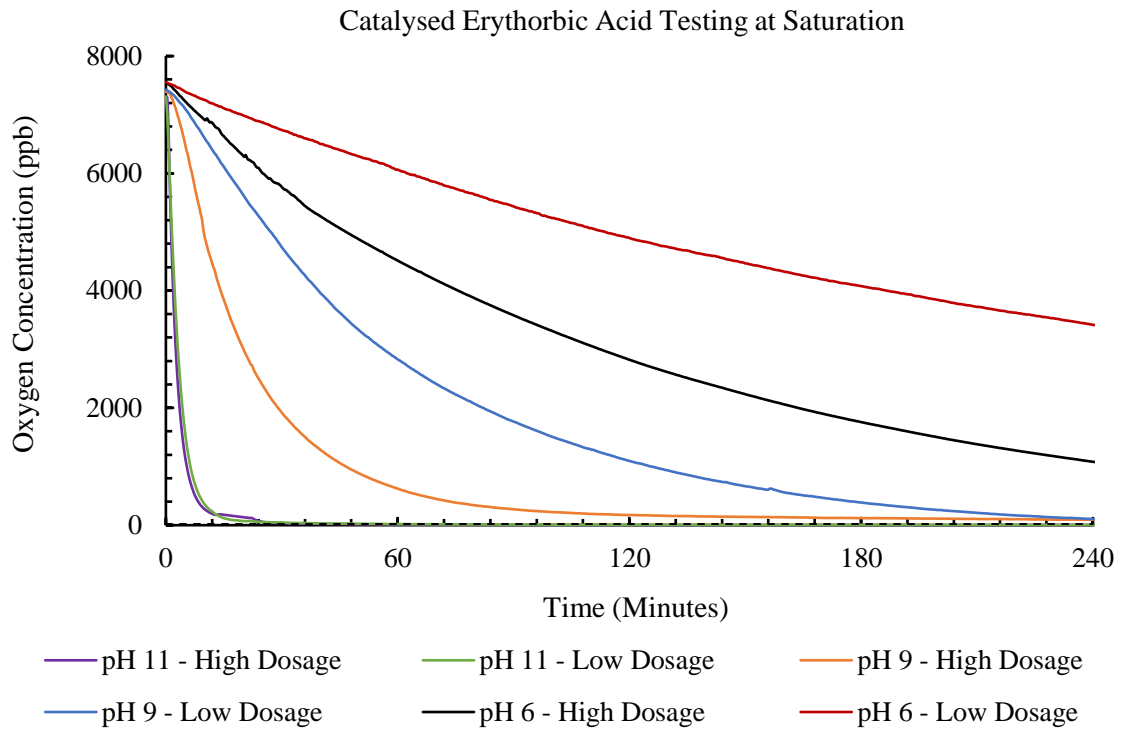


Figure 8-7 Effect of pH upon erythorbic acid performance in high salinity TAL-MEG

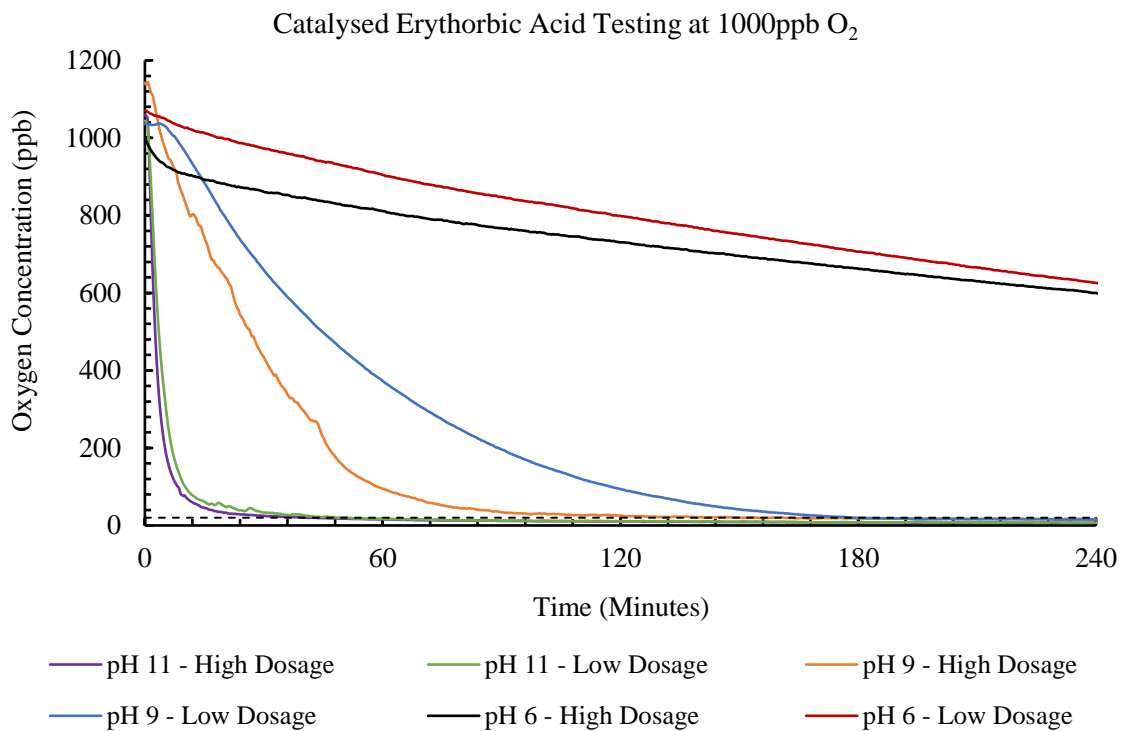


Figure 8-8 Effect of pH upon erythorbic acid performance in MEG no salts TAL-MEG

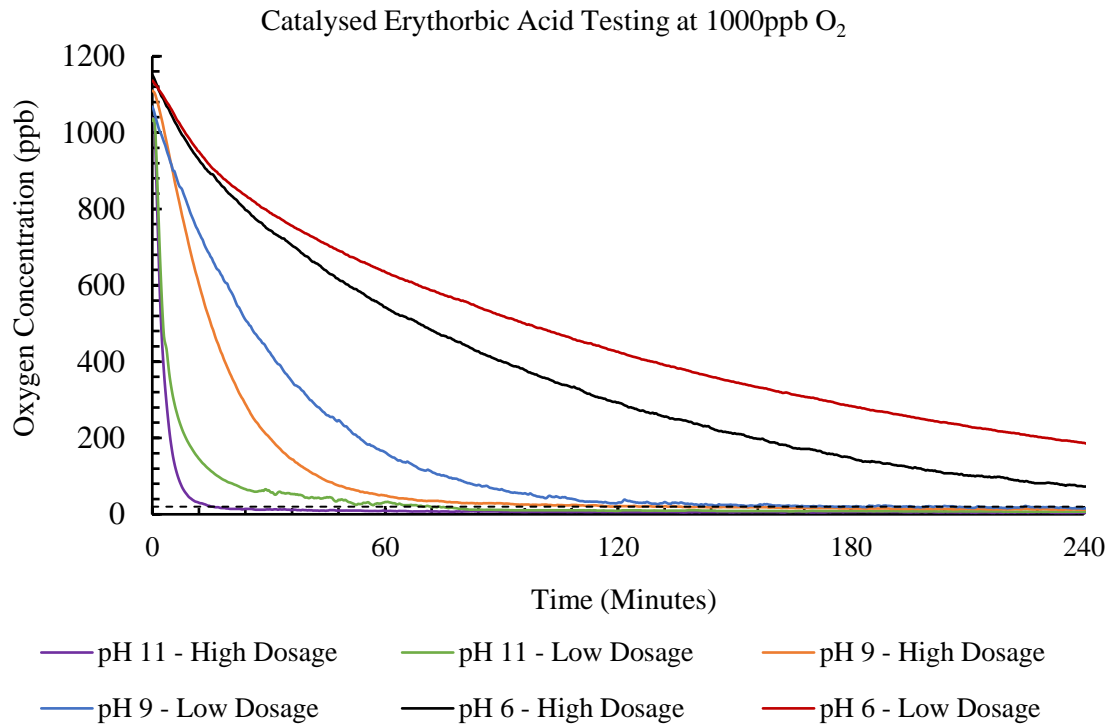


Figure 8-9 Effect of pH upon erythorbic acid performance in MEG low organic acids
(condensed water only) TAL-MEG

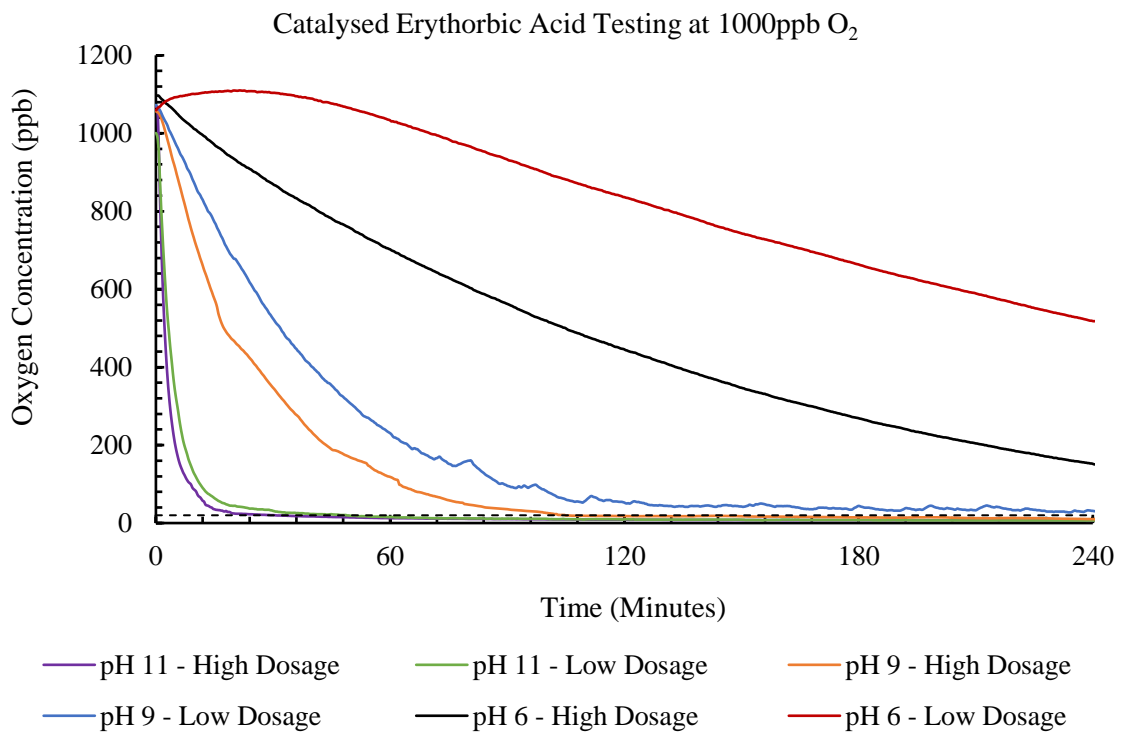


Figure 8-10 Effect of pH upon erythorbic acid performance in high salts MEG (full formation
water) TAL-MEG

8.5 Conclusions

Erythorbic acid as an oxygen scavenger has been extensively recognized for its strong performance as a preservative within the food industry [260, 261, 263, 265, 364]. However, little to no investigation has been performed to assess its applicability for use within the oil and gas industry, specifically under field conditions. The application of erythorbic acid in the oil and gas industry may provide a strong performing non-hazardous alternative to commonly used oxygen scavengers including sulfites to prevent oxygen-based corrosion issues in transportation pipelines and subsea equipment. Therefore, bench-scale evaluation of erythorbic acid has been performed to assess its performance under conditions typically found within industrial MEG regeneration systems including the effects of MEG thermal aging and the presence of common industrial contaminants such as salts and organic acids.

Previous evaluation of erythorbic acid as an oxygen scavenger has been performed within fresh MEG [230] but may not provide an accurate representation of field use. The performance of erythorbic acid has hence been evaluated within TAL-MEG to confirm its suitability for use within TAL-MEG post-regeneration. The results of the testing performed showed a noticeable decrease in oxygen scavenger performance at pH 9.0. However, erythorbic acid was still capable of achieving the desired 20 ppb oxygen concentration within an acceptable time frame (sub 4 hours). As such, this study strongly suggests that erythorbic acid is suitable for use within TAL-MEG and applicable for use in industrial MEG regeneration systems.

However at a pH of 6.0, erythorbic acid demonstrated poor oxygen removal performance is limiting its applicability at low pH. The reduced performance at pH 6.0 was attributed to the inability to fully neutralize the erythorbic acid molecule to its conjugate base (erythorbate) a step necessary to initiate the oxygen scavenging mechanism. Conversely, strong oxygen removal performance was demonstrated at pH 9.0 and 11.0 with little to no impact observed due to the presence of mineral salt ions typically found in MEG regeneration systems. Furthermore, through the testing conducted it was discovered that the presence of organic acids (acetic) did not have a significant impact on the performance of the tested erythorbic acid oxygen scavenger. Overall, the pH of the test solution was found to be the primary factor in determining the performance of erythorbic acid as an oxygen scavenger.

Chapter 9 The Performance of Erythorbic Acid Oxygen Scavenger within Salty Fresh and Degraded Mono Ethylene Glycol under Magnetic Memory Effect

9.1 Introduction

The performance of erythorbic acid oxygen scavenger in food industries has been reported to be effective, suggesting that it is a proper alternative for utilization in the oil and gas industry [20, 230, 256, 263, 282]. However, the performance of erythorbic acid oxygen scavenger under magnetic memory effects has not been studied yet. This study was conducted with 85 vol. % of fresh and degraded mono ethylene glycol solutions (F-MEG and D-MEG) that were pre-adjusted to a pH of 9.0 and pre-treated with a magnetic field (MF). Furthermore, the study was conducted at two levels of oxygen concentration, ~7000 and ~1000 ppb, and high saline concentrations (HF-MEG and HD-MEG) and organic acid contents. The strength of the applied MF, which was generated by a cylindrical permanent magnet, was 0.65 T.

As the dosage rate of oxygen scavenger, pH, and oxygen content in the treated solution containing contaminating species are important parameters to evaluate the performance of oxygen scavengers in the oil and gas industry, the presence of magnetized MEG solutions could change the scavenging dosage rates and their performance as well.

9.2 Experimental Methodology

9.2.1 Equipment Used and Setup

A pair of specially designed glass cells was used and fitted with a closed sealant Teflon cover, as shown in Figure 9-1. Each cell contained a dissolved-oxygen probe and pH probe provided by the Mettler Toledo. The probes were connected to a digital device monitor (M800) from Mettler Toledo to record, monitor the experiments, and then transfer the data to a computer to analyze the results. Each cell was equipped with stainless-steel tubing to allow nitrogen gas to enter the test fluid to release the dissolved oxygen, especially in low-oxygen experiments. This nitrogen source also allows the formation of a blanket of nitrogen gas between the cell cover and surface of the solution to isolate it from possible leakage from the outside. A rubber port was designed to inject the oxygen scavenger via a syringe into the cell without causing oxygen leakage. Both cells were connected to gas wash bottles to avoid accumulation of pressure and to prevent airflow reflection.

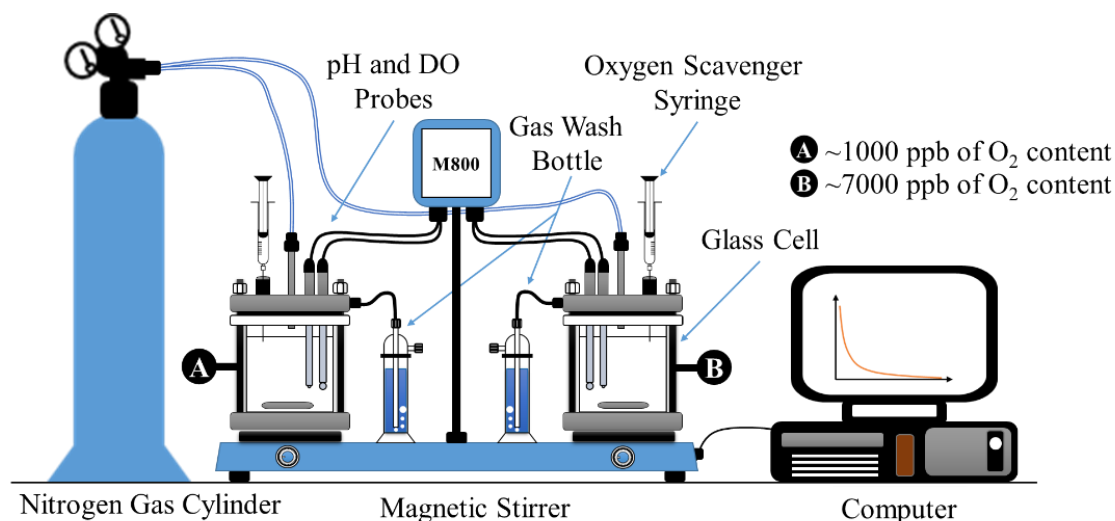


Figure 9-1 Bench-scale oxygen scavenger experimental apparatus

9.2.2 Chemicals Used

Erythorbic acid, manganese(II) chloride tetrahydrate, and diethylaminoethanol (DEAE) were supplied by Sigma Aldrich, at a purity greater than 99.0 wt.%. The oxygen scavenger composition was formulated by following the Institute for Energy Technology (IFE) [365] procedure to prepare erythorbate radicals (see Table 9-1). Manganese(II) ions were used to stimulate erythorbate radical formation. Full dissociation of the erythorbic acid oxygen scavenger was expected during the trial, through the neutralization process with DEAE [256]. All the experiments were performed at room temperature with MEG solutions sourced from Chem-Supply, at a purity greater than 99.9 wt.%. An Edgetech Industries LLC company from China supplied the permanent magnetic cylinder (diameter, 7.62 cm; length 22.86 cm). The magnetic strength at the center of the permanent magnetic (Teslameter, Wuntronic GmbH) was ~0.65 T. Thermally oxidized MEG (D-MEG) was produced in the laboratory using a distillation column setup at 130°C with exposure to air sparging for 5 h to stimulate the thermal oxidation process. The degradation experiment was stopped when significant discoloration was observed.

The degraded MEG solution was analyzed using Inductively Coupled Plasma Mass Spectrometry (ICP-MS) to identify the formed organic acids. High salt concentrations and two levels of oxygen concentration were used for magnetized and non-magnetized solutions to evaluate the oxygen scavenger performance. $\text{CaCl}_2 \cdot 2\text{H}_2\text{O}$, NaCl , $\text{MgCl}_2 \cdot 6\text{H}_2\text{O}$, SrCl_2 , NaHCO_3 , and NaSO_4 were supplied by Chem-Supply, at a purity greater than 99.9 wt.%, and were used to prepare high-salinity F-MEG and D-MEG solutions. Acetic acid and formic acid were supplied by Chem-Supply, at a purity greater than 99.9 wt.%. The synthetic solutions were prepared using ultra-deionized water, to avoid contaminations.

Table 9-1 Evaluated erythorbic-acid-based oxygen scavenger [230]

Component	Concentration (wt.%)	Component Purity (wt.%)
Erythorbic Acid	17.0	99.0
DEAE	25.0	99.5
MnCl ₂ .4H ₂ O	0.5	99.0
Distilled ultrapure water	57.5	Deoxygenated with N ₂

9.2.3 Magnetized Synthetic MEG Solution and Setup

Two synthetic F-MEG and D-MEG solutions of 85 vol. % in ultra-deionized water (18.20 MΩ.cm) were subjected to a homogeneous MF of 0.65 T, generated by a permanent Neodymium magnet, at a pH of 9.0 (see Figure 9-2). The specifications of the magnet are shown in Table 9-2. The laboratory tests were based on the method of circulating the solvents for 15 days, at a circulation rate of 5 ml/min, as described in Fig. 1. After 15 days of exposure, both the glass cells were filled with 750 g of these solutions in preparation for the start of the test. The oxygen levels in the first and second cells were set at ~1000 and ~7000 ppb, respectively. The oxygen scavenger at the first concentration level was injected via syringe and the oxygen probe reading was recorded over time until it reached less than 20 ppb, indicating the end of the experiment. A minimum oxygen concentration of 20 ppb was recommended by several publications to mitigate the corrosion issues in the oil and gas industry [2, 230, 233-235]. The next experiment was conducted with the same steps as before but at the second concentration level of the oxygen scavenger. The influence of the memory effect was the focus of this study to investigate the performance of the oxygen scavenger in pre-magnetized glycolic solutions.

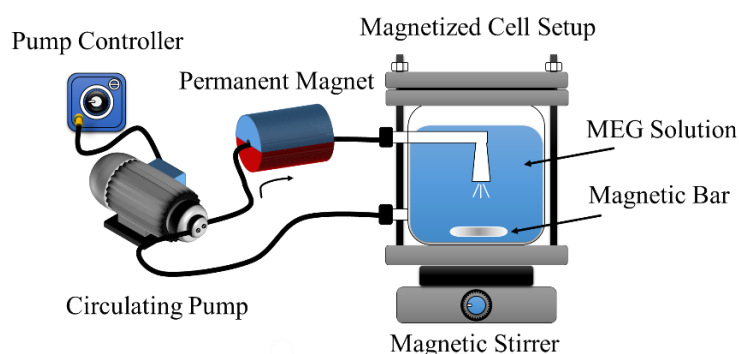


Figure 9-2 Magnetic treatment setup to circulate MEG solutions

Table 9-2 Magnet Specifications and Dimensions

Property	Specification
Magnet Grade and Materials	N45SH, NdFeB
Magnetization Direction	Diametrically
The Maximum Energy Product	44.38 MGOe
Magnetic Field Strength at the	0.65 T

9.2.4 Experimental Setup

Erythorbic acid oxygen scavenger was evaluated using the experimental set-up rig detailed in detail in Table 9-3. The conditions for the synthetic thermally oxidized MEG solutions used in this study were considered the worst thermal oxidation conditions in the MEG regeneration process, to assess erythorbic acid performance in transportation pipelines, whereas F-MEG solutions were considered as ideal MEG solutions. The potential erythorbic acid performance for MEG application was assessed under a range of conditions, including various oxygen scavenger dosage rates, salinities, MFs, and dissolved oxygen concentrations. The experiment was carried out using two oxygen concentration levels, ~7000 and ~1000 ppb, which represent different levels of dissolved O₂ content experienced in MEG regeneration plants. 100 and 200 ppm oxygen scavenger dosages were employed to evaluate the efficacy of the erythorbate radical in degraded and fresh MEG solutions.

Additionally, two typical F-MEG solutions and two D-MEG solutions with varying concentrations of organic acid and salts were prepared for the oxygen scavenger experiments. These solutions included F-MEG without salt or organic acids (uncontaminated fluid), F-MEG with a high content of salt and organic acid (contaminated fluid), thermally oxidized MEG without salt but with a high content of organic acids (representing thermal oxide solution), and thermally oxidized MEG with a high content of salt and organic acids (representing contaminated thermal oxide solution). A logarithmic scale was used during plotting the charts to illustrate the scavenging performance of erythorbic acid with time. The logarithmic scale gives a good insight into the extent of scavenging performance in different experimental conditions. The volume fractions of the fresh and degraded MEG solutions were confirmed using the Al Helal, et al. (2018) models, to ensure that the concentrations of the MEG mixtures were within the proposed level. The chemical compositions of the F-MEG and D-MEG mixtures are outlined in Table 9-4. The scavenging performance of manganese ions, formic acid, and manganese ions with formic acid in the absence of erythorbic acid oxygen scavenger was also determined for salt-free F-MEG solutions under alkaline conditions. These evaluations were done at 1000 ppb oxygen concentration and ambient temperature. The concentration of injected magnesium ions was set at 20 ppm and the formic acid dosage was 250 ppm. The same set-up rig illustrated in detail in Table 9-3 was used to perform this validation.

Table 9-3 Experimental design for fresh and degraded MEG solutions under magnetized and non-magnetized conditions

Test Conditions		Oxygen Scavenger Concentration, ppm		Oxygen Concentration, ppb		Salinity Level	
		100	200	~1000	~7000	Free	High
Fresh MEG	Non-Magnetized	•		•			•
		•			•		•
			•	•			•
			•		•		•
	Magnetized	•		•			•
		•			•		•
			•	•			•
			•		•		•
Degraded MEG	Non-Magnetized	•		•		•	
		•			•	•	
			•	•		•	
			•		•	•	
		•		•			•
		•			•		•
			•	•		•	•
	Magnetized	•		•		•	
		•			•	•	
			•	•		•	
			•		•	•	
		•		•			•
		•			•		•
			•	•			•

Table 9-4 Fresh and degraded MEG solutions at different salinities and organic acid concentrations

Salts/Organic Acids, ppm*	F-MEG Solutions	D-MEG Solutions	
	High Salinity (HF-MEG)	(D-MEG)	High Salinity (HD-MEG)
Na ⁺	7724.72	0	7724.72
K ⁺	28.35	0	28.35
Ca ²⁺	43.65	0	43.65
Mg ²⁺	1.95	0	1.95
Fe ²⁺	0.72	0	0.72
Sr ²⁺	3.645	0	3.65
Ba ²⁺	3.105	0	3.11
Cl ⁻	11641.75	0	11641.75
HCO ₃ ⁻	87.0	0	87.0
SO ₄ ²⁻	23.55	0	23.55
Formic Acid	0	242.66	242.66
Acetic Acid	462.90	1474.69	1937.59

*The salinity levels were analyzed using inductively coupled plasma mass spectrometry.

9.3 Results and Discussion

9.3.1 Validation of Mn^{2+} ion Effect on the Scavenging Process in High-Salt Fresh MEG

The effect of Mn^{2+} ions on the oxygen scavenging process was investigated in salt-free 85 vol. % F-MEG solutions and in the absence of erythorbic acid oxygen scavenger. A 20 ppm Mn^{2+} ion solution was injected into a re-adjusted F-MEG solution at a pH of 9.0 and oxygen concentration of 1000 ppb. The deoxygenation rates over time were monitored using the M800 interface and are presented in Figure 9-3. These results showed that Mn^{2+} ions have oxygen scavenging potential within salt-free F-MEG solutions under alkaline conditions. However, they demonstrated poor deoxygenation performance. The poor performance of Mn^{2+} was due to the initial step of the reaction where Mn^{2+} is converted to $Mn(OH)_2$, which was oxidized to form a dark brown MnO_2 compound. The initial step of $Mn(OH)_2$ formation led to a reduction in the pH level of the MEG solution, which had an effect on the scavenging performance of Mn^{2+} ions; the oxidation performance of Mn^{2+} ions was reported to be excellent at highly alkaline conditions [366]. As shown in Figure 9-3, the deoxygenation period demonstrated this poor performance, wherein the oxygen level reached 200 ppb within 18 operational hours. The scavenged oxygen level with Mn^{2+} ions was not appropriate for the oil and gas industry operational requirements to mitigate the corrosion issue. The generated results confirm that the role of Mn^{2+} ions in erythorbic acid oxygen scavenging is accelerating the scavenging reaction to attain high oxygen removal, which is described in the following sections.

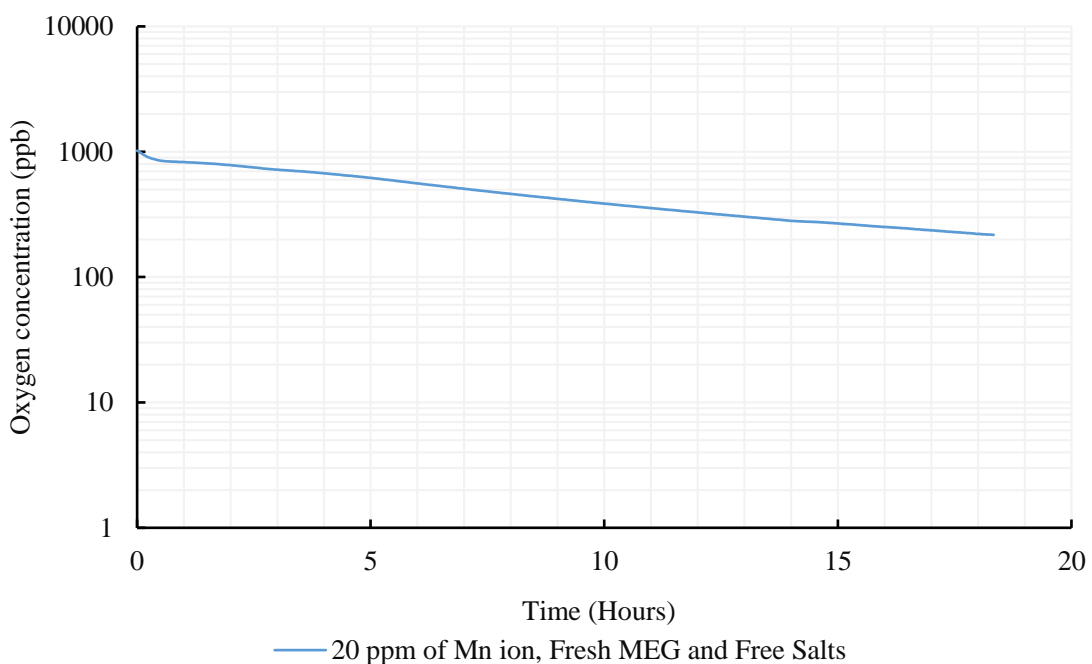


Figure 9-3 Scavenging performance of Mn^{2+} ions in F-MEG solution under alkaline conditions

9.3.2 Effect of pH on the Erythorbic Acid Oxygen Scavenging Performance

It is important to explain why the experiments of this study were performed at a pH of 9.0. It was reported that the performance of erythorbic acid oxygen scavenger at pH below 7.0 fails to achieve the desired 20 ppb oxygen concentration for both ~7000 and ~1000 ppb initial concentrations [230, 281]. Therefore, two experiments were conducted at a high oxygen scavenger dosage to evaluate the performance of erythorbic acid at pH of 9.0 and 11.0, using a salt-free F-MEG solution. As shown in Figure 9-4, an increase in the efficiency of the oxygen scavenger in salt-free F-MEG solutions was observed when the pH was raised from 9.0 to 11.0. This finding is in line with the results of earlier studies, which concluded that the effectiveness of erythorbate radicals increases in highly alkaline environments. However, in this study, a pH of 9.0 was preferred because MEG regeneration plants or oil product transportation pipelines are not commonly operated under such highly alkaline conditions (pH of 11.0). Furthermore, the oxygen scavenging results for pH 9.0 are relatively acceptable, although it takes slightly longer to reach a level close to 20 ppb.

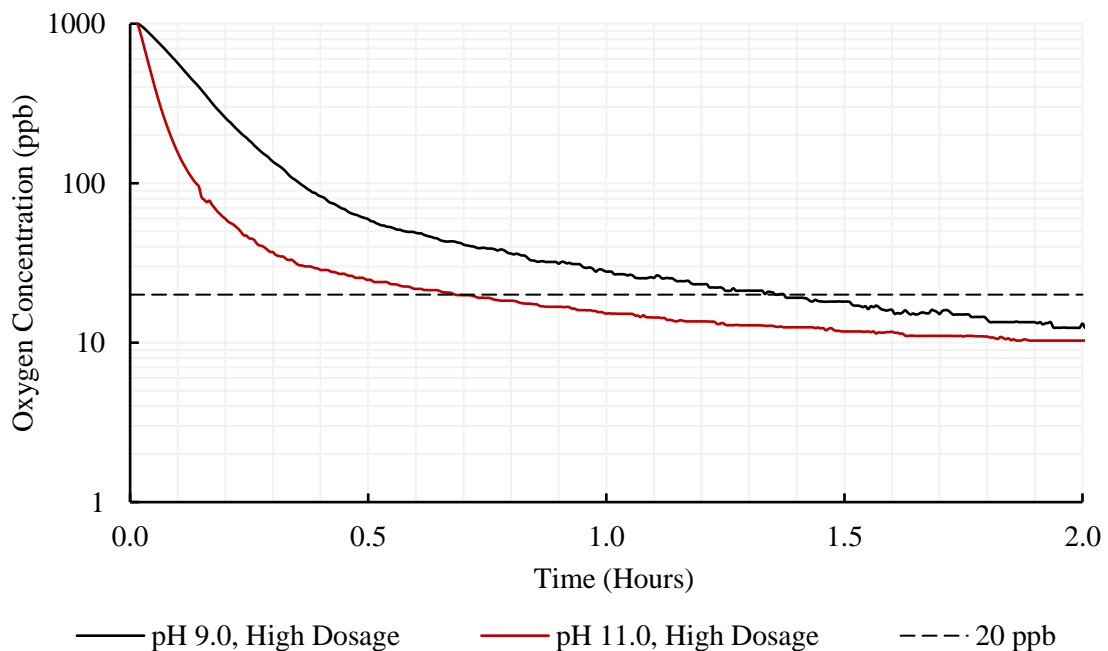


Figure 9-4 Effect of pH level on high-dosage erythorbic acid performance in salt-free F-MEG solutions

9.3.3 Effect of the Magnetic Field on the Erythorbic Acid Performance in High-Salt Fresh MEG Solutions

9.3.3.1 Low Oxygen Scavenger Dosage at ~1000 and ~7000 ppb O₂ Content

The scavenging performance of erythorbic acid in magnetized and non-magnetized HF-MEG solutions was evaluated at a low oxygen scavenger dosage and ~1000 ppb oxygen content. As

shown in Figure 9-5, erythorbic acid showed a low removal performance in oxygen removal to 20 ppb for non-magnetized HF-MEG solutions. However, the scavenging performance increased by 12.5% due to the memory effect, specifically after exposing the HF-MEG solution for 15 days. The generated results confirm the positive effect of the MF to promote oxygen scavenger performance in HF-MEG solutions. The reason behind this could be the influence of the memory effect on the O₂-H₂O binding strength in MEG solutions, which weakens and distorts the hydrogen bond interactions. Furthermore, the magnetized H-bonds facilitate the release of oxygen molecules from the solution and promote oxygen scavenging. In addition, the spin chemistry of the erythorbic acid radical oxygen scavenger pair was improved by the external MF, and magnetization could promote the forward reaction more than the backward reaction, resulting in the faster removal of oxygen molecules (see Figure 9-6). The internal low MF effect resulted from consistent superpositions of the degraded nuclear-electron spin states in spin-correlated radical pairs in zero field. The magnetic memory effect caused these microstructures to fluctuate and reposition, leading to recombined inter-transformation of triplet and singlet electronic states of the radical pair, and therefore changed the yields of the recombination products and free radicals that distributed into the MEG solutions. For singlet radical pairs, the magnetic memory effect leads to an advancement in the group of free radicals. Using experimental approaches, the memory effect was confirmed to change the yield and concentration of singlet radical pairs that change the scavenging performance within HF-MEG solutions. This hypothesis will be a suitable explanation for the generated results, to describe the influence of the memory effect on scavenging performance.

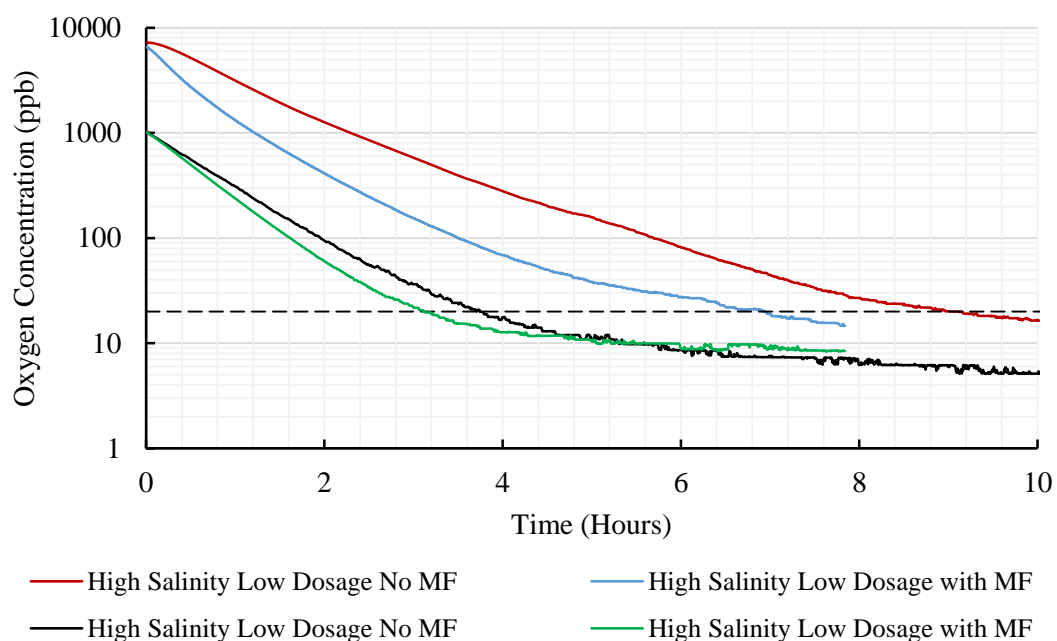


Figure 9-5 Effect of the MF on low-dosage erythorbic acid performance for ~1000 and ~7000 ppb O₂ in the high salinity fresh Monoethylene Glycol solutions

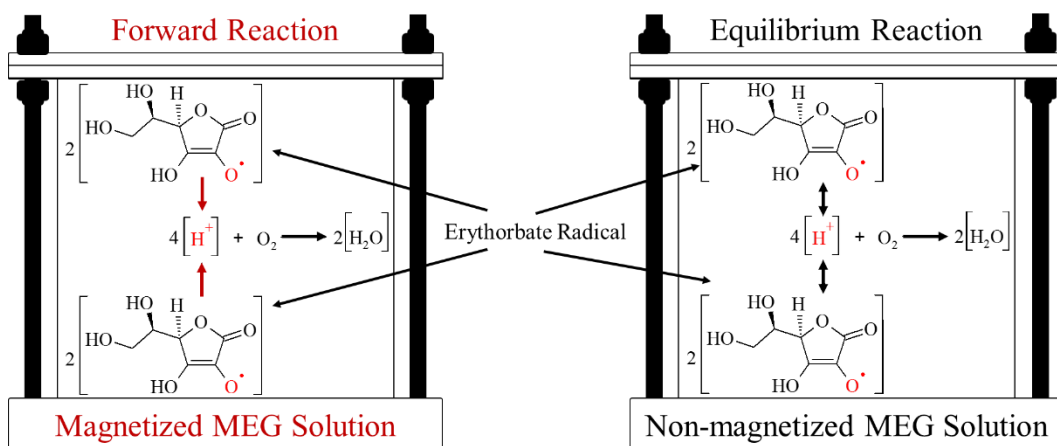


Figure 9-6 Magnetic memory effect on erythorbic acid scavenging reaction

The experiments described in the previous section were re-tested, but at a saturated concentration level of dissolved oxygen of about ~7000 ppb. The results of oxygen scavenging over time are plotted in Figure 9-5. The previous pattern of oxygen removal in magnetized and non-magnetized HF-MEG solutions was the same as that for the saturated-oxygen-level experiments. Also striking was the high performance of the oxygen scavenger in the experiments with solutions exposed to the MF for a fairly long recording period. As a result, the experiments with solutions exposed to MFs were able to reduce the scavenging time during exposure to about 65%. The results also highlighted the ability of MFs to improve the performance of erythorbic acid at high saline contents.

9.3.3.2 High Oxygen Scavenger Dosage at ~1000 and ~7000 ppb O₂ Content

Two HF-MEG solutions with 1000 ppb oxygen content were tested to evaluate the performance of a high dosage of oxygen scavenger under magnetized and non-magnetized conditions. The readings of the oxygen concentration removal over time are illustrated in Figure 9-7. It was observed that the performance of the high-dosage oxygen scavenger was similar to that of the low-dosage oxygen scavenger. This finding is interesting and highlights the potential of the memory effect to improve the scavenging performance to obtain a low oxygen concentration. In addition, the generated results confirmed the effectiveness of the magnetic memory effects on erythorbic acid in increasing the removal performance in non-aqueous solutions.

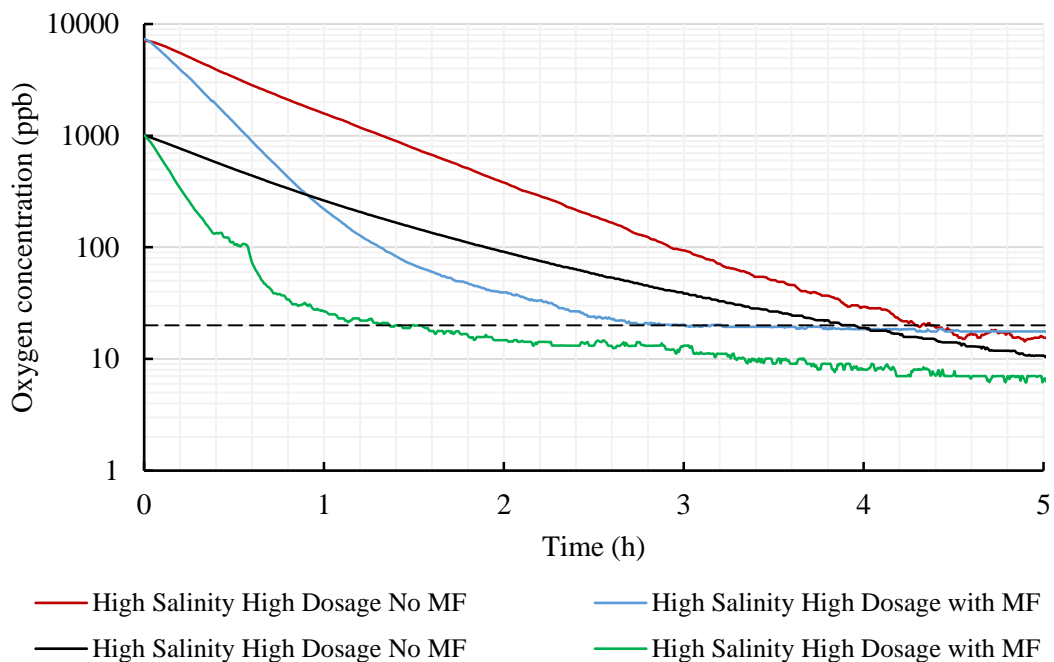


Figure 9-7 Effect of the MF on high-dosage erythorbic acid performance for ~1000 and ~7000 ppb O₂ in high salinity fresh Monoethylene Glycol solutions

The influence of the memory effect on the rate of removal of oxygen molecules was tested in pre-prepared HF-MEG solutions with a high oxygen concentration, which was ~7000 ppb. The generated results were compared with the results of the non-magnetized tests of HF-MEG solutions to illustrate the effect of magnetization on the oxygen scavenging performance, especially for high scavenger dosages. The results are plotted in Figure 9-7. The illustrated results show the positive influence of the memory effect on the oxygen removal over time. This explains the improved performance of the oxygen-removal process due to an enhancement in the forward reactions of the free radicals. As the backward reactions are inhibited under the influence of MFs, the forward reactions promote oxygen scavenging. According to the theory of spin chemistry, there are two types of MF effects in any micro molecular system, wherein the internal field effect is known as the Hyperfine effect, and the external field effect is known as the Zeeman effect, as the latter reflects the direct influence of external MFs, which inhibit the re-bonding of broken bonds during the chemical reaction, leading to the formation of the triplet coupled spin states instead of singlets, by flipping the electron spin of the anisotropic radical pair.

9.3.4 Effect of MF on Erythorbic Acid Performance in Salt-Free Degraded MEG Solutions

9.3.4.1 Low Oxygen Scavenger Dosage at ~1000 and ~7000 ppb O₂ Content

Salt-free degraded MEG solutions were tested under magnetic and non-magnetic conditions to evaluate the performance of the oxygen scavenger at low dosages. The results obtained are plotted in Figure 9-8 to compare the performance of the oxygen scavenger at these conditions. The figure

clearly shows that the performance of erythorbic acid in non-magnetized salt-free D-MEG solutions was faster than that in the magnetized salt-free D-MEG solutions; it also seemed faster than that in the HF-MEG solution tests. However, the time difference between magnetized solutions and the non-magnetized salt free D-MEG solution is not very high, indicating that the effect of the MF on these solutions was insignificant. Moreover, the presence of formic acid in these D-MEG solutions seemed to assist the erythorbic acid scavenging performance to reduce the oxygen concentration rapidly. This hypothesis is in line with several studies that have reported that oxygen molecules can be removed when oxidizing formic acid using a metal-ion-catalyzed process to form water and carbon dioxide at ambient temperature [367-369] (see Figure 9-9). The formation of carbon dioxide may contribute to the formation of aqueous carboxylic acid, leading to a reduction in the pH level of the salt-free D-MEG solutions, which in turn affects the scavenging process period. Although acetic acid is present in the HF-MEG and salt-free D-MEG solutions, it does not show a significant effect on the scavenging performance (see Table 9-4). Furthermore, it has not been evidenced in the literature that acetic acid can be oxidized at ambient conditions (see Figure 9-9) [370]; hence, we excluded the acetic acid effect in this study.

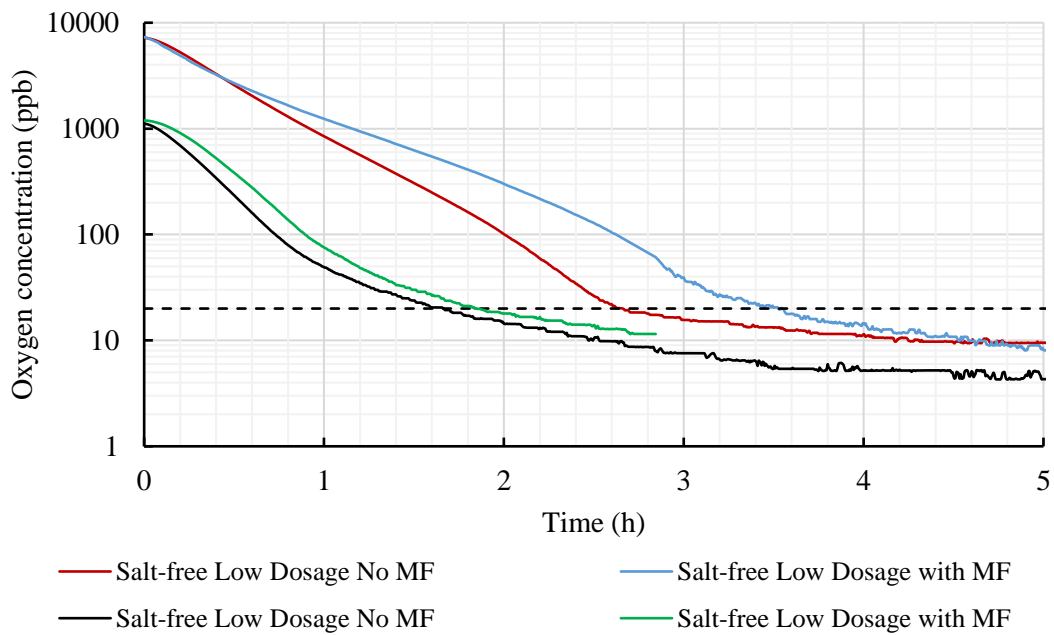


Figure 9-8 Effect of the MF on low-dosage erythorbic acid performance for ~1000 and ~7000 ppb O₂ in salt-free degraded Monoethylene Glycol solutions

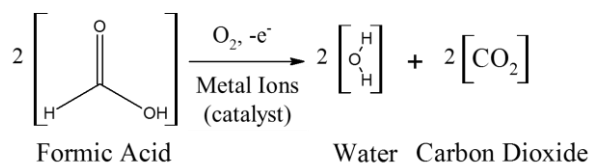


Figure 9-9 Product formation in aerobic oxidation of formic acid with metal-ion catalyst [368]

For the next experiment, the same conditions of the previous experiments were used, except for an oxygen concentration level of ~7000 ppb, to test the performance of erythorbic acid within magnetized D-MEG solutions. The generated results are plotted in Figure 9-8 to determine the variations in oxygen scavenger performance over time. It was interesting to observe the same oxygen removal pattern that was obtained for low oxygen concentration levels. The performance was perfect in non-magnetized D-MEG solutions, compared to that in magnetized tests of D-MEG solutions and HF-MEG solutions. However, the time frame difference between the magnetized and non-magnetized tests was slightly larger and up to 50 min. This may have been due to the rapid decline in the pH level of the magnetized D-MEG solutions, which is illustrated in Section 9.3.6. In fact, MFs tend to accelerate forward reactions, especially when free radical pairs are produced [57, 371]. Therefore, the oxidation of formic acid may enhance the formation of carbon dioxide in magnetized D-MEG solutions, leading to a decline in the pH during the scavenging process [368] (see Figure 9-10). This decline has a negative effect on the erythorbic acid scavenger in magnetized D-MEG solutions. Furthermore, it has been reported that formic acid can form a free radical group that can interact with hydroxyl ions [284, 288]. This kind of reaction contributes to a reduction in the total pH level of D-MEG solutions, as described in the previous section. The reaction between formic acid and hydroxyl radicals can proceed via either an acid or a formyl H-abstraction pathway, because the free radical intermediate decomposes rapidly to hydrogen radical and carbon dioxide [284, 372]. Furthermore, the rate coefficient of this reaction was reported to be relatively temperature-independent between 25 and 127°C [372, 373]. This indicates that this reaction can occur at ambient temperature. Hence, this reaction significantly reduces the performance of the oxygen scavenger, which prefers to operate at a pH of 9.0, generating an obvious difference in the scavenging time.

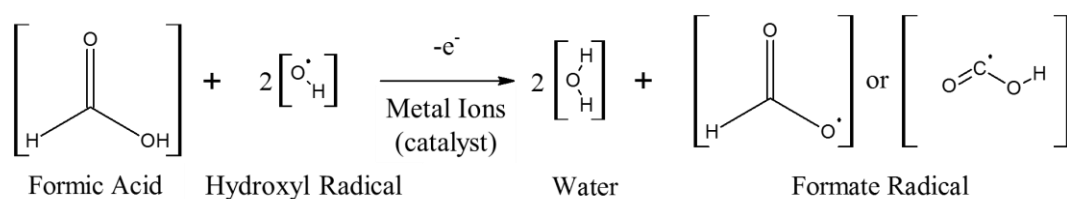


Figure 9-10 Product formation in aerobic oxidation of formic acid with metal-ion catalyst

9.3.4.2 High Oxygen Scavenger Dosage at ~1000 and ~7000 ppb O₂ Content

Two sets of tests were conducted at pH 9.0, using two solutions of magnetized and non-magnetized salt-free D-MEG (No salts) with high dosages of the erythorbic acid oxygen scavenger, as listed in Table 3. These experiments were carried out to evaluate the impact of the memory effect upon high-dosage erythorbic acid oxygen scavenger performance in salt-free D-MEG solutions. For each experiment, the initial O₂ concentration in the salt-free D-MEG solution was adjusted to ~1000 ppb or saturation (~7000 ppb), to simulate actual industrial field

conditions. As shown in Figure 9-11, the performance of the erythorbic acid oxygen scavenger was significantly improved by the thermal oxidation products and high dosage of the oxygen scavenger. Furthermore, for both the magnetized and non-magnetized trials, it was observed that the scavenging removes the oxygen concentrations within the same time periods for both the 1000 ppb and saturation concentrations. The time required to reduce the oxygen concentration from ~1000 ppb to below 20 ppb was 45 min (Figure 9-11), whereas, for saturated salt-free D-MEG solutions, it was 75 min. These results may have been due to the presence of a high dosage of manganese catalyst along with the oxygen scavenger, which boosted the oxidation of formic acid under highly alkaline conditions. The generated results are in line with the conclusions of the previous sections. Furthermore, these outcomes confirm the poor influence of the magnetic memory effect on the scavenging performance at high dosages of erythorbic acid within the salt-free D-MEG that contains formic acid. The scavenging performance was improved by formic acid, when performed in either magnetized or non-magnetized salt-free D-MEG solutions.

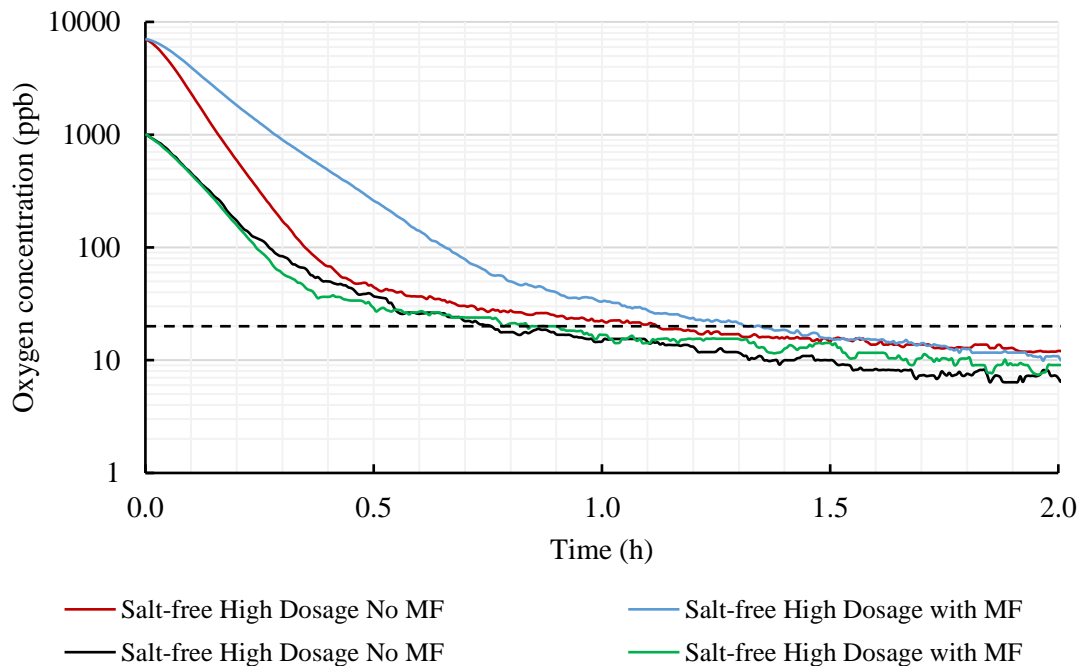


Figure 9-11 Effect of the MF on high-dosage erythorbic acid performance for ~1000 and ~7000 ppb O₂ in salt-free degraded Monoethylene Glycol solutions

9.3.5 Effect of MF on Erythorbic Acid Performance in High Salinity Degraded MEG Solutions

9.3.5.1 High and Low Oxygen Scavenger Dosages at ~1000 and ~7000 ppb O₂ Contents

To evaluate the influence of high salt contents on the performance of erythorbic acid as an oxygen scavenger under magnetized conditions, two sets of tests using HD-MEG solutions were conducted with high and low oxygen scavenger dosages, for 1000 ppb and saturation (~7000 ppb)

oxygen levels, wherein the pH of the solutions was maintained at 9.0. The reason behind using high salinity was to investigate the effects of the mineral ions that accompanied water formation breakthrough during oil and gas production on the oxygen scavenger performance when D-MEG is used as a gas hydrate inhibitor. Furthermore, the performance of the oxygen scavenger was examined in magnetized and non-magnetized salty D-MEG solutions to determine the impact of the magnetic memory effect on the scavenging process.

The results generated for low and high oxygen scavenger dosages showed that the performance of the erythorbic acid oxygen scavenger was significantly advanced within the magnetized HD-MEG solutions when compared with that for the non-magnetized solutions (see Figure 9-12 and Figure 9-13). This was due to the presence of transition-metal ions in the magnetized HD-MEG solutions, which induced a more rapid scavenging performance than that observed in the magnetized and non-magnetized salt-free D-MEG solution trials. The transition-metal ions enhance both the formic and erythorbic acid oxygen scavenging processes by acting as an additional catalyst, together with the pre-added manganese ions, and enhancing free radical formation. In addition, the magnetic memory effect improved the scavenging performance of these organic acids by controlling the pH of the treated HD-MEG solutions, which showed a slight decrease over that observed in the non-magnetized experiments; this positively affected the course of the oxygen molecule scavenging reactions (Figure 9-14). Iron ions are the most likely ions to improve the scavenging performance [242]. Iron is the most similar transition metal to manganese in terms of chemical and physical properties [242]. Therefore, it is expected to exhibit an excellent performance in the removal of oxygen molecules with the availability of metal ions in the HD-MEG solutions. Furthermore, iron ions are highly ferromagnetic with high paramagnetic behaviour over that of the other mineral ions mixed with the HD-MEG solutions [78, 374]. This leads to the rapid response of these ions toward MF environments, which improves the scavenging reactions. The reaction mechanism of this behaviour is not yet understood; however, the explanation still falls within the ambit of spin chemistry theory. Thus, the ability to remove oxygen molecules in saline HD-MEG solutions exposed to MFs improves due to an improved free radical generation, owing to the presence of iron and manganese ions and the stability of the pH level of the magnetized HD-MEG solutions.

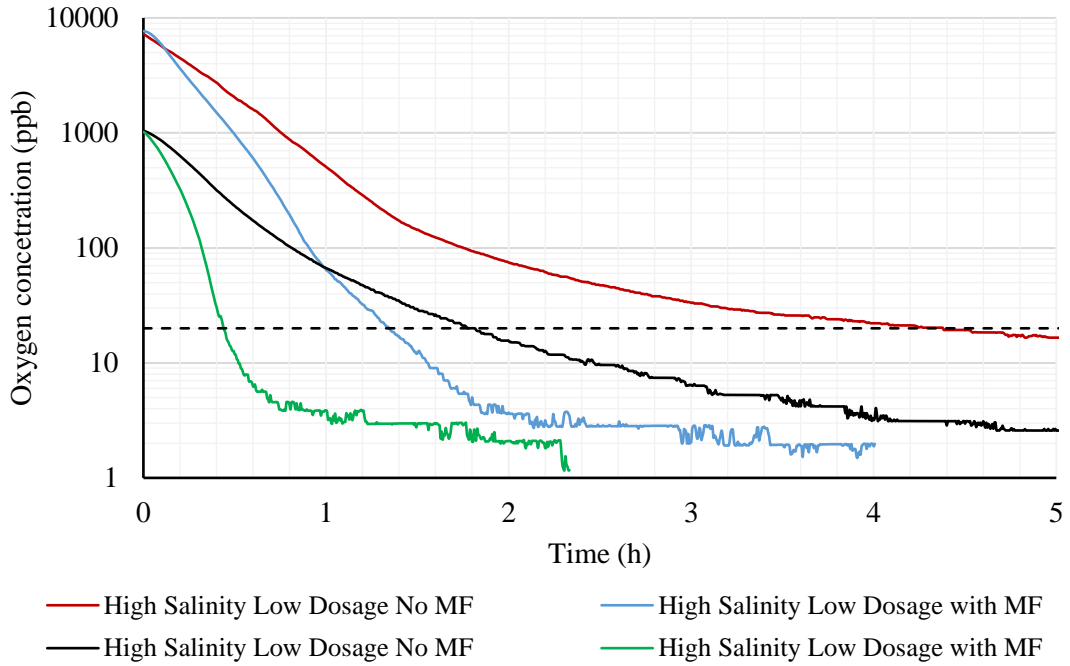


Figure 9-12 Influence of the memory effect on low-dosage erythorbic acid performance for ~1000 and ~7000 ppb O₂ content in high salinity degraded Monoethylene Glycol solutions

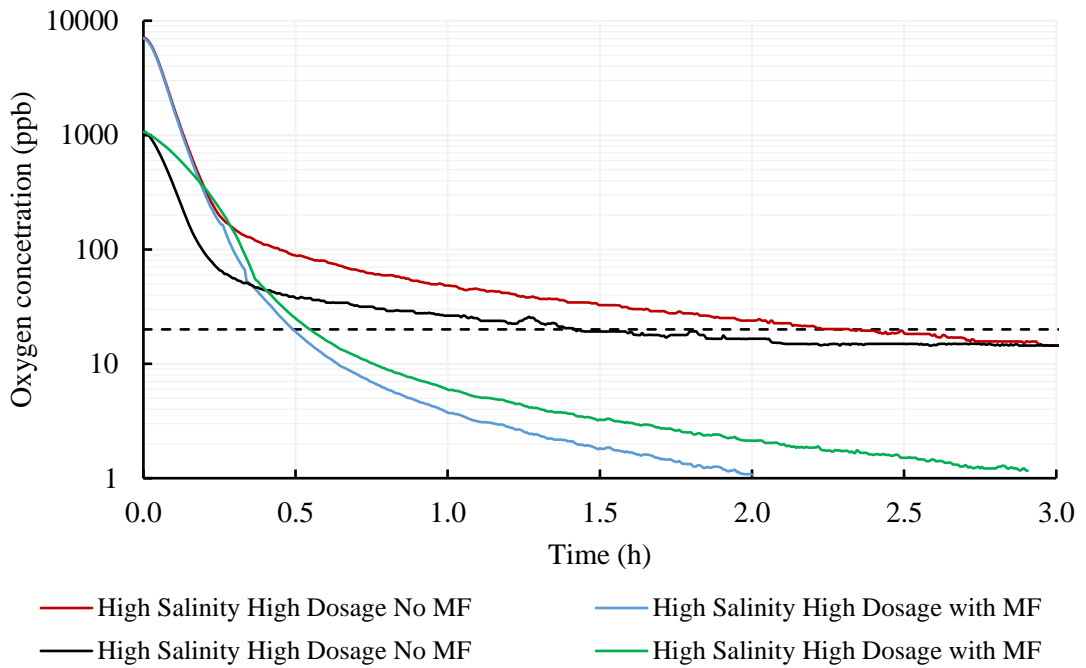


Figure 9-13 Influence of the memory effect on high-dosage erythorbic acid performance for ~1000 and ~7000 ppb O₂ content in high salinity degraded Monoethylene Glycol solutions

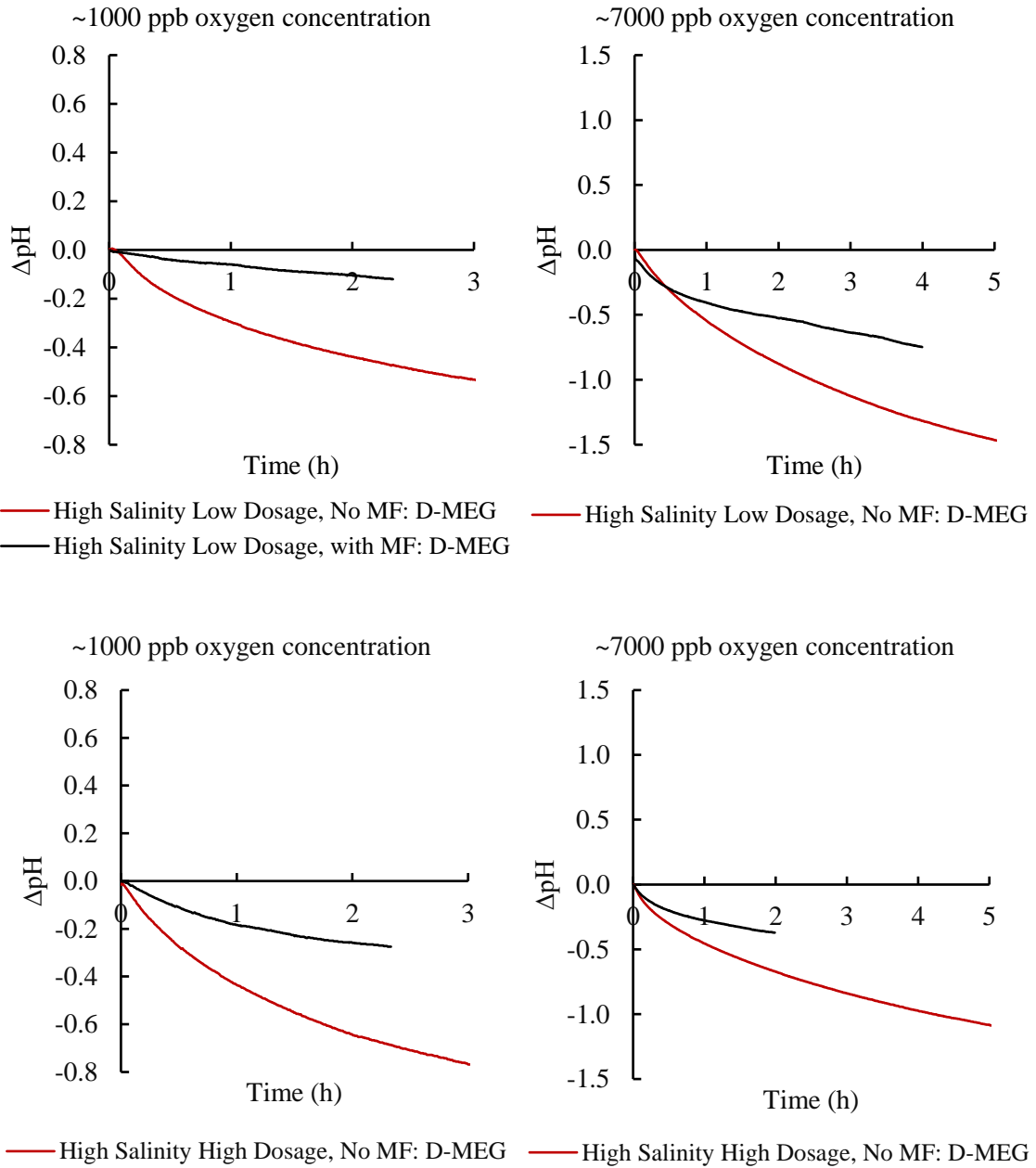


Figure 9-14 Magnetic memory effect on the pH of the magnetized and non-magnetized high salinity degraded Monoethylene Glycol solutions

These results show that the best performance of erythorbic acid for the removal of oxygen molecules was achieved in the D-MEG solutions and not in F-MEG solutions because D-MEG solutions contained organic degradation products that advanced the oxygen scavenging process. They also proved that there is a direct effect of iron ions on the efficiency of the scavenging process in magnetized D-MEG solutions, due to the contribution of iron and manganese ions and the stabilized alkaline environment, which improved free radical formation.

9.3.6 pH of Magnetized and Non-magnetized High Fresh MEG and Degraded MEG Solutions

The pH changes in the magnetized and non-magnetized F-MEG and D-MEG solutions with ~1000 and ~7000 ppb oxygen contents were measured next (Figure 9-15). An increase in pH was evident in the magnetized HF-MEG solutions, while the non-magnetized HF-MEG solutions showed a continuous decrease in pH. These observations are in line with previously published reports of the effect of MFs on the hydroxide species activity in solution leading to elevated pH readings [375, 376]. These results are due to the modifications in the thermodynamic properties and direction of the proton spin of the anion microscopic structures. This phenomenon is partly contributed towards the maintenance of pH values >9.0 in the exposed solutions, leading to enhanced oxygen-scavenging performance, as mentioned in the previous sections.

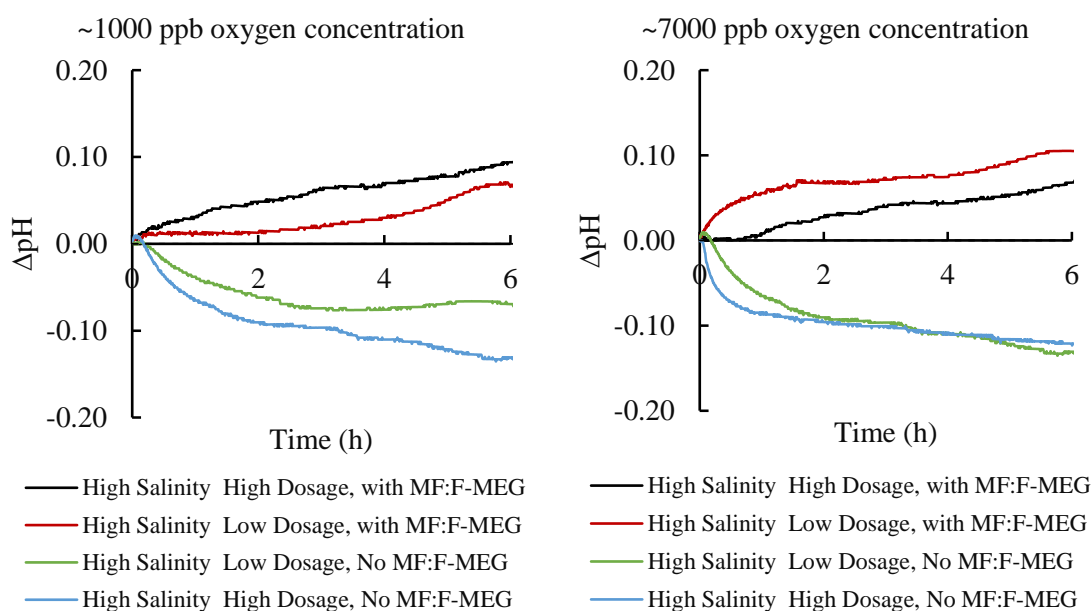


Figure 9-15 pH measurements after and before exposure to an MF for ~1000 and ~7000 ppb oxygen concentrations in the fresh Monoethylene Glycol solutions

However, due to the presence of formic acid in the D-MEG solution, the pH levels in each experiment did not exhibit an increase in response with time, as was observed in the magnetized F-MEG tests (Figure 9-16). These results were expected because the interaction between formic acid and the hydroxyl groups under ambient conditions caused a reduction in the solution pH. In addition, the magnetized D-MEG solutions induce forward rather than reversing the chemical reactions, especially for organic chemical reactions that involve radical intermediate steps. The bonds between the atoms are ruptured during the chemical reactions and the electrons on either side of the broken bond spin in opposite directions to form two radical pairs [57, 58]. At this point, the recombination mechanism begins to reform the bond based on the chemical reaction

equilibrium state of the backward reaction. However, the interaction between the external MF and spin is more likely to advance the formation of the products and disrupt the equilibrium. This occurs because the external MF produces triplets rather than singlets by flipping the electron spin of the anisotropic radical pair (Zeeman interaction) [57, 58]. Thus, the magnetic polarization phenomena demonstrate the dependency of the radical-pair reaction mechanism on the direction of the external MF, which converts singlet radical pairs to triplets to prevent the reverse reaction [57].

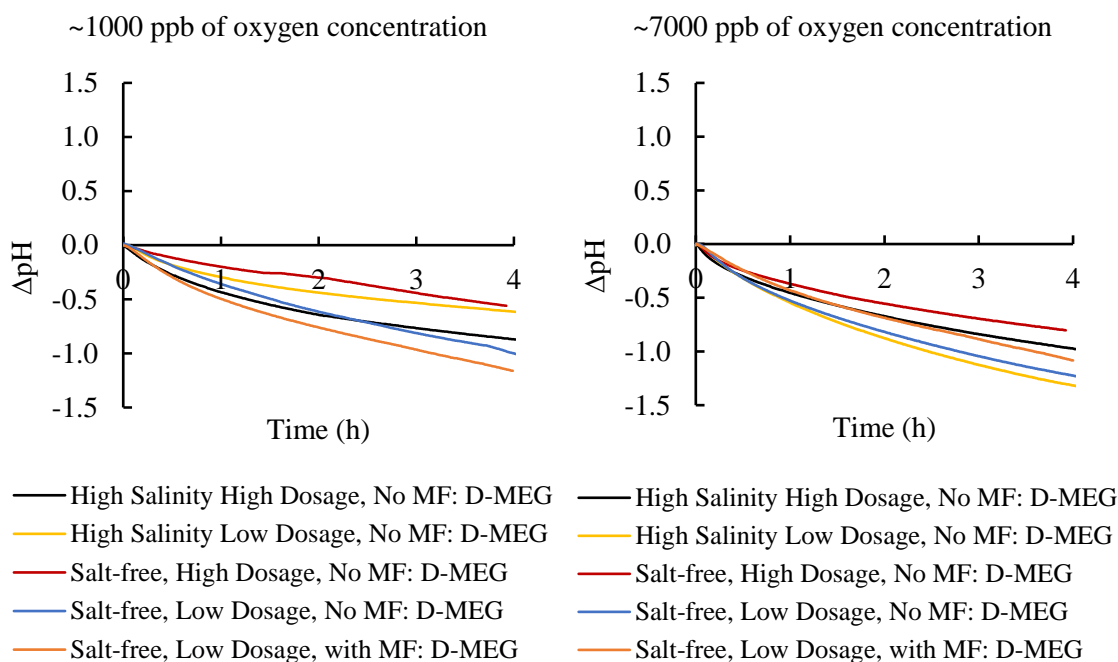


Figure 9-16 pH measurements after and before exposure to an MF for ~1000 and ~7000 ppb oxygen concentrations in the degraded Monoethylene Glycol solutions

9.3.7 Validation of Formic Acid Effect in Combination with Mn^{2+} Ions on the Scavenging Process in F-MEG

The effect of formic acid on the erythorbic acid scavenging performance was evaluated at two pH levels, 9.0 and 10.0, of D-MEG. The obtained scavenging results over time are plotted and illustrated in Figure 9-17. It was observed that the oxygen scavenging process by formic acid is sensitive to the pH levels. The trial with an operational pH of 9.0 showed slow scavenging performance, whereas the trial with a pH of 10.0 showed an improvement in the scavenging performance. This performance is illustrated in detail in Figure 9-18. Although the initial scavenging performance was good, it showed a decline over time due to the reduction in the pH of the solution, which reached 8.5. At this point, we boosted the pH of the remaining solution to 10.0 and kept monitoring the scavenging performance. The oxygen scavenging performance improved significantly and the solution reached 10 ppb of oxygen concentration within approximately 40 min, as shown in Figure 9-18. The generated results confirm the positive effect

of formic acid on the scavenging process, in combination with the erythorbic acid agent. Furthermore, they explain why the oxygen scavenging period for the D-MEG solution was shorter than that in the F-MEG tests. In addition, they explain why the period of magnetized tests was longer than that of non-magnetized tests for D-MEG. Although the magnetic treatment could boost the alkalinity level in the solution, as reported in different publications, free radicals could enhance the reaction between formic acid and hydroxyl ions in magnetized D-MEG solutions, leading to a decline in pH and reduction in oxygen removal performance.

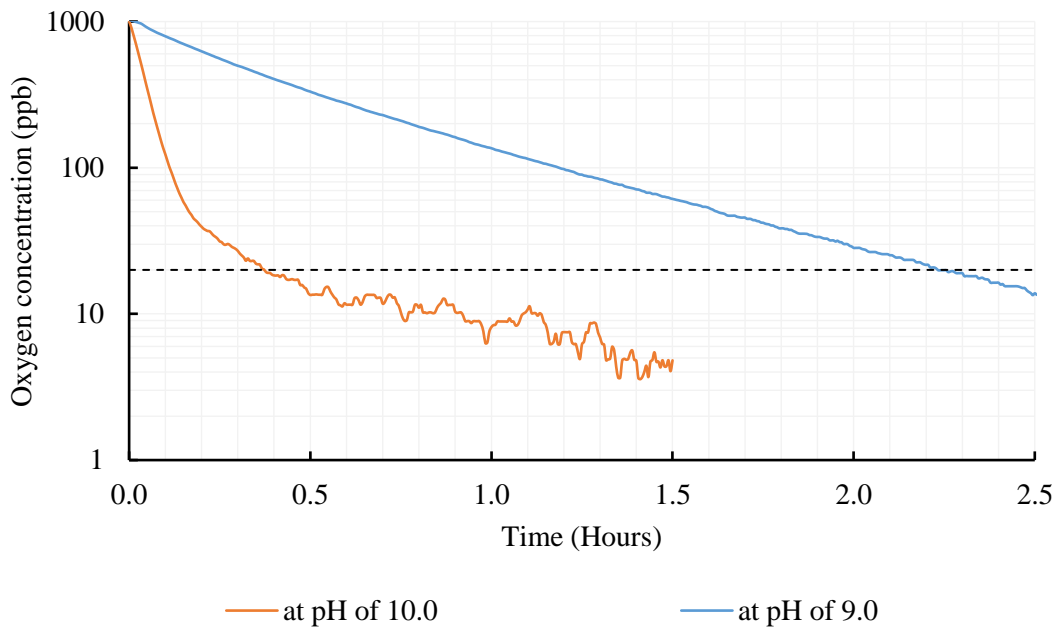


Figure 9-17 Performance of formic acid as oxygen scavenger in F-MEG solutions at pH of 9.0 and 10.0

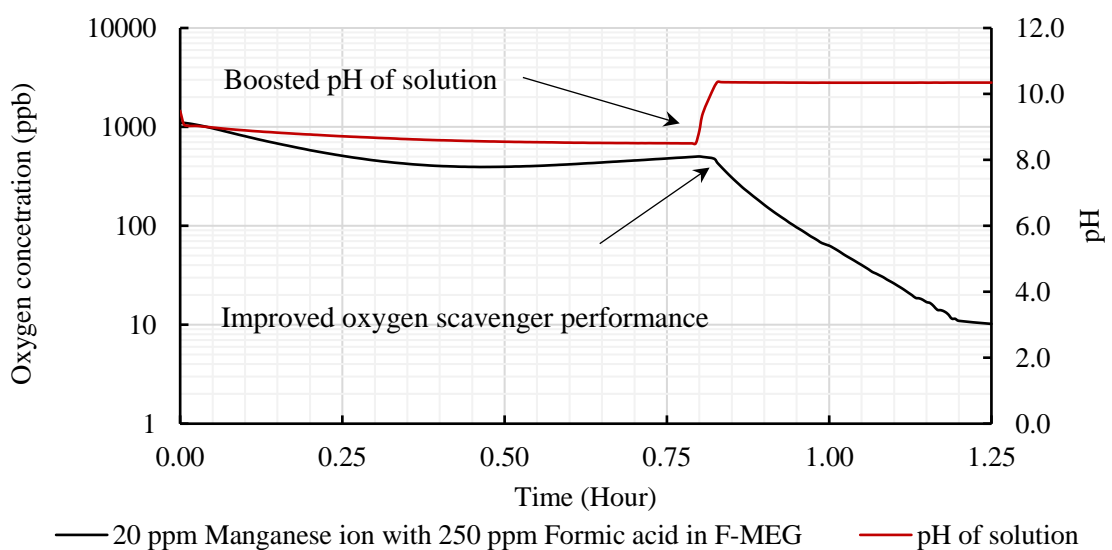


Figure 9-18 Effect of pH level on the scavenging performance of formic acid in F-MEG solution

9.4 Conclusions

The erythorbic acid oxygen scavenger performance was evaluated for different salt contents of 85 vol. % F-MEG and D-MEG solutions, with and without the magnetic memory effect. The magnetic memory effect improved the scavenging performance of erythorbic acid in F-MEG solutions, whereas non-magnetized D-MEG solutions performed better than magnetized solutions. These contrary results are due to the magnetic memory effect, which advanced the forward reaction of the free radical pair to form hydrogen molecules that scavenge oxygen from the F-MEG solution; the presence of degradation products formed during thermal oxidation of MEG solutions, such as formic acid, promoted the erythorbic acid performance to remove the oxygen molecules rapidly. On the other hand, the presence of formic acid in magnetized D-MEG solutions slowed the performance compared with that in non-magnetized D-MEG solutions, due to the interaction of formic acid with hydroxyl groups under alkaline conditions, which led to a rapid reduction in the pH of the solutions. Contrary results were obtained for magnetized HD-MEG due to the presence of iron ions and the more stable alkaline environment. The spin chemistry mechanism was adopted to explain how the magnetic memory effect can change the kinetics and yields of the recombination interactions of oxygen molecules and free radicals of erythorbic acid in MEG solutions. Finally, it is important to acknowledge that in the worst thermal oxidation environments of MEG hydrates, degradation products such as formic acid can act as additional oxygen scavengers if a proper metal catalyst is present at stable alkaline conditions.

Chapter 10 Measurement of the Mono Ethylene Glycol Volume Fraction at Varying Ionic Strengths and Temperatures

10.1 Introduction

MEG concentration is an essential criterion during the industrial regeneration of MEG, required to evaluate the efficiency of the regeneration process and to control the concentration of MEG reinjected at the wellhead. Although many laboratory methods to determine MEG concentration exist, their application can be costly in terms of the time required to perform sampling and laboratory analysis. For this reason, an alternative method for the determination of MEG concentrations has been proposed. This method can be performed on-site utilizing physical properties that can be readily measured using portable measurement devices such as the refractive index (n_D), Electrical Conductivity (EC) and Total Dissolved Salts (TDS). The volume fraction (F_{vm}), n_D , EC, and TDS of MEG solutions were measured at 10, 25, and 50°C in 10–100 vol. % (MEG) and with ionic strengths of 0, 0.125, 0.25, 0.5, and 1.0 M NaCl solutions.

10.2 Experimental Equipment and Chemicals

10.2.1 Equipment

To measure the physical properties of MEG solutions at varying temperatures and salinity levels, three hand-held laboratory devices were acquired from the ATAGO Company. The ATAGO PAL-BX/RI instrument was utilized to measure the refractive index of test solutions and the PAL-EC instrument was used to measure EC and TDS at lower ionic strengths. Due to the measurement limitations of the PAL-EC device at high ionic strengths, the *EC* at high ionic strength was measured using a GMH 5450 instrument. TDS was calculated at a high ionic strength according to the relationship between TDS and EC (refer to Table 10-1). Both electrical conductivity devices were calibrated with a standard aqueous KCl solution having a conductivity of 50.0 mS/cm (± 0.5 mS/cm) at a temperature of 25°C.

The PAL-91S device was employed to measure the volume fraction of MEG (F_{vm}). The measured volume fraction of MEG represents an un-calibrated value that deviated significantly if any dissolved salts were present. The PAL-91S device was designed to measure the volume fraction of MEG without taking into account the effect of dissolved salts or other impurities. In other words, this device was intended to measure the volume fraction of MEG solution under ideal conditions where zero salts were present. Two boundaries must be taken into the account when testing MEG samples with ATAGO devices. Firstly, when measuring any sample the maximum temperature cannot exceed 75°C due to instrument operating condition limits. Secondly, the PAL-91S was intended to measure a maximum MEG volume fraction of 90%. The

temperature of the test solutions was measured by using a built-in temperature sensor in each device with an accuracy of $\pm 0.1^\circ\text{C}$. The operating temperature parameter was adjusted in each test by using a Haake A28 cooling and heating water bath from Thermo Scientific with an accuracy $\pm 0.1^\circ\text{C}$.

Table 10-1 Specifications of measurement devices

Device	Type of Measurement	Range	Accuracy
PAL-BX/RI	Refractive Index, n_D	1.3306 – 1.5284	± 0.0003
GMH 5450	Electrical Conductivity, EC	0 – 1000 mS/cm	± 0.001
PAL-91S	Ethylene Glycol vol. %	0 – 90%	± 0.004
PAL-EC	TDS	0 – 9950 ppm	± 0.4
	Electrical Conductivity, EC	0 – 19.9 mS/cm	

10.2.2 Chemicals

The MEG solution and sodium chloride used within this study were sourced from Chem-Supply, with a purity of 99.8 wt. % and 99.5 wt. %, respectively. Before being utilized, the sodium chloride was dried within an oven for 24 hours at 102°C to remove excess water to ensure a constant and accurate weight. To produce the MEG solutions, deionized water with an electrical resistivity of $18.2 \text{ M}\Omega\cdot\text{cm}$ was used for all experiments.

10.3 Experimental Methodology

10.3.1 Experimental Procedure:

All solutions were prepared by volume, using an analytical micropipette supplied by Thermo Fisher with a measurement accuracy of $\pm 0.001 \text{ ml}$, using the procedure outlined in Section 10.3.2. The resultant solutions were stored in sealed plastic vials and subsequently mechanically shaken for two hours to produce completely homogenous solutions. Prior to taking measurements, the samples were maintained at the required temperatures within a controlled water bath. Once a stable temperature was reached, the solutions were analyzed by the devices listed in Table 10-1 to determine the solutions' n_D , EC , TDS and volume fraction at the adjusted temperature. All measurements were repeated three times to achieve good repeatability and accuracy of the readings.

10.3.2 Preparation of Sample Solutions

In order to prepare the solutions analyzed for this study, two initial stock solutions of 100 vol. % MEG and 100 vol. % distilled water were prepared with 1 M salt concentration (NaCl, 58.44 gm in 1.0 liter of total volume solution). Thus, ionic strength will be a measure of all ions in solution (i.e., NaCl equivalents). Known volumes of each stock solution were then mixed to prepare ten samples with volume fractions ranging from 10 to 100 vol. % in increments of 10 to obtain

samples of known salt and MEG content. To produce samples of lesser salt molarity, the same procedure was repeated using fresh MEG and water stock solutions prepared with the new molarity. Table 10-2 outlines the solutions of varying ionic strengths and volume fractions of MEG that were tested by the listed devices below.

Table 10-2 Summary of experimental solutions

IS, M	F _{vi} , Vol. %	Temperature	Independent Parameters
1.0	10 to 100 in increments of 10	10, 25, and 50°C	Refractive Index Electrical Conductivity TDS F _{vm} by PAL-91S
0.5			
0.25			
0.125			
0			

10.4 Results and Discussions

To ensure the accuracy of the testing procedure, an initial test was conducted using the refractive index measurement device listed in Table 10-1. The refractive index of varying concentration MEG solutions at 25°C along with their respective literature values are presented in Figure 10-1. The refractive index of MEG solutions measured within this study were found to be in good agreement with the literature data reported by Fogg, Hixson [302] measured in weight fraction and Chu and Thompson [377], of which was converted to volume fraction to facilitate the comparison as shown in Figure 10-1. The reported experimental data represents the average of 3-5 measurements with error bars indicated the standard deviation of the repeated measurements.

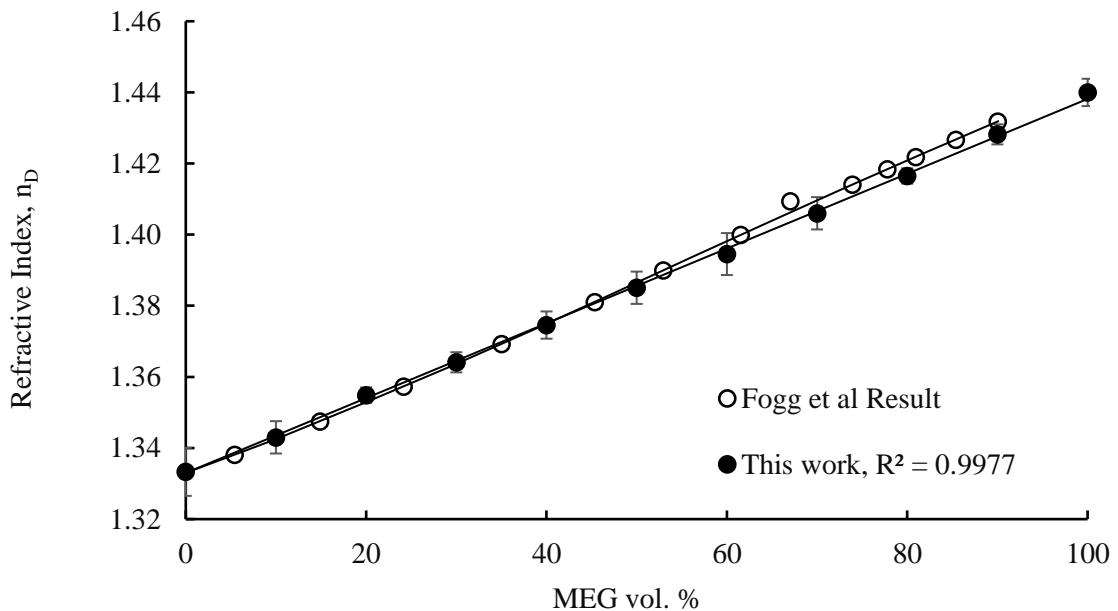


Figure 10-1 Refractive index (n_D) for this work and Fogg et al. (1955) as a function of MEG volume fraction at 25°C

10.4.1 Application and Testing of the Experimental Data

The electrical conductivity and refractive index of the prepared solutions were measured at varying ionic strengths and initial MEG volume fractions and are present by Figure 10-2, Figure 10-3 and Figure 10-4 respectively. The measurements were conducted to monitor the NaCl solubility behavior during the preparation of the sample solutions. When NaCl was present, a clear increase in electrical conductivity was observed with increasing NaCl content. Conversely, a decrease in electrical conductivity was measured with increasing MEG volume fraction at constant molarity, refer to Figure 10-2. These experimental results are in line with the findings of Sandengen and Kaasa [292] who reported similar responses.

Furthermore, with increasing MEG volume fraction and NaCl molarity, an increase in the solutions refractive index was measured as per Figure 10-3, which is in line with the reporting of Zhou, Li [378]. It was noted that the influence of salinity on the refractive index readings was more pronounced at high salinity readings (0.25 to 1 M, Figure 10-2) compared to low levels of salinity (0 to 0.25 M, Figure 10-4). Therefore, using the refractive index solely as a measure of MEG volume fraction will provide inaccurate results when the concentration of mineral ions is high within the solution. Consequently, to accurately predict the volume fraction of MEG in the presence of mineral ions, a combination of the refractive index and a measure of the salt content such as electrical conductivity or total dissolved solids is required.

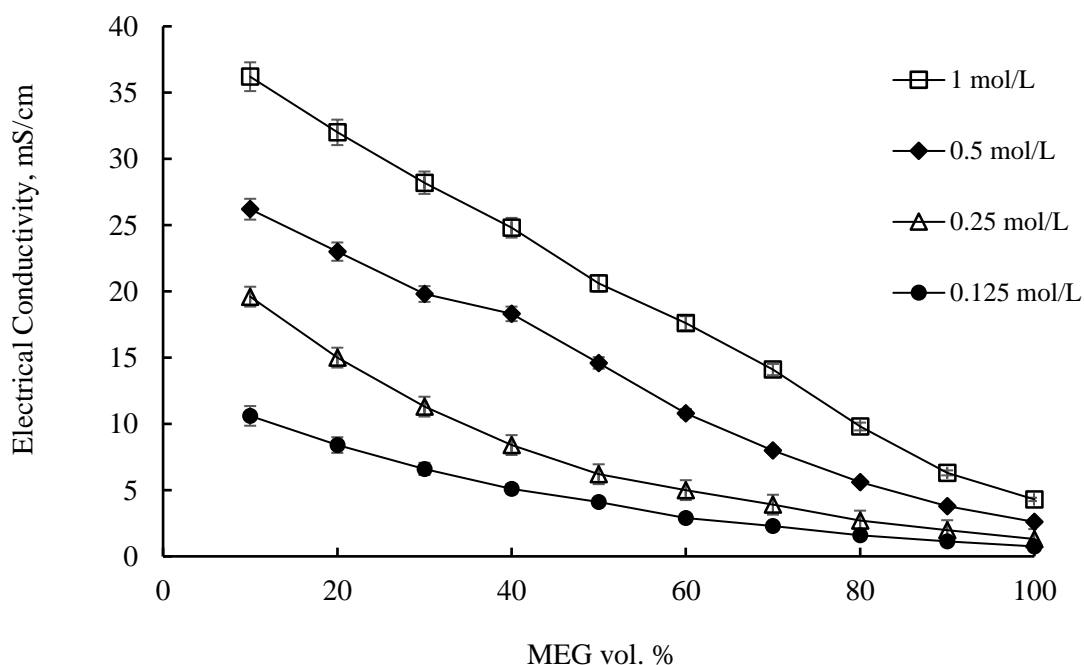


Figure 10-2 Electrical conductivity (*EC*) at a temperature of 25°C as a function of MEG volume fraction and NaCl

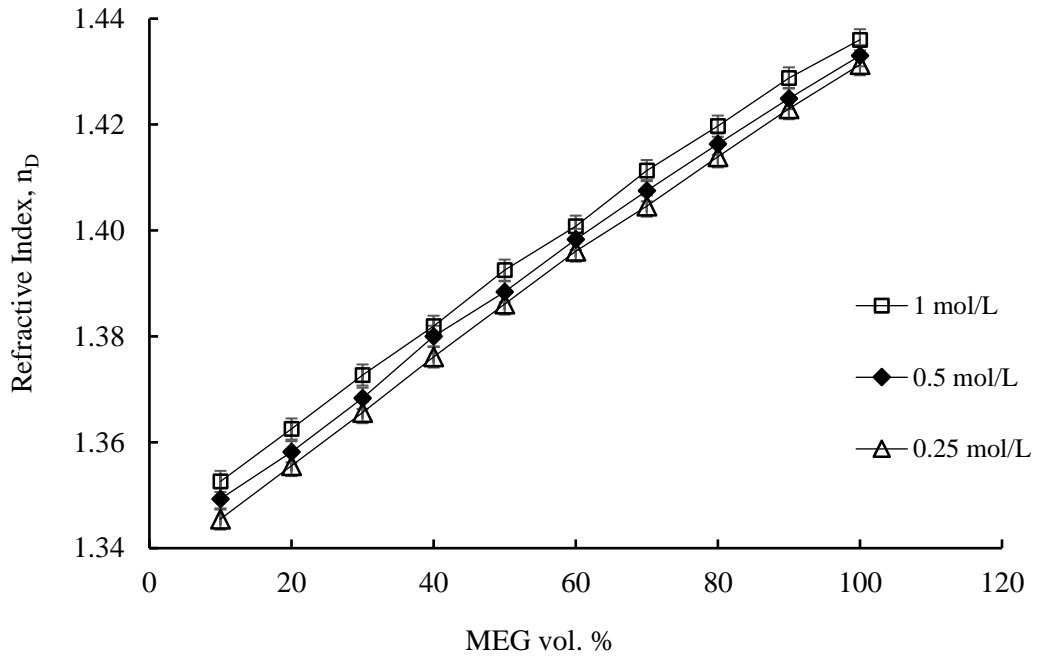


Figure 10-3 Refractive index (n_D) as a function of MEG volume fraction and ionic strength at 25°C

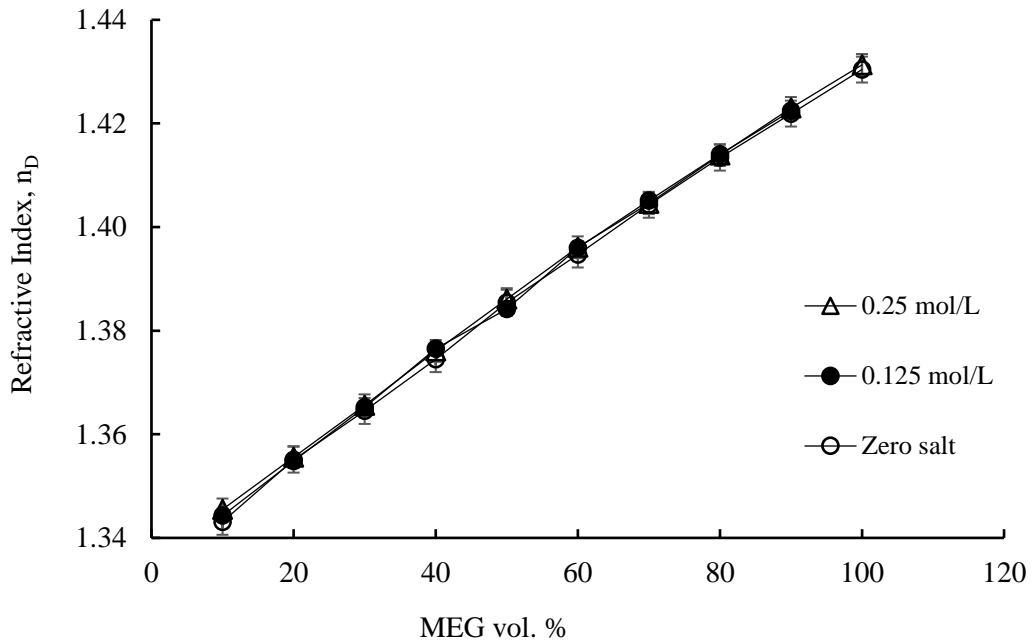


Figure 10-4 Refractive index (n_D) as a function of MEG volume fraction and ionic strength at 25°C

10.4.2 Effect of Ionic Strength on the MEG Volume Fraction Measurements

The primary results of this study outlining the effect of ionic strength upon the refractive index (n_D), EC and TDS of varying volume fraction MEG solution are presented within Table 10-10

for ionic strengths of 1, 0.5, 0.25, and 0.125 M of NaCl respectively. NaCl was chosen as the basis of ionic strength as the majority of mineral salt experienced within industrial MEG regeneration occurs as NaCl. The values reported with respect to refractive index, EC and TDS represent the values measured by the measuring devices listed in Table 10-1 and were subsequently used to calculate the corrected volume fraction MEG, F_{vc} . Furthermore, the volume fraction of MEG, F_{vm} measured by the PAL-91S device is reported. Definitions of the respective parameters used within each model are outlined by Table 10-3.

Table 10-3 Mathematical model nomenclature

Symbol	Definition
F_{vi}	Initial prepared volume fraction of MEG
F_{vm}	Measured volume fraction using PAL-91S without correction
F_{vc}	Calculated volume fraction of MEG as a function of salt content
IS_e	Calculated ionic strength as a function of n_D and EC.
EC_e	Calculated electrical conductivity as a function of TDS.

Figure 10-5 and Figure 10-6 show the response of refractive index and the MEG volume fraction measured by using portable devices versus initial prepared volume fraction (F_{vi}) for solutions at zero and one molar of NaCl. The plots demonstrate that the presence of ionic species such as NaCl can deviate the volume fraction of MEG solution measurements. The results were obtained by measuring the refractive indexes and volume fraction of MEG (F_{vm}) using the PAL-RI/Brix and PAL-91S devices respectively. The error bars associated with the measurements have been included indicating one standard deviation of the one molar measurements away from the respective zero molar measurements. It can be clearly recognized that the dissolved NaCl at one molar concentration has influenced the measurements of the refractive index in comparison to the zero molar test solution. This result means that the dissolved salt has effectively increased the reading of the refractive index and subsequently the volume fraction of MEG reported by the measuring devices.

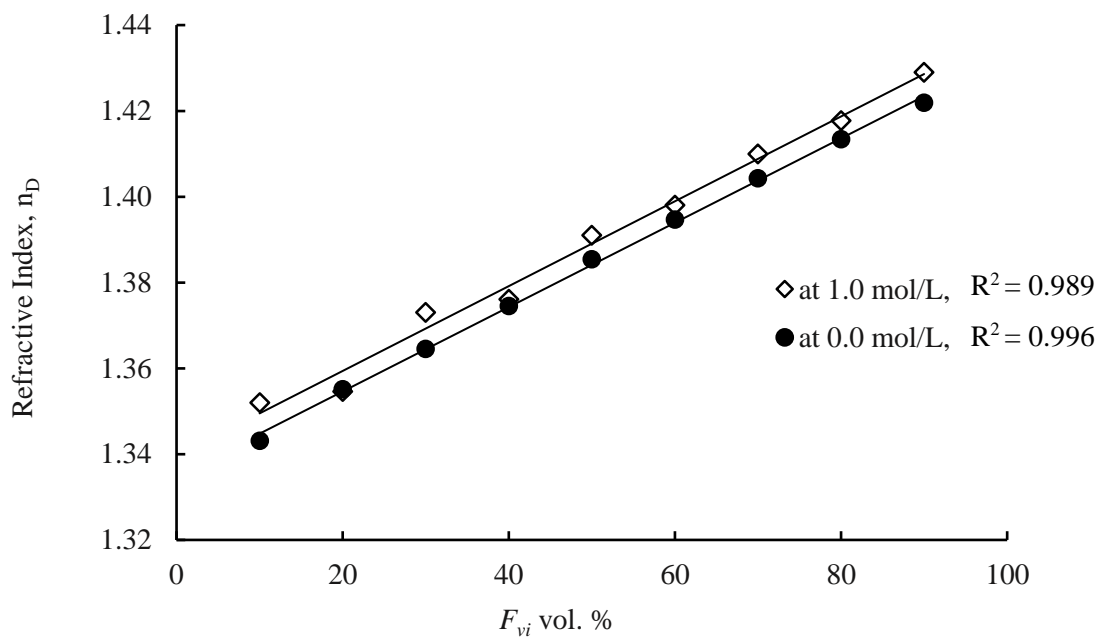


Figure 10-5 Effect of ionic strength on the refractive index measurements at 25°C

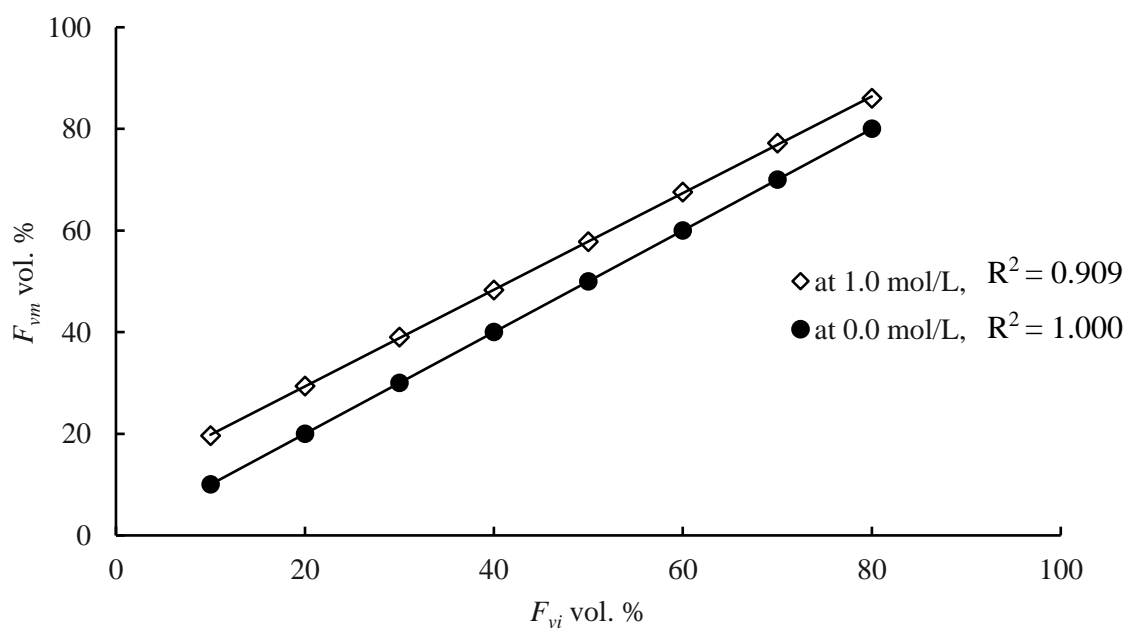


Figure 10-6 Effect of ionic strength on MEG volume fraction measurement at 25°C

10.4.3 Correlation Analysis of Experimental Variables Using SPSS Statistics

The polynomial model [379] described by Equation 10-1 was used to calculate the MEG volume fraction (dependent variable) by associating the field-readable variables (independent variables), such as refractive index, electrical conductivity, and uncorrected MEG volume fraction at different ionic concentrations. In addition, the same model was used to estimate the ionic strength

of these solutions mathematically from values of MEG volume measured by the PAL-91S device and electrical conductivity.

$$Y = A_0 + A_1 * x + A_2 * y + A_3 * x^2 + A_4 * x * y + A_5 + y^2 + A_6 * y * x^2 + A_7 * x * y^2 + A_8 * y^3 + A_9 * x^3 \quad 10-1$$

Where Y denotes to the estimated MEG volume fraction or ionic strength, while x and y are denoted to independent values. A_0 to A_9 are model coefficient parameters.

By using a bivariate analysis tool [182, 380], variables that have a mathematical correlation can be identified by determining the Pearson factor. The closer the Pearson factor is to 1.0, the more variables are affected by each other, and vice versa. The Pearson factor values are tabulated in Table 10-4, showing that the temperature parameter has a Pearson factor that is equal to approximately 0, and can, therefore, be neglected.

Table 10-4 Relationships between experimental variables by using SPSS statistics

Variable		Pearson Correlation					
		F_{vc}	n_D	T	EC	TDS	IS
Dependent	F_{vc}	1	0.991	0	-0.470	-0.058	0
	IS	0	0.085	0.001	0.501	0.501	1
Independent	n_D	0.991	1	-0.025	-0.365	0.025	0.085
	T	0	-0.025	1	0.037	-0.102	0.001
	EC	-0.470	-0.365	0.037	1	0.557	0.501
	TDS	-0.058	0.025	-0.102	0.557	1.000	0.501

10.4.4 Corrected Volume Fraction of MEG as a Function of Refractive Index, Electrical Conductivity, and TDS

To evaluate the effects of dissolved mineral salt ions upon the refractive index and hence measured volume fraction, the electrical conductivity of the test solutions was measured and incorporated into the proposed model. Electrical conductivity provides a measure of the total amount of ionic species (NaCl) within the solution and is easily measured using portable devices which are readily accessible in industry or through inline measurement systems. The electrical conductivity of varying volume fraction MEG solutions at different NaCl concentrations are outlined within Table 10-10 and Figure 10-2 showing an increase in electrical conductivity occurring with higher NaCl concentrations. The proposed model outlined by Equation 10-2, corrects for the effect associated with the dissolved mineral salt ions when calculating the volume fraction of MEG from the measured refractive index. Comparison of initially prepared MEG fractions and those calculated by application of Equation 10-2 are presented in Table 10-10.

$$F_{vc} = A_0 + A_1 * n_D + A_2 * EC + A_3 * n_D^2 + A_4 * n_D * EC + A_5 * EC^2 + A_6 * EC * n_D^2 + A_7 * n_D * EC^2 + A_8 * EC^3 + A_9 * n_D^3 \quad 10-2$$

Where, F_{vc} denotes the corrected MEG volume fraction with the model coefficient parameters given in Table 10-5. For solutions containing no ionic species, Equation 10-3 provides a more accurate estimation of the corrected volume fraction (F_{vc}) with respect to refractive index.

$$F_{vc} = 343.352 - 826.909 * n_D + 320.749 * n_D^3 \quad 10-3$$

Table 10-5 Values of parameters of equation 10-2

No.	Constants	Parameter Estimate
1	A ₀	24449.441
2	A ₁	-54357.031
3	A ₂	26.521
4	A ₃	39615.692
5	A ₄	-35.637
6	A ₅	0.089
7	A ₆	11.693
8	A ₇	-0.064
9	A ₈	-1.834E-05
10	A ₉	-9449.331

To evaluate the accuracy of the proposed model (Equation 10-2), the F_{vc} was calculated for varying MEG-water volume fraction solutions at ionic strengths ranging from 0.125 to 1.0 M and compared to the initial prepared MEG concentrations. Comparison was made by calculating the residual error ($F_{vc} - F_{vi}$), with the residual with respect to initial MEG concentration plotted in Figure 10-7 for ionic strengths of 0.125, 0.25, 0.5 and 1.0 M respectively. The negative and positive values are showing the deviation of the equation accuracy from the target values. The calculated volume fractions were found to be in close agreement with the corresponding initially prepared volume fractions with the residual error found to be typically less than 2.0 vol. % of MEG with an average measurement error of 1.77% by volume. Furthermore, the calculated volume fraction for solutions, containing no dissolved salts estimated through Equation 10-3 is illustrated graphically in Figure 10-8.

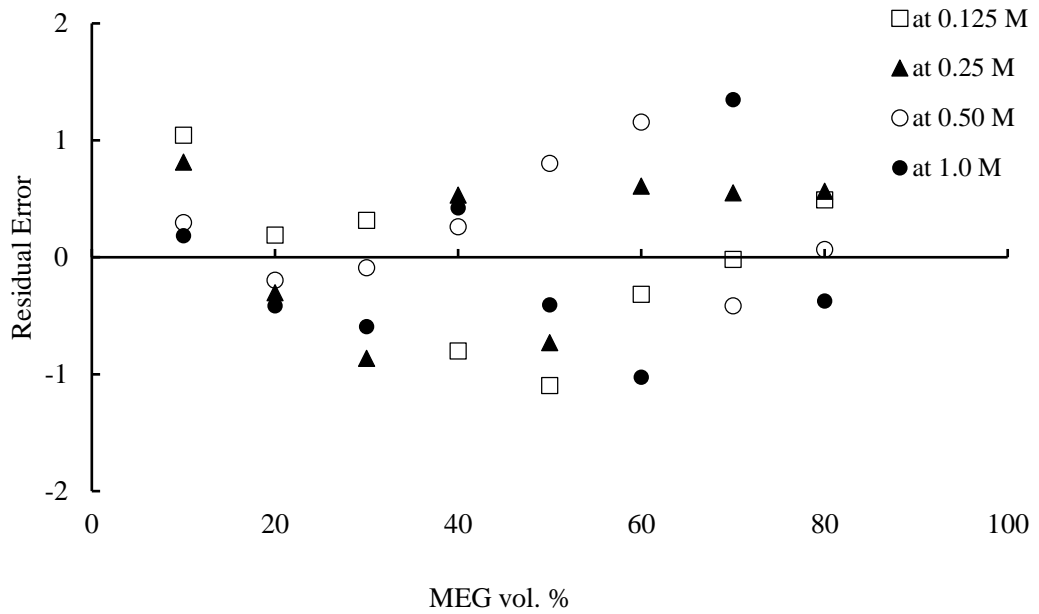


Figure 10-7 MEG volume fraction residual error between actual and calculated values

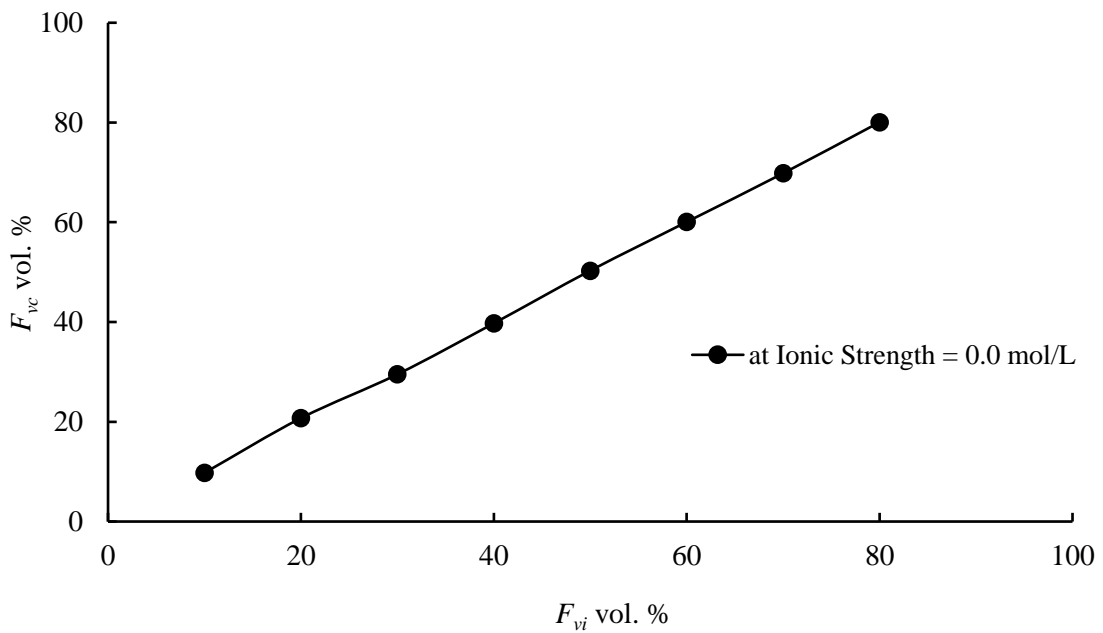


Figure 10-8 Estimated volume fraction of MEG solutions at no salt content, $R^2 = 1.0$

Alternatively, the corrected volume fraction of MEG may also be calculated using a measure of the TDS within solution where electrical conductivity cannot otherwise be measured. The TDS of a solution can be measured using commercially available hand-held measurement devices in a similar manner to electrical conductivity or using laboratory equipment. The corrected volume fraction of MEG can thus be estimated using the proposed model outlined by Equation 10-2 by first convert TDS to EC. To allow application of TDS measurements in place of EC, an empirical relationship was generated to convert the TDS measurements to the equivalent EC (Equation 10-4). The F_{vc} of varying volume fraction solutions was calculated with respect to the measured

TDS and is outlined within Table 10-10. Application of Equation 10-2 using TDS parameter as measurements of EC produced similar accuracy as that obtained by Equation 10-2 when using measured EC, demonstrating that the EC and TDS can be used interchangeable [381] when estimating the corrected volume fraction of MEG.

$$EC = \frac{TDS - 0.004694}{500} \quad 10-4$$

10.4.5 Correct Volume Fraction of MEG as a Function of Measured Volume Fraction, and Electrical Conductivity

Furthermore, if the MEG volume fraction of the solution can be readily measured using a portable device similar to that of PAL-91S used within this study, the following model. The model described by Equation 10-5, utilizes the measured volume MEG fraction reported by the PAL-91S or alternative device representing the MEG volume fraction without taking into account the effects of dissolved salts within the mixture. However, it should be noted that the PAL-91S device used within this study to produce MEG volume fraction measurements is only capable of doing so up to volumetric measurements up to 90%. The volume fraction of MEG measured by the portable device can then be corrected using the proposed model using electrical conductivity as a measure of dissolved salt content. The model covers a wide ranges of ionic strengths from 0.0 to 1.0 M. Figure 10-9 illustrates the application of the model and the resulting residual error at all NaCl molarities with the calculated values for all molarities summarized in Table 10-10. The average measurement error with corresponding of initially prepared volume fractions was found equal to 1.34% by volume.

$$F_{vc} = A_0 + A_1 * F_{vm} + A_2 * EC + A_3 * F_{vm}^2 + A_4 * F_{vm} * EC + A_5 * EC^2 + A_6 * EC * F_{vm}^2 + A_7 * F_{vm} * EC^2 + A_8 * EC^3 + A_9 * F_{vm}^3 \quad 10-5$$

Table 10-6 Values of parameters of equation 10-5

No.	Constants	Parameter Estimate
1	A ₀	0.833
2	A ₁	0.910
3	A ₂	-0.177
4	A ₃	0.002
5	A ₄	0
6	A ₅	0.002
7	A ₆	-1.541E-5
8	A ₇	0
9	A ₈	1.147E-7
10	A ₉	-1.730E-5

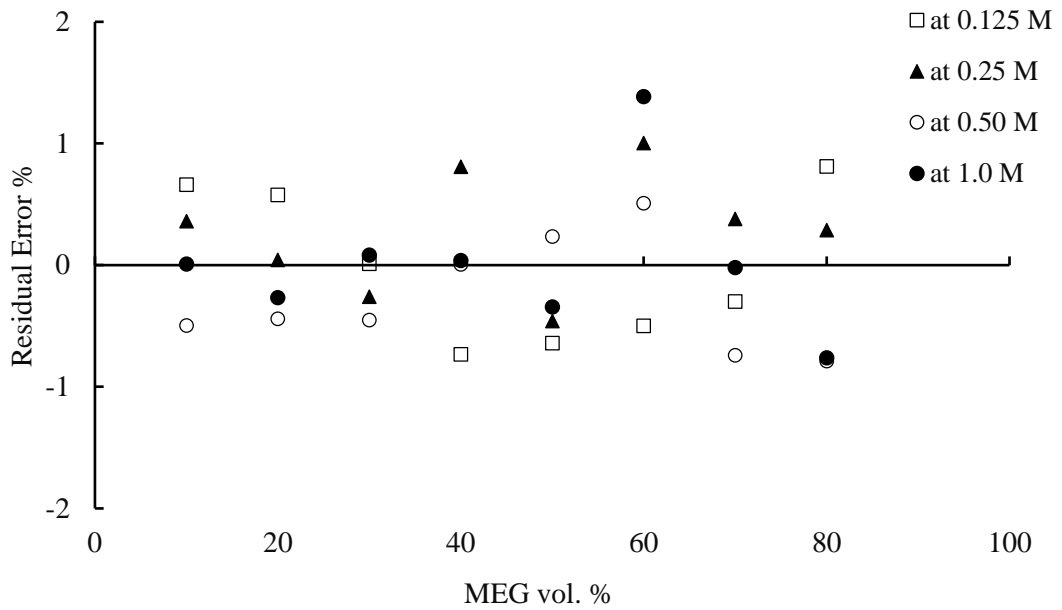


Figure 10-9 Residual error between the estimated and actual volume fraction of MEG solutions at ionic strength using measured volume fraction

10.4.6 Solution Ionic Strength as a Function of Measured MEG Volume Fraction and Electrical Conductivity

Unlike electrical conductivity or TDS, the ionic strength of a solution must be calculated or estimated via analytical means. The ionic strength of MEG solution can be accurately predicted using laboratory analytical techniques including Inductively Coupled Plasma Mass Spectrometry (ICP-MS) however such analysis may take time to be performed [49, 148, 382]. Alternatively, the electrical conductivity of the solution can be used as an essential parameter combined with the uncorrected measurements of MEG solution to predict the ionic strength using the model defined by Equation 10-6. Equation 10-6 represents a quick method for estimating the ionic strength of a MEG solution within the ionic strength range of 0.125 to 1.0 M without the need for time-consuming laboratory analysis. The resultant residual error is presented in Figure 10-10 with the average error produced by Equation 6 being 6.6%.

$$IS_e = A_0 + A_1 * F_{vm} + A_2 * EC + A_3 * F_{vm}^2 + A_4 * F_{vm} * EC + A_5 * EC^2 + A_6 * EC * F_{vm}^2 + A_7 * F_{vm} * EC^2 + A_8 * EC^3 + A_9 * F_{vm}^3 \quad 10-6$$

Table 10-7 Values of parameters of equation 10-6

No.	Constants	Parameter Estimate
1	A ₀	0.233
2	A ₁	0.003
3	A ₂	-0.043
4	A ₃	0
5	A ₄	0.001
6	A ₅	0.003
7	A ₆	6.377E-06
8	A ₇	-1.138E-05
9	A ₈	-2.780E-05
10	A ₉	1.833E-06

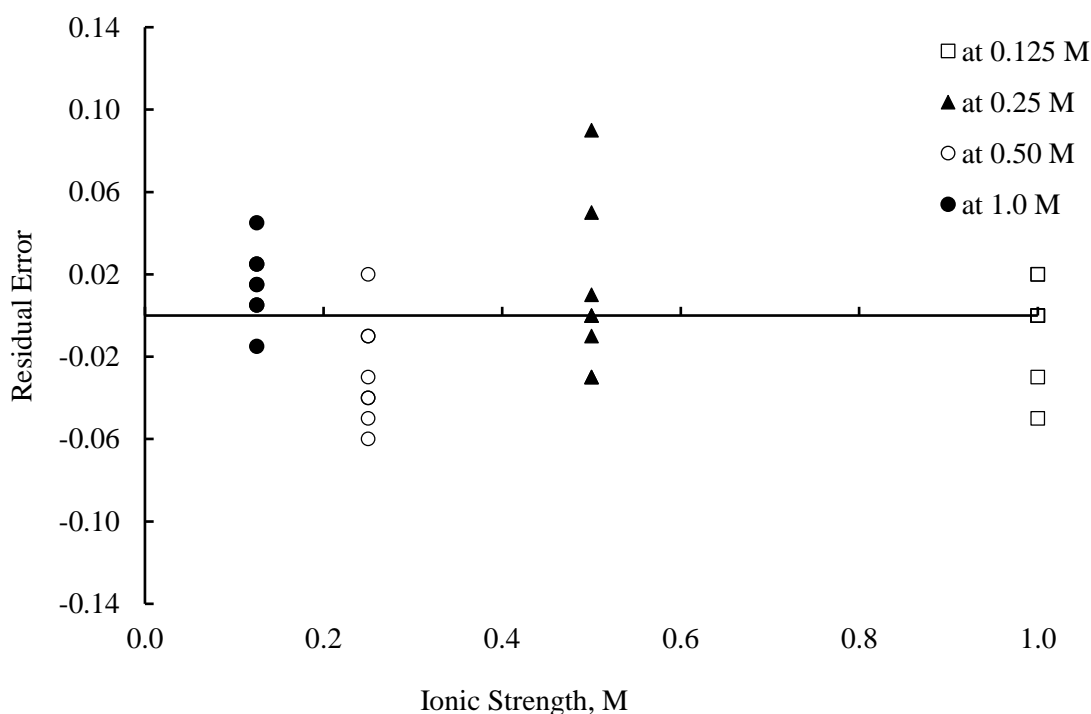


Figure 10-10 Ionic strength residual error between actual and estimated values of MEG volume fraction ranging from 10 to 80%.

10.5 Validation of Proposed Models

To test the proposed models, a set of solutions was prepared with different MEG concentrations at different ionic strengths. The solutions were then analyzed in several ways to determine the volume fraction of MEG. The first method utilized was to completely evaporate the water from the salt containing MEG and the remaining MEG volume measured and compared to the known mass of water evaporated. This method was performed using a convection furnace at 90°C for two days. Secondly, Gas Chromatography (GC) was utilized to accurately determine the concentration of MEG within each solution.

Finally, the parameters of refractive index, electrical conductivity, and uncorrected volume fraction of MEG were measured by the measurement devices listed in Table 10-8. Table 10-8 represents the concentration values of the prepared solutions, while Table 10-9 describes the values derived from the respective laboratory tests and the proposed models. Comparison of corrected MEG concentrations compared to the concentrations determined by alternative analytical means showed good agreement. Therefore, the adoption of these models may provide a means of quickly and accurately determining the concentration of MEG solutions in the field.

Table 10-8 Test sample solutions for models validation

MEG vol. %	n_D	EC, mS/cm	PAL91S Measurements	IS, M
80%	1.4177	8.3	86.0%	0.6850
60%	1.3980	11.3	64.2%	0.5138
40%	1.3761	11.5	42.6%	0.3425
20%	1.3546	11.7	21.6%	0.1712

Table 10-9 Validation of proposed models

Sample	Boiling Methods	GC Methods	F_{vc} Equation 10-2	F_{vc} Equation 10-5	IS_e Equation 10-6
80%	79.75%	80.20%	80.80%	80.39%	0.70 M
60%	60.10%	60.15%	60.25%	60.46%	0.51 M
40%	39.20%	39.21%	39.23%	39.80%	0.30 M
20%	19.21%	19.25%	19.37%	19.37%	0.17 M

10.6 Conclusions

The presence of dissolved mineral ions within industrial MEG regeneration systems presents a major limitation to generate quick and accurate measurements of MEG volume fraction within the field. The purpose of this study was to generate models capable of accurately calculating the volume fraction of MEG when mineral salts are present using portable measuring devices that are easily accessible within the field allowing quick measurements to be made without extensive laboratory analysis (see Figure 10-11). The proposed models utilize a combination of refractive index (n_D) alongside either Electrical Conductivity (EC), Total Dissolved Solids (TDS), Ionic Strength (IS) or uncorrected volume fraction measurements (F_{vm}) to incorporate the effects of dissolved salts. Experimental measurements of n_D and EC, TDS and F_{vm} have been performed in varying volume fraction of MEG + water solutions in the presence of NaCl, the most common mineral salt experienced during industrial MEG regeneration.

Through bivariate analysis, it was possible to demonstrate that temperature has no significant effect on the laboratory-read parameters. This is due to the fact that the laboratory devices used in this study are temperature compensating. Thus, the effect of temperature is eliminated during the generation of these mathematical models and the use of temperature compensated

measurement devices. The developed models allow the accurate prediction of the corrected volumetric fractions of MEG (F_{vc}), by using the measured refractive index and either EC, TDS or IS to correct the effects of NaCl at molarities ranging from 0.125 to 1.0 M. The proposed models were found to be most accurate when applied between volume fractions of 10-80 vol. % of brine/MEG solution with approximant average error of 1.7 vol. %. Furthermore, ionic strength could be measured within acceptable accuracy at salt concentrations, ranging from 0.125 to 1.0 M and with residual error of 0.078 M.



Figure 10-11 Digital Hand-held Devices from ATAGO company, LTD

10.7 Appendix

Table 10-10 Experimental values for refractive index (n_D), TDS, EC, uncorrected volume fraction, estimated values of MEG volume fraction and ionic strength for the MEG + NaCl + H₂O system

Dependent Variable		Independent Variable				Estimated Parameters by Equation Models			
IS	F_{vc}	n_D	TDS	EC	F_{vm}	F_{vc}		IS_e	EC_e
1.000	10.0	1.352	21172.50	42.345	19.600	11.043	10.661	1.02	42.345
1.000	20.0	1.362	16666.50	33.333	29.400	20.190	20.576	0.95	33.333
1.000	30.0	1.373	14533.50	29.067	39.000	30.316	30.012	0.97	29.067
1.000	40.0	1.382	12900.00	25.800	48.267	39.198	39.266	1.00	25.800
1.000	50.0	1.391	10900.00	21.800	57.800	48.902	49.360	1.00	21.800
1.000	60.0	1.401	9216.50	18.433	67.533	59.684	59.501	1.02	18.433
1.000	70.0	1.410	7416.50	14.833	77.200	69.981	69.700	1.00	14.833
1.000	80.0	1.419	5617.00	11.234	88.133	80.491	80.811	1.00	11.234
0.500	10.0	1.348	12966.50	25.933	15.200	10.814	10.362	0.50	25.933
0.500	20.0	1.358	11166.50	22.333	25.333	19.697	20.044	0.50	22.333
0.500	30.0	1.368	9733.50	19.467	35.133	29.136	29.739	0.51	19.467
0.500	40.0	1.380	8900.00	17.800	46.533	40.532	40.810	0.59	17.800
0.500	50.0	1.388	7283.50	14.567	54.667	49.270	49.540	0.55	14.567
0.500	60.0	1.398	5266.50	10.533	65.333	60.609	61.003	0.49	10.533
0.500	70.0	1.407	4016.50	8.033	74.467	70.551	70.379	0.47	8.033
0.500	80.0	1.416	2816.50	5.633	84.467	80.565	80.288	0.47	5.633
0.250	10.0	1.346	9666.65	19.333	12.933	10.296	9.504	0.27	19.333
0.250	20.0	1.356	7400.00	14.800	22.933	19.805	19.558	0.24	14.800
0.250	30.0	1.366	5550.00	11.100	32.533	29.910	29.547	0.22	11.100
0.250	40.0	1.376	4200.00	8.400	42.600	40.262	40.005	0.21	8.400
0.250	50.0	1.386	3100.00	6.200	52.467	50.804	50.234	0.19	6.200
0.250	60.0	1.396	2500.00	5.000	62.733	61.157	60.509	0.20	5.000
0.250	70.0	1.404	1950.00	3.900	71.600	69.586	69.260	0.21	3.900
0.250	80.0	1.414	1366.50	2.733	82.000	80.066	79.212	0.24	2.733
0.125	10.0	1.344	5300.00	10.600	11.867	10.184	10.009	0.11	10.600
0.125	20.0	1.354	4266.50	8.533	21.733	19.585	19.732	0.14	8.533
0.125	30.0	1.364	3350.00	6.700	32.000	29.406	30.082	0.15	6.700
0.125	40.0	1.375	2650.00	5.300	41.800	40.423	40.038	0.15	5.300
0.125	50.0	1.384	2166.50	4.333	51.333	49.594	49.657	0.14	4.333
0.125	60.0	1.393	1600.00	3.200	63.067	58.973	61.385	0.13	3.200
0.125	70.0	1.405	1133.50	2.267	71.800	71.349	69.981	0.13	2.267
0.125	80.0	1.413	811.50	1.623	81.600	79.625	79.238	0.17	1.623

Chapter 11 CONCLUSIONS AND RECOMMENDATIONS

11.1 CONCLUSIONS

11.1.1 Effect of Pretreatment on Scale Formation in the Reboiler Section of a Mono Ethylene Glycol Regeneration Plant

The results allow operators to evaluate the use of the reboiler unit under harsh conditions to prevent the worst-case scenario during field operations. The primary results obtained from these experiments show the high probability of scale precipitation from solutions with low divalent ion concentrations inside the capillary tubing and the reboiler bundle when using a pretreatment vessel in a MEG regeneration plant. Thus, the pretreatment vessel cannot be minimized without harming the MEG regeneration process because of the formation of scale deposits on the heater bundle, pipelines, filters, and equipment in the presence of low concentrations of divalent ions in the rich MEG stream.

From the results, the following conclusions can be made.

1. The primary scaling products identified in the rich MEG case were calcium carbonate in the form of calcite, vaterite, and dolomite.
2. For both cases 1 and 2, complete blockage of the capillary coil occurred during the DSL tests at a pretreatment pH of 7.24 at 1.0 and 2.0 mol. % CO₂ content, whereas semi-blockage occurred at 0.5 mol. % CO₂ content.
3. The formation of calcium carbonate scale primarily occurred inside the DSL capillary tube for divalent cation concentrations of 10 and 5 ppm at 5.0 mol. % CO₂ content without significant pressure build-up.
4. The DSL results were consistent with those measured in a MEG regeneration pilot plant.
5. The blocking of the capillary tubing was more likely for high initial CO₃²⁻ concentrations.
6. Operating under highly alkaline conditions with a high concentration of magnesium ions resulted in the precipitation of magnesium hydroxide, which precipitated in the inline filters and on hot surfaces.

11.1.2 Influence of Magnetic Fields on Calcium Carbonate Scaling in Aqueous Solutions at 150°C and 1 Bar

In this study, the use of MF treatment to reduce scale formation in sodium bicarbonate solutions of varying concentrations was investigated. The extent of scale formation was evaluated using a DSL system by measuring the increase in pressure drop across a capillary tube as scale was

formed. In contrast to similar studies used to evaluate the effects of magnetic exposure upon the behavior of ionic species, an appreciable effect on particle behavior, as shown by inhibited scale formation and electrical conductivity, was achieved by short exposure to a magnetic field. Many studies have used long-term exposure to MFs to evaluate its impact, but the results of this study have conclusively demonstrated that only short exposure (2.5 s) to a strong diametric MF can significantly affect particle behavior. Furthermore, earlier studies evaluating the use of magnetic treatment have used single or multiple rectangular magnets arranged around the fluid flow using either a class 1 or class 4 magnetic arrangement as shown in Figure 2-13. By comparison, the results of this study were generated using a class 4-A magnetic arrangement utilizing a ring-shaped magnet with fluid flow occurring through the center of the magnet Figure 5-4 making the results of this study unique.

From the results using the DSL system, three conclusions were drawn regarding the use of MF treatment to inhibit the formation of calcium carbonate scale in aqueous systems. First, the extent of scale formation, whether inhibited or promoted, is dependent upon the ratio of bicarbonate to calcium ions. From these tests, it is apparent that the amount of bicarbonate present has a key role in magnetic treatment for preventing scale formation in brine solutions. When bicarbonate was present in greater or equal concentration to that of calcium ions, appreciable inhibition of scale formation was achieved, suggesting that bicarbonate is more responsive to the effects of the applied MF compared to the cations. The inhibition of scale formation was attributed to the intermolecular separation of the calcium and bicarbonate ionic species arising from the induced Lorentz force as the solution flowed through the MF.

Following exposure to the MF, the separated ions within the solution had sufficient magnetic memory to ensure that the formation of scale was inhibited. However, because of the large concentration of calcium ions present during testing, the same behavior was not observed, possible because of the formation of clots within the capillary tube that led to interactions between the calcium and bicarbonates, thus forming scale deposits. Furthermore, it should be noted that the separation of charged particles achieved through magnetic exposure can only be maintained during laminar flow. The turbulent flow of the solution promotes the mixing of the separated charged particles, nullifying the effects of magnetic exposure.

Secondly, the exposure of brine solutions to the applied MF had a significant impact on the electrical conductivity. A considerable reduction in electrical conductivity of the high concentration bicarbonate and equal concentration solutions was observed during testing, and this was attributed to the influence of the MF on the structure of the ionic species. These results are consistent with previous results, which have shown that the hydration shell thickness of the bicarbonate and calcium ions are affected by MFs, leading to changes in the electrical conductivity of the solution. Furthermore, it was observed that the electrical conductivity

measured at the outlet of the DSL system steadily increased as scale formation proceeded. Therefore, it was concluded that the measurement of electrical conductivity may provide an indirect measure of the extent of scale formation with a pipeline.

Finally, because of the successful inhibition of scale formation via MF treatment, MF treatment may be an eco-friendly scale inhibition strategy that could replace the use of traditional chemical scale inhibitors. Furthermore, MF treatment for scale inhibition may provide a more cost-effective method to prevent the formation of scale because of the one-time cost of a magnetic treatment system being outweighed by the continued cost of chemical scale inhibitors. However, the applicability of MF treatment in large scale pipelines has yet to be fully evaluated.

11.1.3 The Influence of Magnetic Fields on Calcium Carbonate Scale Formation within Mono Ethylene Glycol Solutions under Regeneration Conditions

It was intended to use a high concentration of both calcium and carbonate ions in this study to make the deposition process inside the capillary faster so that we can observe the effects of magnetic fields on scale formation. Five conclusions have been made concerning the applications of MF treatment in inhibiting the scale formation of CaCO_3 in aqueous solutions at different MEG concentrations. Firstly, the degree of scale formation, whether inhibited or promoted, is conditional on MEG content. Secondly, exposure of the MEG and brine solutions to the applied MF had a significant impact on the measured EC. The results were consistent with previous studies of aqueous solutions where it was concluded that the solvation shell thickness of the Ca^{2+} and HCO_3^- ions were subject to manipulation by MFs leading to variations in EC [109, 169, 194]. Thirdly, following trials at 50 vol. % MEG concentration, bulky, and rough crystals were formed that may enhance a hypothesized clot-like build-up inside the transportation pipelines [109]. Similarly, jar tests highlighted the shift in crystallization processes that may occur at high MEG concentrations and high temperatures, although the jar test results could not explain the morphology of real crystals in pipelines they could clarify the kinetic parameters that control crystals formed under different conditions.

Fourthly, previous studies have suggested the external radius of ions to be the outer radius of hydration shells, not the actual ion radius in calculating the ionic activity coefficient [219, 220, 342]. This hypothesis has been reinforced after an improvement in the activity coefficient of ions occurring following exposure to MFs. Finally, due to the effective inhibition of scale formation produced by the external MF treatment within 50 % by volume of MEG, it can be proposed that MF treatment could provide an environmentally friendly scale inhibition approach that could replace/reduce the use of traditional chemical inhibitors in industry. In this regard, it is believed that research into the thermodynamic properties of an aqueous and non-aqueous solution in MFs is more promising.

11.1.4 Evaluation of Chemical Scale Inhibitor Performance under an External Magnetic Field using a Dynamic Scale Loop

The most important findings of this study are summarized as follows.

1. The effects of MF exposure on the MEG–brine solution continued even after the solution was subjected to high temperatures.
2. In the presence of a high concentration of MEG, the formation of inorganic deposits was faster after exposure to a MF than without exposure.
3. This acceleration in the scale formation rate caused by the applied MF negatively affected the performance of the chemical inhibitors used in this study, irrespective of their concentrations.
4. The measured EC values of the solutions exposed to the MF were lower than those of the unexposed solutions.
5. Irrespective of concentration, chemical scale inhibitors B (CSI-B) failed to inhibit scale formation. In contrast, CSI-A showed acceptable initial inhibitory performance, although it later failed when exposed to the MF.
6. Trials of CSI-B at high concentrations showed higher turbidity values than other experiments carried out in this study.
7. Exposure to the MF produced a stable phase of calcium carbonate (calcite) in the case of a high MEG concentration, even when CSIs were used.
8. In the presence of MEG, the ζ potential under the applied MF was lower than that without MF exposure.
9. The relationship between the thickness of the hydration shell and EC values agreed with previously reported results for MF exposure.

The findings presented above are significant in determining the effect of an applied MF on scale formation, irrespective of whether a CSI is used. The most significant finding is the apparent difference in the ζ potential values. Although the measured values were not large, the clear difference in these values before and after exposure to the MF highlight the ability of the MF to change the external charge on the surface of the molecules and, thus, change the thickness of the hydration shell surrounding the ions. Investigations into the ability of MFs to fundamentally affect scale formation are still in their early stages and require intensive studies. This study gives a reasonable assessment of the effects of the various treatments employed for preventing scale formation or scale removal.

11.1.5 Performance of Erythorbic Acid as an Oxygen Scavenger in Thermally Aged Lean MEG

Erythorbic acid as an oxygen scavenger has been extensively recognized for its good performance as a preservative within the food industry [260, 261, 263, 265, 364]. However, little to no investigation has been performed to assess its applicability for use in the oil and gas industry under practical conditions. The application of erythorbic acid in the oil and gas industry may provide an effective, non-sulfite product, non-hazardous alternative to commonly used oxygen scavengers, including sulfites, to prevent oxygen-based corrosion issues in transportation pipelines and subsea equipment. Therefore, bench-scale evaluation of erythorbic acid was done to assess its performance under conditions typically found within industrial MEG regeneration systems, including the effects of MEG thermal aging and the presence of common industrial contaminants, such as salts and organic acids.

Previous evaluation of erythorbic acid as an oxygen scavenger has been performed in fresh MEG [230], but this may not provide an accurate representation of real usage conditions. The performance of erythorbic acid was, thus, evaluated in thermally aged MEG (TAL-MEG) to confirm its suitability for use in TAL-MEG post-regeneration. The results showed a noticeable decrease in oxygen scavenger performance at pH 9.0. However, erythorbic acid was still capable of achieving the desired 20 ppb oxygen concentration within an acceptable time frame (under 4 h). As such, this study strongly suggests that erythorbic acid is suitable for use within TAL-MEG and applicable for use in industrial MEG regeneration systems.

However, at pH 6.0, erythorbic acid demonstrated poor oxygen removal performance, limiting its applicability at low pH value. The reduced performance at pH 6.0 was attributed to the inability to fully neutralize the erythorbic acid molecule to its conjugate base (erythorbate), a step necessary to initiate the oxygen scavenging mechanism. Conversely, good oxygen removal performance was demonstrated at pH 9.0 and 11.0, and the presence of the mineral salt ions typically found in MEG regeneration systems had no impact. Furthermore, it was found that the presence of organic acids (acetic) did not have a significant impact on the performance of the erythorbic acid oxygen scavenger. Overall, the pH of the test solution was found to be the primary factor in determining the performance of erythorbic acid as an oxygen scavenger.

11.1.6 The Performance of Erythorbic Acid Oxygen Scavenger within Salty Fresh and Degraded Mono Ethylene Glycol under Magnetic Memory Effect

The erythorbic acid oxygen scavenger performance was evaluated for different salt contents of 85 vol. % F-MEG and D-MEG solutions, with and without the magnetic memory effect. The magnetic memory effect improved the scavenging performance of erythorbic acid in F-MEG solutions, whereas non-magnetized D-MEG solutions performed better than magnetized

solutions. These contrary results are due to the magnetic memory effect, which advanced the forward reaction of the free radical pair to form hydrogen molecules that scavenge oxygen from the F-MEG solution; the presence of degradation products formed during thermal oxidation of MEG solutions, such as formic acid, promoted the erythorbic acid performance to remove the oxygen molecules rapidly. On the other hand, the presence of formic acid in magnetized D-MEG solutions slowed the performance compared with that in non-magnetized D-MEG solutions, due to the interaction of formic acid with hydroxyl groups under alkaline conditions, which led to a rapid reduction in the pH of the solutions. Contrary results were obtained for magnetized HD-MEG due to the presence of iron ions and the more stable alkaline environment. The spin chemistry mechanism was adopted to explain how the magnetic memory effect can change the kinetics and yields of the recombination interactions of oxygen molecules and free radicals of erythorbic acid in MEG solutions. Finally, it is important to acknowledge that in the worst thermal oxidation environments of MEG hydrates, degradation products such as formic acid can act as additional oxygen scavengers if a proper metal catalyst is present at stable alkaline conditions.

11.1.7 Measurement of Mono Ethylene Glycol Volume Fraction at Varying Ionic Strengths and Temperatures

The presence of dissolved mineral ions in industrial MEG regeneration systems prevents the rapid and accurate on-site assessment of the MEG volume fraction. The purpose of this study was to generate models capable of accurately calculating the volume fraction of MEG when mineral salts are present using portable measuring devices that are easily accessible in the field, allowing quick measurements to be made without extensive laboratory analysis. The proposed models utilize a combination of refractive index (n_D) alongside either EC, TDS, IS, or uncorrected volume fraction measurements (F_{vm}) to incorporate the effects of dissolved salts. Experimental measurements of n_D and EC, TDS, and F_{vm} have been performed in MEG + water solutions with varying MEG volume fractions in the presence of NaCl, the most common mineral salt encountered in industrial MEG regeneration.

Through bivariate analysis, it was possible to demonstrate that temperature has no significant effect on the laboratory-read parameters. This is because the laboratory devices used in this study are temperature compensating. Thus, the effect of temperature is eliminated during the generation of these mathematical models and the use of temperature compensated measurement devices. The developed models allow the accurate prediction of the corrected volumetric fractions of MEG (F_{vc}), by using the measured refractive index and either EC, TDS, or IS to correct for the effects of NaCl at molarities ranging from 0.125 to 1.0 M. The proposed models were found to be most accurate when applied between MEG volume fractions of 10–80 vol. % in the MEG–brine solution with an approximate average error of 1.7 vol. %. Furthermore, the ionic strength could

be measured within acceptable accuracy at salt concentrations, ranging from 0.125 to 1.0 M with a residual error of 0.078 M.

11.2 RECOMMENDATIONS

1. It is suggested that the application of magnetic fields with dynamic scale flow loop technology should be developed to include the use of an ion-selective electrode to monitor the reduction of calcium ions rate in line with monitoring the pressure drop within the capillary tube. This additional electrode would add more parameters to evaluate the effect of magnetic fields on the chemical activity of calcium ion in non-aqueous solutions.
2. The ion activity coefficient of calcium ions could be studied by measuring the ion hydration shell thickness at different magnetic fields' strengths and different magnetic polar and arrangements by using method Nuclear Magnetic Resonance (NMR), use of colligative properties and x-ray and neutron diffraction, X-ray spectroscopy, Raman spectroscopy, electro-osmosis, or gel exclusion chromatography.
3. It is suggested that the internal microstructure behaviour of particles with external magnetic fields should be studied by using Molecular Dynamic Simulation programs.
4. For the oil and natural gas industry, as the inorganic scale formation develops with increasing flow rate, the flow rate parameter should be taken into account to evaluate the scale formation growth in pipelines under magnetized conditions.
5. The behavior of scale formation under magnetic field treatments should be studied to include several non-aqueous solutions to provide different scale formation performance.
6. The modified DSL test showed promising potential. It is suggested that the DSL test should be developed to evaluate magnetized scale formation solutions at higher pressures and temperatures.
7. Due to different arrangements morphology of calcium carbonate generated at different thermodynamic conditions, the morphology of the calcium carbonate precipitation at different temperatures and different magnetic fields strength need to be further scrutinized.
8. The modified DSL test develops in this study could be applied to evaluate the inorganic deposition of other mineral ions substances such as strontium, magnesium, barium in non-aqueous systems.
9. The modified DSL test should be developed by using electrical magnetic field coils to generate different intensity and polarity during the scale formation test.

10. The effect of magnetic field treatments on the performance of other chemical scale inhibitors should be also be considered.
11. Developing an industrial type of magnetic field generator to be installed on the equipment or pipelines to develop this work for a practical industry applications.
12. The modified DSL could be used to determine the performance of other oxygen scavengers at higher temperatures and higher pressures.
13. The flow rate of deoxygenated non-aqueous solutions should also be considered.
14. The scavenging performance of erythorbic acid oxygen scavenger at room temperature could also be re-evaluated at high operating conditions using the modified DSL.
15. The concentration of erythorbic acid used in this work are high. Therefore, the scavenging capability of erythorbic acid could be further evaluated at a lower concentrations.
16. Effect of magnetic fields treatment on the oxygen scavenging and scale inhibitory performances with non-aqueous solutions should be studied using a modified DSL test.
17. Effect of other mineral salts and impurities on the refractive index measurement on MEG solutions should be studied.
18. Effect of other hydrocarbon mixture components on the refractive index measurement on MEG solutions should be studied.
19. Inline refractive index measurement system should be developed to measure MEG concentration on site.

Chapter 12 REFERENCES

1. Sandengen, K., *Prediction of mineral scale formation in wet gas condensate pipelines and in MEG (mono ethylene glycol) regeneration plants*. 2006, Norwegian University of Science and Technology.
2. AlHarooni, K., et al., *Influence of Regenerated Monoethylene Glycol on Natural Gas Hydrate Formation*. *Energy & Fuels*, 2017. **31**(11): p. 12914-12931.
3. Bonyad, H., et al. *Field Evaluation of a hydrate inhibition monitoring system*. in *Offshore Mediterranean Conference and Exhibition*. 2011. Offshore Mediterranean Conference.
4. Brustad, S., K.-P. Løken, and J.G. Waalmann. *Hydrate Prevention using MEG instead of MeOH: Impact of experience from major Norwegian developments on technology selection for injection and recovery of MEG*. in *Offshore Technology Conference*. 2005. Offshore Technology Conference.
5. Flaten, E.M., et al., *Impact of Monoethylene Glycol and Fe²⁺ on Crystal Growth of CaCO₃*, in *CORROSION*. 2015, NACE International.
6. Hyllestad, K., *Scaling of Calcium Carbonate on a Heated Surface in a Flow Through System with Mono Ethylene Glycol*. 2013, Norwegian University of Science and Technology.
7. Navabzadeh Esmaeely, S., et al., *Effect of Calcium on the Formation and Protectiveness of Iron Carbonate Layer in CO₂ Corrosion*. *Corrosion*, 2013. **69**(9): p. 912-920.
8. Muryanto, S., et al., *Calcium carbonate scale formation in pipes: effect of flow rates, temperature, and malic acid as additives on the mass and morphology of the scale*. International Conference and Workshop on Chemical Engineering Unpar 2013 (Icce Unpar 2013), 2014. **9**: p. 69-76.
9. Amjad, Z., *Mineral Scales in Biological and Industrial Systems*. 2013: CRC Press.
10. Amjad, Z. and K.D. Demadis, *Mineral Scales and Deposits: Scientific and Technological Approaches*. 2015: Elsevier.
11. Cole, K., *An Experimental Comparison of Three Scale Control Materials*. 2015: University of Louisiana at Lafayette.
12. Cavano, R.R. *Understanding Scaling Indices and Calculating Inhibitor Dosages*. in *CORROSION 2005*. 2005. NACE International.
13. Dariva, C.G. and A.F. Galio, *Corrosion Inhibitors—Principles, Mechanisms and Applications*. 2014.
14. Barmatov, E., T. Hughes, and M. Nagl, *Efficiency of film-forming corrosion inhibitors in strong hydrochloric acid under laminar and turbulent flow conditions*. *Corrosion Science*, 2015. **92**: p. 85-94.
15. Bikkina, C., et al. *Development of MEG regeneration unit compatible corrosion inhibitor for wet gas systems*. in *SPE Asia Pacific Oil and Gas Conference and Exhibition*. 2012. Society of Petroleum Engineers.
16. Chilingar, G.V., *The Fundamentals of Corrosion and Scaling for Petroleum & Environmental Engineers*, ed. R. Mourhatch and A. Al-Qahtani. 2013, Burlington: Burlington : Elsevier Science.
17. Dalas, E. and P.G. Koutsoukos, *The Effect of Magnetic-Fields on Calcium-Carbonate Scale Formation*. *Journal of Crystal Growth*, 1989. **96**(4): p. 802-806.
18. Coey, J., *Magnetic water treatment—how might it work?* *Philosophical Magazine*, 2012. **92**(31): p. 3857-3865.
19. Baker, J.S. and S.J. Judd, *Magnetic amelioration of scale formation*. *Water Research*, 1996. **30**(2): p. 247-260.
20. Amjad, Z., *The science and technology of industrial water treatment*. 2010: CRC Press.
21. Chen, T., Q. Wang, and F. Chang. *CaCO₃ Scale Risk Assessment-Thermodynamics vs Kinetics*. in *CORROSION 2016*. 2016. NACE International.

22. Alabi, A., et al., *Advances in anti-scale magnetic water treatment*. Environmental Science: Water Research & Technology, 2015. **1**(4): p. 408-425.
23. Grutsch, J.F. and J.W. McClintock, *Corrosion and deposit control in alkaline cooling water using magnetic water treatment at AMOCO's largest refinery*. Corrosion84, 1984: p. 1984.
24. Glater, J., J.L. York, and K.S. Campbell, *Scale formation and prevention*. Vol. 627. 1980: Academic Press.
25. Boak, L.S., *Factors that impact scale inhibitor mechanisms*. 2013, Heriot-Watt University.
26. Montazaud, T., *Precipitation of carbonates in the pretreatment process for regeneration of ethylene glycol*. 2011, Norwegian University of Science and Technology: Institutt for kjemisk prosesssteknologi.
27. Jiang, L., et al., *Effect of permanent magnetic field on scale inhibition property of circulating water*. Water Sci Technol, 2017. **76**(7-8): p. 1981-1991.
28. Esmailnezhad, E., et al., *Characteristics and applications of magnetized water as a green technology*. Journal of Cleaner Production, 2017. **161**: p. 908-921.
29. Silva, I.B., J.C.Q. Neto, and D.F.S. Petri, *The effect of magnetic field on ion hydration and sulfate scale formation*. Colloids and Surfaces a-Physicochemical and Engineering Aspects, 2015. **465**: p. 175-183.
30. Hasaani, A.S., Z.L. Hadi, and K.A. Rasheed, *Experimental study of the interaction of magnetic fields with flowing water*. International Journal of Basics and Applied Science, 2015. **3**(3): p. 1-8.
31. Chibowski, E. and A. Szczes, *Magnetic water treatment-A review of the latest approaches*. Chemosphere, 2018. **203**: p. 54-67.
32. Zaidi, N.S., et al., *Magnetic Field Application and its Potential in Water and Wastewater Treatment Systems*. Separation & Purification Reviews, 2013. **43**(3): p. 206-240.
33. Moosavi, F. and M. Gholizadeh, *Magnetic effects on the solvent properties investigated by molecular dynamics simulation*. Journal of Magnetism and Magnetic Materials, 2014. **354**: p. 239-247.
34. Koshoridze, S.I. and Y.K. Levin, *The influence of a magnetic field on the coagulation of nanosized colloid particles*. Technical Physics Letters, 2014. **40**(8): p. 716-719.
35. Zhu, L., et al., *Molecular dynamics simulation for the impact of an electrostatic field and impurity Mg^{2+} ions on hard water*. RSC Advances, 2017. **7**(75): p. 47583-47591.
36. Kumar, P.P., A.G. Kalinichev, and R.J. Kirkpatrick, *Hydrogen-Bonding Structure and Dynamics of Aqueous Carbonate Species from Car- Parrinello Molecular Dynamics Simulations*. The Journal of Physical Chemistry B, 2008. **113**(3): p. 794-802.
37. Jalilehvand, F., et al., *Hydration of the calcium ion. An EXAFS, large-angle x-ray scattering, and molecular dynamics simulation study*. J Am Chem Soc, 2001. **123**(3): p. 431-41.
38. Chang, K.T. and C.I. Weng, *The effect of an external magnetic field on the structure of liquid water using molecular dynamics simulation*. Journal of Applied Physics, 2006. **100**(4): p. 043917.
39. Barrett, R.A. and S.A. Parsons, *The influence of magnetic fields on calcium carbonate precipitation*. Water Research, 1998. **32**(3): p. 609-612.
40. Rajczykowski, K. and K. Loska, *Stimulation of Heavy Metal Adsorption Process by Using a Strong Magnetic Field*. Water Air Soil Pollut, 2018. **229**(1): p. 20.
41. Wang, Y., et al., *Rapid onset of calcium carbonate crystallization under the influence of a magnetic field*. Water Research, 1997. **31**(2): p. 346-350.
42. Sophie, V.T.I., *Magnetic treatment device for liquids*. 1953, US Patents.
43. Vermeiren, T., *Magnetic treatment of liquids for scale and corrosion prevention*. Anti-Corrosion Methods and Materials, 1958. **5**(7): p. 215-219.
44. Bruns, S., V. Klassen, and A. Konshina, *Change in extinction of light by water after treatment in a magnetic field*. Colloid Journal-USSR, 1966. **28**(1): p. 153-155.

45. Liberman, G.V. and V.I. Galaktionova, *Influence of Magnetic Treatment on Interaction of Beta-Dicalcium Silicate with Water and Added Salts*. Journal of Applied Chemistry of the Ussr, 1975. **48**(1): p. 29-32.
46. Zubarev, V., *Role of colloidal ferric hydroxide in magnetic treatment of water*. COLLOID JOURNAL-USSR, 1971. **33**(4): p. 445-&.
47. Grutsch, J., *USA/USSR symposium of physical mechanical treatment of wastewaters*. EPA, Cincinnati, 1977. **44**.
48. Luo, L.Q. and A.V. Nguyen, *A review of principles and applications of magnetic flocculation to separate ultrafine magnetic particles*. Separation and Purification Technology, 2017. **172**: p. 85-99.
49. Ambashta, R.D. and M. Sillanpaa, *Water purification using magnetic assistance: a review*. J Hazard Mater, 2010. **180**(1-3): p. 38-49.
50. Kochmarsky, V., *Magnetic treatment of water: possible mechanisms and conditions for applications*. Physical Separation in Science and Engineering, 1996. **7**(2): p. 77-107.
51. Oshitani, J., et al., *Magnetic Effect on Ion-Exchange Kinetics*. J Colloid Interface Sci, 1999. **210**(1): p. 1-7.
52. Higashitani, K., K. Okuhara, and S. Hatade, *Effects of Magnetic-Fields on Stability of Nonmagnetic Ultrafine Colloidal Particles*. Journal of Colloid and Interface Science, 1992. **152**(1): p. 125-131.
53. Colic, M. and D. Morse, *Effects of amplitude of the radiofrequency electromagnetic radiation on aqueous suspensions and solutions*. Journal of Colloid and Interface Science, 1998. **200**(2): p. 265-272.
54. Colic, M. and D. Morse, *The elusive mechanism of the magnetic 'memory' of water*. Colloids and Surfaces a-Physicochemical and Engineering Aspects, 1999. **154**(1-2): p. 167-174.
55. Saksono, N., et al., *Effects of magnetic field on calcium carbonate precipitation: Ionic and particle mechanisms*. Korean Journal of Chemical Engineering, 2009. **25**(5): p. 1145-1150.
56. Kney, A.D. and S.A. Parsons, *A spectrophotometer-based study of magnetic water treatment: assessment of ionic vs. surface mechanisms*. Water Res, 2006. **40**(3): p. 517-24.
57. Timmel, C.R., et al., *Effects of weak magnetic fields on free radical recombination reactions*. Molecular Physics, 1998. **95**(1): p. 71-89.
58. Steiner, U.E. and T. Ulrich, *Magnetic-Field Effects in Chemical-Kinetics and Related Phenomena*. Chemical Reviews, 1989. **89**(1): p. 51-147.
59. Rodgers, C.T., *Magnetic field effects in chemical systems*. Pure and Applied Chemistry, 2009. **81**(1): p. 19-43.
60. NACE International, N., *Dynamic Scale Inhibitor Evaluation Apparatus and Procedures in Oil and Gas Production*. NACE International, 2005.
61. Bhandari, N., et al. *Effect of Hydrodynamic Pressure on Mineral Precipitation Kinetics and Scaling Risk at HPHT*. in *SPE International Oilfield Scale Conference and Exhibition*. 2016. Society of Petroleum Engineers.
62. Bazin, B., N. Kohler, and A. Zaitoun. *Some Insights Into the Tube-Blocking-Test Method To Evaluate the Efficiency of Mineral Scale Inhibitors*. in *SPE Annual Technical Conference and Exhibition*. 2005. Society of Petroleum Engineers.
63. Guan, H., *Scale Deposition Control and Management in Subsea Fields*. 2015, NACE International.
64. Halvorsen, A.M.K., et al. *The Relationship Between Internal Corrosion Control Method, Scale Control And Meg Handling Of A Multiphase Carbon Steel Pipeline Carrying Wet Gas With CO2 And Acetic Acid*. 2007. NACE International.
65. Yong, A. and E.O. Obanijesu, *Influence of natural gas production chemicals on scale production in MEG regeneration systems*. Chemical Engineering Science, 2015. **130**: p. 172-182.

66. Charpentier, T.V.J. and A. Neville, *Controlling the Kinetic Versus Thermodynamic Growth of Calcium Carbonate Scale in the Bulk and on Surfaces*. 2016, NACE International.
67. Latta, T.M., M.E. Seiersten, and S.A. Bufton. *Flow assurance impacts on lean/rich MEG circuit chemistry and MEG regenerator/reclaimer design*. in *Offshore Technology Conference*. 2013. Offshore Technology Conference.
68. Wang, S. and J. Wylde. *Scale inhibitor selection for deepwater high temperature applications*. in *CORROSION 2009*. 2009. NACE International.
69. Halvorsen, E.N., et al. *Scale Inhibitor Testing for Multiphase Pipelines in a Subsea to Shore Development with a closed MEG-loop system*. in *SPE International Oilfield Scale Symposium*. 2006. Society of Petroleum Engineers.
70. Fan, C., et al., *Scale Prediction and Inhibition for Oil and Gas Production at High Temperature/High Pressure*. *SPE Journal*, 2013. **17**(02): p. 379-392.
71. Graham, A.L., et al. *How Minimum Inhibitor Concentration (MIC) and sub-MIC concentrations affect bulk precipitation and surface scaling rates*. in *SPE International Symposium on Oilfield Chemistry*. 2005. Society of Petroleum Engineers.
72. Zenker, H.C., *Thermal stability of squeeze scale inhibitors at high temperature*. 2014.
73. Graham, G., et al. *Selection and Application of a Non-Damaging Scale Inhibitor Package for Pre-Emptive Squeeze in Mungo Production Wells*. in *International Symposium on Oilfield Scale*. 2002. Society of Petroleum Engineers.
74. Garnett, P.J., *Foundations of chemistry*. 1996: Addison Wesley Longman Australia.
75. Wu, S.L., et al., *The miscibility of hydrogenated bio-oil with diesel and its applicability test in diesel engine: A surrogate (ethylene glycol) study*. *Fuel Processing Technology*, 2017. **161**: p. 162-168.
76. Gölle, A., *Dielectric Characteristics of Ionic Liquids and Usage in Advanced Energy Storage Cells*, in *Progress and Developments in Ionic Liquids*. 2017, InTech.
77. Scott, L., *Reduced calcium carbonate scaling through turbulent physical conditioning*. 2012.
78. Lide, D.R., *CRC handbook of chemistry and physics : a ready-reference book of chemical and physical data*. 90th ed. ed. Handbook of chemistry and physics. 2009, Boca Raton, Fla. London: Boca Raton, Fla. London : CRC.
79. Rozhkova, M.V., A.G. Rozhkova, and E.V. Butyrskaya, *Separation of mineral salts and nonelectrolytes (ethylene glycol) by dialysis through ion-exchange membranes*. *Journal of Analytical Chemistry*, 2007. **62**(8): p. 710-715.
80. Schmid, R., *Recent advances in the description of the structure of water, the hydrophobic effect, and the like-dissolves-like rule*. *Monatshefte Fur Chemie*, 2001. **132**(11): p. 1295-1326.
81. Smith, W.L., *Selective solubility: " Like dissolves like"*. *Journal of Chemical Education*, 1977. **54**(4): p. 228.
82. Kan, A.T., G.M. Fu, and M.B. Tomson, *Effect of methanol and ethylene glycol on sulfates and halite scale formation*. *Industrial & Engineering Chemistry Research*, 2003. **42**(11): p. 2399-2408.
83. Babu, D.R., et al., *Carbonates precipitation in MEG loops - A comparative study of South Pars and Bass Strait gas fields*. *Journal of Natural Gas Science and Engineering*, 2015. **27**: p. 955-966.
84. Wang, P.M., et al., *Ethylene Glycol and Its Mixtures with Water and Electrolytes: Thermodynamic and Transport Properties*. *Industrial & Engineering Chemistry Research*, 2013. **52**(45): p. 15968-15987.
85. Matvejev, V., M. Zizi, and J. Stiens, *Hydration shell parameters of aqueous alcohols: THz excess absorption and packing density*. *J Phys Chem B*, 2012. **116**(48): p. 14071-7.
86. Marcus, Y., *Effect of ions on the structure of water: structure making and breaking*. *Chem Rev*, 2009. **109**(3): p. 1346-70.
87. Pálincás, G. and K. Heinzinger, *Hydration shell structure of the calcium ion*. *Chemical Physics Letters*, 1986. **126**(3-4): p. 251-254.

88. Glueckauf, E., *The influence of ionic hydration on activity coefficients in concentrated electrolyte solutions*. Transactions of the Faraday Society, 1957. **53**: p. 305-305.
89. Harris, D.C., *Quantitative chemical analysis*. 2010: Macmillan.
90. Silberberg, M.S. and R. Duran, *Chemistry: The Molecular Nature of Matter and Change With Advanced Topics*. 2018: McGraw-Hill New York.
91. Zavitsas, A.A., *Aqueous solutions of calcium ions: hydration numbers and the effect of temperature*. J Phys Chem B, 2005. **109**(43): p. 20636-40.
92. Badyal, Y.S., et al., *Understanding the effects of concentration on the solvation structure of Ca²⁺ in aqueous solutions. II: Insights into longer range order from neutron diffraction isotope substitution*. Journal of Physical Chemistry A, 2004. **108**(52): p. 11819-11827.
93. Fulton, J.L., et al., *Understanding the effects of concentration on the solvation structure of Ca²⁺ in aqueous solution. I: The perspective on local structure from EXAFS and XANES*. Journal of Physical Chemistry A, 2003. **107**(23): p. 4688-4696.
94. Megyes, T., et al., *Solvation of calcium ion in polar solvents: An X-ray diffraction and ab initio study*. Journal of Physical Chemistry A, 2004. **108**(35): p. 7261-7271.
95. Mahler, J. and I. Persson, *A study of the hydration of the alkali metal ions in aqueous solution*. Inorg Chem, 2012. **51**(1): p. 425-38.
96. Di Tommaso, D., et al., *Modelling the effects of salt solutions on the hydration of calcium ions*. Phys Chem Chem Phys, 2014. **16**(17): p. 7772-85.
97. Cai, R., et al., *The effects of magnetic fields on water molecular hydrogen bonds*. Journal of Molecular Structure, 2009. **938**(1-3): p. 15-19.
98. Papic, P., *Scaling and corrosion potential of selected geothermal waters in Serbia*. 1991: United Nations University.
99. Bustos-Serrano, H., *The carbonate system in natural waters*, F.J. Millero, et al., Editors. 2010, ProQuest Dissertations Publishing.
100. Linert, W., *Highlights in Solute-Solvent Interactions*. 2002: Springer.
101. Dhanaraj, G., et al., *Springer handbook of crystal growth*. 2010: Springer Science & Business Media.
102. Hartkamp, R. and B. Coasne, *Structure and transport of aqueous electrolytes: from simple halides to radionuclide ions*. J Chem Phys, 2014. **141**(12): p. 124508.
103. Marcus, Y., *Concentration dependence of ionic hydration numbers*. J Phys Chem B, 2014. **118**(35): p. 10471-6.
104. Marcus, Y., *On Water Structure in Concentrated Salt Solutions*. Journal of Solution Chemistry, 2009. **38**(5): p. 513-516.
105. Waluyo, I., et al., *A different view of structure-making and structure-breaking in alkali halide aqueous solutions through x-ray absorption spectroscopy*. J Chem Phys, 2014. **140**(24): p. 244506.
106. Flaten, E.M., M. Seiersten, and J.P. Andreassen, *Polymorphism and morphology of calcium carbonate precipitated in mixed solvents of ethylene glycol and water*. Journal of Crystal Growth, 2009. **311**(13): p. 3533-3538.
107. Flaten, E.M., M. Seiersten, and J.P. Andreassen, *Growth of the calcium carbonate polymorph vaterite in mixtures of water and ethylene glycol at conditions of gas processing*. Journal of Crystal Growth, 2010. **312**(7): p. 953-960.
108. Flaten, E.M., et al. *Precipitation of iron and calcium carbonate in pipelines at varying MEG contents*. in *SPE International Oilfield Scale Conference*. 2008. Society of Petroleum Engineers.
109. Al Helal, A., et al., *Influence of Magnetic Fields on Calcium Carbonate Scaling in Aqueous Solutions at 150° C and 1 Bar*. Journal of Colloid and Interface Science, 2018. **509**: p. 472-484.
110. Dickinson, S.R., G.E. Henderson, and K.M. McGrath, *Controlling the kinetic versus thermodynamic crystallisation of calcium carbonate*. Journal of Crystal Growth, 2002. **244**(3-4): p. 369-378.
111. Moriarty, B.E., et al. *Methods to monitor and control scale in cooling water systems*. in *CORROSION 2001*. 2001. NACE International.

112. Yang, Q., et al., *Investigation of Calcium Carbonate Scaling Inhibition and Scale Morphology by AFM*. J Colloid Interface Sci, 2001. **240**(2): p. 608-621.
113. Gorna, K., et al., *Amorphous calcium carbonate in form of spherical nanosized particles and its application as fillers for polymers*. Materials Science and Engineering a-Structural Materials Properties Microstructure and Processing, 2008. **477**(1-2): p. 217-225.
114. Dai, Z., et al. *A Thermodynamic Model for The Solution Density and Mineral Solubility Predictions up to 250° C, 1,500 Bars for Na-K-Mg-Ca-Ba-Sr-Cl-CO₃-HCO₃-SO₄-CO₂ aq Systems*. in *SPE International Oilfield Scale Conference and Exhibition*. 2016. Society of Petroleum Engineers.
115. Hu, Y.B., et al., *Effect of pH and Phosphate on Calcium Carbonate Polymorphs Precipitated at near-Freezing Temperature*. Crystal Growth & Design, 2015. **15**(4): p. 1596-1601.
116. Liu, X., et al. *Understanding Mechanisms of Scale inhibition Using Newly Developed Test Method and Developing Synergistic Combined Scale Inhibitors*. in *SPE International Conference on Oilfield Scale*. 2012. Society of Petroleum Engineers.
117. Väisänen, H., *CaCO₃ scale inhibition in paper making processes—evaluation of testing methods and inhibitor performance*. 2011.
118. Lu, H., A.T. Kan, and M.B. Tomson. *Effects of Monoethylene Glycol on Carbonate Equilibrium and Calcite Solubility in Gas/Monoethylene Glycol/Water/Salt Mixed Systems*. in *SPE International Symposium on Oilfield Chemistry*. 2009. Society of Petroleum Engineers.
119. Kan, A.T., H.P. Lu, and M.B. Tomson, *Effects of Monoethylene Glycol on Carbon Dioxide Partitioning in Gas/Monoethylene Glycol/Water/Salt Mixed Systems*. Industrial & Engineering Chemistry Research, 2010. **49**(12): p. 5884-5890.
120. Plummer, L.N. and E. Busenberg, *The solubilities of calcite, aragonite and vaterite in CO₂-H₂O solutions between 0 and 90°C, and an evaluation of the aqueous model for the system CaCO₃-CO₂-H₂O*. Geochimica et Cosmochimica Acta, 1982. **46**(6): p. 1011-1040.
121. Kan, A.T., et al. *Effect of hydrate inhibitors on oilfield scale formation and inhibition*. in *International Symposium on Oilfield Scale*. 2002. Society of Petroleum Engineers.
122. Lu, H., A.T. Kan, and M.B. Tomson, *Effects of Monoethylene Glycol on Carbonate Equilibrium and Calcite Solubility in Gas/Monoethylene Glycol/NaCl/Water Mixed Systems*. SPE Journal, 2013. **15**(03): p. 714-725.
123. Evans, T., *Influence of Ionic strength on calcium carbonate (CaCO₃) polymorphism*. arXiv preprint arXiv:1209.3333, 2012.
124. Guan, H., *Carbonate Scaling Prediction: The Importance of Valid Data Input*. Journal of Materials Science and Engineering, 2011. **5**(2): p. 220.
125. Ferguson, R.J. *mineral scale prediction and control at extreme TDS*. in *International Water Conference*. 2011. ESWP Orlando, FL, USA.
126. Kan, A., G. Fu, and M. Tomson. *Prediction of Scale Inhibitor Squeeze and Return in Calcite-Bearing Formation*. in *SPE International Symposium on Oilfield Chemistry*. 2005. Society of Petroleum Engineers.
127. Fosbøl, P.L., K. Thomsen, and E.H. Stenby, *Modeling of the mixed solvent electrolyte system CO₂-Na₂CO₃-NaHCO₃- monoethylene glycol- water*. Industrial & Engineering Chemistry Research, 2009. **48**(9): p. 4565-4578.
128. Daniels, J.K., et al., *Laboratory Methods for Scale Inhibitor Selection for HP/HT Fields*, in *SPE International Oilfield Scale Conference and Exhibition*. 2014, Society of Petroleum Engineers: Aberdeen, Scotland. p. 12.
129. Saifelnasr, A., et al., *Calcium Carbonate Scale Formation, Prediction and Treatment (Case Study Gumry Oilfield-PDOC)*. International Letters of Chemistry, Physics and Astronomy, 2013. **12**: p. 47--58.
130. Gal, J.Y., et al., *Calcium carbonate solubility: a reappraisal of scale formation and inhibition*. Talanta, 1996. **43**(9): p. 1497-509.

131. AlHarooni, K., et al., *Inhibition effects of thermally degraded MEG on hydrate formation for gas systems*. Journal of Petroleum Science and Engineering, 2015. **135**: p. 608-617.
132. Tomson, M.B., et al. *Scale formation and prevention in the presence of hydrate inhibitors*. in *International Symposium on Oilfield Chemistry*. 2003. Society of Petroleum Engineers.
133. Shipley, H.J., et al. *Effect of hydrate inhibitors on calcite, sulfates and halite scale formation*. in *SPE International Oilfield Scale Symposium*. 2006. Society of Petroleum Engineers.
134. Ehsani, H., *Influence of Monoethylene Glycol (MEG) on the corrosion inhibition of wet-gas flow lines*, in *Department of Chemistry*. 2013, Curtin University.
135. Psarrou, M.N., et al., *Carbon Dioxide Solubility and Monoethylene Glycol (MEG) Degradation at MEG Reclaiming/Regeneration Conditions*. Journal of Chemical and Engineering Data, 2011. **56**(12): p. 4720-4724.
136. Zaboon, S., et al., *Recovery of mono-ethylene glycol by distillation and the impact of dissolved salts evaluated through simulation of field data*. Journal of Natural Gas Science and Engineering, 2017. **44**: p. 214-232.
137. AlHarooni, K., et al., *Analytical Techniques for Analyzing Thermally Degraded Monoethylene Glycol with Methyl Diethanolamine and Film Formation Corrosion Inhibitor*. Energy & Fuels, 2016. **30**(12): p. 10937-10949.
138. Stewart, E. and R. Lanning, *Reduce amine plant solvent losses; Part 1*. Hydrocarbon Processing;(United States), 1994. **73**(5).
139. Nizzer, C. and J. Keogh. *Advances in glycol reclamation technology*. in *Offshore Technology Conference*. 2006. Offshore Technology Conference.
140. Flaten, E.M., M. Seiersten, and J.P. Andreassen, *Induction time studies of calcium carbonate in ethylene glycol and water*. Chemical Engineering Research & Design, 2010. **88**(12a): p. 1659-1668.
141. Kan, A.T., G.M. Fu, and M.B. Tomson, *Effect of methanol on carbonate equilibrium and calcite solubility in a gas/methanol/water/salt mixed system*. Langmuir, 2002. **18**(25): p. 9713-9725.
142. Xu, B., et al. *Influence of Calcium and Bicarbonate Ions on the Kinetics of CaCO₃ Formation at HTHP in the Absence and Presence of Scale Inhibitors*. in *SPE International Oilfield Scale Conference and Exhibition*. 2014. Society of Petroleum Engineers.
143. Jordan, M.M., N.D. Feasey, and C. Johnston. *Inorganic Scale Control Within MEG/Methanol Treated Produced Fluids*. in *SPE International Symposium on Oilfield Scale*. 2005. Society of Petroleum Engineers.
144. Williams, H., et al. *The Impact of Thermodynamic Hydrate Inhibitors (MEG and Methanol) on Scale Dissolver Performance*. in *SPE International Oilfield Scale Conference and Exhibition*. 2016. Society of Petroleum Engineers.
145. Hills, E.J., et al. *Hydrate-Inhibited Scale Inhibitor for Use on Sub-Sea Templates*. in *SPE International Oilfield Scale Symposium*. 2006. Society of Petroleum Engineers.
146. Schilter, R., et al. *Field-Detectable Scale Inhibitor for Severe Oilfield Environments*. in *SPE Deepwater Drilling and Completions Conference*. 2014. Society of Petroleum Engineers.
147. NACE International, N., *Laboratory Screening Tests to Determine the Ability of Scale Inhibitors to Prevent the Precipitation of Calcium Sulfate and Calcium Carbonate from Solution (for Oil and Gas Production Systems)*. 2016, NACE International.
148. Bhandari, N., et al. *The Effect of Pressure and TDS on Barite Scaling Kinetics*. in *SPE International Symposium on Oilfield Chemistry*. 2015. Society of Petroleum Engineers.
149. Kohler, N., G. Courbin, and F. Ropital. *Static and Dynamic Evaluation of Calcium Carbonate Scale Formation and Inhibition*. in *SPE European Formation Damage Conference*. 2001. Society of Petroleum Engineers.
150. Yuan, M., E. Jamieson, and P. Hammonds, *Investigation of scaling and inhibition mechanisms and the influencing factors in static and dynamic inhibition tests*. 1998, NACE International, Houston, TX (United States).

151. Baraka-Lokmane, S., et al. *Prediction of Mineral Scaling in a MEG Loop System of a gas production offshore*. in *SPE International Conference on Oilfield Scale*. 2012. Society of Petroleum Engineers.
152. Abidoeye, L.K. and D.B. Das, *Scale dependent dynamic capillary pressure effect for two-phase flow in porous media*. *Advances in Water Resources*, 2014. **74**: p. 212-230.
153. Reddy, M.M. and A.R. Hoch, *Calcite Crystal Growth Rate Inhibition by Polycarboxylic Acids*. *J Colloid Interface Sci*, 2001. **235**(2): p. 365-370.
154. Smothers, K.W., et al., *Demonstration and Evaluation of Magnetic Descalers*. 2001, DTIC Document.
155. Koutsoukos, P.G., et al. *Calcium Carbonate Crystal Growth And Dissolution Inhibitors*. in *CORROSION 2007*. 2007. NACE International.
156. M. Ramzia, R.H., M. El-Sayedb*, M. Fathyc and and T.A. Moghny, *Evaluation of scale inhibitors performance under simulated flowing field conditions using dynamic tube blocking test*. *Int. J. Chem. Sci.*, 2016. **14**(1): p. 16-28.
157. Kelland, M.A., *Effect of Various Cations on the Formation of Calcium Carbonate and Barium Sulfate Scale with and without Scale Inhibitors*. *Industrial & Engineering Chemistry Research*, 2011. **50**(9): p. 5852-5861.
158. Valiakhmetova, A., et al. *Novel Studies on Precipitated Phosphate Ester Scale Inhibitors for Precipitation Squeeze Application*. in *SPE International Conference on Oilfield Chemistry*. 2017. Society of Petroleum Engineers.
159. Kelland, M.A., *Production chemicals for the oil and gas industry*. 2014: CRC press.
160. Fraser, A., et al. *Limitations of Common Oilfield Scale Inhibitor Chemistries*. in *CORROSION 2016*. 2016. NACE International.
161. Demadis, K.D. and M. Preari, "Green" scale inhibitors in water treatment processes: the case of silica scale inhibition. *Desalination and Water Treatment*, 2015. **55**(3): p. 749-755.
162. Kim, W.T. and Y.I. Cho, *A study of physical water treatment methods for the mitigation of mineral fouling*. 2001: ProQuest Dissertations Publishing.
163. Cho, Y.I., et al., *Physical water treatment for the mitigation of mineral fouling in cooling-tower water applications*. 2003.
164. Lee, S.H. and Y.I. Cho, *A study of physical water treatment technology to mitigate the mineral fouling in a heat exchanger*. 2002: Drexel University.
165. Halvorsen, A.M.K., J.I. Skar, and K. Reiersølmoen. *Qualification of scale and corrosion inhibitor for a subsea HPHT field with a MEG-loop*. 2012. NACE International.
166. Crupi, V., et al., *Raman spectroscopic study of water in the poly(ethylene glycol) hydration shell*. *Journal of Molecular Structure*, 1996. **381**(1-3): p. 207-212.
167. ACD/ChemSketch Freeware, A.C.D., Inc., Toronto, ON, Canada, www.acdlabs.com, 2015.
168. Tansel, B., et al., *Significance of hydrated radius and hydration shells on ionic permeability during nanofiltration in dead end and cross flow modes*. *Separation and Purification Technology*, 2006. **51**(1): p. 40-47.
169. Holysz, L., A. Szczes, and E. Chibowski, *Effects of a static magnetic field on water and electrolyte solutions*. *J Colloid Interface Sci*, 2007. **316**(2): p. 996-1002.
170. Rozhkova, A.G., et al., *Quantum chemical calculation of cation interaction with water molecules and ethylene glycol*. *Journal of Structural Chemistry*, 2007. **48**(1): p. 166-169.
171. Pang, X.F. and B. Deng, *Investigation of changes in properties of water under the action of a magnetic field*. *Science in China Series G-Physics Mechanics & Astronomy*, 2008. **51**(11): p. 1621-1632.
172. Tai, C.Y., et al., *Magnetic effects on crystal growth rate of calcite in a constant-composition environment*. *Journal of Crystal Growth*, 2008. **310**(15): p. 3690-3697.
173. Pang, X. and B. Deng. *Investigation of magnetic-field effects on water*. in *Applied Superconductivity and Electromagnetic Devices*, 2009. *ASEMD 2009. International Conference on*. 2009. IEEE.
174. Higashitani, K., et al., *Effects of a Magnetic-Field on the Formation of Caco3 Particles*. *Journal of Colloid and Interface Science*, 1993. **156**(1): p. 90-95.

175. Fathi, A., et al., *Effect of a magnetic water treatment on homogeneous and heterogeneous precipitation of calcium carbonate*. Water Res, 2006. **40**(10): p. 1941-50.
176. Busch, K.W., et al., *Studies of a Water-Treatment Device That Uses Magnetic-Fields*. Corrosion, 1986. **42**(4): p. 211-221.
177. Busch, K.W. and M.A. Busch, *Laborator studies on magnetic water treatment and their relationship to a possible mechanism for scale reduction*. Desalination, 1997. **109**(2): p. 131-148.
178. Okada, I., M. Ozaki, and E. Matijevic, *Magnetic-Interactions between Platelet-Type Colloidal Particles*. Journal of Colloid and Interface Science, 1991. **142**(1): p. 251-256.
179. Higashitani, K., et al., *Magnetic Effects on Zeta-Potential and Diffusivity of Nonmagnetic Colloidal Particles*. Journal of Colloid and Interface Science, 1995. **172**(2): p. 383-388.
180. Johan, S., *Effect of magnetic field on the sedimentation of suspended solids of sewage*. 2003, Thesis of Philosophy of Doctorate: Universiti Teknologi Malaysia.
181. Anthony, R. and B. Stuart, *Solvent extraction and characterization of neutral lipids in Oocystis sp*. Advancements in Algal Biofuels Research—Recent Evaluation of Algal Biomass Production and Conversion Methods of into Fuels and High Value Co-products, 2017.
182. Reitsma, J.B., et al., *Bivariate analysis of sensitivity and specificity produces informative summary measures in diagnostic reviews*. J Clin Epidemiol, 2005. **58**(10): p. 982-90.
183. Vick, W.S. *Magnetic fluid conditioning*. in *Environmental Engineering*:. 1991. ASCE.
184. Wang, Y.M., R.J. Pugh, and E. Forssberg, *The Influence of Interparticle Surface Forces on the Coagulation of Weakly Magnetic Mineral Ultrafines in a Magnetic-Field*. Colloids and Surfaces a-Physicochemical and Engineering Aspects, 1994. **90**(2-3): p. 117-133.
185. Prykarpatsky, A.K. and N.N. Bogolubov, *The Maxwell Electromagnetic Equations and the Lorentz Type Force Derivation—The Feynman Approach Legacy*. International Journal of Theoretical Physics, 2011. **51**(1): p. 237-245.
186. Sackey, J., *Theoretical And Computational Modeling Of The Effects Of Electromagnetic Field On The Plasmodium Falciparum*. 2011, Princeton University.
187. Ghosh, B., M.I. Hashmi, and L. Sun, *Acceleration-Retardation of Calcium Carbonate Scale Deposition under Static Electric Potential*. 2015.
188. Madsen, H.E.L., *Influence of Magnetic-Field on the Precipitation of Some Inorganic Salts*. Journal of Crystal Growth, 1995. **152**(1-2): p. 94-100.
189. Higashitani, K. and J. Oshitani, *Magnetic Effects on Thickness of Adsorbed Layer in Aqueous Solutions Evaluated Directly by Atomic Force Microscope*. J Colloid Interface Sci, 1998. **204**(2): p. 363-8.
190. Alimi, F., et al., *Influence of magnetic field on calcium carbonate precipitation*. Desalination, 2007. **206**(1-3): p. 163-168.
191. Powell, M.R., *Magnetic Water and Fuel Treatment: Myth, Magic, or Mainstream Science? Skeptical Inquirer*, 1998. **22**: p. 27-31.
192. Krauter, P., et al., *Test of a Magnetic Device for the Amelioration of Scale Formation at Treatment Facility D*. Internal Rep. OSTI, 1996. **567404**.
193. Szczeń, A., et al., *Effects of static magnetic field on water at kinetic condition*. Chemical Engineering and Processing: Process Intensification, 2011. **50**(1): p. 124-127.
194. Szczeń, A., et al., *Effects of static magnetic field on electrolyte solutions under kinetic condition*. J Phys Chem A, 2011. **115**(21): p. 5449-52.
195. Ahmed, A.W. and S.I. Mohammed, *Kinetic model of aerobic Agro Strain Growth under Constant Magnetic Field in Batch system*. Jornal of Biotechnology Research Center, 2011. **5**(3).
196. Chang, M.-C. and C.Y. Tai, *Effect of the magnetic field on the growth rate of aragonite and the precipitation of CaCO₃*. Chemical Engineering Journal, 2010. **164**(1): p. 1-9.
197. Rao, M.S. and O. Sahu, *Study of Electromagnetic Waves on Industrial Waste Water*. Physics and Materials Chemistry, 2013. **1**(2): p. 34-40.
198. Yan, L., et al., *Magnetotactic bacteria, magnetosomes and their application*. Microbiol Res, 2012. **167**(9): p. 507-19.

199. Ghauri, S. and M. Ansari, *Increase of water viscosity under the influence of magnetic field*. 2006, AIP.
200. Hosoda, H., et al., *Refractive indices of water and aqueous electrolyte solutions under high magnetic fields*. *Journal of Physical Chemistry A*, 2004. **108**(9): p. 1461-1464.
201. Parsons, S.A., et al., *Magnetic treatment of calcium carbonate scale - Effect of pH control*. *Water Research*, 1997. **31**(2): p. 339-342.
202. Tai, C.Y., C.-K. Wu, and M.-C. Chang, *Effects of magnetic field on the crystallization of CaCO₃ using permanent magnets*. *Chemical Engineering Science*, 2008. **63**(23): p. 5606-5612.
203. Ge, H.-H., et al. *Scale Inhibition of Electromagnetic Water Treatment and Corrosion Behavior of Carbon Steel in Simulated Water*. in *Bioinformatics and Biomedical Engineering (iCBBE), 2010 4th International Conference on*. 2010. IEEE.
204. Burgos-Cara, A., et al., *Hydration Effects on the Stability of Calcium Carbonate Pre-Nucleation Species*. *Minerals*, 2017. **7**(7): p. 126.
205. Tomson, M., et al. *Mechanisms of mineral scale inhibition*. in *International Symposium on Oilfield Scale*. 2002. Society of Petroleum Engineers.
206. Zeng, B., et al., *Application of 1-hydroxyethylidene-1, 1-diphosphonic acid in boiler water for industrial boilers*. *Water Sci Technol*, 2013. **67**(7): p. 1544-50.
207. Sorbie, K. and N. Laing. *How scale inhibitors work: Mechanisms of selected barium sulphate scale inhibitors across a wide temperature range*. in *SPE International Symposium on Oilfield Scale*. 2004. Society of Petroleum Engineers.
208. Fan, C., et al., *Ultrahigh-Temperature/Ultrahigh-Pressure Scale Control for Deepwater Oil and Gas Production*. *SPE Journal*, 2013. **17**(01): p. 177-186.
209. Perez, L.A., Z. Amjad, and R.W. Zuhl, *Stressed Cooling Water System Deposit Control Management*. NACE International, CORROSION, 2016.
210. Racke, K.D., *Degradation of organophosphorus insecticides in environmental matrices*, in *Organophosphates Chemistry, Fate, and Effects*. 1992, Elsevier. p. 47-78.
211. Tai, C.Y., M.C. Chang, and S.W. Yeh, *Synergetic effects of temperature and magnetic field on the aragonite and calcite growth*. *Chemical Engineering Science*, 2011. **66**(6): p. 1246-1253.
212. Messiha, H.L., et al., *Magnetic field effects as a result of the radical pair mechanism are unlikely in redox enzymes*. *J R Soc Interface*, 2015. **12**(103): p. 20141155.
213. Till, U. and P.J. Hore, *Radical pair kinetics in a magnetic field*. *Molecular Physics*, 1997. **90**(2): p. 289-296.
214. Daniels, J., et al. *Laboratory Methods for Scale Inhibitor Selection for HP/HT Fields*. in *SPE International Oilfield Scale Conference and Exhibition*. 2014. Society of Petroleum Engineers.
215. Goss, D.J. and R.H. Petrucci, *General Chemistry Principles & Modern Applications, Petrucci, Harwood, Herring, Madura: Study Guide*. 2007: Pearson/Prentice Hall.
216. Sherman, A., S.J. Sherman, and L. Russikoff, *Basic concepts of chemistry*. 1984: Houghton Mifflin Harcourt (HMH).
217. Lide, D.R., *CRC handbook of chemistry and physics*. 2004.
218. Akbarzadeh, A., M. Samiei, and S. Davaran, *Magnetic nanoparticles: preparation, physical properties, and applications in biomedicine*. *Nanoscale Res Lett*, 2012. **7**(1): p. 144.
219. Truesdell, A.H. and B.F. Jones, *WATEQ, a computer program for calculating chemical equilibria of natural waters*. *J. Res. US Geol. Surv*, 1974. **2**(2): p. 233-248.
220. Marcus, Y., *Ionic-Radii in Aqueous-Solutions*. *Chemical Reviews*, 1988. **88**(8): p. 1475-1498.
221. Hem, J.D., *Calculation and use of ion activity*. 1961, US Govt. Print. Off.
222. Kielland, J., *Individual activity coefficients of ions in aqueous solutions*. *Journal of the American Chemical Society*, 1937. **59**(9): p. 1675-1678.
223. Pitzer, K.S., *Thermodynamics of electrolytes. I. Theoretical basis and general equations*. *The Journal of Physical Chemistry*, 1973. **77**(2): p. 268-277.

224. Olsen, R., B. Kvamme, and T. Kuznetsova, *Hydrogen Bond Lifetimes and Statistics of Aqueous Mono-, Di- and Tri-Ethylene Glycol*. *Aiche Journal*, 2017. **63**(5): p. 1674-1689.
225. Ellingsen, F. and H. Kristiansen, *Does magnetic treatment influence precipitation of calcium carbonate from supersaturated solutions*. *Vatten*, 1979. **35**(4): p. 309-315.
226. Tombacz, E., et al., *Effect of a weak magnetic field on hematite sol in stationary and flowing systems*. *Colloid & Polymer Science*, 1991. **269**(3): p. 278-289.
227. Lychagin, N.I., *Change of Properties of Magnetized Water*. *Izvestiya Vysshikh Uchebnykh Zavedenii Fizika*, 1974. **17**(2): p. 99-103.
228. Soames, A., et al., *Operation of a MEG pilot regeneration system for organic acid and alkalinity removal during MDEA to FFCI switchover*. *Journal of Petroleum Science and Engineering*, 2018. **169**: p. 1-14.
229. Pojtanabuntoeng, T., et al., *Assessment of corrosion control by pH neutralisation in the presence of glycol at low temperature*. *Corrosion Science*, 2017. **126**: p. 94-103.
230. Kundu, S.S. and M. Seiersten, *Development of a non-sulphite oxygen scavenger for monoethylene glycol (MEG) used as gas hydrate inhibitor*. *Journal of Petroleum Science and Engineering*, 2017. **158**: p. 120-128.
231. Haque, M.E., *Ethylene glycol regeneration plan: a systematic approach to troubleshoot the common problems*. *Journal of Chemical Engineering*, 2013. **27**(1): p. 21-26.
232. Rudenko, A., A. Gershuni, and L. Kalabina, *Some characteristics of ethylene glycol as a heat-transfer agent for closed two-phase systems*. *Journal of engineering physics and thermophysics*, 1997. **70**(5): p. 799-804.
233. Ivonye, I., C. Wang, and A. Neville, *The Corrosion of Carbon Steel in the Presence of Monoethylene Glycol (MEG)–Assessing the Influence of an Iron Carbonate Scale*, in *Corrosion 2015*. 2015, NACE International: Dallas, Texas. p. 11.
234. Salasi, M., et al., *Efficacy of Bisulfite Ions as an Oxygen Scavenger in Monoethylene Glycol (At Least 20 wt%)/Water Mixtures*. *SPE Journal*, 2017. **22**(05): p. 1467-1477.
235. Lehmann, M., et al. *Corrosion Inhibitor and Oxygen Scavenger for use as MEG Additives in the Inhibition of Wet Gas Pipelines*. in *Offshore Technology Conference-Asia*. 2014. Offshore Technology Conference.
236. Matsumoto, T., et al., *CO₂-free power generation on an iron group nanoalloy catalyst via selective oxidation of ethylene glycol to oxalic acid in alkaline media*. *Scientific reports*, 2014. **4**: p. 5620.
237. King, C.S., et al., *Short contact, elevated temperature meg reclamation*. 2017, Patent App. 20170015613A1.
238. Clifton, J.R., W.J. Rossiter, and P.W. Brown, *Degraded Aqueous Glycol Solutions - Ph Values and the Effects of Common Ions on Suppressing Ph Decreases*. *Solar Energy Materials*, 1985. **12**(1): p. 77-86.
239. Rossiter, W.J., et al., *An Investigation of the Degradation of Aqueous Ethylene-Glycol and Propylene-Glycol Solutions Using Ion Chromatography*. *Solar Energy Materials*, 1985. **11**(5-6): p. 455-467.
240. Brown, P.W., K.G. Galuk, and W.J. Rossiter, *Characterization of Potential Thermal-Degradation Products from the Reactions of Aqueous Ethylene-Glycol and Propylene-Glycol Solutions with Copper Metal*. *Solar Energy Materials*, 1987. **16**(4): p. 309-313.
241. Finkbeiner, H. and J.B. Bush, *Oxidation of acetic acid by manganese (III) salts*. *Discussions of the Faraday Society*, 1968. **46**: p. 150-157.
242. Brandt, C. and R. Vaneldik, *Transition-Metal-Catalyzed Oxidation of Sulfur(IV) Oxides - Atmospheric-Relevant Processes and Mechanisms*. *Chemical Reviews*, 1995. **95**(1): p. 119-190.
243. Kotronarou, A. and L. Sigg, *Sulfur dioxide oxidation in atmospheric water: role of iron (II) and effect of ligands*. *Environmental science & technology*, 1993. **27**(13): p. 2725-2735.
244. Nurmi, D., et al., *Sulfite Oxidation in Organic Acid Solutions*. 1982, ACS Publications.
245. Dugstad, A. and M. Seiersten. *pH-stabilisation, a reliable method for corrosion control of wet gas pipelines*. in *SPE International Symposium on Oilfield Corrosion*. 2004. Society of Petroleum Engineers.

246. Joosten, M.W., et al., *Materials Considerations for MEG (Mono Ethylene Glycol) Reclamation Systems*, in *Corrosion 2007*. 2007, NACE: Nashville, Tennessee. p. 19.
247. Mansoori, H., R. Mirzaee, and A. Mohammadi. *Pitting Corrosion Failures of Natural Gas Transmission Pipelines*. in *IPTC 2013: International Petroleum Technology Conference*. 2013.
248. Olsen, S. *Corrosion Control by Inhibition, Environmental Aspects, and pH Control: Part II: Corrosion Control by pH Stabilization*. 2006. NACE.
249. Gui, F., et al. *Inhibition of Carbon Steel Stress Corrosion Cracking in Fuel Grade Ethanol by Chemical Addition or Oxygen Control: A Feasibility Evaluation*. in *CORROSION 2013*. 2013. NACE.
250. Crowe, C.W., *Evaluation of Agents for Preventing Precipitation of Ferric Hydroxide From Spent Treating Acid*. *Journal of Petroleum Technology*, 2013. **37**(04): p. 691-695.
251. Abbadi, A., et al., *New food antioxidant additive based on hydrolysis products of lactose*. *Green Chemistry*, 2003. **5**(1): p. 47-51.
252. Crovetto, R., E. Murtagh, and A.M. Rossi. *Research evaluation of polyamine chemistry for boiler treatment: Corrosion Protection*. 2011. NACE International.
253. Backstrom, H., *The chain mechanism in the autoxidation of sodium sulfite solutions*. *Z. Physik. Chem. B*, 1934. **25**: p. 122-138.
254. Snively, E.S., *Chemical Removal of Oxygen from Natural Waters*. *Journal of Petroleum Technology*, 2013. **23**(04): p. 443-446.
255. Hobson, D.B., et al., *Kinetics of the Oxygen Sulfite Reaction at Waterflood Concentrations - Effect of Catalysts and Seawater Medium*. *Industrial & Engineering Chemistry Research*, 1987. **26**(9): p. 1818-1822.
256. Christensen, R.J. and L.H. Steimel, *Oxygen scavenger for boiler water and method of use*. 1990, US Patent App. 4,891,141.
257. Snively, E.S. and F.E. Blount, *Rates of Reaction of Dissolved Oxygen With Scavengers in Sweet and Sour Brines*. *Corrosion*, 1969. **25**(10): p. 397-404.
258. Dooley, R.B. and V.K. Chexal, *Flow-accelerated corrosion of pressure vessels in fossil plants*. *International Journal of Pressure Vessels and Piping*, 2000. **77**(2-3): p. 85-90.
259. Uchida, S., et al., *Evaluation of flow accelerated corrosion by coupled analysis of corrosion and flow dynamics. Relationship of oxide film thickness, hematite/magnetite ratio, ECP and wall thinning rate*. *Nuclear Engineering and Design*, 2011. **241**(11): p. 4585-4593.
260. May, R.D., *Oxygen removal with carbon catalyzed erythorbate or ascorbate*. 1989, US Patent App. 4851130A.
261. Kramarenko, G.G., et al., *Ascorbate reacts with singlet oxygen to produce hydrogen peroxide*. *Photochem Photobiol*, 2006. **82**(6): p. 1634-7.
262. Nimse, S.B. and D. Pal, *Free radicals, natural antioxidants, and their reaction mechanisms*. *RSC Advances*, 2015. **5**(35): p. 27986-28006.
263. Barrita, J.L.S. and M.d.S.S. Sánchez, *Antioxidant role of ascorbic acid and his protective effects on chronic diseases*, in *Oxidative Stress and Chronic Degenerative Diseases-A Role for Antioxidants*. 2013, InTech.
264. Elmore, A., *Final report of the safety assessment of L-Ascorbic Acid, Calcium Ascorbate, Magnesium Ascorbate, Magnesium Ascorbyl Phosphate, Sodium Ascorbate, and Sodium Ascorbyl Phosphate as used in cosmetics*. *International journal of toxicology*, 2005. **24**: p. 51-111.
265. Suman, S.P., et al., *Effect of erythorbate, storage and high-oxygen packaging on premature browning in ground beef*. *Meat Sci*, 2005. **69**(2): p. 363-9.
266. Pischetsrieder, M., et al., *Reaction of ascorbic acid with aliphatic amines*. *Journal of Agricultural and Food Chemistry*, 1995. **43**(12): p. 3004-3006.
267. Wenner, W., *The reaction of L-ascorbic and D-isoascorbic acid with nicotinic acid and its amide*. *J Org Chem*, 1949. **14**(1): p. 22-6.
268. Colton, C. and D. Gilbert, *Reactive Oxygen Species in Biological Systems: An Interdisciplinary Approach*. 2007: Springer Science & Business Media.
269. Fridovich, I., *The biology of oxygen radicals*. *Science*, 1978. **201**(4359): p. 875-80.

270. Wilson, R.J., A.E. Beezer, and J.C. Mitchell, *A Kinetic-Study of the Oxidation of L-Ascorbic-Acid (Vitamin-C) in Solution Using an Isothermal Microcalorimeter*. *Thermochimica Acta*, 1995. **264**: p. 27-40.
271. Ikari, Y., *Composition containing divalent manganese ion*. 1997, Patent App. 5,618,526.
272. Andrews, G.C., *Derivatives of L-ascorbic acid and D-erythorbic acid*. 1983, US Patent App. 4,368,330.
273. Silberberg, M.S., *Chemistry : the molecular nature of matter and change / Martin S. Silberberg*. 4th ed.. ed. 2006, Boston: Boston : McGraw-Hill.
274. Ahrens, G., *Method of preparing high concentration calcium ascorbate reaction products and products produced by same*. 1971, US Patent App. 3/755,592.
275. Schreur, C., *Method of making a solid crystalline composition consisting essentially of calcium ascorbate*. 1981, US Patent App. 4,251,449.
276. Suresh, S.J. and V.M. Naik, *Hydrogen bond thermodynamic properties of water from dielectric constant data*. *Journal of Chemical Physics*, 2000. **113**(21): p. 9727-9732.
277. Tromans, D., *Temperature and pressure dependent solubility of oxygen in water: a thermodynamic analysis*. *Hydrometallurgy*, 1998. **48**(3): p. 327-342.
278. Urquidi, J., et al., *Temperature and pressure effects on the structure of liquid water*. *Journal of Molecular Structure*, 1999. **485**: p. 363-371.
279. Guo, Y.Z., et al., *Evaporation rate of water as a function of a magnetic field and field gradient*. *Int J Mol Sci*, 2012. **13**(12): p. 16916-28.
280. Otsuka, I. and S. Ozeki, *Does magnetic treatment of water change its properties? The Journal of Physical Chemistry B*, 2006. **110**(4): p. 1509-1512.
281. Al Helal, A., et al., *Performance of erythorbic acid as an oxygen scavenger in thermally aged lean MEG*. *Journal of Petroleum Science and Engineering*, 2018. **170**: p. 911-921.
282. Miyake, N. and T. Kurata, *Autoxidation Reaction Mechanism for L-Ascorbic Acid-related Compounds in Methanol without Metal Ion Catalysis*. *Biosci Biotechnol Biochem*, 1998. **62**(4): p. 811-3.
283. March, J., *Advanced organic chemistry: reactions, mechanisms, and structure*. 1992: John Wiley & Sons.
284. Olivella, S., et al., *Mechanism of the hydrogen transfer from the OH group to oxygen-centered radicals: proton-coupled electron-transfer versus radical hydrogen abstraction*. *Chemistry*, 2004. **10**(14): p. 3404-10.
285. Gomberg, M., *An Instance of Trivalent Carbon: Triphenylmethyl*. *Journal of the American Chemical Society*, 1900. **22**(11): p. 757-771.
286. Paneth, F., *The Transmutation of Hydrogen into Helium*. *Nature*, 1927. **119**(3002): p. 706-707.
287. Paneth, F. and W. Hofeditz, *Über die Darstellung von freiem Methyl*. *Berichte der deutschen chemischen Gesellschaft (A and B Series)*, 1929. **62**(5): p. 1335-1347.
288. Anglada, J.M., *Complex mechanism of the gas phase reaction between formic acid and hydroxyl radical. Proton coupled electron transfer versus radical hydrogen abstraction mechanisms*. *J Am Chem Soc*, 2004. **126**(31): p. 9809-20.
289. Hore, P.J. and H. Mouritsen, *The Radical-Pair Mechanism of Magnetoreception*. *Annu Rev Biophys*, 2016. **45**: p. 299-344.
290. Miessler, G.L. and D.A. Tarr, *Coordination compounds*. *Inorganic chemistry*, 1999. **642**: p. 315-316.
291. Booser, E.R., *CRC Handbook of Lubrication and Tribology, Volume III: Monitoring, materials, synthetic lubricants, and applications*. Vol. 3. 1993: CRC Press.
292. Sandengen, K. and B. Kaasa, *Estimation of Monoethylene Glycol (MEG) Content in Water + MEG + NaCl + NaHCO₃ Solutions*. *Journal of Chemical & Engineering Data*, 2006. **51**(2): p. 443-447.
293. MacLeod, S.K., *Moisture determination using Karl Fischer titrations*. *Analytical chemistry*, 1991. **63**(10): p. 557A-566A.
294. Meyer Jr, A. and C. Boyd, *Determination of water by titration with coulometrically generated Karl Fischer reagent*. *Analytical Chemistry*, 1959. **31**(2): p. 215-219.

295. Peters, E. and J. Jungnickel, *Improvement in Karl Fischer Method for Determination of Water*. Analytical Chemistry, 1955. **27**(3): p. 450-453.
296. Scholz, E., *Karl Fischer titration: determination of water*. 2012: Springer Science & Business Media.
297. Porter, W.H. and A. Auansakul, *Gas-chromatographic determination of ethylene glycol in serum*. Clin Chem, 1982. **28**(1): p. 75-8.
298. Bost, R.O. and I. Sunshine, *Ethylene glycol analysis by gas chromatography*. J Anal Toxicol, 1980. **4**(2): p. 102-103.
299. Zafarani-Moattar, M.T. and N. Tohidifar, *Vapor-liquid equilibria, density, speed of sound, and viscosity for the system poly(ethylene glycol) 400+ethanol at different temperatures*. Journal of Chemical and Engineering Data, 2008. **53**(3): p. 785-793.
300. Moosavi, M., et al., *Investigation on some thermophysical properties of poly(ethylene glycol) binary mixtures at different temperatures*. Journal of Chemical Thermodynamics, 2013. **58**: p. 340-350.
301. Kolská, Z., et al., *Refractometric study of systems water-poly (ethylene glycol) for preparation and characterization of Au nanoparticles dispersion*. Arabian Journal of Chemistry, 2016.
302. Fogg, E.T., A.N. Hixson, and A.R. Thompson, *Densities and refractive indexes for ethylene glycol-water solutions*. Analytical Chemistry, 1955. **27**(10): p. 1609-1611.
303. Wiederseiner, S., et al., *Refractive-index and density matching in concentrated particle suspensions: a review*. Experiments in Fluids, 2010. **50**(5): p. 1183-1206.
304. Yang, C.S., et al., *Excess molar volumes, viscosities, and heat capacities for the mixtures of ethylene glycol plus water from 273.15 K to 353.15 K*. Journal of Chemical and Engineering Data, 2003. **48**(4): p. 836-840.
305. Trimble, H. and W. Potts, *Glycol-water mixtures vapor pressure-boiling point-composition relations*. Industrial & Engineering Chemistry, 1935. **27**(1): p. 66-68.
306. Aly, K.M. and E. Esmail, *Refractive index of salt water: effect of temperature*. Optical Materials, 1993. **2**(3): p. 195-199.
307. Chiao, T.-T. and A. Thompson, *Densities and Refractive Indices for Glycol-Water Solutions... Triethylene Glycol, Dipropylene Glycol, and Hexylene Glycol*. Analytical Chemistry, 1957. **29**(11): p. 1678-1681.
308. *Application - Water in Glycols - Keit Spectrometers*. 2017; Available from: <https://keit.co.uk/irmadillo-water-glycols/>.
309. NSTM0374, N.S., *Laboratory Screening Tests to Determine the Ability of Scale Inhibitors to Prevent the Precipitation of Calcium Sulfate and Calcium Carbonate from Solution (for Oil and Gas Production Systems)*. National Association of Corrosion Engineers, 2007.
310. Hamoshi, T.N.M.a.E.A., *The Effect of Magnetic Field on The Solubility of NaCl and CaCl₂. 2H₂O at Different Temperature and pH Values*. Basrah Journal of Agricultural Sciences, 2012. **25**(1): p. 19-26.
311. Chang, K.T. and C.I. Weng, *An investigation into the structure of aqueous NaCl electrolyte solutions under magnetic fields*. Computational Materials Science, 2008. **43**(4): p. 1048-1055.
312. Impey, R.W., P.A. Madden, and I.R. McDonald, *Hydration and Mobility of Ions in Solution*. Journal of Physical Chemistry, 1983. **87**(25): p. 5071-5083.
313. Wang, Y.F., et al., *The effect of a static magnetic field on the hydrogen bonding in water using frictional experiments*. Journal of Molecular Structure, 2013. **1052**: p. 102-104.
314. Patrick, E.L. and W.L. Vault, *Bioelectromagnetic Effects of the Electromagnetic Pulse (EMP)*. 1990, HARRY DIAMOND LABS ADELPHI MD.
315. Bassett, C.A., *Beneficial effects of electromagnetic fields*. J Cell Biochem, 1993. **51**(4): p. 387-93.
316. Tsai, M.T., et al., *Modulation of osteogenesis in human mesenchymal stem cells by specific pulsed electromagnetic field stimulation*. J Orthop Res, 2009. **27**(9): p. 1169-74.
317. Beebe, S.J., et al., *Nanosecond, high-intensity pulsed electric fields induce apoptosis in human cells*. FASEB J, 2003. **17**(11): p. 1493-5.

318. Kaszuba, M., et al., *High-concentration zeta potential measurements using light-scattering techniques*. Philos Trans A Math Phys Eng Sci, 2010. **368**(1927): p. 4439-51.
319. Pitzer, K.S. and J.M. Simonson, *Thermodynamics of Multicomponent, Miscible, Ionic Systems - Theory and Equations*. Journal of Physical Chemistry, 1986. **90**(13): p. 3005-3009.
320. Mehrbach, C., et al., *Measurement of the apparent dissociation constants of carbonic acid in seawater at atmospheric pressure I*. Limnology and Oceanography, 1973. **18**(6): p. 897-907.
321. Sandengen, K., B. Kaasa, and T. Østvold, *pH Measurements in Monoethylene Glycol (MEG) + Water Solutions*. Industrial & Engineering Chemistry Research, 2007. **46**(14): p. 4734-4739.
322. Al Helal, A., et al., *Measurement of mono ethylene glycol volume fraction at varying ionic strengths and temperatures*. Journal of Natural Gas Science and Engineering, 2018. **54**: p. 320-327.
323. Al-Gharbi, M.S., *Dynamic pore-scale modelling of two-phase flow*. 2004, Imperial College.
324. Al-Rawajfeh, A.E., et al., *Scale formation model for high top brine temperature multi-stage flash (MSF) desalination plants*. Desalination, 2014. **350**: p. 53-60.
325. Al-Anezi, K. and N. Hilal, *Scale formation in desalination plants: effect of carbon dioxide solubility*. Desalination, 2007. **204**(1-3): p. 385-402.
326. Green, D.W. and R.H. Perry, *Perry's chemical engineers' handbook*. 1999, McGraw-Hill Professional.
327. Kim, J. and C. Vipulanandan, *Effect of pH, sulfate and sodium on the EDTA titration of calcium*. Cement and Concrete Research, 2003. **33**(5): p. 621-627.
328. Kawano, M. and M. Tokonami, *Effect of organic acids on the precipitation rate and polymorphism of calcium carbonate minerals in solutions with Mg²⁺ IONS*. Clay Science, 2014. **18**(1): p. 1-10.
329. Alsaïari, H.A., *Effect of Ca²⁺ and Fe²⁺ on the precipitation of calcium carbonate and iron carbonate solid solutions and on scale inhibitors retention*. 2011, RICE University.
330. Marcus, Y., *Thermodynamics of solvation of ions. Part 5.—Gibbs free energy of hydration at 298.15 K*. Journal of the Chemical Society, Faraday Transactions, 1991. **87**(18): p. 2995-2999.
331. Waluyo, I., et al., *The structure of water in the hydration shell of cations from x-ray Raman and small angle x-ray scattering measurements*. J Chem Phys, 2011. **134**(6): p. 064513.
332. Ayrapetyan, S.N., et al., *Magnetic fields alter electrical properties of solutions and their physiological effects*. Bioelectromagnetics, 1994. **15**(2): p. 133-42.
333. Fu, S. and C.A. Lucy, *Prediction of electrophoretic mobilities. 1. Monoamines*. Anal Chem, 1998. **70**(1): p. 173-81.
334. Railsback, L.B., *Some fundamentals of mineralogy and geochemistry*. On-line book, quoted from: www.gly.uga.edu/railsback, 2006.
335. Persson, I., *Hydrated metal ions in aqueous solution: how regular are their structures?* Pure and Applied Chemistry, 2010. **82**(10): p. 1901-1917.
336. Jones, B. and M.G. Kenward, *Design and analysis of cross-over trials*. 2014: Chapman and Hall/CRC.
337. Montgomery, D.C., *Design and analysis of experiments*. 2017: John Wiley & Sons.
338. Zhou, K.X., et al., *Monte Carlo simulation of liquid water in a magnetic field*. Journal of Applied Physics, 2000. **88**(4): p. 1802-1805.
339. Jung, W.M., et al., *Particle morphology of calcium carbonate precipitated by gas-liquid reaction in a Couette-Taylor reactor*. Chemical Engineering Science, 2000. **55**(4): p. 733-747.
340. Alamdari, A. and M. Saffari, *Kinetic study of calcium carbonate precipitation in gas field brine containing methanol*. Journal of Natural Gas Science and Engineering, 2012. **5**: p. 17-24.

341. Merkel, B. and F.P.B.G. Geochemistry, *A practical Guide to modeling of Natural and Contaminated Aquatic Systems*. Volume, 2005. **1**: p. 20.
342. Langmuir, D., *Aqueous environmental geochemistry*. 1997.
343. Cowan, J.C. and D.J. Weintritt, *Water-formed scale deposits*. 1976: Gulf Publishing Company, Book Division.
344. Schwierz, N., D. Horinek, and R.R. Netz, *Anionic and cationic Hofmeister effects on hydrophobic and hydrophilic surfaces*. *Langmuir*, 2013. **29**(8): p. 2602-14.
345. Collins, K.D., *Ions from the Hofmeister series and osmolytes: effects on proteins in solution and in the crystallization process*. *Methods*, 2004. **34**(3): p. 300-11.
346. Daintith, J., *A dictionary of chemistry*. 2008: OUP Oxford.
347. Hem, J.D., *Chemical equilibria and rates of manganese oxidation*. 1963, USGPO.
348. Shen, X. *Increased dielectric constant in the water treated by extremely low frequency electromagnetic field and its possible biological implication*. in *Journal of Physics: Conference Series*. 2011. IOP Publishing.
349. Pang, X.F. and G.F. Shen, *The Changes of Physical Properties of Water Arising from the Magnetic Field and Its Mechanism*. *Modern Physics Letters B*, 2013. **27**(31): p. 1350228.
350. Flaten, E.M., *The effect of MEG (mono ethyleneglycol) on the precipitation kinetics of calcium carbonate related to natural gas production from subsea wells*, F.f.N.O.T.I.f.K.P. Norges Teknisk-Naturvitenskapelige Universitet, Editor. 2010, NTNU.
351. TM, N., *Laboratory Screening Test to Determine the Ability of Scale Inhibitors to Prevent the Precipitation of Calcium Sulfate and Calcium Carbonate from Solutions (for Oil and Gas production Systems)*. 2007. National Association of Corrosion Engineers, 2007.
352. Ryu, M., et al., *Synthesis of calcium carbonate in ethanol-ethylene glycol solvent*. *Journal of the Ceramic Society of Japan*, 2009. **117**(1361): p. 106-110.
353. Han, Y.S., et al., *Factors affecting the phase and morphology of CaCO₃ prepared by a bubbling method*. *Journal of the European Ceramic Society*, 2006. **26**(4-5): p. 843-847.
354. Krylov, O., et al., *Influence of magnetic treatment on the electrokinetic properties of a suspension of calcium carbonate*. *Coll. J. USSR*, 1985. **47**: p. 31-38.
355. Lv, W., et al., *Self-assembly and pH response of electroactive liquid core-tetra(aniline) shell microcapsules*. *Journal of Materials Chemistry B*, 2014. **2**(29): p. 4720-4725.
356. Ding, J.M. and H.J. Keh, *The Electrophoretic Mobility and Electric Conductivity of a Concentrated Suspension of Colloidal Spheres with Arbitrary Double-Layer Thickness*. *J Colloid Interface Sci*, 2001. **236**(1): p. 180-193.
357. Gouverneur, M., et al., *Direct determination of ionic transference numbers in ionic liquids by electrophoretic NMR*. *Phys Chem Chem Phys*, 2015. **17**(45): p. 30680-6.
358. Shen, D., et al. *Seawater injection, inhibitor transport and rock-brine interactions*. in *SPE International Oilfield Scale Conference*. 2008. Society of Petroleum Engineers.
359. Al Helal, A., et al., *The influence of magnetic fields on calcium carbonate scale formation within monoethylene glycol solutions at regeneration conditions*. *Journal of Petroleum Science and Engineering*, 2019. **173**: p. 158-169.
360. Soames, A., A. Barifcani, and R. Gubner, *Removal of Organic Acids during Monoethylene Glycol Distillation and Reclamation To Minimize Long-Term Accumulation (Book review)*. 2019.
361. Tran, T., et al., *Investigation of the electrochemical mechanisms for acetic acid corrosion of mild steel*. *Corrosion*, 2013. **70**(3): p. 223-229.
362. Brown, T.L., *Chemistry: the central science*. 2009: Pearson Education.
363. Kaasa, B., *Prediction of pH, mineral precipitation and multiphase equilibria during oil recovery*. 1998, Norges teknisk-naturvitenskapelige universitet.
364. Pisoschi, A.M., A.F. Danet, and S. Kalinowski, *Ascorbic acid determination in commercial fruit juice samples by cyclic voltammetry*. *Journal of Analytical Methods in Chemistry*, 2009. **2008**.
365. Institutt for energiteknikk. *Material Technology*. 2018; Available from: https://www.ife.no/en/ife/main_subjects_new/petroleum_research/corrosion.

366. Brauer, G., *Handbook of preparative inorganic chemistry*. Vol. 2. 2012: Elsevier.
367. Fukuzumi, S., T. Kobayashi, and T. Suenobu, *Formic acid acting as an efficient oxygen scavenger in four-electron reduction of oxygen catalyzed by a heterodinuclear iridium-ruthenium complex in water*. *J Am Chem Soc*, 2010. **132**(34): p. 11866-7.
368. Khurana, M., P.K. Sharma, and K.K. Banerji, *Kinetics and mechanism of the oxidation of formic and oxalic acids by quinolinium fluorochromate*. *Proceedings of the Indian Academy of Sciences-Chemical Sciences*, 2000. **112**(2): p. 73-81.
369. Suenobu, T., S. Shibata, and S. Fukuzumi, *Catalytic oxidation of formic acid by dioxygen with an organoiridium complex*. *Catalysis Science & Technology*, 2014. **4**(10): p. 3636-3639.
370. Van Haasterecht, T., et al., *Transformations of polyols to organic acids and hydrogen in aqueous alkaline media*. *Catalysis Science & Technology*, 2014. **4**(8): p. 2353-2366.
371. Blank, M. and L. Soo, *Electromagnetic acceleration of electron transfer reactions*. *J Cell Biochem*, 2001. **81**(2): p. 278-83.
372. Wine, P., R. Astalos, and R. Mauldin III, *Kinetic and mechanistic study of the hydroxyl+ formic acid reaction*. *The Journal of Physical Chemistry*, 1985. **89**(12): p. 2620-2624.
373. Jolly, G.S., et al., *Rates of hydroxyl radical reactions. Part 14. Rate constant and mechanism for the reaction of hydroxyl radical with formic acid*. *The Journal of Physical Chemistry*, 1986. **90**(24): p. 6557-6562.
374. Schenck, J.F., *The role of magnetic susceptibility in magnetic resonance imaging: MRI magnetic compatibility of the first and second kinds*. *Med Phys*, 1996. **23**(6): p. 815-50.
375. Hassan, S. and R.A. Rahman, *Effects of exposure to magnetic field on water properties and hatchability of Artemia salina*. *ARPJ Journal of Agricultural & Biological Sciences*, 2016. **11**(11): p. 416-423.
376. Amor, H.B., A. Elaoud, and M. Hozayn, *Does Magnetic Field Change Water pH?* *Asian Research Journal of Agriculture*, 2018. **8**(1): p. 1-7.
377. Chu, K.-Y. and A. Thompson, *Densities and Refractive Indices of Glycol Ether-Water Solutions*. *Journal of Chemical and Engineering Data*, 1960. **5**(2): p. 147-149.
378. Zhou, Y.H., et al., *Compositions, Densities, and Refractive Indices for the Ternary Systems Ethylene Glycol + NaCl + H₂O, Ethylene Glycol + KCl + H₂O, Ethylene Glycol + RbCl + H₂O, and Ethylene Glycol + CsCl + H₂O at 298.15 K*. *Journal of Chemical and Engineering Data*, 2010. **55**(3): p. 1289-1294.
379. Neter, J., et al., *Applied linear statistical models*. Vol. 4. 1996: Irwin Chicago.
380. Opsomer, J.D. and D. Ruppert, *Fitting a bivariate additive model by local polynomial regression*. *Annals of Statistics*, 1997. **25**(1): p. 186-211.
381. Walton, N., *Electrical conductivity and total dissolved solids—what is their precise relationship?* *Desalination*, 1989. **72**(3): p. 275-292.
382. Ordoñez, G.D., *Geochemical kinetics during CO₂ sequestration: the reactivity of the Hontomín caprock and the hydration of MgO*. Thesis, 2015.

APPENDIX A : PUBLICATIONS FROM THIS RESEARCH

Effect of Pretreatment Process on Scale Formation in the Re-Boiler Section of Monoethylene Glycol Regeneration Plant

Ammar Al Helal^{1,2,*}, Adam Soames¹, Stefan Iglauer³, Ahmed Barifcani¹, Rolf Gubner¹

¹Curtin University, Kent St, Bentley WA 6102, Perth, Australia

²Al-Khawarizmi College of Engineering, University of Baghdad, Jadriyah, Baghdad, Iraq

³Edith Cowan University, Joondalup WA, Australia

*Corresponding author: 17610661@student.curtin.edu.au

Abstract. Monoethylene glycol (MEG) regeneration plants often use pretreatment vessels to precipitate divalent cations, such as Fe^{2+} , Ca^{2+} , and Mg^{2+} , in order to avoid or reduce fouling in downstream reboilers and heat exchangers. This pretreatment process operates under alkaline conditions and moderate temperatures ($\sim 80^\circ\text{C}$) to accelerate the formation of low-solubility divalent salts. The objective of the present research was to determine whether the pretreatment process could be minimized, without negatively impacts on the MEG regeneration process from to the formation of scale on the heater bundle in the presence of low concentrations of divalent cations in the rich MEG stream. Scale formation was analyzed under MEG regeneration process conditions using a dynamic scale loop (DSL) test and verification experiments were performed in a MEG regeneration and reclamation pilot plant, both with and without pretreatment conditions. The scaling tendencies of several rich MEG-brine mixtures were evaluated at different pH pretreatment levels and dissolved CO_2 concentrations. An evaluation temperature of 180°C was chosen to match the skin temperature of the reboiler heater bundle during the MEG regeneration process. The experiments of pH 7.24 showed high amounts of precipitation scale within the reboiler due to high remaining concentrations of mineral ions. In addition, small concentrations of calcium and magnesium ions led to the precipitation of calcite, dolomite, and magnesium hydroxide on the reboiler bundle and within associated filtered outputs even when a pretreatment vessel was present. These results were confirmed by the differential pressure build-up and Scanning Electron Microscopy analyses for each experimental condition. Another interesting finding is that pH increased within the reboiler due to CO_2 gas boiling off at high operating temperatures, thus contributing to increased alkalinity levels, which in turn promoted scale formation. These results indicate that pretreatment should not be reduced, even with divalent ion concentrations as low as ~ 5 ppm TDS, due to the harsh conditions within the reboiler heater bundle.

1. Introduction

Natural gas transportation and production systems face significant operational concerns from the formation of scale, which can restrict or block flow and cause fouling issues [1, 2]. Chemical analyses and laboratory studies have shown that calcium carbonate, barium sulfate, and strontium sulfate are



Al Helal, A.; Soames, A.; Iglauer, S.; Barifcani, Gubner, R., Effect of Pretreatment Process on Scale Formation in the Re-Boiler Section of Monoethylene Glycol Regeneration Plant. in IOP Conference Series: Materials Science and Engineering. 2019. IOP Publishing.

Authors and full affiliations:

	Conception and design	Acquisition of data and method	Data conditioning and manipulation	Analysis and statistical method	Interpretation and discussion	Final approval
Ammar Al Helal	x	x	x	x	x	x
I acknowledge that these represent my contribution to the above research output						
Adam Soames				x	x	x
I acknowledge that these represent my contribution to the above research output						
Dr Stefan Iglauer				x	x	x
I acknowledge that these represent my contribution to the above research output						
Dr Ahmed Barifcani	x				x	x
I acknowledge that these represent my contribution to the above research output						
Dr Rolf Gubner	x			x	x	x
I acknowledge that these represent my contribution to the above research output						

Signature:



Signature:



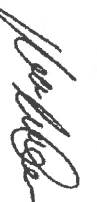
Signature:



Signature:



Signature:



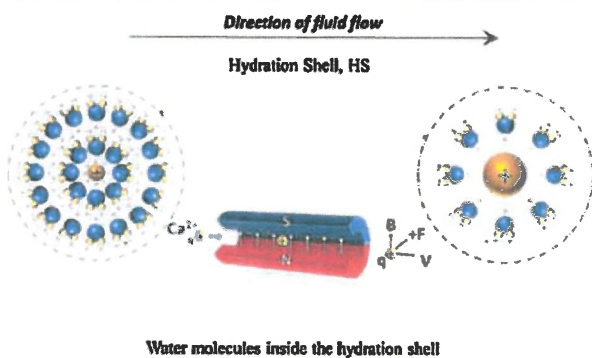


Regular Article

Influence of magnetic fields on calcium carbonate scaling in aqueous solutions at 150 °C and 1 bar

Ammar Al Helal^{a,*}, Adam Soames^a, Rolf Gubner^a, Stefan Iglauer^b, Ahmed Barifcani^a^a Chemical Engineering Department, Curtin University, Perth, W.A., Australia^b Petroleum Engineering Department, Curtin University, Perth, W.A., Australia

GRAPHICAL ABSTRACT



ARTICLE INFO

Article history:

Received 10 July 2017

Revised 7 September 2017

Accepted 7 September 2017

Available online 8 September 2017

Keywords:

Scaling

Scale inhibition

Diametrically magnetic treatment

Dynamic scale loop

DSL

ABSTRACT

The experiments performed as a part of this study were conducted to evaluate the effect of magnetic field treatment upon the scale forming tendency of brine solution composed primarily of calcium bicarbonate ions. The reported results were generated using a Dynamic Scale Loop system with the brine solution exposed to a magnetic field generated by a 6480 Gauss magnet of grade N45 SH in a diametrical orientation for 2.5 s. Following magnetic exposure, the brine solution was exposed to an elevated temperature 150 °C at 1 bar to promote the formation of scale within a capillary tube. The extent of scaling was measured by recording the differential pressure across the tube as scaling proceeded.

Three important conclusions regarding the effect of magnetic field treatment upon scale formation in calcium bicarbonate solutions were reached. Firstly, the ratio of calcium to bicarbonate plays a key role in determining how magnetic fields influence scale formation, whether promoting or inhibiting it. Solutions containing high concentrations of the bicarbonate, or equal concentrations of the bicarbonate and calcium species showed inhibited scale formation following magnetic exposure. Secondly, the electrical conductivity of the calcium carbonate solution was noticeably impacted by the exposure to the magnetic field through manipulation of the ionic hydration shell and may also provide a measure of the extent of scale formation. Finally, the application of magnetic field treatment for scale inhibition may provide an alternative eco-friendly scale inhibition strategy in place of traditional chemical scale inhibitors.

© 2017 Elsevier Inc. All rights reserved.

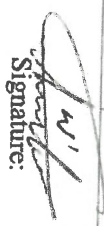
* Corresponding author.

E-mail address: ammar.waadallah@yahoo.com (A. Al Helal).

Al Helal A, Soames A, Gubner R, Iglauer S, Barifcani A. Influence of Magnetic Fields on Calcium Carbonate Scaling in Aqueous Solutions at 150° C and 1 Bar. Journal of Colloid and Interface Science. 2018;509:472-84.

Authors and full affiliations:

	Conception and design	Acquisition of data and method	Data conditioning and manipulation	Analysis and statistical method	Interpretation and discussion	Final approval
Ammar Al Helal	x	x	x	x	x	x
I acknowledge that these represent my contribution to the above research output						
Adam Soames				x	x	x
I acknowledge that these represent my contribution to the above research output						
Dr Stefan Iglauer					x	x
I acknowledge that these represent my contribution to the above research output						
Dr Rolf Gubner	x	x		x	x	x
I acknowledge that these represent my contribution to the above research output						
Dr Ahmed Barifcani	x			x	x	x
I acknowledge that these represent my contribution to the above research output						


Signature:


Signature:


Signature:


Signature:


Signature:



The influence of magnetic fields on calcium carbonate scale formation within monoethylene glycol solutions at regeneration conditions

Ammar Al Helal^{a,c,*}, Adam Soames^a, Stefan Iglauer^b, Rolf Gubner^a, Ahmed Barifcani^a

^a WA School of Mines: Minerals, Energy and Chemical Engineering, Curtin University, Perth, W.A, Australia

^b School of Engineering, Edith Cowan University, Joondalup, W.A, Australia

^c Al-Khawarizmi College of Engineering, University of Baghdad, Jadriyah, Baghdad, Iraq

ARTICLE INFO

Keywords:

Magnetic fields
MEG
Calcium carbonate
Morphology
Scale formation
Dynamic scale loop

ABSTRACT

One of the most discussed topics related to the effects of external magnetic fields (MF) on aqueous solutions is the influence on the scale formation of calcium carbonate (CaCO_3). However, the extent of the effect of these forces on the scale formation in the non-aqueous solutions has not been investigated so far. So MFs will be applied to non-aqueous mixtures to find out the behavior of scale formation. This study presents the results of inorganic scale formation within MEG solutions containing Ca^{2+} and HCO_3^- ions, which has been investigated using both static and dynamic scale loop (DSL) evaluation techniques. Furthermore, the influence of MFs on scale formation using the dynamic technique has also been studied. Results were generated using brine/MEG solutions exposed to an external MF produced by a 0.65 T Neodymium magnet for 2.5 s. The degree of scale formation was examined by measuring the pressure build-up across a capillary coil as scale was developed. Moreover, differences in CaCO_3 morphologies were evaluated for the exposed and blank trials via the DSL technique and compared with the results obtained from the static scale evaluation method.

The results of this research have demonstrated that the short exposure (2.5 s) to a powerful MF can significantly reduce scale-formation in the rich MEG solutions within the capillary coil. This is due to the alteration of the proton spin inversion in the field of diamagnetic salts. Furthermore, a significant difference in CaCO_3 morphology was observed for the scale formed during dynamic and static conditions. The generating results help to reduce the use of chemical scale inhibitors with MEG solution during the gas hydrate treatments, especially when the concentration of MEG in formation water is low and scale formation is more likely to occur.

1. Introduction

Calcium carbonate is a common mineral scale experienced in a wide range of industries including water treatment (Al Helal et al., 2018a; Amjad, 2010), paper mill industries (Dickinson et al., 2002), cooling water systems (Moriarty et al., 2001), natural gas transportation pipelines and MEG regeneration systems following the breakthrough of formation water (Babu et al., 2015; Yong and Obanijesu, 2015). The formation of CaCO_3 occurs upon the surface of heat transfer equipment operating at high temperatures, such as heat exchangers and reboilers, leading to reduced heat transfer efficiency (Yang et al., 2001) and potential blockages or restrictions of flow along the inner surfaces of pipelines and tubing (Amjad, 2010; Chilingar et al., 2013). Several studies have been conducted to investigate the scale formation behavior of CaCO_3 by examining various characteristics including crystalline phase, size distribution, and morphology (Muryanto et al., 2014; Flaten et al.,

2009; Gorna et al., 2008). The saturation index (SI) of calcium and carbonate ions have been the subject of extensive prior studies and represent a key factor in determining the tendency of CaCO_3 to form (Al Helal et al., 2018a; Dai et al., 2016).

Muryanto et al. (Muryanto et al., 2014) reported that CaCO_3 crystals are formed in three anhydrous polymorphs: calcite, aragonite, and vaterite. Calcite is known as the most stable form of CaCO_3 crystal while aragonite and vaterite exhibit poor thermodynamic stability with the potential to convert to calcite after readjustment of certain conditions including fluid pH, temperature, supersaturation, and the presence of additives (Muryanto et al., 2014; Hu et al., 2015). For instance, Hu et al. (Hu et al., 2015) reported that at pH 9.0, the anhydrous polymorph (vaterite) is more likely to form compared to the hydrated polymorphs of CaCO_3 such as monohydrate and hexahydrate (ikaite), which forms at high pH conditions of approximately 13.4 and greater within low temperature (Hu et al., 2015). However, in the presence of

* Corresponding author. WA School of Mines: Minerals, Energy and Chemical Engineering, Curtin University, Perth, W.A, Australia.

E-mail address: a.ahmed11@postgrad.curtin.edu.au (A. Al Helal).

<https://doi.org/10.1016/j.petrol.2018.09.100>

Received 30 July 2018; Received in revised form 28 September 2018; Accepted 29 September 2018

Available online 09 October 2018

0920-4105/ © 2018 Elsevier B.V. All rights reserved.

Al Helal A, Soames A, Iglauer S, Gubner R, Barficani A. The influence of magnetic fields on calcium carbonate scale formation within monoethylene glycol solutions at regeneration conditions. Journal of Petroleum Science and Engineering. 2019;173:158-69.

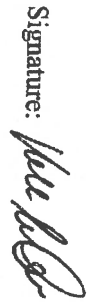
Authors and full affiliations:

	Conception and design	Acquisition of data and method	Data conditioning and manipulation	Analysis and statistical method	Interpretation and discussion	Final approval
Ammar Al Helal	x	x	x	x	x	x
I acknowledge that these represent my contribution to the above research output						
Adam Soames				x	x	x
I acknowledge that these represent my contribution to the above research output						
Dr Stefan Iglauer					x	x
I acknowledge that these represent my contribution to the above research output						
Dr Rolf Gubner	x	x		x	x	x
I acknowledge that these represent my contribution to the above research output						
Dr Ahmed Barficani	x			x	x	x
I acknowledge that these represent my contribution to the above research output						

Signature: 

Signature: 

Signature: 

Signature: 

Signature: 



Evaluating chemical-scale-inhibitor performance in external magnetic fields using a dynamic scale loop



Ammar Al Helal^{a,b,*}, Adam Soames^a, Stefan Iglauer^c, Rolf Gubner^a, Ahmed Barifcani^a

^a WA School of Mines: Minerals, Energy and Chemical Engineering, Curtin University, Perth, W.A, Australia

^b Al-Khawarizmi College of Engineering, University of Baghdad, Jadriyah, Baghdad, Iraq

^c Petroleum Engineering Department, Edith Cowan University, Joondalup, W.A, Australia

Keywords:

Monoethylene glycol
Chemical scale inhibitor
Magnetic-field treatment
Scale formation
Electrical conductivity
Zeta potential

ABSTRACT

Monoethylene glycol (MEG) is extensively used in oil and gas pipelines to prevent the formation of gas hydrates. However, the injection of MEG may inadvertently contribute to mineral-ion precipitation through reduced solubility of ionic species and operation under alkaline conditions for corrosion control. As a result, the injection of chemical scale inhibitors (CSI) to manage scaling is often required. Non-chemical inhibitors, such as external magnetic fields (MFs) have also been shown to inhibit scaling in aqueous solutions. With this in mind, we investigated the combined application of CSIs and MF treatment to study the formation of scale under conditions representative of a MEG regeneration system's reboiler, a system under a high risk of scale formation. Two commercial CSIs were examined in the presence and absence of a 0.650-T external MF using a dynamic-scale-loop device. The CSIs were injected into ionic solutions containing 1656.9 ppm calcium ions and 2628 ppm carbonate ions in aqueous MEG (80 vol%), and experiments were performed at 130 °C and pH 9.5. Despite the presence of a CSI, the MF promoted scale formation and afforded a stable calcium carbonate phase morphology at high MEG concentrations. Moreover, the zeta potential under the applied MF was lower than that in the absence of the MF, which led to greater scaling, implying that the magnetic field had an ionic interfacial effect. These results provide significant insight into the effect of a MF on scale formation, irrespective of the use of a CSI, and help to interpret the effects of various treatments for scale removal or the prevention of scale formation during the MEG regeneration process.

1. Introduction

Inorganic deposits (scale) in oil and gas pipelines are one of the most critical problems encountered in the oil and gas industry owing to their direct adverse impact on flow assurance, which ultimately leads to a decrease in production (Babu et al., 2015; Wang et al., 2013). Scale can form due to changes in operating conditions; i.e., temperature, pressure, pH, and the use of additives such as gas-hydrate inhibitors (Yong and Obanijesu, 2015; BARAKA-Lokmane et al., 2012; Østvold and Randhol, 2001, Flaten et al., 2015). The primary source of mineral ions that form scale is the seawater injected into oil wells or formation water breakthrough during oil production (Shen et al., 2008; Halvorsen et al., 2007). For instance, sulfate scale is formed during recovery operations following the downhole injection of seawater, which is used to increase wellhead pressure and prompt production flow (Amiri et al., 2013;

Bader, 2006). Meanwhile, carbonate scales are formed following the breakthrough of formation water through the mixing of different mineral ions, such as calcium, magnesium, and barium, present in the formation water with the carbonate ions formed under alkaline conditions from dissolved CO₂ gas (Halvorsen et al., 2007). On-shore analyses using scanning electron microscopy (SEM), X-ray diffraction (XRD), and chemical analysis have shown that the most common scale deposit in most oil fields is CaCO₃ (Flaten et al., 2009; Kan et al., 2005; Yong and Obanijesu, 2015).

Furthermore, during oil and gas recovery operations, gas-hydrate inhibitors are often injected to prevent the formation of hydrates that hinder hydrocarbon flow in transportation pipelines (Yong and Obanijesu, 2015; Brustad et al., 2005; Sandengen, 2006; Tomson et al., 2002; Soames et al., 2018; Halvorsen et al., 2007). However, gas-hydrate inhibitors such as monoethylene glycol (MEG), lower the

Abbreviations: CSI, chemical scale inhibitor; DSL, dynamic-scale-loop device; EC, electrical conductivity; HEDP, 1-hydroxyethane-1,1-diphosphonic acid; MEG, monoethylene glycol; MF, magnetic field; SEM, scanning electron microscopy; XRD, X-ray diffraction

* Corresponding author. WA School of Mines: Minerals, Energy and Chemical Engineering, Curtin University, Perth, W.A, Australia.

E-mail address: 17610661@student.curtin.edu.au (A. Al Helal).

<https://doi.org/10.1016/j.petrol.2019.04.093>

Received 10 November 2018; Received in revised form 26 April 2019; Accepted 26 April 2019

Available online 05 May 2019

0920-4105/ © 2019 Elsevier B.V. All rights reserved.

Al Helal A, Soames A, Iglauer S, Gubner R, Barifani A. Evaluating chemical-scale-inhibitor performance in external magnetic fields using a dynamic scale loop. Journal of Petroleum Science and Engineering. 2019;179:1063-77.

Authors and full affiliations:

	Conception and design	Acquisition of data and method	Data conditioning and manipulation	Analysis and statistical method	Interpretation and discussion	Final approval
Ammar Al Helal	x	x	x	x	x	x
I acknowledge that these represent my contribution to the above research output						
Adam Soames				x	x	x
I acknowledge that these represent my contribution to the above research output						
Dr Stefan Iglauer					x	x
I acknowledge that these represent my contribution to the above research output						
Dr Rolf Gubner	x	x		x	x	x
I acknowledge that these represent my contribution to the above research output						
Dr Ahmed Barifani	x			x	x	x
I acknowledge that these represent my contribution to the above research output						

Adam Soames
Signature:

Stefan Iglauer
Signature:

Rolf Gubner
Signature:

Ahmed Barifani
Signature:

A. S. Soames
Signature:



Performance of erythorbic acid as an oxygen scavenger in thermally aged lean MEG

Ammar Al Helal^{a,b,*}, Adam Soames^a, Rolf Gubner^a, Stefan Iglauer^c, Ahmed Barifcani^a

^a WA School of Mines: Minerals, Energy and Chemical Engineering, Curtin University, Perth, W.A., Australia

^b Al-Khawarizmi College of Engineering, University of Baghdad, Jadriyah, Baghdad, Iraq

^c Petroleum Engineering Department, Edith Cowan University, Joondalup, W.A., Australia

ARTICLE INFO

Keywords:

Oxygen scavenger
Mono-ethylene glycol
Salts
Corrosion
Erythorbic acid

ABSTRACT

The objective of this work is to further evaluate the performance of the erythorbic acid oxygen scavenger designed by (Kundu and Seiersten, 2017) within 85% wt. Thermally Aged Lean Mono Ethylene Glycol (TAL-MEG). Experiments were performed at two levels of dissolved oxygen concentrations including 1000 ppb and > 7500 ppb at pH values of 6, 9 and 11. Furthermore, the erythorbic acid oxygen scavenger was evaluated under conditions representative of an industrial MEG regeneration system in terms of salt and organic acid concentrations to replicate field usage. Strong performance of erythorbic acid in combination with manganese and diethylethanolamine (DEAE) was observed under field conditions suggesting that erythorbic acid may provide an attractive alternative oxygen scavenger for use in the oil and gas industry in place of traditional sulfite based scavengers.

However, the results generated within TAL-MEG showed a reduction in the performance of erythorbic acid oxygen scavenger when compared to fresh MEG solution. Moreover, results confirmed that varying acetic acid concentration did not affect oxygen scavenger performance within TAL-MEG. It was observed that the pH of the solution was the primary factor in determining the performance of the erythorbic oxygen scavenger tested with insufficient oxygen removal achieved at a pH of 6. In contrast, strong performance was achieved at pH 9 and 11 successfully reaching below 20 ppb dissolved oxygen concentration within a reasonable timeframe with little to no impact due to the presence of mineral salt ions and organic acids.

1. Introduction

Mono Ethylene Glycol (MEG) is well known in the oil and gas industry as a hydrate inhibitor by controlling gas hydrate formation profile (AlHarooni et al., 2015, 2016; Baraka-Lokmane et al., 2012; Halvorsen et al., 2007; Joosten et al., 2007; Sandengen, 2006). MEG is favoured as an alternative gas hydrate inhibitor in place of methanol and ethanol due to its high thermal stability, non-flammable nature with a high flash point and relatively lower solubility in the gas phase (Bikkina et al., 2012; Lehmann et al., 2014; Lu et al., 2010). To achieve continuous gas hydrate inhibition and sustained flow assurance, the continual dosage of MEG solution is required. In such systems, MEG solution is often regenerated to minimize operational costs and inventory requirements (Lehmann et al., 2014; Sandengen, 2006; Yong and Obanijesu, 2015). To recover MEG at a concentration suitable for reinjection back into hydrocarbon transportation pipelines (typically above 80% wt.), regeneration occurs using onshore or topsides facilities to remove excess water and contaminants including mineral salt ions

(Platen et al., 2015; Halvorsen et al., 2007; Joosten et al., 2007; Pojtanabuntoeng et al., 2017; Sandengen, 2006).

However, during the regeneration process if MEG is exposed to high temperatures and/or excessive oxygen levels degradation of the MEG may occur (AlHarooni et al., 2015, 2016; Kundu and Seiersten, 2017; Yong and Obanijesu, 2015). The thermal degradation of MEG may result in the formation of organic acids including glycolic, acetic and formic acids. These organic acids represent a limitation in the number of MEG regeneration cycles that can be performed before replacement is required (AlHarooni et al., 2015; Haque, 2013; Nazzar and Keogh, 2006) if the build-up is not being otherwise managed by removal of the organic acids from the closed glycol loop on a continuous basis. Numerous studies in the oil and gas industry have been conducted to evaluate the effects of MEG thermal aging on various operational parameters, such as regeneration temperature (AlHarooni et al., 2016; King et al., 2017), pH (Clifton et al., 1985; Rossiter et al., 1985), organic acid formation (Clifton et al., 1985; Rossiter et al., 1985), corrosion rate (AlHarooni et al., 2016; Rossiter et al., 1985), gas hydrate

* Corresponding author. WA School of Mines: Minerals, Energy and Chemical Engineering, Curtin University, Perth, W.A., Australia.
E-mail address: 17610561@student.curtin.edu.au (A. Al Helal).

<https://doi.org/10.1016/j.petrol.2018.06.073>

Received 13 December 2017; Received in revised form 5 June 2018; Accepted 24 June 2018

Available online 28 June 2018

0920-4105/ © 2018 Elsevier B.V. All rights reserved.

Al Helal A, Soames A, Gubner R, Iglauer S, Barficani A. Performance of erythorbic acid as an oxygen scavenger in thermally aged lean MEG. Journal of Petroleum Science and Engineering. 2018;170:911-21.

Authors and full affiliations:

	Conception and design	Acquisition of data and method	Data conditioning and manipulation	Analysis and statistical method	Interpretation and discussion	Final approval
Ammar Al Helal	x	x	x	x	x	x
I acknowledge that these represent my contribution to the above research output						
Adam Soames	x	x		x	x	x
I acknowledge that these represent my contribution to the above research output						
Dr Stefan Iglauer					x	x
I acknowledge that these represent my contribution to the above research output						
Dr Rolf Gubner	x	x		x	x	x
I acknowledge that these represent my contribution to the above research output						
Dr Ahmed Barficani	x			x	x	x
I acknowledge that these represent my contribution to the above research output						

Signature: [Handwritten Signature]
Signature:

Signature: [Handwritten Signature]
Signature:

Signature: [Handwritten Signature]
Signature:

Signature: [Handwritten Signature]
Signature:

Signature: [Handwritten Signature]
Signature:

Performance of erythorbic acid as an oxygen scavenger in salted fresh and degraded monoethylene glycol under a magnetic memory effect

Ammar Al Helal^{1,2} | Stefan Iglauer³ | Rolf Gubner¹ | Ahmed Barifcani¹

¹WA School of Mines: Minerals, Energy and Chemical Engineering, Curtin University, Perth, WA, Australia

²Al-Khwarizmi College of Engineering, University of Baghdad, Baghdad, Iraq

³Petroleum Engineering Department, Edith Cowan University, Joondalup, WA, Australia

Correspondence

Ammar Al Helal, WA School of Mines: Minerals, Energy and Chemical Engineering, Curtin University, Perth, WA, Australia.
Email: 17610661@student.curtin.edu.au

Funding information

Department of Chemical Engineering; Curtin Corrosion Engineering Industry Centre

Abstract

Studies show that erythorbic acid is an effective oxygen scavenger in the food industry, thereby suggesting its potential for use in monoethylene glycol (MEG) regeneration systems. However, its performance under magnetic memory effects has not been studied. This study was conducted with 85-vol.% fresh MEG (F-MEG) and degraded MEG (D-MEG) solutions, preadjusted to pH 9.0 and pretreated with a magnetic field (MF). Two oxygen concentrations, ~7,000 and ~1,000 ppb, high-salinity concentrations (HF-MEG and HD-MEG), and organic acids were also employed. The applied MF strength, generated by a cylindrical permanent magnet, was ~0.65 T.



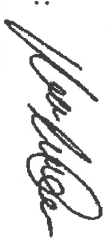

The erythorbic acid scavenging performance was enhanced upon exposure of the HF-MEG solutions to an MF. Conversely, the magnetized salt-free D-MEG solutions displayed a lower scavenging performance than the nonmagnetized solutions: Oxygen removal was more effective in the D-MEG solutions than in the HF-MEG solutions, regardless of magnetization, due to formic acid formation during the thermal oxidization process. Furthermore, the magnetized HF-MEG solutions exhibited a progressive increase in pH over time, whereas the nonexposed and D-MEG solutions presented different responses. Iron ions, acting as metal catalysts, also affected the oxygen scavenging performance in the D-MEG tests. The results suggest that the erythorbic acid scavenging performance can be improved by promoting the forward reaction using an MF. In addition, in the presence of erythorbic acid and only under specific conditions, formic acid can be used as secondary oxygen scavenger in oil and gas industry. Stable alkaline conditions are also necessary to achieve better scavenging performance. These results can be attributed to the influence of the MF on the spin state mechanism, given that the electron spin dynamics are affected by the Zeeman effect.

KEYWORDS

degraded monoethylene glycol, erythorbic acid, formic acid, fresh monoethylene glycol, magnetic memory effect, oxygen scavenger

Al Helal A, Iglauer S, Gubner R, Barifciani A, Performance of erythorbic acid as an oxygen scavenger in salted fresh and degraded monoethylene glycol under a magnetic memory effect. Asia-Pacific Journal of Chemical Engineering 2019, 14 (5), e2364.

Authors and full affiliations:

	Conception and design	Acquisition of data and method	Data conditioning and manipulation	Analysis and statistical method	Interpretation and discussion	Final approval
Ammar Al Helal	x	x	x	x	x	x
I acknowledge that these represent my contribution to the above research output						
 Signature:						
Dr Stefan Iglauer				x	x	x
I acknowledge that these represent my contribution to the above research output						
 Signature:						
Dr Rolf Gubner	x				x	
I acknowledge that these represent my contribution to the above research output						
 Signature:						
Dr Ahmed Barifciani	x			x	x	x
I acknowledge that these represent my contribution to the above research output						
 Signature:						



Contents lists available at ScienceDirect

Journal of Natural Gas Science and Engineering

journal homepage: www.elsevier.com/locate/jngse

Measurement of mono ethylene glycol volume fraction at varying ionic strengths and temperatures

Ammar Al Helal^{a,*}, Adam Soames^a, Rolf Gubner^a, Stefan Iglauer^b, Ahmed Barifcani^a^a WA School of Mines: Minerals, Energy and Chemical Engineering, Curtin University, Perth W.A., Australia^b Petroleum Engineering Department, Edith Cowan University, Perth W.A., Australia

ARTICLE INFO

Keywords:

MEG volume fraction
MEG field measurement
MEG regeneration
Refractive index
Electrical conductivity
Ionic strength

ABSTRACT

The estimation of Mono Ethylene Glycol (MEG) concentration is an essential criterion during the industrial regeneration of MEG to evaluate the efficiency of regeneration process and to control the concentration of MEG reinjected at the wellhead. Although many laboratory methods to determine MEG concentration exist, their application may be costly in terms of the time required to perform sampling and laboratory analysis. For this reason, an alternative method for determination of MEG concentrations has been proposed. This method can be performed on-site utilizing physical properties that can be readily measured using portable measurement devices including refractive index (n_D), electrical conductivity (EC) and total dissolved solids (TDS).

The volume fraction (F_m), n_D , EC, and TDS of MEG solutions have been measured at (283.15, 298.15, and 323.15) K, (10–100) vol. %, and at (0, 0.125, 0.25, 0.5, 1.0) M NaCl total volume of solution) ionic strength (IS). The experimental results were then correlated to develop a simplistic model capable of estimating the volume fraction of MEG mixtures at varying ionic strengths. The proposed models will therefore allow a quick and convenient method for the determination of MEG concentrations in the field to quickly identify undesirable changes in produced lean MEG concentration.

1. Introduction

Hydrate inhibitors play a major role in sustaining the flow of hydrocarbon products within the transportation pipelines preventing the formation of natural gas hydrates (Brustad et al., 2005; Flaten et al., 2010; Lu et al., 2010; Latta et al., 2013; Mazloum et al., 2011; Kaasa et al., 2005). The oil and gas industry has recently begun to adopt the use of Mono-Ethylene Glycol (MEG) as an efficient gas hydrate inhibitor in place of the traditional hydrate inhibitors, including ethanol and methanol (AlHarooni et al., 2015; Brustad et al., 2005). Although MEG is more expensive, the switchover has occurred due to the ability to regenerate and reuse MEG following the hydrate inhibition process without significant changes in its inhibition properties, therefore, reducing operational costs (Zaboon et al., 2017; Brustad et al., 2005). Following the injection of MEG at the wellhead, it is separated onshore alongside the condensed water phase and subsequently regenerated to regain a typical purity above 80 wt % MEG (Zaboon et al., 2017; Halvorsen et al., 2007; Brustad et al., 2005). Furthermore, the regeneration process can be utilized to remove mineral ions and organic acids present in formation water and other process chemicals, including scale and corrosion inhibitors (Halvorsen et al., 2007; Flaten et al.,

2010; Latta et al., 2013).

The measurement of the MEG concentration is an important criterion during the regeneration process to evaluate the efficiency of the distillation system and to control the MEG concentration injected into the pipeline (Zaboon et al., 2017; Sandengen, 2006; Sandengen and Kaasa, 2006). However, conventional methods of MEG concentration measurement during the operational process pose a significant challenge to plant operators (Sandengen, 2006; Sandengen and Kaasa, 2006). The main obstacles faced by the plant operators in accurately determining the concentration of MEG can be summarized as: 1) the time required to determine MEG concentration, which may involve shipping samples to an external laboratory for analysis, 2) the accuracy of the measurement after dilution to reach the limits of the testing devices, 3) the flexibility of the measurement process under different conditions, and finally, 4) the presence of mineral ions and impurities dissolved within the solution, which may cause inaccuracy of the measurement (Sandengen and Kaasa, 2006).

Numerous researchers have suggested the adoption of Karl Fischer's method for the determination of water content, and hence, the concentration of MEG (MacLeod, 1991; Meyer Jr and Boyd, 1959; Peters and Jungnickel, 1955; Scholz, 2012). While others have suggested

* Corresponding author.

E-mail address: a.ahmed11@posigrad.curtin.edu.au (A. Al Helal).<https://doi.org/10.1016/j.jngse.2018.04.012>

Received 4 August 2017; Received in revised form 9 April 2018; Accepted 11 April 2018

Available online 16 April 2018

1875-5100/ Crown Copyright © 2018 Published by Elsevier B.V. All rights reserved.


Al Helal A, Soames A, Gubner R, Iglauer S, Barifcani A. Measurement of mono ethylene glycol volume fraction at varying ionic strengths and temperatures. Journal of Natural Gas Science and Engineering. 2018;54:320-7.

Authors and full affiliations:

	Conception and design	Acquisition of data and method	Data conditioning and manipulation	Analysis and statistical method	Interpretation and discussion	Final approval
Ammar Al Helal	x	x	x	x	x	x
I acknowledge that these represent my contribution to the above research output						
Adam Soames				x	x	x
I acknowledge that these represent my contribution to the above research output						
Dr Stefan Iglauer					x	x
I acknowledge that these represent my contribution to the above research output						
Dr Rolf Gubner	x	x		x	x	x
I acknowledge that these represent my contribution to the above research output						
Dr Ahmed Barifcani	x			x	x	x
I acknowledge that these represent my contribution to the above research output						


Signature:

Signature: 

Signature: 

Signature: 

Signature: 



Operation of a MEG pilot regeneration system for organic acid and alkalinity removal during MDEA to FFCI switchover



Adam Soames^{a,*}, Edith Odeigah^a, Ammar Al Helal^a, Sami Zaboon^a, Stefan Iglauer^b, Ahmed Barifcani^a, Rolf Gubner^a

^a WA School of Mines: Minerals, Energy and Chemical Engineering, Curtin University, Perth W.A., Australia

^b Petroleum Engineering Department, Edith Cowan University, Perth W.A., Australia

ARTICLE INFO

Keywords:

Mono-ethylene glycol
Distillation
Corrosion
MDEA
Organic acids
Film forming corrosion inhibitors

ABSTRACT

The switch over from pH stabilisation using MDEA to film forming corrosion inhibitors (FFCI) may be beneficial following formation water breakthrough during hydrocarbon transportation and processing to prevent scaling at elevated pH and to extend the operational lifespan of a field. Where formation water is present, organic acids including acetic can be expected within MEG regeneration systems and can impose a corrosion risk together with carbon dioxide. A case study was performed to evaluate the potential of simultaneous removal of organic acids and MDEA/alkalinity during the switch over from pH stabilisation to film forming corrosion inhibitors (FFCI). Experimental testing was conducted using a MEG pilot regeneration plant operated by the Curtin Corrosion Engineering Industry Centre. Sufficient removal of organic acids was achieved to prevent accumulation within the MEG regeneration loop and subsequent corrosion issues through distillation by lowering the pH of the rich glycol feed to six to promote removal of organic acids with the water distillate. Simultaneously, removal of MDEA and reduction of lean glycol alkalinity was achieved through the reclamation system to facilitate FFCI switchover more rapidly than a comparative industrial operational methodology.

1. Introduction

The formation of natural gas hydrates in hydrocarbon transportation pipelines represents a major flow assurance concern with major implications upon safe and economical process operation. The inhibition of hydrate formation is of critical importance in maintaining process flow and the prevention of damage to process equipment and piping. The annual cost associated with preventing hydrate formation has been estimated to be greater than \$500 million through inhibition by methanol injection alone (Daraboina et al., 2013). In many recent oil and gas developments, Mono-Ethylene Glycol (MEG) has seen increasing popularity replacing methanol as the thermodynamic hydrate inhibitor of choice (Haghighi et al., 2009; Pojtanabuntoeng et al., 2017; Zaboon et al., 2017). The preference for MEG over methanol stems from its low volatility, toxicity and flammability, favourable thermodynamic behaviour and simple and proven technology requirements (Bikkina et al., 2012; Haque, 2012).

Post hydrate inhibition, the recovery and reuse of MEG is essential due to the significant volume required to provide effective hydrate control, its high cost and its effects on downstream processes (Haghighi et al., 2009; Pojtanabuntoeng et al., 2017; AlHarouni et al., 2015).

Following the three-phase separation from gaseous and liquid hydrocarbons, MEG is removed in combination with water and must be regenerated before it is recycled back to the wellhead for reinjection. The regeneration of MEG is typically performed by distillation to remove surplus water in order to regain a glycol purity between 80 and 90% by weight (Latta et al., 2013; Carroll, 2003).

Alongside hydrate inhibition, the prevention of corrosion in piping and processing systems is a critical aspect of hydrocarbon flow assurance. The majority of natural gas pipelines are manufactured from carbon steel and are susceptible to 'sweet' corrosion due to the presence of carbon dioxide and free water during transport and processing (Pojtanabuntoeng et al., 2017; Papavinasam et al., 2007; Nam et al., 2014). The annual global cost associated with corrosion has been estimated by Koch et al. (Koch et al., 2017) at roughly US \$2.5 trillion with up to 60% of corrosion experienced in the oil and gas industry resulting from CO₂ based corrosion (López et al., 2003). To combat corrosion in hydrocarbon pipelines two methods of corrosion control can be applied including the injection of film forming corrosion inhibitors (FFCI) and/or pH stabilisers (Pojtanabuntoeng et al., 2017; Latta et al., 2013; Dong et al., 2008). The presence of MEG itself has also been shown to impede CO₂ corrosion of carbon steels (Pojtanabuntoeng et al., 2017;

* Corresponding author.

E-mail address: Adam.Soames@postgrad.curtin.edu.au (A. Soames).

<https://doi.org/10.1016/j.petrol.2018.05.047>

Received 3 February 2018; Received in revised form 1 May 2018; Accepted 16 May 2018

Available online 18 May 2018

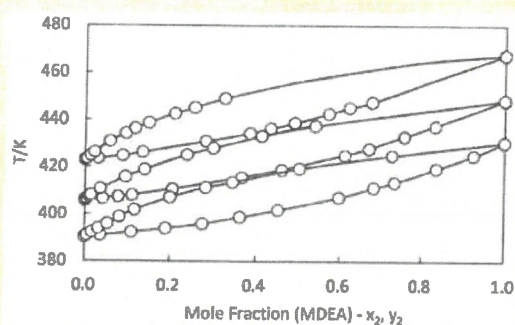
0920-4105/ © 2018 Elsevier B.V. All rights reserved.

Experimental Vapor–Liquid Equilibrium Data for Binary Mixtures of Methyldiethanolamine in Water and Ethylene Glycol under Vacuum

Adam Soames,^{*,†} Ammar Al Helal,[†] Stefan Iglauer,[‡] Ahmed Barifcani,[†] and Rolf Gubner[†][†]WA School of Mines: Minerals, Energy and Chemical Engineering, Curtin University, Bentley Western Australia 6102, Australia[‡]Petroleum Engineering Department, Edith Cowan University, Joondalup Western Australia 6027, Australia

Supporting Information

ABSTRACT: Methyldiethanolamine (MDEA) is a widely used chemical in the natural gas processing industry as a solvent for CO₂ and H₂S capture and as a basic compound for pH stabilization corrosion control. During pH stabilization corrosion control, the removal of MDEA during the (mono)ethylene glycol (MEG) regeneration process may occur under vacuum conditions during reclamation in which the removal of salt cations is performed. Isobaric vapor–liquid equilibrium data for the binary MEG–MDEA system is presented at (20, 10 and 5) kPa and water–MDEA system at (40, 20, 10) kPa to simulate its behavior during MEG reclamation under vacuum. Vapor and liquid equilibrium concentrations of MDEA were measured using a combination of ion chromatography and refractive index. The generated experimental VLE data were correlated to the UNIQUAC, NRTL, and Wilson activity coefficient models, and the respective binary parameters were regressed.



INTRODUCTION

Ethylene glycol (EG) and *N*-methyldiethanolamine (MDEA) are common chemicals used in the natural gas processing industry. The injection of EG is performed to prevent the formation of natural gas hydrates within transportation pipelines.^{1–3} Whereas MDEA and other alkanolamines are typically used as chemical absorbents for the removal of carbon dioxide and hydrogen sulfide during natural gas processing.^{4,5} Furthermore, the application of MDEA within natural gas transportation extends to its use as a basic compound suitable for pH stabilization corrosion control.^{2,6}

pH stabilization corrosion control is performed to promote the formation of an iron carbonate protective film by artificially increasing the system pH.^{2,6–8} MDEA as a pH stabilizer may be preferable to salt based (hydroxide or carbonate) chemicals because of its ability to be recovered during vacuum reclamation minimizing operational losses and dosing requirements.^{2,9} Moreover, the thermal stability of MDEA is advantageous during industrial EG regeneration where exposure to high temperature (120–140 °C)³ is required allowing multiple regeneration cycles before thermal degradation occurs.^{10,11}

Vacuum reclamation is often performed to prevent the accumulation of salts within the EG regeneration loop.^{12–14} The vacuum reclamation process entails the vaporization of EG to remove nonvolatile salt compounds. Vacuum reclamation of EG is typically performed at low pressure (≈ 100 mbar^{12,15,16}) to minimize the required operational temperature (120–150 °C^{13,16}). Low temperature vaporization of EG is desired to prevent its degradation.^{14,15} However, the vacuum reclamation process may

inadvertently lead to MDEA losses due its higher boiling point in comparison to EG. Therefore, ensuring the vaporization of MDEA alongside EG is an important aspect of EG regeneration during pH stabilization to minimize MDEA losses.

Alternatively, the removal of MDEA within EG regeneration systems operating under pH stabilization control is essential following formation water breakthrough.^{14,15} The combined presence of MDEA (high pH) and divalent cations including calcium, magnesium, and barium presents a scaling risk within both transportation lines and equipment operating at high temperature (heat exchangers, EG regeneration system).^{14,17} MDEA will react in the presence of CO₂ to form bicarbonate^{2,14,17} facilitating the formation of scaling products including CaCO₃. pH stabilization chemicals such as MDEA must therefore be removed to facilitate switch over to more scaling friendly film forming corrosion inhibitors (FFCIs). The removal of MDEA can be achieved via vacuum reclamation systems alongside mineral salts.¹⁴

Therefore, knowledge of the vapor–liquid equilibrium (VLE) of MDEA with respect to EG at low pressure is essential for the design of separation equipment. Current literature for MDEA VLE data in EG and water solutions is limited at the low-pressure conditions necessary for EG vacuum reclamation. This work outlines the VLE of MDEA with respect to water and EG under low pressure conditions (40–10 kPa) and (20–5 kPa), respectively. However, the operating conditions of reclamation

Received: January 16, 2018

Accepted: March 21, 2018

Published: March 28, 2018



Oxygen scavenging performance of carboxylic acids formed during the degradation of monoethylene glycol regeneration products

Ammar Al Helal^{a,b,*}, Peter Milner^a, Ahmed Barifcani^a

^a WA School of Mines: Minerals, Energy and Chemical Engineering, Curtin University, Perth, W.A, Australia

^b Al-Khwarizmi College of Engineering, University of Baghdad, Jadriyah, Baghdad, Iraq

ARTICLE INFO

Article history:

Received 21 October 2019

Received in revised form 13 February 2020

Accepted 17 February 2020

Available online 25 February 2020

Keywords:

Salty aged lean MEG

Oxygen scavenger

Formic acid

Glycolic acid

DEHA

MEKO

Degraded MEG product

Natural gas processing

ABSTRACT

Previous studies have demonstrated that formic and glycolic acids could scavenge oxygen from aqueous solutions via complex radical mechanisms similar to that of erythorbic acid. Therefore, it is important to study the feasibility of using these common thermal degradation products obtained from the regeneration of monoethylene glycol (MEG). By replacing commercially used oxygen scavengers, such as sulfites, with these organic acids, the toxicity and subsequent environmental impact of oil and gas products could be easily reduced. Furthermore, these organic acids are rapid oxygen scavengers at low concentration, and they could be cost-effective; in addition, the chemical inventory could be reduced and project costs could be further optimized. The experimental results confirmed the potential of formic and glycolic acids to be used as oxygen scavengers downstream of the MEG regeneration process in the presence of manganese (II) ions as catalyst. Of the two commercial aqueous industrial oxygen scavengers tested, diethylhydroxylamine was an extremely rapid oxygen scavenger in salty aged lean MEG solutions under alkaline conditions, whereas methyl ethyl ketoxime exhibited extremely poor performance under similar conditions; therefore, it was ruled out as potential oxygen scavenger.

© 2020 Institution of Chemical Engineers. Published by Elsevier B.V. All rights reserved.

1. Introduction

Natural gas production platforms and subsea facilities experience fluctuating conditions that affect the wellhead production (AlHarooni et al., 2015; Amjad, 2010; Soames et al., 2018a; Ehsani, 2013; Alamdari and Saffari, 2012; Kim et al., 2018) (Fig. 1). These conditions include pressure, temperature, water formation breakthrough, and the partial pressure of the acid gases generated in the oil and gas industry (Halvorsen et al., 2007; Jordan et al., 2005; AlHarooni et al., 2017; Kavianpour et al., 2014; Cao et al., 2019). Such environments promote the formation of gas hydrates, corrosion, microbial contamination, and formation of scale at the top of the wellheads and inside the networks of natural gas production and transmission pipelines (Ehsani, 2013; Halvorsen et al., 2007; AlHarooni et al., 2017; Soames et al., 2019; An et al., 2019). Thermodynamic gas hydrate inhibitors, such as monoethylene glycol (MEG), are used to minimize these concerns by shifting the equilibrium conditions toward lower temperatures, which are commonly experienced during subsea oil and gas operations, and thus, miti-

gate the pipeline blockage concerns (Ehsani, 2013; AlHarooni et al., 2017; Al Helal et al., 2019a; Yong and Obanijesu, 2015; Tavasoli et al., 2011; Amouei Torkmahalleh et al., 2016). Furthermore, the major effects on the project cost, including the corrosion and scale formation inside natural gas transmission lines could be avoided by adding pH stabilizers, such as methyl diethanolamine (MDEA), film-forming corrosion inhibitors, scale inhibitors, and oxygen scavengers (Halvorsen et al., 2007; Brustad et al., 2005; Dugstad and Seiersten, 2004; Al Helal et al., 2019b, c; Dyer et al., 2004). These additives promote flow assurance without affecting other processes or the performance of other injected chemicals (Soames et al., 2019; Bhandari et al., 2016; Charpentier and Neville, 2016; Soames et al., 2018b; Gbaruko et al., 2007).

The recovered rich MEG solution (<50 wt.%) used for inhibiting the formation of gas hydrates is separated from the oil and gas stream and is reconcentrated at a concentration greater than 80 wt.% inside the MEG regeneration units to avoid economic capital cost (AlHarooni et al., 2017; Halvorsen et al., 2013; Zaboony et al., 2017). Once regenerated, lean MEG can be reinjected into the natural gas wellhead and used for multiple cycles throughout the reservoir lifespan until thermal ageing and degradation inhibit its performance (Zaboony et al., 2017; AlHarooni et al., 2016). The regeneration process, including the selected specific processes implemented (reclamation process), chemical additives, and oper-

* Corresponding author at: WA School of Mines: Minerals, Energy and Chemical Engineering, Curtin University, Perth, W.A, Australia.

E-mail address: 17610661@student.curtin.edu.au (A. Al Helal).